

# UNCLASSIFIED

AD NUMBER
AD404861
NEW LIMITATION CHANGE
TO Approved for public release, distribution unlimited
FROM Distribution authorized to U.S. Gov't. agencies and their contractors; Administrative/Operational Use; NOV 1962. Other requests shall be referred to U.S. Army Signal Corps, Washington, DC.
AUTHORITY
USAEC ltr, 3 Nov 1966

THIS PAGE IS UNCLASSIFIED

NOTICE: When government or other drawings, specifications or other data are used for any purpose other than in connection with a definitely related government procurement operation, the U. S. Government thereby incurs no responsibility, nor any obligation whatsoever; and the fact that the Government may have formulated, furnished, or in any way supplied the said drawings, specifications, or other data is not to be regarded by implication or otherwise as in any manner licensing the holder or any other person or corporation, or conveying any rights or permission to manufacture, use or sell any patented invention that may in any way be related thereto.

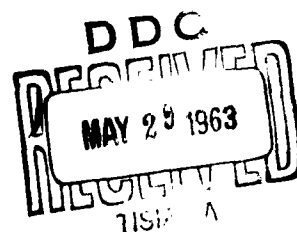
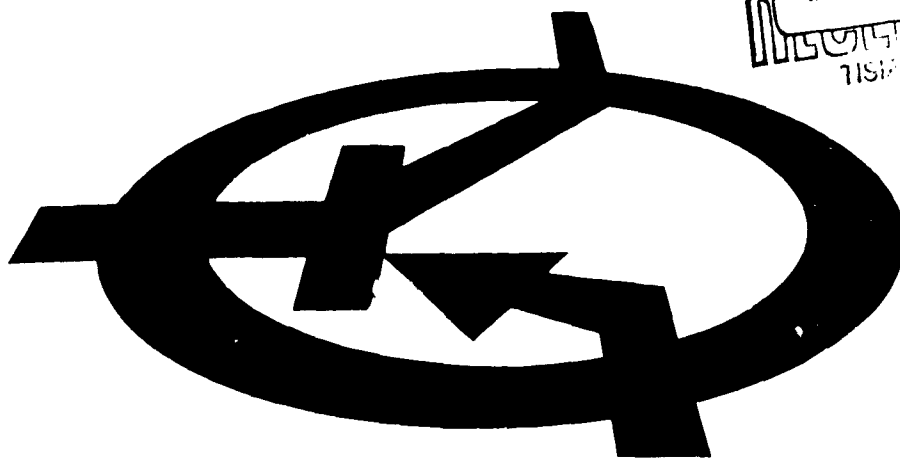
404 861

CATALOGED BY ASTIA

AS AC 100



404861



NO OTS

**Best  
Available  
Copy**

"QUALIFIED REQUESTORS MAY OBTAIN COPIES OF THIS  
REPORT FROM ASTIA. ASTIA RELEASE TO OTS NOT  
AUTHOR. LD."

HIGH-CAPACITY MAGNESIUM BATTERIES  
REPORT NO. 10

SIGNAL CORPS CONTRACT NO.  
DA-36-039-SC-85340

DEPARTMENT OF THE ARMY  
PROJECT NO. 3A99-09-002

FINAL REPORT

1 June 1960 to 30 November 1962

Prepared for

U.S. ARMY ELECTRONICS RESEARCH AND DEVELOPMENT LABORATORY  
Fort Monmouth, New Jersey

Submitted by

RADIO CORPORATION OF AMERICA  
Semiconductor and Materials Division  
Somerville, New Jersey

HIGH-CAPACITY MAGNESIUM BATTERIES  
REPORT NO. 10

SIGNAL CORPS CONTRACT  
DA-36-039-SC-85340

DEPARTMENT OF THE ARMY  
PROJECT NO. 3A99-09-002

FINAL REPORT

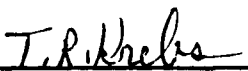
1 June 1960 to 30 November 1962

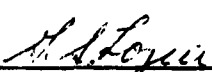
The objective of this research and development project is the development of high-capacity magnesium primary batteries using the perchlorate electrolyte systems.

This report prepared by:

Approved by:

  
\_\_\_\_\_  
R.J. Ryan

  
\_\_\_\_\_  
T.R. Krebs

  
\_\_\_\_\_  
G.S. Lozier, Manager  
Electrochemical Systems,  
Semiconductor and Materials Division

## CONTENTS

	<u>Page</u>
1. PURPOSES . . . . .	1-1
2. SUMMARY	
2.1 General . . . . .	
2.2 Reserve Cells . . . . .	
2.3 Dry Cells . . . . .	
2.4 Research Studies. . . . .	
3. EXPERIMENTAL AND FACTUAL DATA. . . . .	3-1
3.1 Prior Work On Magnesium Primary Cells with a Magnesium Perchlorate Electrolyte . . . . .	3-1
3.2 Reserve Cells . . . . .	3-2
3.2.1 Magnesium/Cupric-Oxide Reserve Cells . . . . .	3-2
3.2.1.1 Magnesium-Cupric Oxide Reserve Cell Design. . . . .	3-2
3.2.2 Research Studies . . . . .	3-6
3.2.2.1 Cathode Grid Studies. . . . .	3-7
3.2.3 Magnesium-Mercuric Oxide Reserve Cells . . . . .	3-9
3.2.3.1 Cell Characterization . . . . .	3-10
3.2.3.2 Cathode Grid Studies. . . . .	3-12
3.2.3.3 Cathode Mix Studies . . . . .	3-13
3.2.3.4 Mix Additive Studies. . . . .	3-14
3.2.3.5 Voltage Control by Heat Sink Techniques . . . . .	3-21
3.2.3.6 Low-Discharge-Rate Cell Studies . . . . .	3-22
3.2.3.7 Low-Temperature Studies . . . . .	3-23
3.2.3.8 Activated Stand Tests . . . . .	3-25
3.2.3.9 Storage Tests . . . . .	3-25



## CONTENTS (Cont'd)

	<u>Page</u>
3.2.4 Comparison of Mercuric-Oxide and Cupric-Oxide Reserve Cells. . . . .	3-26
3.2.4.1 High-Rate Polarization Studies. . . . .	3-26
3.2.5 Magnesium-Manganese Dioxide Reserve Cells. . . . .	3-27
3.2.5.1 Low-Temperature Studies . . . . .	3-28
3.2.5.2 Anode Efficiency. . . . .	3-28
3.2.5.3 Efficiency vs. Temperature Study. . . . .	3-28
3.2.5.4 Correlation of Anode Efficiency with Magnesium Corrosion Film Studies. . . . .	3-33
3.3 Electrolyte Research Studies. . . . .	3-34
3.3.1 Low-Temperature Electrolyte Conductivity . . . . .	3-34
3.3.2 Specific Conductivity of Various Perchlorates. . . . .	3-34
3.3.2.1 Effect of Various Perchlorate Electrolytes On The Performance of Magnesium/Mercuric-Oxide Cells . . . . .	3-35
3.3.3 Variation of Electrolyte Viscosity with Temperature. . . . .	3-35
3.4 Dry Cells . . . . .	3-36
3.4.1 Synthetic $MnO_2$ Study . . . . .	3-37
3.4.2 Dry Cell Parameter Studies . . . . .	3-38
3.4.2.1 Cell Formulation. . . . .	3-39
3.4.2.2 Capacity Data . . . . .	3-39
3.4.3 Low Temperature Studies. . . . .	3-40
3.4.3.1 Cell Formulation. . . . .	3-41
3.4.3.2 Variations in Cell Construction . . . . .	3-41
3.4.3.3 Excess-Electrolyte Studies. . . . .	3-41
3.4.3.4 Prepelled Cathode Electrodes. . . . .	3-42
3.4.3.5 Studies of Electrode Surface Area . . . . .	3-43
3.4.4 Magnesium Can Studies. . . . .	3-44
3.4.4.1 Can Seal Studies. . . . .	3-46
3.4.4.2 Delayed Action Shelf Study. . . . .	3-46

## CONTENTS (Cont'd)

	<u>Page</u>
3.5 Basic Research. . . . .	3-48
3.5.1 Impedance of Dry Cells . . . . .	3-48
3.5.1.1 Introduction. . . . .	3-48
3.5.1.2 Measurements and Equations. . . . .	3-49
3.5.1.3 Cell Analysis . . . . .	3-50
3.5.1.4 Test Procedure. . . . .	3-56
3.5.1.5 Comparison of AZ-21 and C.P. Magnesium Anode Cells . . . . .	3-56
3.5.2 Impedance Studies. . . . .	3-58
3.5.2.1 CuO Cells . . . . .	3-59
3.5.2.2 Effect of Storage on Cell Impedance . . . . .	3-59
3.5.2.3 AZ-21 Impedance . . . . .	3-59
3.5.2.4 Magnesium Impedance . . . . .	3-60
3.6 Meteorological Battery. . . . .	3-61
3.6.1 Design . . . . .	3-61
3.6.2 Activation Procedure . . . . .	3-61
3.6.3 Experimental Data. . . . .	3-61
3.6.3.1 Results Obtained. . . . .	3-61
3.6.4 Conclusions. . . . .	3-62
4. RECOMMENDATIONS FOR FUTURE WORK. . . . .	4-1
4.1 Reserve Cells . . . . .	4-1
4.2 Dry Cells . . . . .	4-1
4.3 Research Studies. . . . .	4-1

## TABLES

### Table No.

- I. Shelf-Life Data for  $\text{Mg}/\text{Mg}(\text{ClO}_4)_2/\text{MnO}_2$  Cells With Various Types of  $\text{MnO}_2$ .
- II. Discharge Data for  $\text{Mg}/\text{CuO}$  Cells at Various Discharge Currents and Temperatures.
- III. Capacity Data for  $\text{Mg}/\text{Mg}(\text{ClO}_4)_2/\text{CuO}$  Reserve Cells at Various Discharge Rates and Temperatures.
- IV.  $\text{Mg}/\text{Mg}(\text{ClO}_4)_2/\text{CuO}$  Reserve Cells with Various Carbon Black Ratios.
- V. Mercuric-Oxide Cathode-Mix-Composition Data.
- VI. High-Rate-Capacity Data for  $\text{Mg}/\text{Mg}(\text{ClO}_4)_2/\text{HgO}$  Cells of Various Cathode Compositions.
- VII. Comparison of  $\text{Mg}/\text{Mg}(\text{ClO}_4)_2/\text{HgO}$  Reserve Cells with Various Grids.
- VIII. Composition and Capacity Data for Mercuric-Oxide Blended Mixes with Various Active-Material-To-Shawinigan-Carbon-Black Ratios.
- IX. Capacity Data for  $\text{Mg}/\text{Mg}(\text{ClO}_4)_2/\text{HgO}$  Reserve Cells at Various Discharge Rates and Temperatures.
- X. Capacity Data for  $\text{Mg}/\text{Mg}(\text{ClO}_4)_2/\text{HgO}$  Reserve Cells at Various Discharge Rates and Temperatures.
- XI. Comparison of Four-Cathode and Five-Anode-Plate Reserve Cells of Equivalent Size.
- XII. Capacity Data for  $\text{Mg}/\text{Mg}(\text{ClO}_4)_2/\text{MnO}_2$  System.
- XIII. Cathode Efficiency of  $\text{Mg}/\text{Mg}(\text{ClO}_4)_2$  at Various Current Drains and Temperatures.
- XIV. Magnesium Efficiency and Capacity Data for  $\text{Mg}(\text{Az-21XA})/\text{Mg}(\text{ClO}_4)_2/\text{MnO}_2$  Cells at Various Constant-Current Drains.
- XV. Magnesium-Anode Efficiency Data at a Current Density of  $0.096 \text{ MA}/\text{CM}^2$  in  $2\text{N Mg}(\text{ClO}_4)_2$  Electrolyte.
- XVI. Magnesium-Anode Efficiency Data in  $2\text{N}$  Magnesium-Perchlorate Electrolyte.

TABLES (Contd.)

Table No.

- XVII. Specific Conductivity Data for Various Perchlorate-Salt Solutions as a Function of Temperature and Concentration.
- XVIII. Viscosity of 5N  $\text{Ca}(\text{ClO}_4)_2$ ,  $\text{Sr}(\text{ClO}_4)_2$ , and  $\text{Mg}(\text{ClO}_4)_2$  Electrolytes at Various Temperatures.
- XIX. Performance Data of Type-L and -M  $\text{MnO}_2$  A-Size Cells Utilizing Both  $\text{MgBr}_2$  and  $\text{Mg}(\text{ClO}_4)_2$  Electrolytes.
- XX. Performance of  $\text{Mg}/\text{Mg}(\text{ClO}_4)_2/\text{MnO}_2$  A-Cells Discharged Continuously at Various Temperatures Through Various Resistances.
- XXI. Shelf-Life Data for Magnesium Cells Discharged Under an Intermittent AN/PRC-35 (XC-2) A2 Current Drain.
- XXII. Voltage Variations of  $\text{Mg}/\text{Mg}(\text{ClO}_4)_2/\text{MnO}_2$  (Type M) A-Cells with AZ-10 and AZ-21 Magnesium Alloy on Intermittent Service.
- XXIII. Constants and Fixed Parameters for Evaluating AZ-21 C.P. Magnesium Anodes.
- XXIV. Summary Data on AZ-21-Alloy Magnesium Anodes.
- XXV. Shelf-Life and Impedance Data for  $\text{Mg}/\text{Mg}(\text{ClO}_4)_2$  and  $\text{Mg}/\text{Mg}(\text{ClO}_4)_2/\text{CuO}$  A-Cells.
- XXVI. Initial Capacity Data for  $\text{Mg}/\text{Mg}(\text{ClO}_4)_2/\text{CuO}$  A-Cells.
- XXVII. Summary of Data on C.P. Magnesium Anodes.
- XXVIII. Impedance Data for  $\text{Mg}/\text{Mg}(\text{ClO}_4)_2/\text{MnO}_2$  (Type M) A-Cells Discharged at a Constant Resistance of 50 Ohms.

## ILLUSTRATIONS

### Figure No.

1. Capacity of Various Dry Cells as a Function of Discharge Time.
2. Capacity of Various Dry Cells as a Function of Discharge Time.
3. Capacity Retention of Magnesium/Cupric-Oxide AA-Cells Stored at  $70 \pm 2^\circ\text{F}$  and  $50 \pm 5\%$  R.H. (Cells Discharged Continuously Through a 50-Ohm Resistance at  $70 \pm 2^\circ\text{F}$ . and  $50 \pm 5\%$  R.H.).
4. AC Impedance vs Load Resistance of AA-Cells. Discharged Continuously Through Various Load Resistances at  $70 \pm 2^\circ\text{F}$  and  $50 \pm 5\%$  R.H. (Impedance Measured at Approximately 50% Discharge).
5. Delayed Action of D-Cells Discharged Through 6.6 Ohms for 4 Min. Each/1/2 Hour for 24 Hours Per Day.
6. Capacity Data for Mg/CuO Reserve Cells Discharged Under a Constant-Current of 20.0 Amperes in  $2\text{N Mg}(\text{ClO}_4)_2$  Electrolyte.
7. Capacity Data for Mg/CuO-Reserve Cell Under a Constant-Current Drain of 25.4 Amperes in  $2\text{N Mg}(\text{ClO}_4)_2$  Electrolyte.
8. Capacity Data for Mg/CuO-Reserve Cell Under a Constant-Current Drain of 10.0 Amperes in  $2\text{N Mg}(\text{ClO}_4)_2$  Electrolyte.
9. Capacity Data for  $\text{Mg}/\text{Mg}(\text{ClO}_4)_2/\text{CuO}$  Reserve Cells at Various Discharge Drains at  $70^\circ\text{F}$ .
10. Effect of Temperature on the Discharge Characteristics of  $\text{Mg}/\text{Mg}(\text{ClO}_4)_2/\text{CuO}$  Reserve Cells.
11. Effect of Temperature on Discharge Characteristics of  $\text{Mg}/\text{Mg}(\text{ClO}_4)_2/\text{CuO}$  Reserve Cells.
12. Effect of Temperature on the Discharge Characteristics of  $\text{Mg}/\text{Mg}(\text{ClO}_4)_2/\text{CuO}$  Reserve Cells.
13. Effect of Temperature on Mg/CuO Reserve Cells with Various Magnesium Anodes.
14. Temperature Dependence of the Mg Anode and CuO Cathode in a Mg/CuO Reserve Cell in  $2\text{N Mg}(\text{ClO}_4)_2$  Electrolyte.
15. Capacity Data for Mg/CuO Reserve Cells with Various Carbon Ratios Under a Constant Current Drain of 20.0 Amperes in  $2\text{N Mg}(\text{ClO}_4)_2$  Electrolyte.
16. Capacity Data for  $\text{Mg}/\text{Mg}(\text{ClO}_4)_2/\text{CuO}$  Reserve Cells under a Constant-Current Drain of 10.0 Amperes.

ILLUSTRATIONS (Cont'd)

Figure No.

17.  $\text{Mg}/\text{Mg}(\text{ClO}_4)_2/\text{CuO}$  Reserve Cell Discharged at 15 Amperes at Room Temperature.
18.  $\text{Mg}/\text{Mg}(\text{ClO}_4)_2/\text{CuO}$  Reserve Cell Made with Milled CuO and Discharged at 10 Amperes Average Volt 0.97 to 20% 6-1 CuO Shawinigan.
19.  $\text{Mg}/\text{Mg}(\text{ClO}_4)_2/\text{HgO}$  (8:1 Mix Plus 10%  $\text{Ag}_2\text{O}$ ) Reserve Cells with .003-inch Cathode Grids.
20. Capacity Data for  $\text{Mg}/\text{Mg}(\text{ClO}_4)_2/\text{HgO}$  Reserve Cells Discharged at a Constant Current of 20 Amperes.
21. Capacity Data for  $\text{Mg}/\text{Mg}(\text{ClO}_4)_2/\text{HgO}$  Reserve Cells with a Titanium Cathode Grid.
22. Capacity Data for  $\text{Mg}/\text{Mg}(\text{ClO}_4)_2/\text{HgO}$  Reserve Cells of Various Active Material-to-Carbon Ratios.
23. Effect of  $\text{Ag}_2\text{O}$  in the  $\text{HgO}$  Cathode on Initial Discharge Voltage at 10.0 Amperes.
24. Effect of  $\text{Ag}_2\text{O}$  in the Cathode Mix on the Discharge Voltage Characteristics of  $\text{Mg}/\text{Mg}(\text{ClO}_4)_2/\text{HgO}$  Reserve Cells.
25. Effect of 5%  $\text{Ag}_2\text{O}$  Added to the Cathode Mix  $\text{Mg}/\text{Mg}(\text{ClO}_4)_2/\text{HgO}$  Reserve Cell.
26. Effect of Various Additives on Initial Voltage Characteristics of  $\text{Mg}/\text{Mg}(\text{ClO}_4)_2/\text{HgO}$  Reserve Cells.
27.  $\text{Mg}/\text{Mg}(\text{ClO}_4)_2/\text{HgO}$  Reserve Cell with 5%  $\text{Ag}_2\text{O}$  Added to the Cathode Mix Discharged at 10.0 Amperes.
28.  $\text{Mg}/\text{Mg}(\text{ClO}_4)_2/\text{HgO}$  Reserve Cell with 5%  $\text{Ag}_2\text{O}$  Added to the Cathode Mix Discharged at 10.0 Amperes at Room Temperature.
29. Low-Temperature Capacity Data for  $\text{Mg}/\text{Mg}(\text{ClO}_4)_2/\text{HgO}$  Reserve Cells.
30. Effect of Partial Reduction of Mercuric Oxide on Voltage Characteristics of  $\text{Mg}/\text{HgO}$  Reserve Cells.
31. Calories Evolved from Magnesium Electrode Per Hour at Various Mg Efficiencies at High Discharge Rates.
32. Calories Evolved from a Magnesium Electrode Per Hour at Various Anode Efficiencies at Low Discharge Rates.
33. Calories Evolved from Magnesium Corrosion Reaction as a Function of Electrode Efficiency at High Discharge Rates.
34. Calories Evolved from Magnesium Corrosion Reaction as a Function of Electrode Efficiency at Low Discharge Rates.

ILLUSTRATIONS (Cont'd)

Figure No.

35. Capacity Data for  $\text{Mg}/\text{Mg}(\text{ClO}_4)_2/\text{HgO}$  Reserve Cell.
36. Three-Cell  $\text{Mg}/\text{Mg}(\text{ClO}_4)_2/\text{HgO}$  Reserve Battery with Copper-Foil Jacket.
37. Capacity Data for a Three-Cell  $\text{Mg}/\text{Mg}(\text{ClO}_4)_2/\text{HgO}$  Reserve Battery with Aluminum-Case Construction.
38. Capacity Data for  $\text{Mg}/\text{Mg}(\text{ClO}_4)_2/\text{HgO}$  Reserve Cells.
39. Capacity Data for  $\text{Mg}/\text{Mg}(\text{ClO}_4)_2/\text{HgO}$  Reserve Cells at Various Discharge Drains at  $-4^\circ\text{F}$ .
40. Effect of Temperature on Discharge Characteristics of  $\text{Mg}/\text{Mg}(\text{ClO}_4)_2/\text{HgO}$  Reserve Cells.
41. Capacity Data for  $\text{Mg}/\text{Mg}(\text{ClO}_4)_2/\text{HgO}$  Reserve Cells at Various Discharge Rates at  $-40^\circ\text{F}$ .
42. Capacity Data for  $\text{Mg}/\text{Mg}(\text{ClO}_4)_2/\text{HgO}$  Reserve Cells at Various Discharge Drains at  $-58^\circ\text{F}$ .
43. Capacity Data for a 3-Cell  $\text{Mg}/\text{Mg}(\text{ClO}_4)_2/\text{HgO}$  Reserve Battery at 1.0 Ampere at  $-40^\circ\text{F}$ .
44. Capacity Data for a 3-Cell  $\text{Mg}/\text{Mg}(\text{ClO}_4)_2/\text{HgO}$  Reserve Battery at 1.0 Ampere at  $-58^\circ\text{F}$ .
45. Discharge Characteristics of a 6-Cell Magnesium/Mercuric-Oxide Battery Discharged at 1.5 Amperes at  $21.1^\circ\text{C}$  and  $-40^\circ\text{C}$ .
46. Capacity Data for  $\text{Mg}/\text{Mg}(\text{ClO}_4)_2/\text{HgO}$  Reserve Cells with Various Activation Time Discharged at 5 Amperes.
47. Characteristics of  $\text{Mg}/\text{Mg}(\text{ClO}_4)_2/\text{HgO}$  Reserve Cell Discharged at 3.0 Amperes after 19-Months Storage.
48. Capacity For a  $\text{Mg}/\text{Mg}(\text{ClO}_4)_2/\text{CuO}$  Reserve Cell Discharged at 20.0 Amperes.
49. Effect of Current Density on the Electrode Potentials of a  $\text{Mg}/\text{Mg}(\text{ClO}_4)_2/\text{CuO}$  Reserve Cell.
50. Effect of Current Density on the Electrode Potentials of a  $\text{Mg}/\text{Mg}(\text{ClO}_4)_2/\text{HgO}$  Reserve Cell.
51.  $\text{Mg}/\text{Mg}(\text{ClO}_4)_2/\text{MnO}_2$  Reserve Cells Discharged at  $70^\circ\text{F}$ .
52.  $\text{Mg}/\text{Mg}(\text{ClO}_4)_2/\text{MnO}_2$  Reserve Cells Discharged at  $70^\circ\text{F}$ .
53.  $\text{Mg}/\text{Mg}(\text{ClO}_4)_2/\text{MnO}_2$  Reserve Cells Discharged at  $-20^\circ\text{F}$ .
54.  $\text{Mg}/\text{Mg}(\text{ClO}_4)_2/\text{MnO}_2$  Reserve Cells Discharged at  $-20^\circ\text{F}$ .
55.  $\text{Mg}/\text{Mg}(\text{ClO}_4)_2/\text{MnO}_2$  Reserve Cells Discharged at  $-40^\circ\text{F}$ .

ILLUSTRATIONS (Cont'd)

Figure No.

56.  $\text{Mg}/\text{Mg}(\text{ClO}_4)_2/\text{MnO}_2$  Reserve Cells Discharged at  $-40^\circ\text{F}$ .
57. Effect of Temperature on Anode Efficiency of Various Magnesium Alloys in  $2\text{N Mg}(\text{ClO}_4)_2$  at Current Density of  $1.5 \text{ ma}/\text{cm}^2$ .
58. Effect of Temperature on Anode Efficiency of Various Magnesium Alloys in  $2\text{N Mg}(\text{ClO}_4)_2$  at a Current Density of  $10.0 \text{ ma}/\text{cm}^2$ .
59. Effect of Open-Circuit Time off on the Anode Efficiency of  $\text{Mg}/\text{Mg}(\text{ClO}_4)_2/\text{CuO}$  Cells Discharged at  $10.0 \text{ ma}/\text{cm}^2$  for 15 Minutes.
60.  $\text{Mg}(\text{AZ-21XA})/\text{Mg}(\text{ClO}_4)_2/\text{MnO}_2$  (Type M) Flat Cell.
61. Magnesium Anode Efficiency as a Function of Current Density in  $2\text{N Mg}(\text{ClO}_4)_2$  Electrolyte.
62. Exposed-Anode Area ( $A_T - A_F$ ) and Anode Efficiency vs. Apparent Current Density of Pure Magnesium in  $2\text{N Mg}(\text{ClO}_4)_2$  Electrolyte.
63. Exposed Anode Area ( $A_T - A_F$ ) and Anode Efficiency vs. Apparent Current Density.
64. Specific Conductivity of Various Perchlorate Electrolytes as a Function of Temperature and Concentration.
65.  $\text{Mg-HgO}$  Cells Discharged at 0.1 Ampere at Room Temperature in Various Electrolytes.
66. Comparison of Magnesium A-Cells Containing Two Different Types of Synthetic  $\text{MnO}_2$  and Electrolyte Discharged at 4 Ohms.
67. Comparison of Magnesium A-Cells Containing Two Different Types of Synthetic  $\text{MnO}_2$  and Electrolyte Discharged at  $16-2/3$  Ohms.
68. Data for  $\text{Mg}/\text{Mg}(\text{ClO}_4)_2/\text{MnO}_2$  A-Cells Discharged Continuously at  $16-2/3$  Ohms at Various Temperatures.
69. Data for  $\text{Mg}/\text{Mg}(\text{ClO}_4)_2/\text{MnO}_2$  A-Cells Discharged Continuously at 50 Ohms at Various Temperatures.
70. Relation of Capacity to Temperature and Rate of Discharge for  $\text{Mg}/\text{Mg}(\text{ClO}_4)_2/\text{MnO}_2$  A-Cells.
71. Relation of  $\text{Mg}/\text{Mg}(\text{ClO}_4)_2/\text{MnO}_2$  Cell Capacity and Efficiency to Temperature and Discharge Rate.
72. Capacity Data for  $\text{Mg}/\text{Mg}(\text{ClO}_4)_2/\text{MnO}_2$  A-Cells Discharged Continuously at  $16-2/3$  Ohms at Various Temperatures.
73.  $\text{Mg}/\text{MnO}_2$  Dry Cells Made with Various Separator Materials and Discharged on  $16-2/3$  Ohms at  $-20^\circ\text{F}$ .



ILLUSTRATIONS (Cont'd)

Figure No.

74. Mg/MnO<sub>2</sub> Dry Cells made with Various Cathode Constructions and Discharged on 16-2/3 Ohms at 70°F.
75. Mg/MnO<sub>2</sub> Dry Cells Made with Various Cathode Constructions and Discharged on 16-2/3 Ohms at -20°F.
76. Basic Construction of Low-Temperature A-Cell having Increased Anode-Surface Area.
77. Mg/Mg(ClO<sub>4</sub>)<sub>2</sub>/MnO<sub>2</sub> (Type M) A-Cells of Increased Anode Area Discharged on 16-2/3 Ohms at -20°F.
78. Mg/MnO<sub>2</sub> A-Cells of Increased Anode Area, Discharged on 16-2/3 Ohms at 70°F.
79. Mg/Mg(ClO<sub>4</sub>)<sub>2</sub>/MnO<sub>2</sub> Flat-Plate Cells of Various Anode Surfaces.
80. Mg/MnO<sub>2</sub> Dry Cells with Spiralled Elements.
81. Capacity Data for Mg/Mg(ClO<sub>4</sub>)<sub>2</sub>/MnO<sub>2</sub> (Type M) A-Cells at 16-2/3 Ohms.
82. Capacity Data for Mg/Mg(ClO<sub>4</sub>)<sub>2</sub>/CuO A-Cells at 10-2/3 Ohms.
83. Capacity Data for Mg/Mg(ClO<sub>4</sub>)<sub>2</sub>/MnO<sub>2</sub> (Type M) AA-Cells.
84. Delayed Action Characteristics of Mg/Mg(ClO<sub>4</sub>)<sub>2</sub>/MnO<sub>2</sub> (Type M) AA-Cells at 150-Ohm to 8.93-Ohm Drain.
85. Delayed Action Characteristics of Mg/Mg(ClO<sub>4</sub>)<sub>2</sub>/CuO AA-Cells at 91-Ohm to 5.39-Ohm Drain.
86. Delayed-Action Characteristics of AZ-21 Mg/Mg(ClO<sub>4</sub>)<sub>2</sub>/MnO<sub>2</sub> (Type M) A-Cells at 150-Ohm to 8.9-Ohm Drain.
87. Delayed Action Characteristics of Mg(AZ-10)/Mg(ClO<sub>4</sub>)<sub>2</sub>/MnO<sub>2</sub> (Type M) A-Cells at 150-Ohm to 8.9-Ohm Drain.
88. Equivalent Circuit of the Magnesium Cell.
89. Ideal Frequency Characteristics of a Two-Component System.
90. Resistance-Ratio Bridge for Magnesium Cell Impedance Measurements.
91. Equivalent Circuit of Magnesium Cell at Frequencies Above the Electrolyte cutoff Frequency.
92. DC Equivalent Circuit of a Magnesium Cell.
93. Total Anode Area vs. Apparent Current Density for AZ-21 Magnesium Alloy and Pure Magnesium
94. Exposed Anode Area ( $A_T - A_F$ ) and Film Volume per Unit Total Area vs Apparent Current Density (AZ-21 Magnesium Alloy)

# ILLUSTRATIONS (Cont'd)

## Figure No.

95. Exposed Anode Area ( $A_m - A_a$ ) and Film Volume Per Unit Total Area vs Apparent Current Density<sup>f</sup> of Pure Magnesium.
96. Experimental Apparatus for Impedance Measurement.
97. AC Impedance vs Load Resistance of  $Mg/Mg(ClO_4)_2/MnO_2$  (Type M) AA-Cells.
98. AC Impedance vs Frequency of  $Mg/Mg(ClO_4)_2/MnO_2$  (Type M) AA-Cells.
99. AC Impedance vs Load Resistance of  $Mg/Mg(ClO_4)_2/CuO$  AA-Cells.
100. AC Impedance vs Frequency of  $Mg/Mg(ClO_4)_2/CuO$  AA-Cells.
101. Four-Cell Magnesium-Mercuric Oxide Meteorological Battery. Discharged through 12 Ohms.
102. Four-Cell Magnesium-Mercuric Oxide Meteorological Battery.

#### ABSTRACT

This abstract describes briefly the final report of the accomplishments and progress made during the U.S. Army Electronics Research and Development Laboratories High-Capacity Magnesium-Battery Program by the Radio Corporation of America, Semiconductor and Materials Division, Somerville, New Jersey. This program was conducted during the period from 1 June 1960 through 30 November 1962.

Characteristic data are presented for magnesium/magnesium-perchlorate reserve cells discharged at temperatures as low as  $-40^{\circ}\text{F}$ . Cathode efficiency data as a function of temperature and current drain are also presented.

Factors affecting the performance of dry cell batteries were investigated. Cathode efficiencies, storage characteristics, and electrode surface phenomena were evaluated.

Data are also presented for a newly-developed magnesium/mercuric-oxide meteorological battery, including discharge data for temperatures as low as  $-58^{\circ}\text{F}$ .

#### ABSTRACT

This abstract describes briefly the final report of the accomplishments and progress made during the U.S. Army Electronics Research and Development Laboratories High-Capacity Magnesium-Battery Program by the Radio Corporation of America, Semiconductor and Materials Division, Somerville, New Jersey. This program was conducted during the period from 1 June 1960 through 30 November 1962.

Characteristic data are presented for magnesium/magnesium-perchlorate reserve cells discharged at temperatures as low as  $-40^{\circ}\text{F}$ . Cathode efficiency data as a function of temperature and current drain are also presented.

Factors affecting the performance of dry cell batteries were investigated. Cathode efficiencies, storage characteristics, and electrode surface phenomena were evaluated.

Data are also presented for a newly-developed magnesium/mercuric oxide meteorological battery, including discharge data for temperatures as low as  $-58^{\circ}\text{F}$ .

# 1. PURPOSE

The purposes of this research and development contract were to:

1. develop practical Mg-CuO and Mg-HgO reserve cells suitable for use in high-rate batteries,
2. characterize the  $\text{Mg/Mg(ClO}_4)_2/\text{MgO}$  and  $\text{Mg/Mg(ClO}_4)_2/\text{CuO}$  dry cells, and
3. perform research studies to determine the factors and mechanisms controlling anode efficiency, inhibitor function, and delayed action of magnesium anode. Emphasis was placed on the perchlorate electrolyte.

## 2. SUMMARY

### 2.1 GENERAL

A two-and-one-half-year study program was carried out to investigate electrochemical phenomena which affect performance characteristics of high-capacity magnesium reserve and dry-cell primary batteries with a perchlorate electrolyte. Areas of investigation which received special attention during this program are the following:

- a. high-rate and low-temperature reserve cells.
- b. dry cells.
- c. basic research.

### 2.2 RESERVE CELLS

The development of practical Mg-HgO and Mg-CuO reserve cells is described. The capacity of the Mg-HgO cell is over 50 watt-hours per pound and 3.3 watt-hours per square inch. Both cells were shown to be affected adversely by the heat generated by the magnesium anode. Data is presented to show that, by the use of heat sinks, efficient operation of both systems can be obtained on a 10-minute discharge rate.

During the course of this program, factors affecting the performance of reserve Mg-HgO and Mg-CuO cells were investigated. It was determined that reserve cell performance can be improved to an appreciable degree by changes and modifications in the following areas:

- a. cathode material formulation.

- b. cathode mix preparation.
- c. cathode mix additives.
- d. cathode grid.
- e. Mg alloy type.
- f. electrolyte type and concentration.

Optimum conditions are given.

#### 2.2.1 Low Temperature Application of Mg-HgO Reserve Cells

A detailed analysis of the heat-generating mechanism of the magnesium anode and its effect on magnesium performance was investigated. The application of this heat generation was used as an approach to the design of low-temperature batteries. Magnesium/mercuric-oxide batteries were designed equivalent to the BA-253/u meteorological battery. This battery gave greatly increased performance.

The use of a polyurethane insulating jacket was shown to be practical for the design of batteries on 24-hour discharge rates. A magnesium/mercuric-oxide battery with 50-w-hr/lb capacity at -40°F on a 24-hour discharge rate was demonstrated.

As part of the low-temperature program, the properties of electrolytes were studied extensively. Such factors as low-temperature conductivity, specific conductivity of various electrolytes, and variations in electrolyte viscosity with temperature changes were investigated.

#### 2.3 DRY CELLS

The basic properties -- shelf life, intermittent performance, impedance, delayed action, operating temperature -- of the magnesium/manganese dioxide dry cell and the magnesium/cupric-oxide dry cell were characterized. The delayed action of Mg/CuO and Mg/MnO<sub>2</sub> A-cells was unaffected by storage at 70° and 113°F., and the impedance was essentially the same after storage for five months at 113°F and six months at 70°F. The capacity retention on the Mg/MnO<sub>2</sub> cells at both temperatures exceeded 90%. The shelf life of the magnesium/cupric-oxide dry cell exhibited a drop-off at 113°F.

The low-temperature properties of the magnesium/manganese-dioxide dry cell was evaluated. Data are presented to show that the low-temperature performance is a function of electrode surface area.

#### 2.4 RESEARCH STUDIES

It was attempted to establish a correlation between the impedance and the film formation of the magnesium anode. Measurements of the capacitance and resistance of the corrosion film showed that the exposed area ( $A_t - A_p$ ) decreased, as predicted, with decreases in current density. A relationship between exposed anode area and anode efficiency, as a function of current density, was developed.



### 3. EXPERIMENTAL AND FACTUAL DATA

#### 3.1 PRIOR WORK ON MAGNESIUM PRIMARY CELLS WITH A MAGNESIUM PERCHLORATE ELECTROLYTE

Prior to this contract, a research program at the RCA Laboratories demonstrated the advantages of a perchlorate electrolyte in magnesium primary cells. Some of the important properties of the perchlorate electrolyte are:

- a. It is less corrosive to a magnesium anode than either a magnesium chloride or a magnesium bromide electrolyte. At high-current drains, magnesium operates at an anode efficiency of 80 percent. This feature reduces the amount of water required for cell reaction and the amount of  $Mg(OH)_2$  formed. These properties are desirable for the efficient design of magnesium primary batteries.
- b. Magnesium has a low level of static corrosion in a perchlorate electrolyte, thereby insuring a good shelf life for dry cells or an extremely long activated-stand capability for reserve cells.
- c. The perchlorate electrolyte does not react with cupric oxide, mercuric oxide, silver II oxide, or nickel dioxide, thereby permitting the coupling of these high-capacity cathode materials to a magnesium anode. These are the most desirable cathode materials for the design of batteries with a high capacity at high discharge rates.

The performance characteristics of the magnesium/magnesium-perchlorate cells are presented in Figures 1, 2, 3, 4, and 5. Presented in Figures 1 and 2 are watt-hour capacity data per unit of weight and volume obtained from single cells.

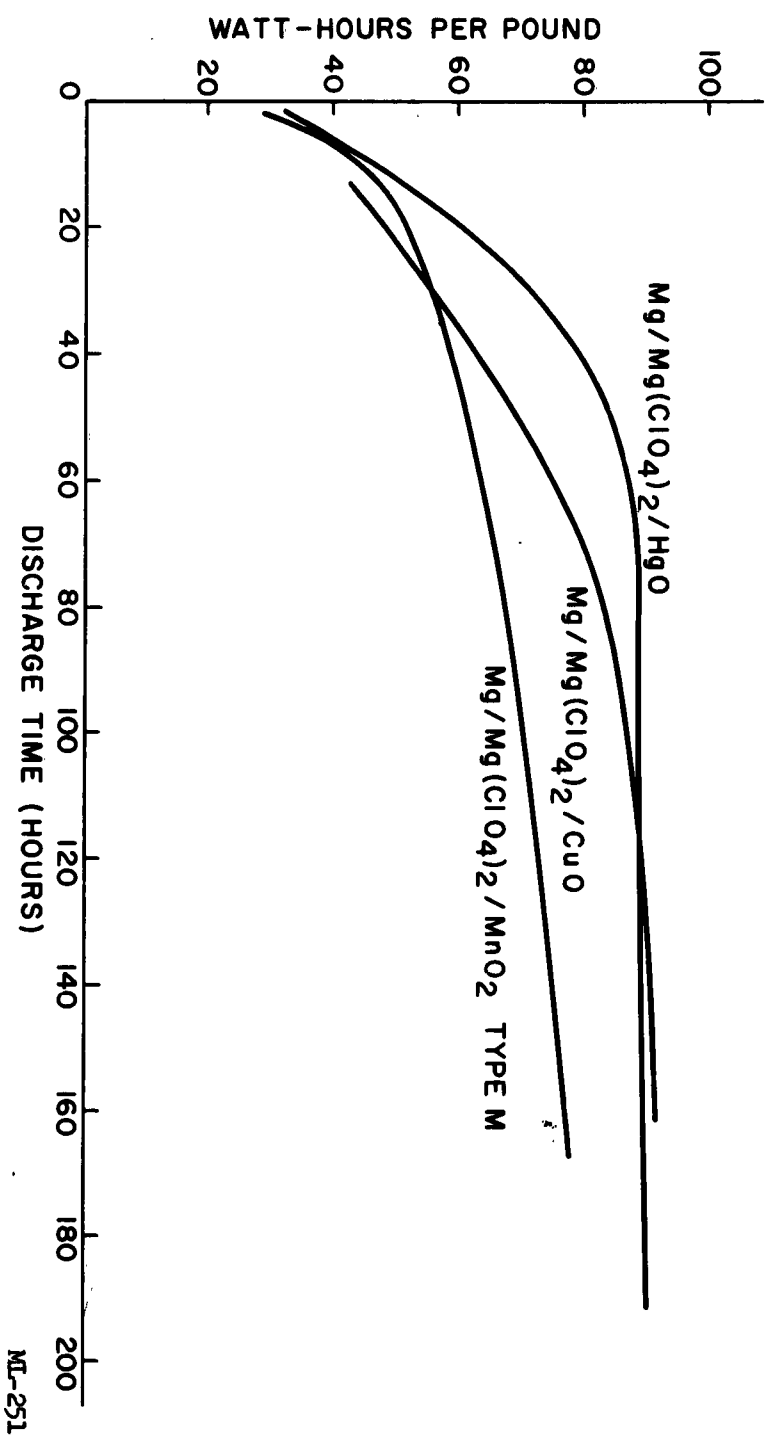


FIGURE 1. CAPACITY OF VARIOUS DRY CELLS AS A FUNCTION OF DISCHARGE TIME.

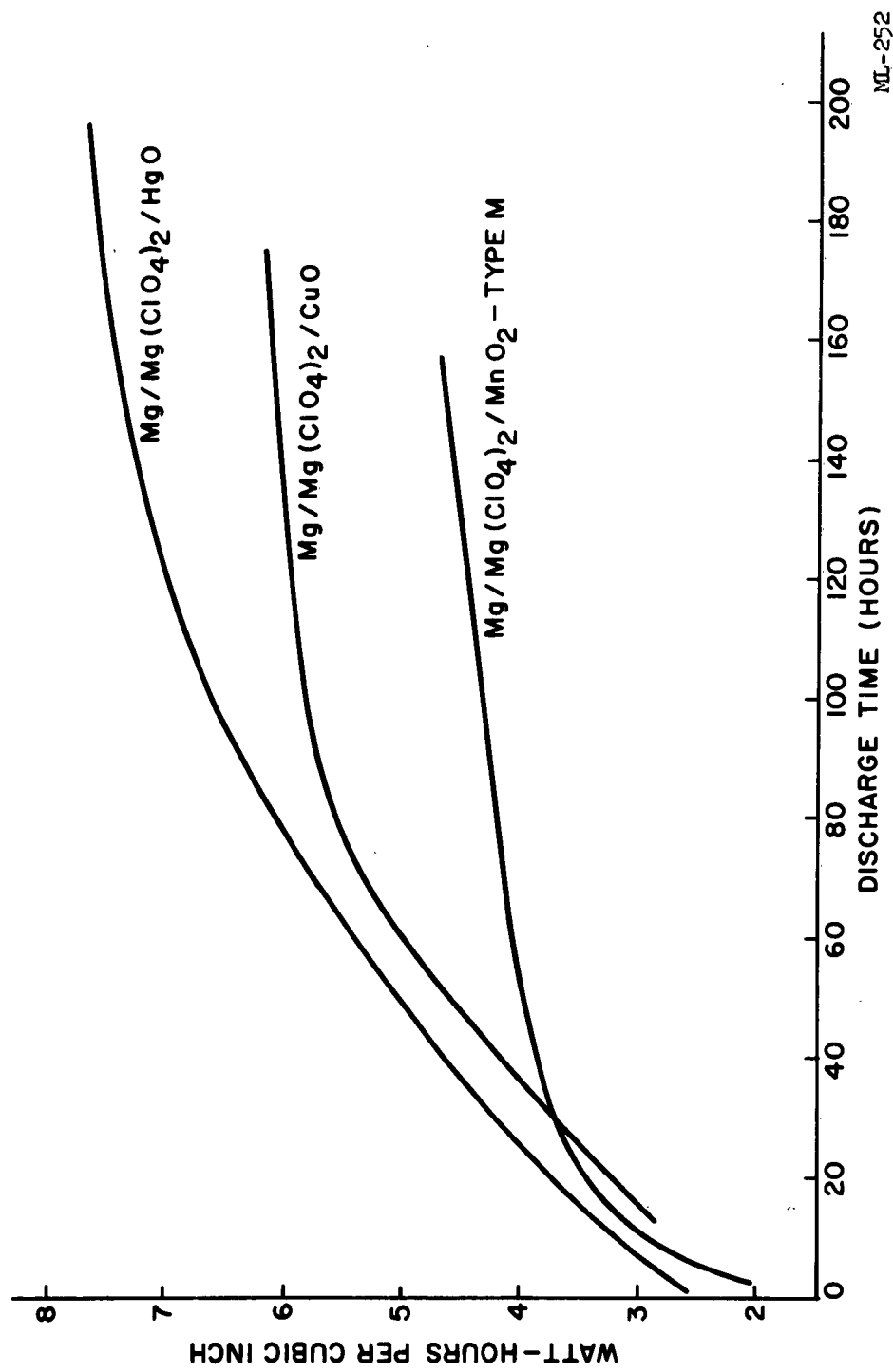


FIGURE 2. CAPACITY OF VARIOUS DRY CELLS AS A FUNCTION OF DISCHARGE TIME.

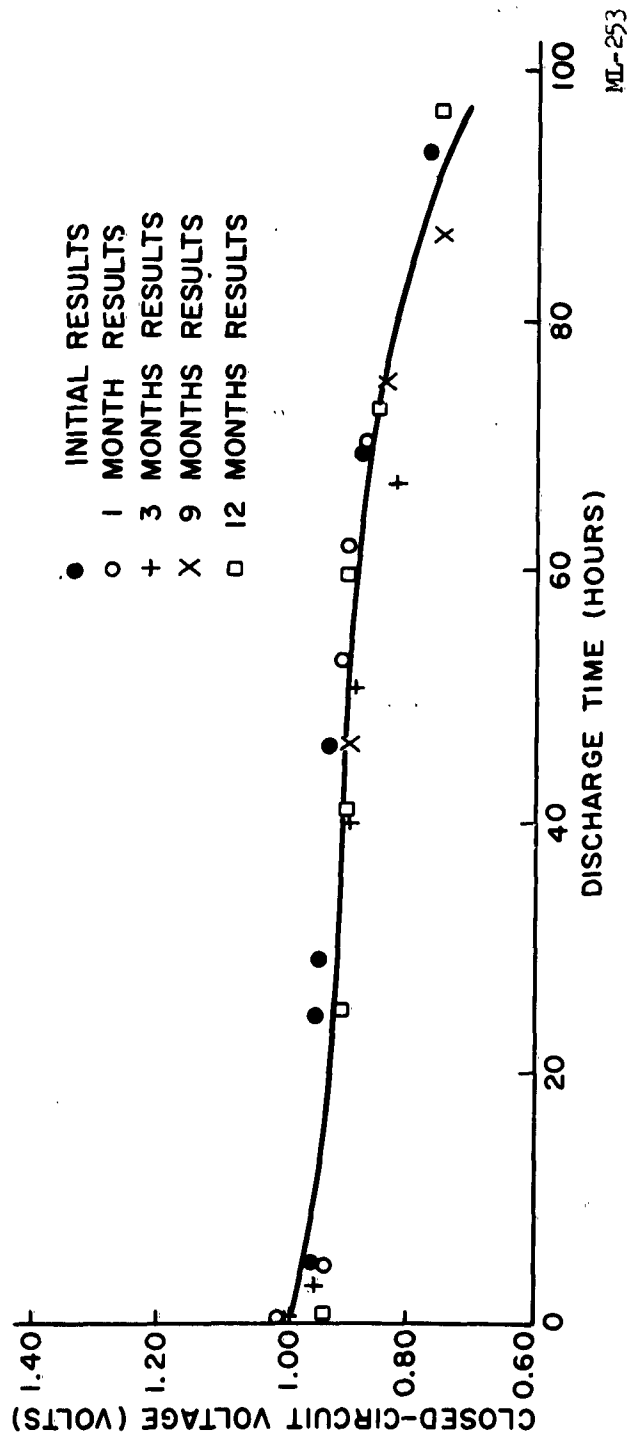
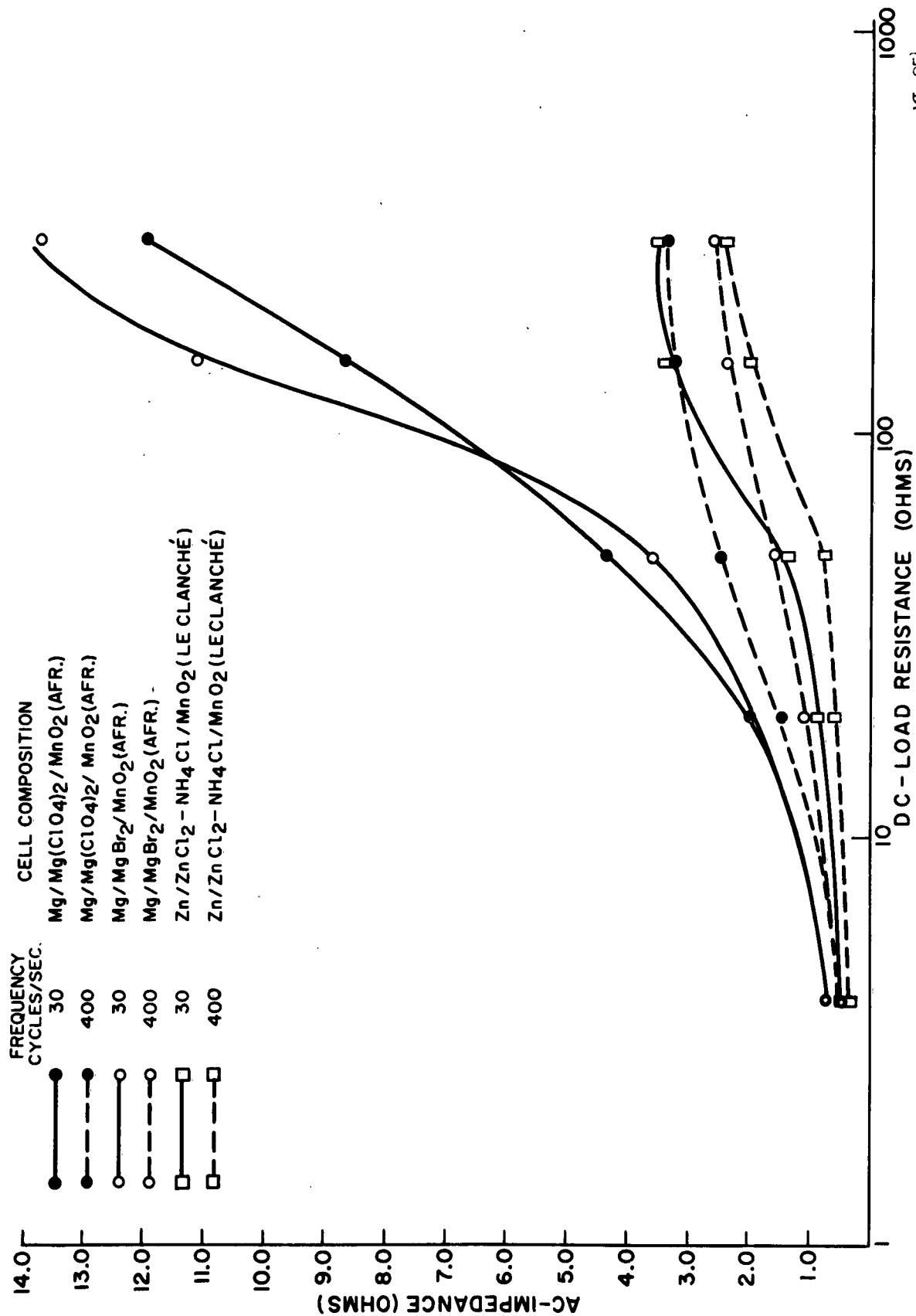


FIGURE 3. CAPACITY RETENTION OF MAGNESIUM/CUPRIC-OXIDE AA-CELLS STORED AT  $70 \pm 2^\circ\text{F}$  AND  $50 \pm 5\%$  R.H. (CELLS DISCHARGED CONTINUOUSLY THROUGH A 50-OHM RESISTANCE AT  $70 \pm 2^\circ\text{F}$ . AND  $50 \pm 5\%$  R.H.)



ML-254

FIGURE 4. AC IMPEDANCE VS LOAD RESISTANCE OF AA-CELLS, DISCHARGED CONTINUOUSLY THROUGH VARIOUS LOAD RESISTANCES AT 70±2°F AND 50±5% R.H. (IMPEDANCE MEASURED AT APPROXIMATELY 50% DISCHARGE)

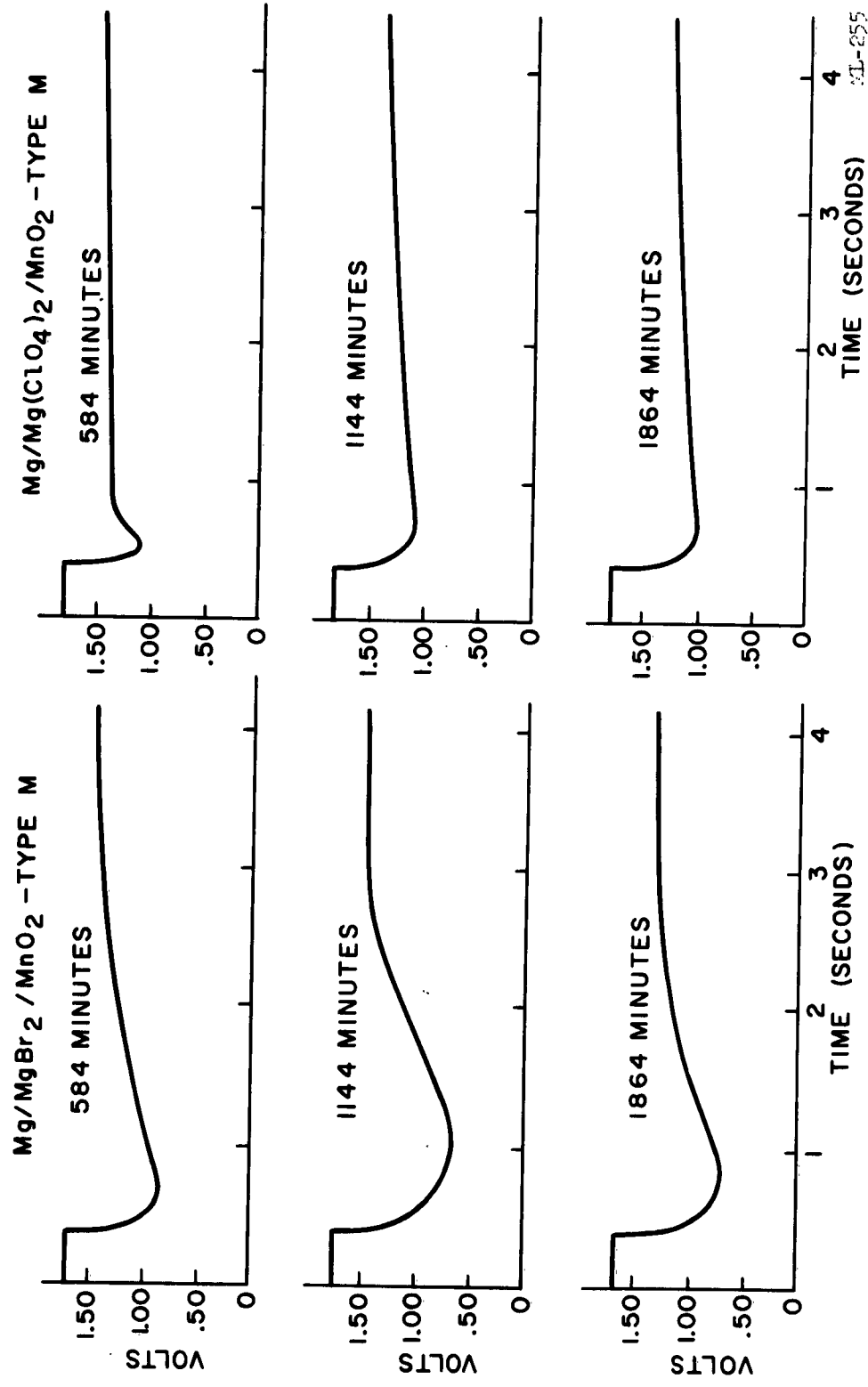


FIGURE 5. DELAYED ACTION OF D-CELLS DISCHARGED THROUGH 6.6 OHMS FOR 4 MIN EACH/1/2 HOUR FOR 24 HOURS PER DAY.

AL-255

As evidenced by the data presented in Figure 3 and in Table I, satisfactory shelf-life data have been obtained from cells made with cupric oxide and synthetic manganese dioxide.

The impedance of  $\text{Mg}/\text{Mg}(\text{ClO}_4)_2/\text{MnO}_2$  (African) AA-size cells has been shown to be similar to that of comparable  $\text{Mg}/\text{MgBr}_2/\text{MnO}_2$  (Afr.) AA-size cells. Data for the impedance of  $\text{Mg}/\text{Mg}(\text{ClO}_4)_2/\text{MnO}_2$  (Afr.),  $\text{Mg}/\text{MgBr}_2/\text{MnO}_2$  (Afr.), and commercial LeClanche cells as a function of load resistance are presented in Figure 4.

The delayed action of magnesium cells containing a magnesium-perchlorate electrolyte in preliminary studies has been shown to be less than that of similar cells containing a magnesium-bromide electrolyte. This is particularly true for applications in which the time between discharges is short as evidenced by the delayed action data for D-size cells on a test simulating the BA-30 test presented in Figure 5.

### 3.2 RESERVE CELLS

#### 3.2.1 Magnesium/Cupric-Oxide Reserve Cells

The magnesium/cupric-oxide system was selected for the development of a high-capacity reserve battery for the following reasons:

- a. High capacity per unit weight and volume.
- b. Flat discharge curve.
- c. Potential low cost.

##### 3.2.1.1 Magnesium-Cupric Oxide Reserve Cell Design

A 3-ampere-hour cell was selected for initial study and characterization because this size cell is readily adapted to laboratory development and comparison to other systems.

The cathode plates were constructed using techniques previously developed in this laboratory. The following steps are used in the assembly of a cupric oxide cathode:

- a. Dry blend cupric oxide with Shawinigan Acetylene Black using standard techniques.

A. 70 ±2°F and 50 ±5% R.H.		DISCHARGE RESISTANCE (ohms)	INITIAL TIME		CAPACITY RETENTION (percent)					
LOT	TYPE MnO <sub>2</sub>		(hours)	(minutes)	3 MOS.	6 MOS.	9 MOS.	12 MOS.	15 MOS.	
29	M	16-2/3 166-2/3	13 166	22 30	98.5 103.0	101 98.5	93.6 93.7	96.7	108	
30	WB-PL	16-2/3 166-2/3	12 157	— —	100.0 102.0	96.6 93.6	101.3 109.0	88.2		
33	Trona C-8	16-2/3 166-2/3	10 144	45	95.4 112.0	81.5 113.0	88.4			
87	M	16-2/3 166-2/3	14 175	37	95.8 104.0	91.7 111.0		87.5 100		
92	WB-PL	16-2/3 166-2/3	13 209	17	91.7 111.0	90.3 86.2		82 66		

B. 113 ±2°F and 95% R.H.		DISCHARGE RESISTANCE (ohms)	INITIAL TIME		CAPACITY RETENTION (percent)					
LOT	TYPE MnO <sub>2</sub>		(hours)	(minutes)	1 MOS.	2 MOS.	3 MOS.	6 MOS.	12 MOS.	
90	M	16-2/3 166-2/3	14 198	2	96.3 113.0	97.3 104.0	92.7 86.3	86.5	85	
94	WB-PL	16-2/3 166-2/3	12 209	55	94.8 112.0	94.1 86.2	89.2 76.0	88.3	94.5	

MT-46

TABLE I. SHELF -LIFE DATA FOR Mg/Mg(ClO<sub>4</sub>)<sub>2</sub>/MnO<sub>2</sub> CELLS WITH VARIOUS TYPES OF MnO<sub>2</sub>. STORED AT 70° AND 113°F.



- b. Prepare a wet mix using a water solution of HV CMC (carboxymethyl cellulose) with suitable wetness to provide maximum ease of handling in steps c and d.
- c. Paste a weighed amount of cathode mix on the metal grid.
- d. Apply the separator material filter paper to the wet cathode plate and press it 3000 to 5000 psi for several seconds.
- e. Air dry overnight.

In the following studies, the anode and cathode specifications are:

a. Cathode:

Size - 2 x 2 inches  
 Grid - 25/0.010-inch woven bronze screen, 0.575 g/in<sup>2</sup>  
           with a 1/2 x 3/4-inch tab for making connections.  
 Wet mix composition - 42.8% CuO  
                           10.7% Shawinigan Acetylene Black  
                           45.7% H<sub>2</sub>O  
                           .7% HV CMC  
 Separator - analytical grade filter paper  
 Theoretical capacity per plate - 85 ampere-minutes.

b. Anode:

Size - 2 x 2 inches with 1/2 x 3/4-inch tab for making connections.  
 Weight - 0.005-inch plate           0.74 g  
           0.010-inch plate           1.06 g  
           0.014-inch plate           1.73 g  
 Theoretical capacity per plate (not including tab)  
           0.005-inch               76.7 amp-min  
           0.010-inch               151 amp-min  
           0.014-inch               200 amp-min

c. Cell Assembly:

The cells were assembled by soldering four cathode plates together and interweaving 5 magnesium anode plates between the cathode plates. The tabs of anode plates were spotwelded together and connected to a copper wire lead.

## Cell Characterization

### Effect of Discharge Rate

The discharge characteristics of 3 amp-hr Mg-CuO cells determined under constant current drains of 10 to 25 amperes are presented below and in Figure 6, 7, and 8.

<u>Amperes</u>	<u>Magnesium Anode</u>	<u>Discharge Time (min)</u>	<u>Average Voltage</u>	<u>Cathode Efficiency</u>
10.0	0.014-inch, C.P.	30	0.835	88
20.0	0.014-inch, C.P.	13	0.82	76.5
25.4	0.005-inch, C.P.	6.5	0.715	49
20.0	0.016-inch, AZ-31B	9.4	0.68	55

### Cell Studies at Low-Discharge Rates

Cupric oxide cells were constructed with five 2 x 2-inch cathode plates onto which was spread a 6:1 ratio of cupric oxide to Shawinigan black mix containing a two-percent mercurous-chromate inhibitor. The theoretical coulombic cathode capacity was 590 ampere-minutes. The anode consisted of six 2 x 2-inch pure magnesium plates.

Discharge characteristics at constant currents of one, two, and four amperes are presented in Figure 9 and Table II. Cells discharged at room temperature used a water heat sink to limit the temperature rise. The data show that a discharge voltage is obtained with good cathode efficiency to the 0.90 voltage cutoff.

### Low Temperature Discharge

Cupric oxide cells of the above construction were discharged at the 2.0 and 4.0-ampere drains at temperatures down to -58°F. Data showing the effect of temperature on the discharge characteristics are presented in Figures 10 thru 12 and Table III. Results show poor low-temperature capacity is obtained for cells discharged in an uninsulated plastic case. However, the use of one-half-inch-thick polyurethane

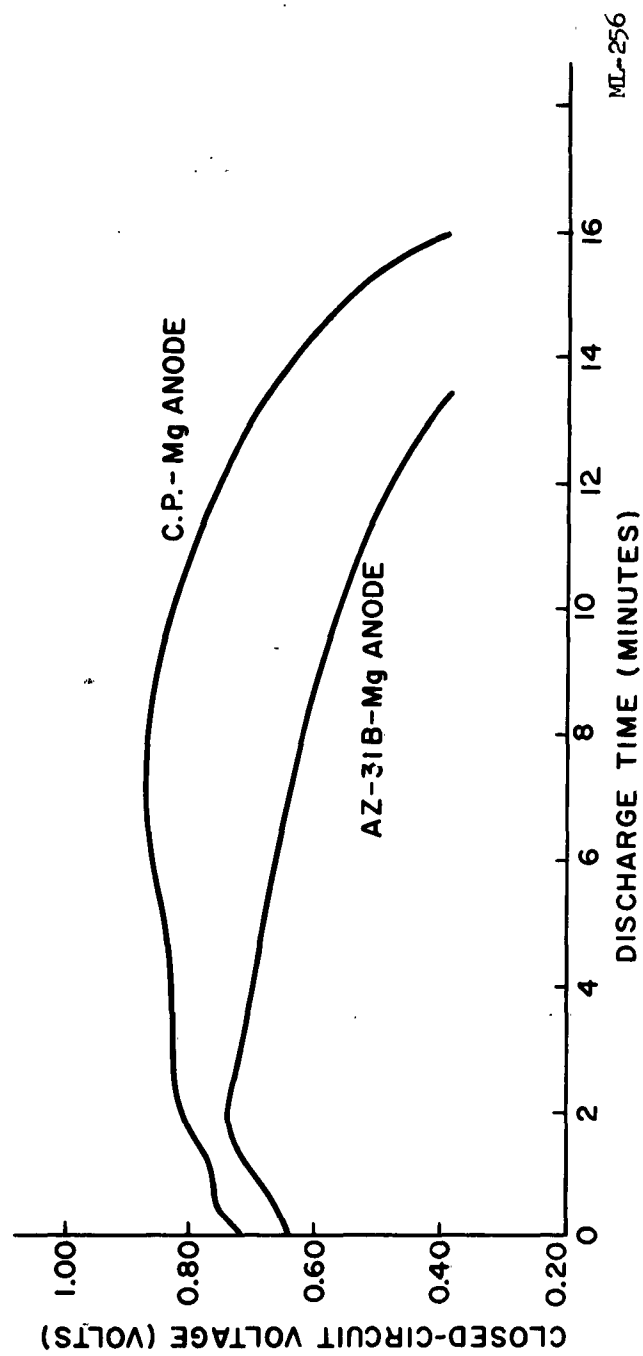


FIGURE 6. CAPACITY DATA FOR  $\text{Mg/CuO}$  RESERVE CELLS DISCHARGED UNDER A CONSTANT-CURRENT OF 20.0 AMPERES IN  $2\text{N Mg(ClO}_4)_2$  ELECTROLYTE.

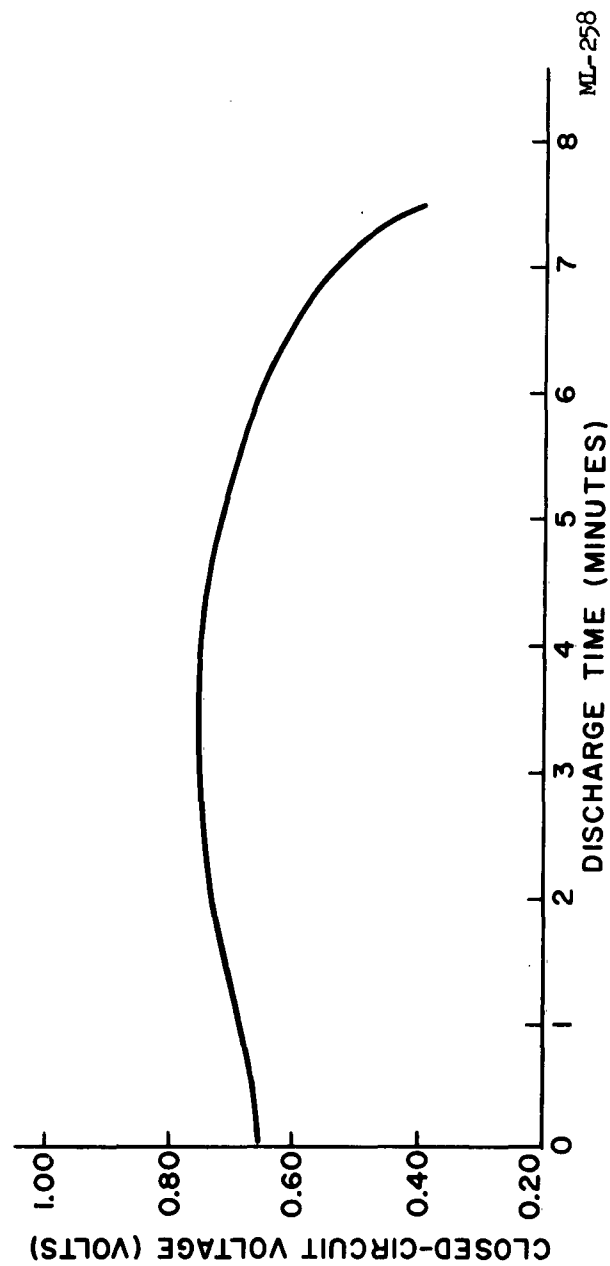


FIGURE 7. CAPACITY DATA FOR  $\text{Mg}/\text{CuO}$ -RESERVE CELL UNDER A CONSTANT-CURRENT DRAIN OF 25.4 AMPERES IN 2N  $\text{Mg}(\text{ClO}_4)_2$  ELECTROLYTE.

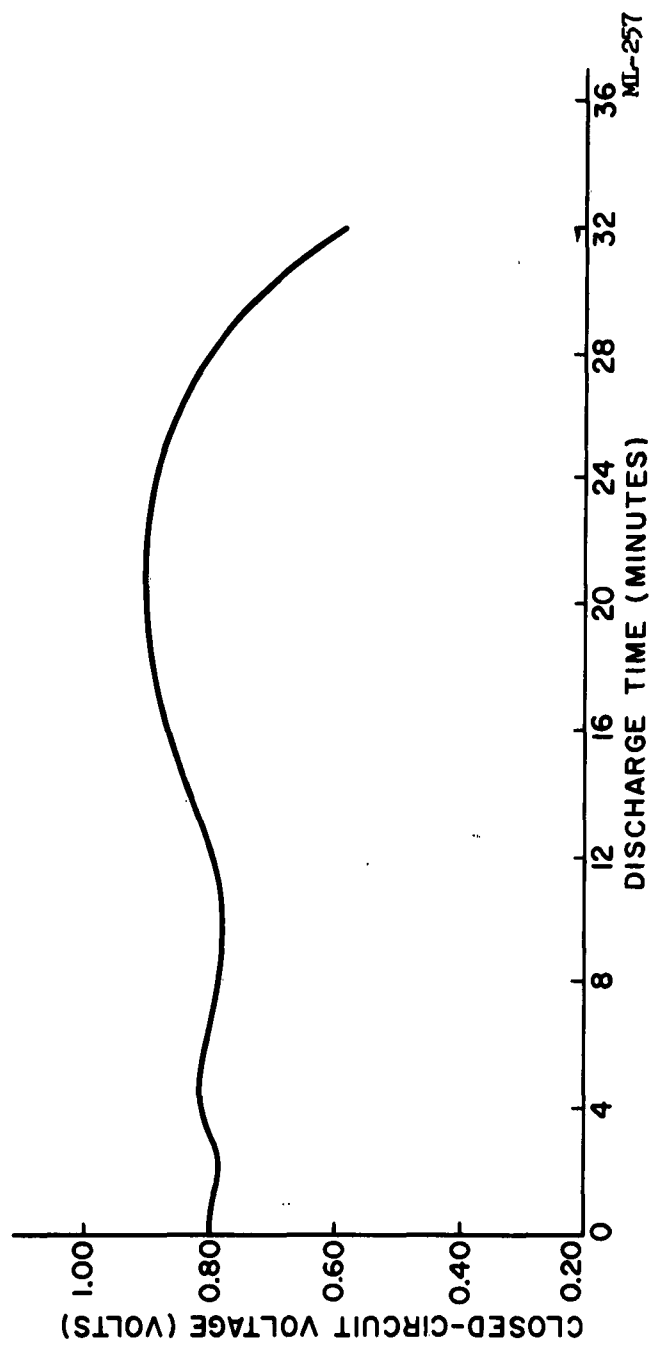


FIGURE 8. CAPACITY DATA FOR  $Mg/CuO$ -RESERVE CELL UNDER A CONSTANT-CURRENT DRAIN OF 10.0 AMPERES IN  $2N\ Mg(ClO_4)_2$  ELECTROLYTE.

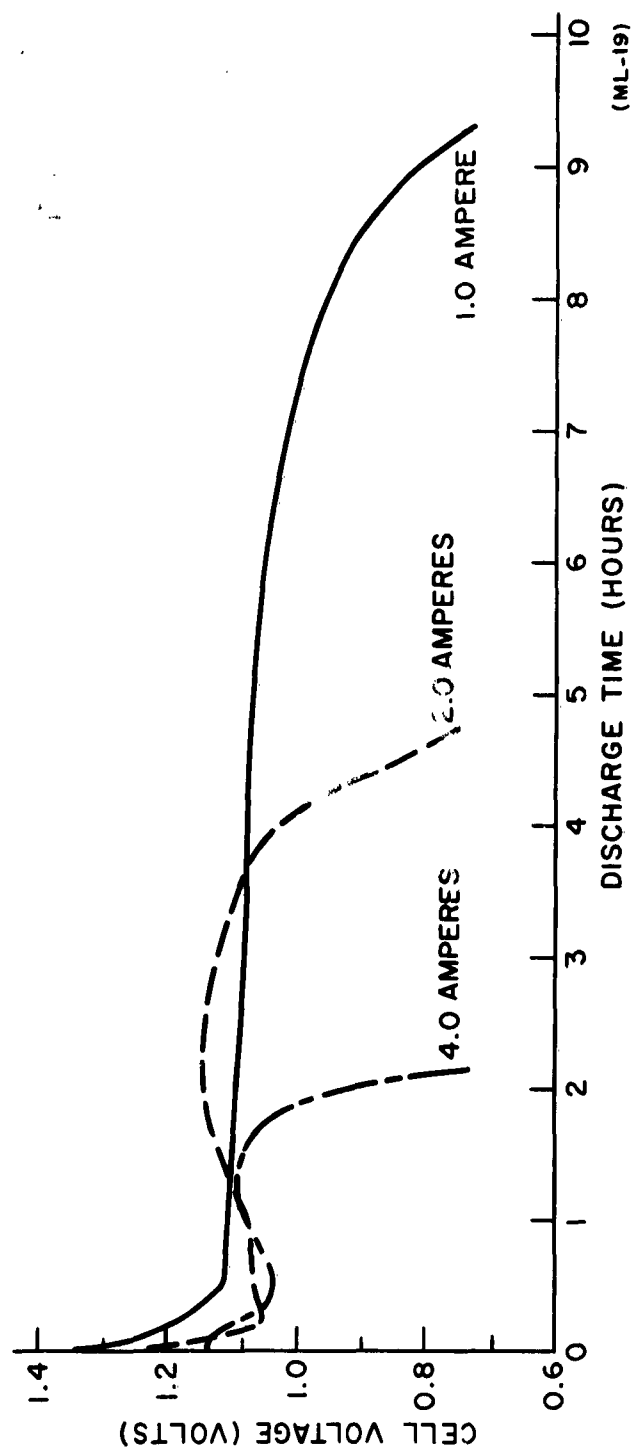


FIGURE 9. CAPACITY DATA FOR  $\text{Mg}/\text{Mg}(\text{ClO}_4)_2/\text{CuO}$  RESERVE CELLS AT VARIOUS DISCHARGE DRAINS AT  $70^\circ\text{F}$ .

DISCHARGE CURRENT (amperes)	AMBIENT TEMPERATURE (°F)	DISCHARGE TIME (TO 0.90 VOLTS)		VOLTS (av)	CATHODE EFFICIENCY (percent)
		Hours	Minutes		
1.0	70° with water heat sink	8	30	1.06	86.5
2.0	70° with water heat sink	4	22	1.10	89
4.0	70° with water heat sink	2	3	1.06	81.8
2.0	- 4°	-	50	1.00	17
2.0	-40°	-	40	1.02	17
2.0	-40°*	4	3	1.02	82.3

\*Cell discharged in 1/2-inch-polyurethane insulation.

MF-47

TABLE II. DISCHARGE DATA FOR Mg/CuO CELLS AT VARIOUS DISCHARGE CURRENTS AND TEMPERATURES.

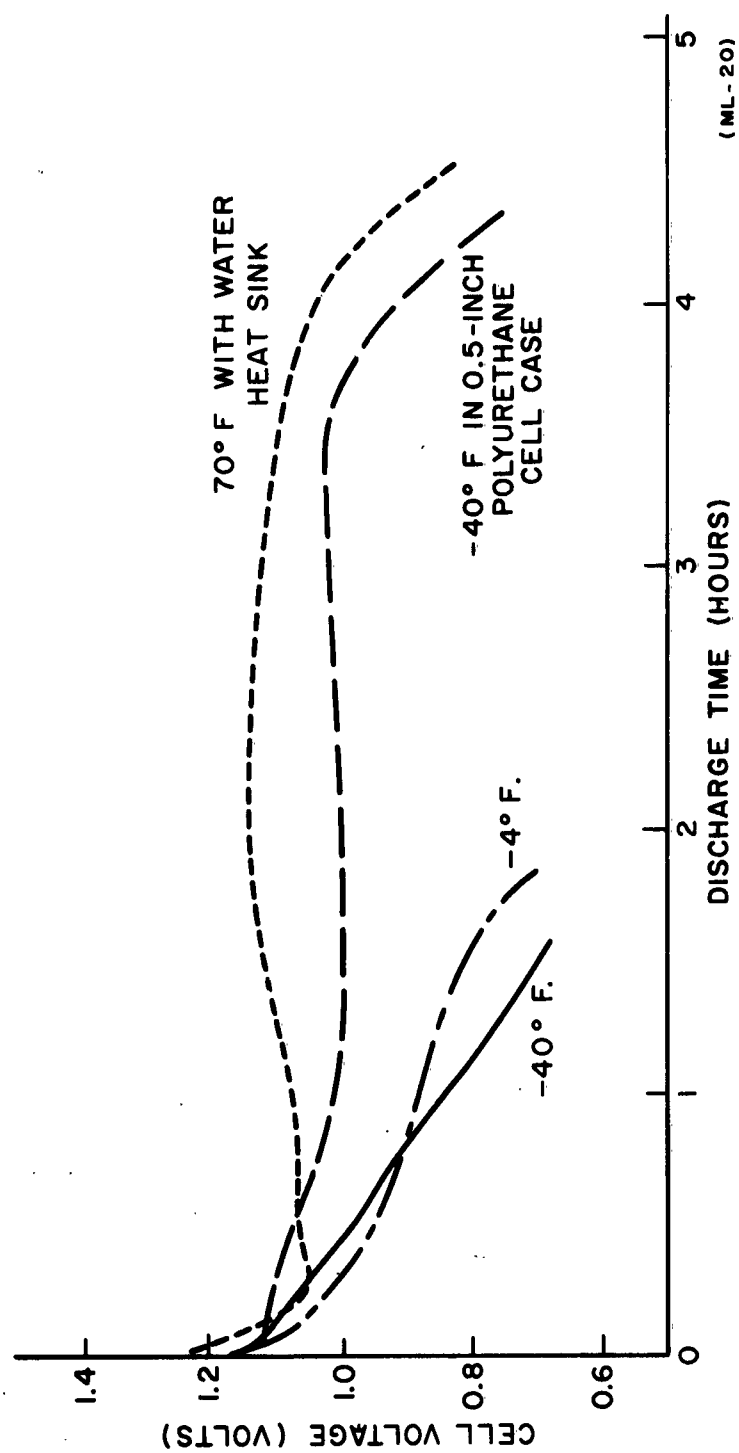


FIGURE 10. EFFECT OF TEMPERATURE ON THE DISCHARGE CHARACTERISTICS OF  $\text{Mg}/\text{Mg}(\text{ClO}_4)_2/\text{CuO}$  RESERVE CELLS  
DISCHARGED AT A CONSTANT-CURRENT DRAIN OF 2.0 AMPERES.



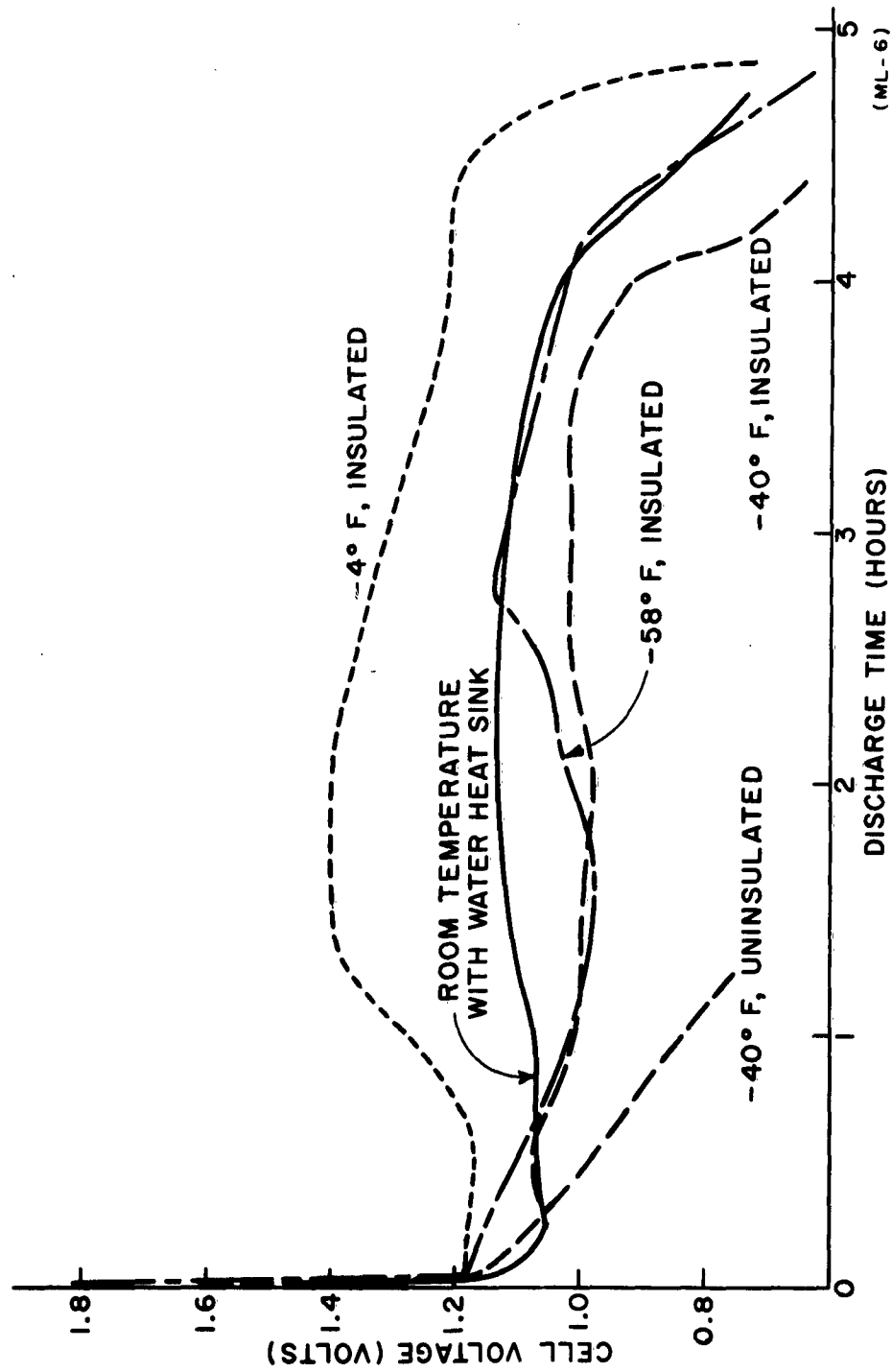


FIGURE 11. EFFECT OF TEMPERATURE ON DISCHARGE CHARACTERISTICS OF  $\text{Mg}/\text{Mg}(\text{ClO}_4)_2/\text{CuO}$  RESERVE CELLS DISCHARGED AT A CONSTANT-CURRENT DRAIN OF 2.0 AMPERES.

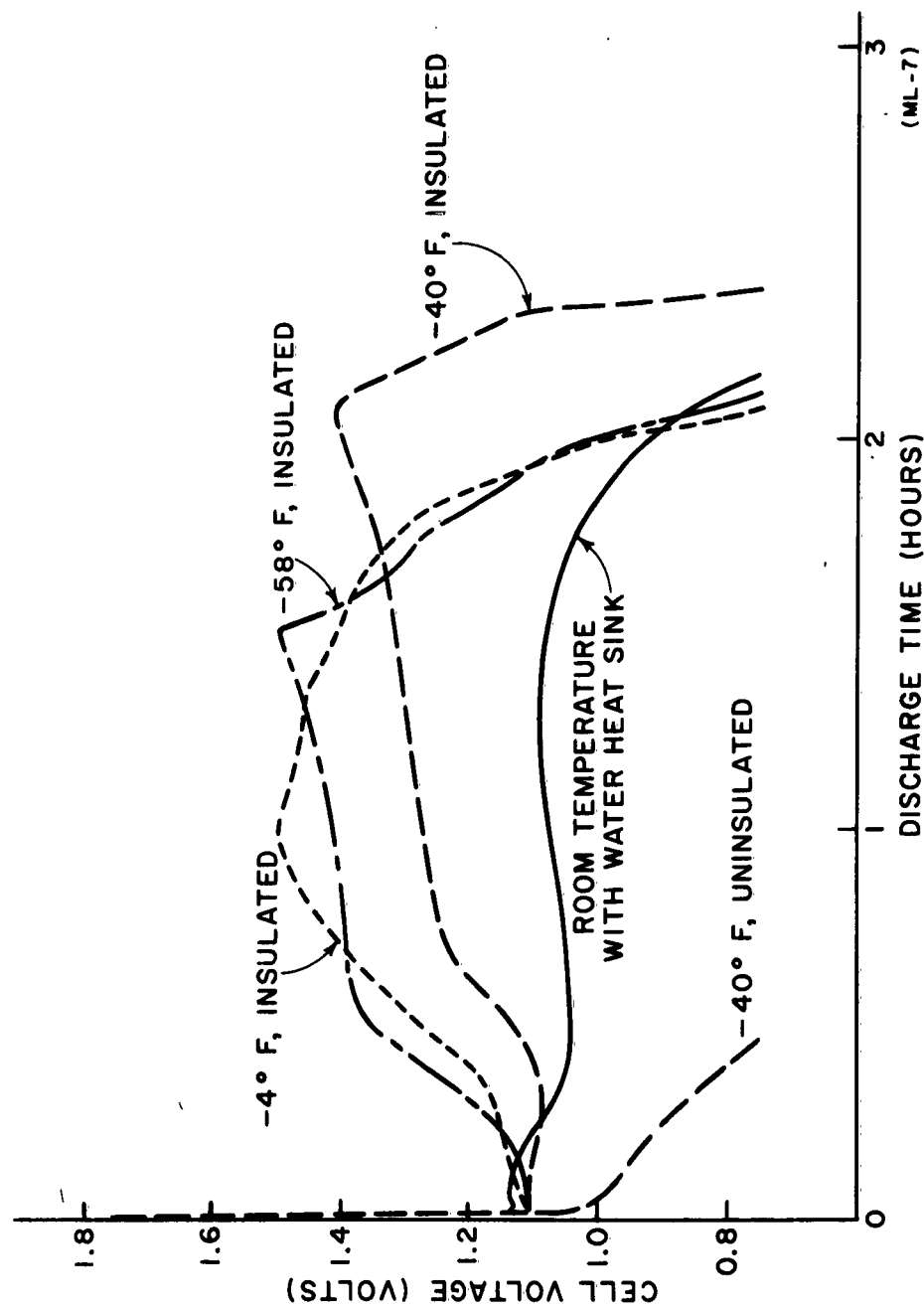


FIGURE 12. EFFECT OF TEMPERATURE ON THE DISCHARGE CHARACTERISTICS OF  $\text{Mg}/\text{Mg}(\text{ClO}_4)_2/\text{CuO}$  RESERVE CELLS DISCHARGED AT A CONSTANT-CURRENT DRAIN OF 4.0 AMPERES.

DISCHARGE CURRENT (amperes)	AMBIENT TEMPERATURE (°F)	CAPACITY TO 20-PER- CENT VOLTAGE DROP			CELL CASE
		DISCHARGE TIME		VOLTS (av)	
		Hours	Minutes		
1.0	70°	8	30	1.06	noninsulated plastic plus heat sink
2.0	70°	4	20	1.10	noninsulated plastic plus heat sink
2.0	- 4°	4	49 <sup>(1)</sup>	1.29	1/2-inch polyurethane
2.0	-40°	4	5	1.02	1/2-inch polyurethane
2.0	-58°	4	23	1.06	1/2-inch polyurethane
4.0	70°	2	3	1.06	noninsulated plastic plus heat sink
4.0	- 4°		2 <sup>(1)</sup>	1.35	1/2-inch polyurethane
4.0	-40°		21 <sup>(1)</sup>	1.26	1/2-inch polyurethane
4.0	-58°	2	4 <sup>(1)</sup>	1.33	1/2-inch polyurethane
1.0	- 4°	4	10 <sup>(2)</sup>	.98	1/2-inch polyurethane
1.0	-40°	4	20 <sup>(2)</sup>	.95	1/2-inch polyurethane
1.0	-58°	4	50 <sup>(2)</sup>	.96	1/2-inch polyurethane
2.0	- 4°		50	1.00	noninsulated plastic
2.0	-40°		48	1.02	noninsulated plastic
4.0	- 4°		27	.89	noninsulated plastic

(1) to 1.10 volts  
(2) to 0.80 volts

MT-48

TABLE III. CAPACITY DATA FOR  $Mg/Mg(ClO_4)_2/CuO$  RESERVE CELLS AT VARIOUS  
DISCHARGE RATES AND TEMPERATURES.

insulation at  $-40^{\circ}\text{F}$  increased the capacity to 92 percent of the capacity obtained at room temperature. The data indicate that the cupric-oxide system can operate at low temperature with good capacity (similar to the other magnesium systems) provided that the dissipated heat is maintained within the cells.

The test data show that room-temperature capacity is obtained at temperatures down to  $-58^{\circ}\text{F}$  for cells with a polyurethane jacket. Capacity of noninsulated-case cells discharged at  $-4^{\circ}$  and  $-40^{\circ}\text{F}$  dropped to less than 20 percent of optimum capacity. These results show that the cupric-oxide cathode is highly temperature dependent and that control of heat within the cell will affect cell capacity. Also, the cupric-oxide cathode has a high temperature coefficient and wide variation of cell voltage can be obtained. Data presented in Figures 13 and 14 show a variation of magnesium/cupric-oxide cell voltage with temperature over a temperature range of 0 to  $80^{\circ}\text{C}$ . This variation is confirmed by the increase in cell voltage of cells enclosed in a one-half inch polyurethane case as shown in Figures 11 and 12. The high operating voltage indicates an internal cell temperature above  $40^{\circ}\text{C}$ .

The low temperature studies of the cupric oxide system described above show that good capacity can be obtained down to at least  $-58^{\circ}\text{F}$ . Cell operating temperature however, must be controlled by the battery design to insure proper operating voltage.

The cells were placed in a plastic test container to restrict volume and were discharged in excess  $2\text{N Mg}(\text{ClO}_4)_2$  five minutes after activation. All cells showed a voltage rise during discharge which was greatest at the lighter drains as evidenced by the 10-ampere discharge data in Figure 8. The voltage changes that occur during discharge are believed to be due mainly to the heat evolved by the cell reactions.

#### Effect of Cupric-Oxide-to-Carbon Ratio on Cell Performance

The effects of the  $\text{CuO}$ -to-carbon ratio on the cathode efficiency and the voltage-time characteristic were determined on cells with a

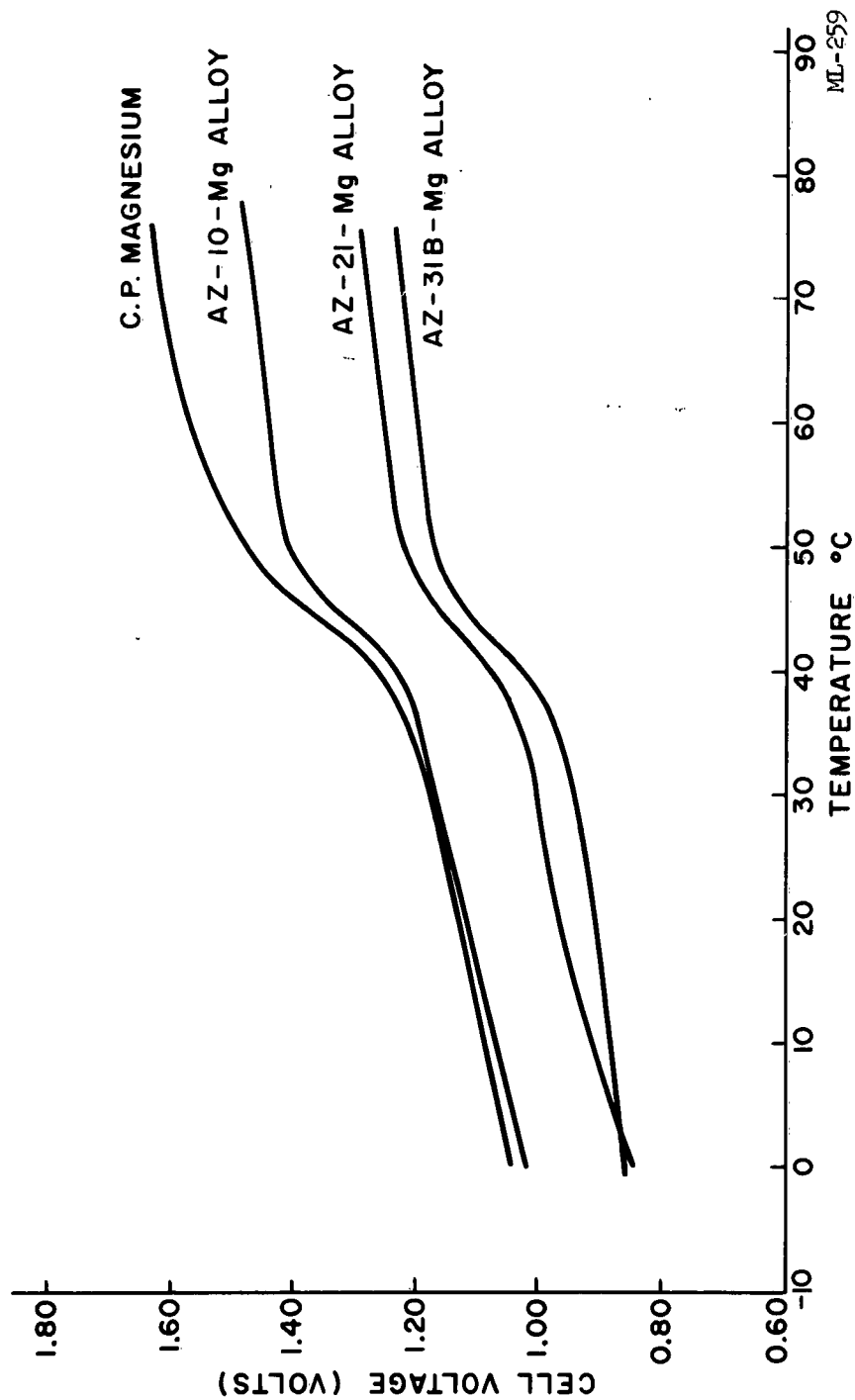


FIGURE 13. EFFECT OF TEMPERATURE ON  $Mg/CuO$  RESERVE CELLS WITH VARIOUS MAGNESIUM ANODES. DISCHARGED UNDER A 50-HOUR RATE IN  $2N\ Mg(ClO_4)_2$  ELECTROLYTE.

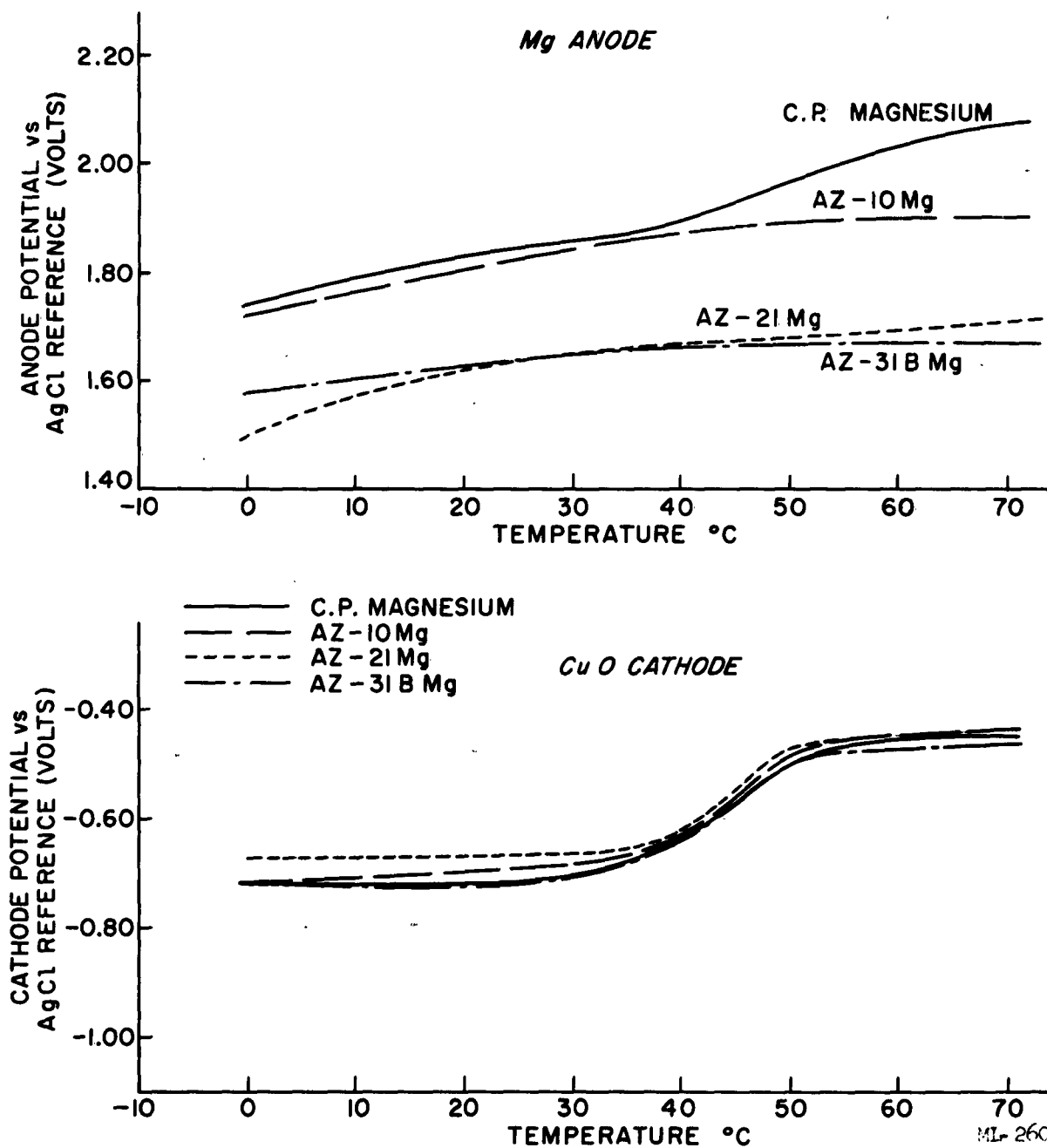


FIGURE 14. TEMPERATURE DEPENDENCE OF THE Mg ANODE AND CuO CATHODE IN A Mg/CuO RESERVE CELL IN 2N  $Mg(ClO_4)_2$  ELECTROLYTE.

Theoretical capacity of 300 to 340 ampere-minutes on a 20-ampere drain. In these cells, the number of plates in the cathode was varied to keep the theoretical capacity approximately constant. The cathode efficiency increases as the active material ratio is decreased and as the plate surface area is increased as shown in Figure 15 and Table IV. As would be expected if the voltage rise is caused by the heat evolved, the CuO-to-carbon ratio had little effect on the percentage voltage increase.

### 3.2.2 Research Studies

A research study was initiated to determine the mechanism by which the heat evolved influences the voltage behavior of the magnesium/cupric-oxide reserve cell system. The temperature rise found on cell discharge is due to the heat evolved by the corrosion reaction and by the irreversibility of the magnesium anode. Since both of these factors are dependent on the current density, the temperature rise will be greatest on high discharge rates.

Test cells were made using two cupric-oxide plates with a 3:1 ratio of Shawinigan carbon black and three anode plates of various magnesium alloys. The cupric-oxide plates were taken from the lot whose test results are shown in Figure 15 with a theoretical capacity of 60 ampere-minutes per plate. AZ-31B, AZ-21, AZ-10, and commercially pure (C.P.) magnesium anodes were used in these studies. The cupric-oxide cathode plates were discharged for 16 hours on an 80-hour rate for stabilization prior to the assembly of the test cells. A silver/silver-chloride reference electrode was included at the end of each cell for half-cell measurements. The cells were placed in beakers with excess 2N  $\text{Mg}(\text{ClO}_4)_2$ , immersed in constant-temperature water and discharged through a 32-ohm resistor, corresponding to a 50-hour rate. The cell, anode-to-reference, and cathode-to-reference potentials were measured over a temperature range of 2°C to 70°C.

The results of this study are presented in Figures 13 and 14. It is seen that the voltage increased linearly with temperature, except for the range

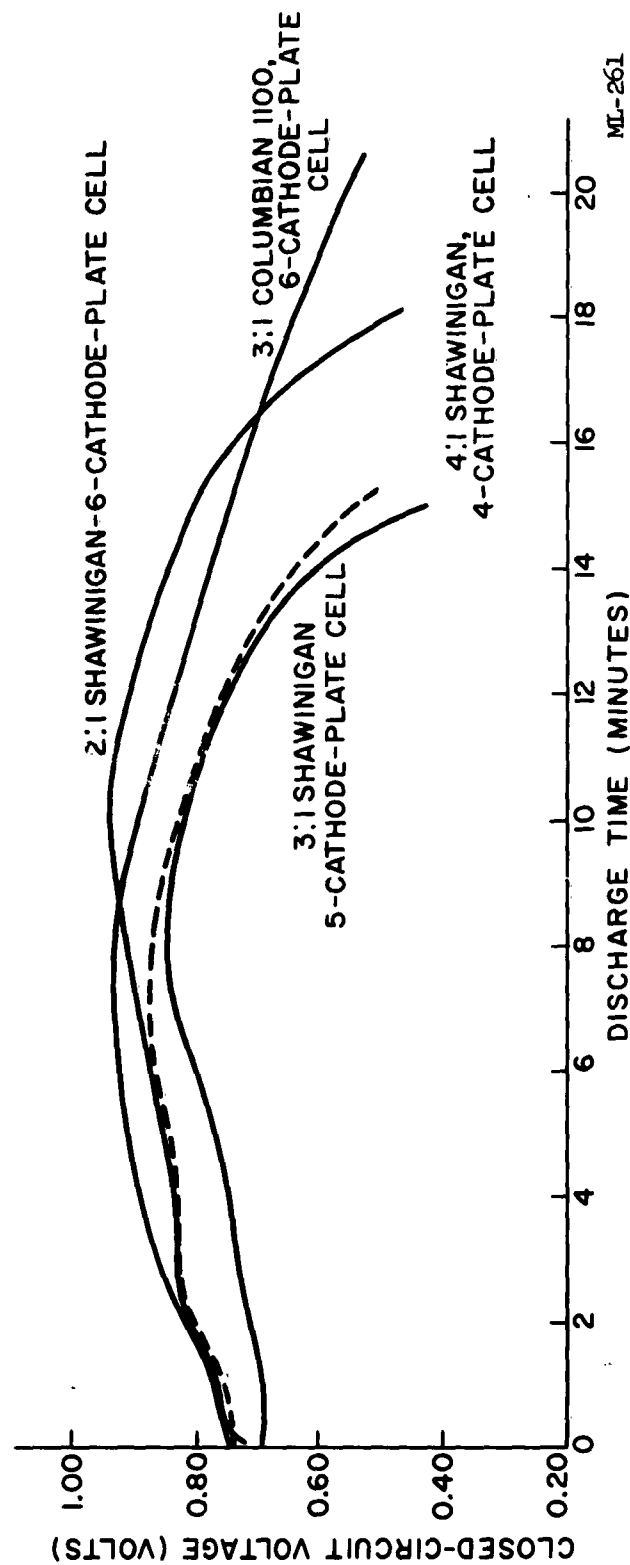


FIGURE 15. CAPACITY DATA FOR  $Mg/CuO$  RESERVE CELLS WITH VARIOUS CARBON RATIOS UNDER A CONSTANT-CURRENT DRAIN OF 20.0 AMPERES IN  $2N\ Mg(ClO_4)_2$  ELECTROLYTE.



CuO-TO-CARBON BLACK RATIO	WET-MIX COMPOSITION	CATHODE PLATES PER CELL	THEORETICAL CATHODE CAPACITY PER CELL (ampere-minutes)	ANODE THICKNESS C. P. MAGNESIUM (inches)	DISCHARGE TIME TO 20-PERCENT VOLTAGE DROP (minutes)	CATHODE EFFICIENCY (percent)
SHAWINIGAN, 4:1	42.8% CuO 10.7% Carbon Black 45.7% H <sub>2</sub> O 0.7% HV CMC 4.9 g mix/plate	4	340	.014	13	77
SHAWINIGAN, 3:1	33.3% CuO 11.1% Carbon Black 54.8% H <sub>2</sub> O 0.83% HV CMC 4.45 g mix/plate	5	300	.010	13.2	88
SHAWINIGAN, 2:1	28.6% CuO 14.3% Carbon Black 56.2% H <sub>2</sub> O 0.86% HV CMC 4.45 g mix/plate	6	308	.010	16	104
COLOMBIAN, 3:1	27.6% CuO 9.2% Carbon Black 62.6% H <sub>2</sub> O 0.48% HV CMC 4.45 g mix/plate	6	298	.010	14.9	100

MT-49

TABLE IV.  $Mg/Mg(ClO_4)_2/CuO$  RESERVE CELLS WITH VARIOUS CARBON BLACK RATIOS.  
DISCHARGED ON A 20-AMPERE CONSTANT-CURRENT DRAIN.

between 35°C and 50°C. The half-cell measurements show that the marked increase in cell voltage in this temperature range is caused by the presence of the cupric-oxide cathode (Figure 14).

A voltage difference of 0.2 volt was found between the AZ-31 and C.P. magnesium anodes. This difference increased at higher temperatures because the corrosion reaction for pure magnesium was greatly accelerated. The effect of corrosion reaction on cell discharge voltage can be seen from the data in Figure 14.

### 3.2.2.1 Cathode Grid Studies

A study was made in order to obtain a light-weight grid material to reduce the electrode element weight. An investigation of various manufacturers' literature showed that an expanded copper foil was the most practical material for minimum-weight design for the CuO cathode.

Three samples of expanded 0.005-inch copper foil\* were obtained for evaluation. The physical characteristics of these materials are summarized in the following table:

<u>Material Designation</u>	<u>Original Sheet Thickness (inches)</u>	<u>Strand Width (inches)</u>	<u>Mesh (center to center) Long- wise (inches)</u>	<u>Short wise (inches)</u>	<u>Weight per square inch (grams)</u>
3 Cu5 - 4/0	0.003	0.005	0.077	0.042	0.11
5 Cu5 - 4/0	0.005	0.005	0.077	0.042	0.18
5 Cu5 - 3/0	0.005	0.005	0.125	0.058	0.12

Cells were assembled with CuO cathodes using the 5 Cu5 - 4/0 screen and were evaluated at high discharge rates. The cells had dry-element weights of 27.3 grams, 6.8 grams lighter than comparable cells made with a 25/0.018-inch woven-screen grid. Element volume was 2.25 x 2.5 x 0.28 inches. Capacity data for a 20 ampere drain are given in Figure 15. Twelve and one-half minutes of discharge were obtained to 20-percent cutoff voltage with an average of 0.81 volts for the cell without added inhibitor. These discharge data compare favorably with previous cells using a woven screen.

\* Emmet Corporation, Tuckahoe, N.Y.

#### Effect of Mercury Compounds:

Previous work in this laboratory, using mercury compounds as inhibitors added to the electrolyte or cathode mix in magnesium dry cells, resulted in improved anode efficiency. Mercuric-oxide reserve-cell studies also showed higher anode efficiency over comparable cupric-oxide cells. This is due to the inhibiting action of the slightly soluble mercuric oxide.

A study was made to determine the effect of mercury compound additives on the discharge characteristics and anode efficiency of  $\text{Mg}/\text{Mg}(\text{ClO}_4)_2/\text{CuO}$  reserve cells. Several cathode batches were made with  $\text{Hg}_2\text{CrO}_4$  inhibitors added to a standard 4:1 CuO mix. Reserve cells were assembled with four cathode plates and five 0.014-inch C.P. magnesium anode plates and discharged at constant-current drains of 5 to 20 amperes.

Capacity data are given in Figures 15 and 16 for the 20- and 10-ampere drains for cells with and without inhibitor. A marked increase and leveling of the voltage was obtained on the 5- and 10-ampere drains with addition of three percent  $\text{Hg}_2\text{CrO}_4$ . The voltage level was lower, however, at the 20-ampere drain. Anode efficiency was increased from 63 to 76 percent at 20-ampere drain, and from 62 to 80 percent by the addition of  $\text{Hg}_2\text{CrO}_4$  inhibitor at 10-ampere drain. On discharge, mercury is plated on the magnesium and inhibits the corrosion reaction by retarding the hydrogen evolution reaction. The higher cell potential is attributed to the partial removal of the oxide film by amalgamation.

To extend the work on cupric oxide, several 10-cathode-plate cells were assembled for capacity testing. The cathode composition consisted of a 4:1 mix with Shawinigan carbon black and contained two percent mercurous chromate as an inhibitor. A curve showing the 15-ampere room-temperature discharge in  $2\text{N Mg}(\text{ClO}_4)_2$  is presented in Figure 17. The cell was placed in a 150 ml water heat sink to control temperature on discharge.

The cathode efficiency of these cells was 62.2 percent to a 10-percent voltage cutoff and 73.4 percent to a 20-percent voltage cutoff. Capacity to a 20-percent cutoff was 41.5 watt-hours per pound and 2.63 watt-hours per cubic inch, neglecting volume for terminal height.

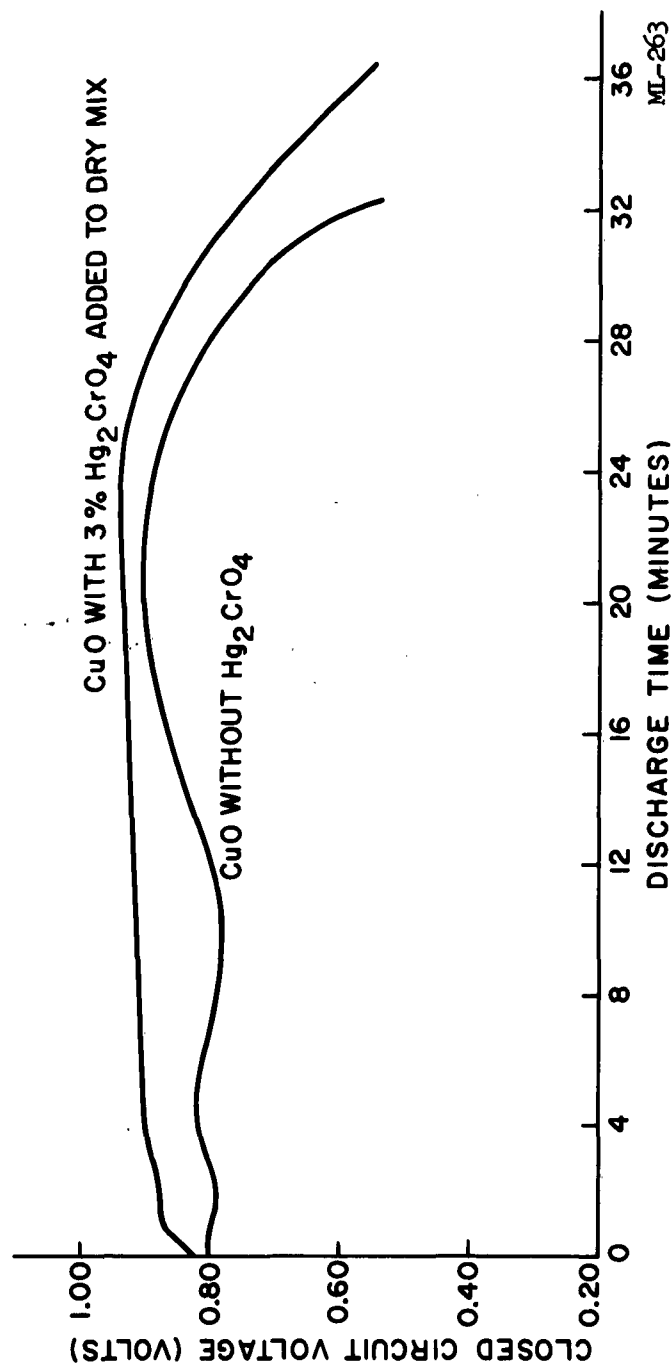


FIGURE 16. CAPACITY DATA FOR  $\text{Mg}/\text{Mg}(\text{ClO}_4)_2/\text{CuO}$  RESERVE CELLS UNDER A CONSTANT-CURRENT DRAIN OF 10.0 AMPERES.

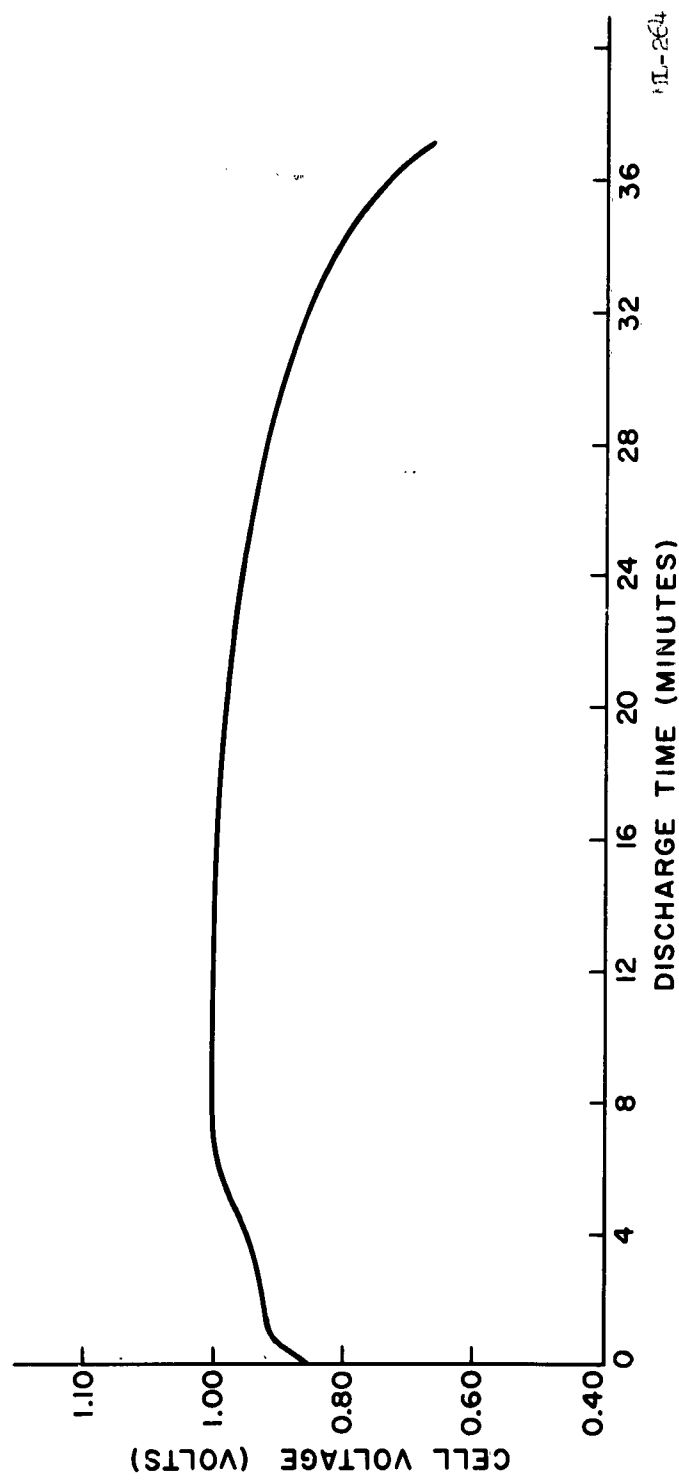


FIGURE 17.  $\text{Mg}/\text{Mg}(\text{ClO}_4)_2/\text{CuO}$  RESERVE CELL DISCHARGED AT 15 AMPERES AT ROOM TEMPERATURE. 10-CATHODE-PLATE  
 4:1 RATIO MIX WITH 2%  $\text{Hg CrO}_4$ . THEORETICAL CAPACITY = 712 AMPERE-MINUTES.

#### Effect of Mix Variations:

Previous test data on cupric oxide reserve cells showed a gradual decrease in cell voltage toward the end of the discharging cycle. This necessitated the choice of a 20-percent cutoff voltage in order to obtain good utilization of the active material.

Various mix blending techniques were also evaluated to determine their effect on voltage level and cell capacity. Cathode mixes were made using reagent-grade cupric-oxide powder, that was ball milled for twenty-four hours to reduce particle size. Further blending was done by milling the cupric oxide with 12 percent of the required carbon for thirty minutes, and with the remainder of the carbon for two minutes. The mix was completed by hand blending with CMC solution.

Capacity data for a four 2 x 2-inch cathode-plate test cell was determined at the thirty minute rate and is given in Figure 18. Results showed that no significant leveling of voltage was obtained. This mix procedure permitted the use of a higher mix ratio with increased cathode efficiency. Eighty-four percent cathode efficiency was obtained for a 20-percent cutoff, compared to 73 percent for the 4:1 mix.

Overheating occurred during the latter part of discharge and cell voltage reached a maximum of 1.04 volts.

#### 3.2.3 Magnesium-Mercuric Oxide Reserve Cells

Prior work in this laboratory demonstrated that HgO reserve-cell cathode plates could be made using techniques developed with the CuO cathode. Discharge data showed that the HgO cathode in a  $\text{Mg}(\text{ClO}_4)_2$  electrolyte operated at good cathode efficiencies and had a flat voltage discharge characteristic on rates above one hour. Cell construction and initial characterization are presented in the following sections.

##### Cell Design

HgO cathode plates were constructed using techniques similar to those used for the CuO system. Two-by-two-inch silver-plated 25/0.010-inch

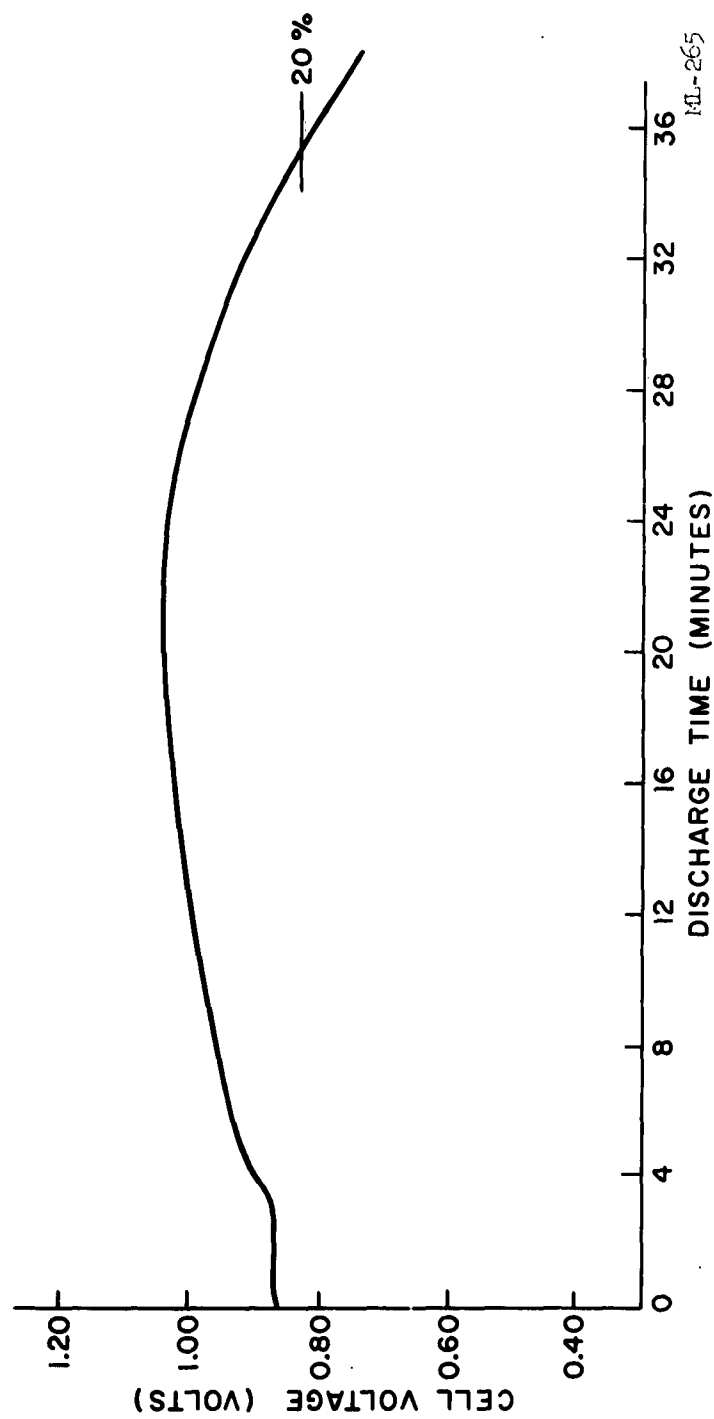


FIGURE 18.  $\text{Mg}/\text{Mg}(\text{ClO}_4)_2/\text{CuO}$  RESERVE CELL MADE WITH MILLED  $\text{CuO}$  AND DISCHARGED AT 10 AMPERES AVERAGE VOLT 0.97 TO 20% 6 TO 1  $\text{CuO}$  SHAWINIGAN. THEORETICAL CATHODE CAPACITY = 420 AMPERES-MINUTES CATHODE EFFICIENCY = 84.3%.

woven copper and silver-plated 5 Cu5 expanded-copper screens were used as grids. The wet-mix composition data are included in Table V. Cells were assembled using four cathode plates and five 2 x 2-inch, 0.014-inch thick C.P. magnesium anode plates. The theoretical cell capacity varied from 122.4 ampere-minutes for the 4:1 HgO-to-carbon mix to 160 ampere-minutes for the 6:1 mix. The dry element weight of cells with 5 Cu5 Ag plated grids and 0.014-inch magnesium anodes averaged 28.2 grams, and the dimensions were 2.25 x 2.5 x 0.28-inches. Cells have been studied using thinner cathode grid material and thinner magnesium sheet to reduce element weight. Cells made with a .003-inch silver-plated copper grid gave two minutes less capacity at the thirty-minute rate than cells using the .005-inch grids. Activated cell weight was reduced from ninety to eighty-five grams.

Although further weight reduction can be obtained by using thinner magnesium sheet, choice of proper thickness is determined by the performance of the anode. In cells where magnesium is the limiting electrode, excess overheating occurs toward the end of the discharge cycle, preventing operation of the cell within a 10-percent voltage tolerance. In addition, an increased corrosion rate is obtained with the use of very thin magnesium, resulting in an increase in cell operation voltage. Capacity data at the thirty-minute rate for cells made with .003-inch grids and with .005-inch magnesium are given in Figure 19. All cells were discharged in 2N  $\text{Hg}(\text{ClO}_4)_2$  using a heat sink of 150 ml water.

#### 3.2.3.1 Cell Characterization

Studies were made to investigate high-rate performance of the mercuric-oxide system. Test cells of thin-plate construction to increase surface area of the electrodes were assembled. A comparison of the characteristics of a cell of this construction discharged at 20 amperes constant current with a cell having thicker plates is presented in Figure 20. Cell data are as follows:



MIX RATIO HgO-TO- SHAWINIGAN CARBON BLACK (Acetylene)	WET-MIX COMPOSITION (percent)				AMOUNT OF MIX PER PLATE (grams)	THEORETICAL CAPACITY/PLATE (Ampere-Minutes)
	HgO	CARBON	CMC	H <sub>2</sub> O		
4:1	41.3	10.3	0.72	47.6	5.0	30.6
6:1	51.8	8.6	0.59	39.0	4.9	37.6
8:1	54.0	6.7	0.59	38.8	5.0	40.0

MT-50

TABLE V. MERCURIC-OXIDE CATHODE-MIX-COMPOSITION DATA.

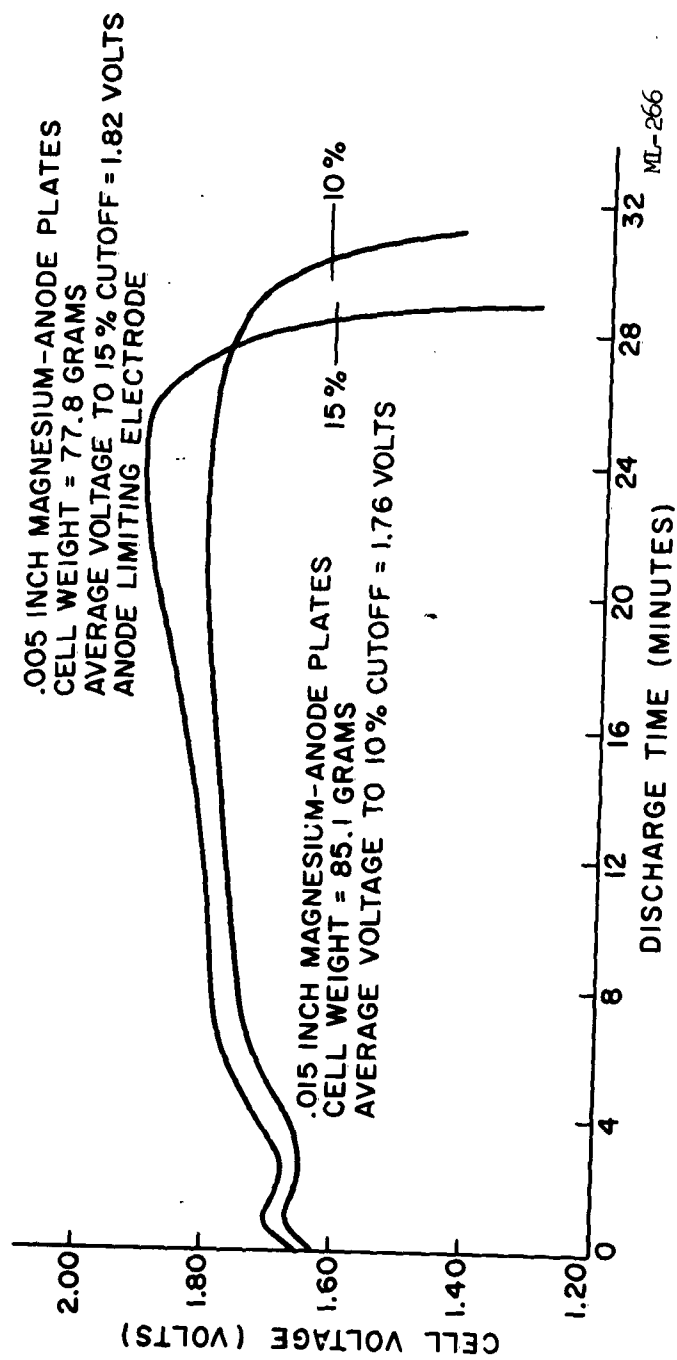


FIGURE 19.  $\text{Mg}/\text{Mg}(\text{ClO}_4)_2/\text{HgO}(8:1 \text{ MDX PLUS } 10\% \text{ Ag}_2\text{O})$  RESERVE CELLS WITH .003-INCH CATHODE GRIDS AND VARIOUS MAGNESIUM THICKNESS DISCHARGED AT 10.0 AMPERES.

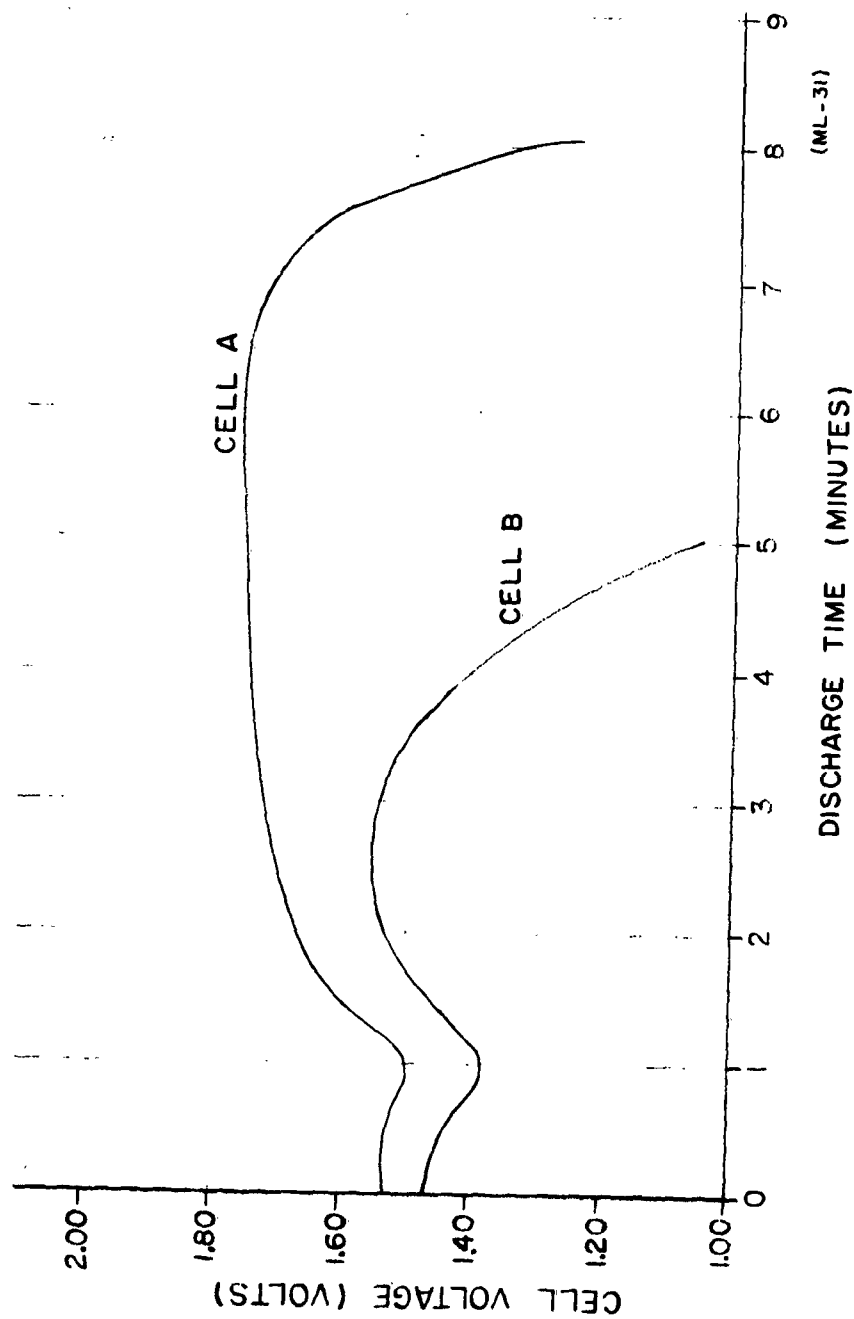


FIGURE 20. CAPACITY DATA FOR  $\text{Mg}/\text{Mg}(\text{C}^{\text{I}}\text{O}_4)_2$  H<sub>2</sub>O RESERVE CELLS DISCHARGED AT A CONSTANT CURRENT OF 20 AMPERES.  
 CELL A: 10 CATHODE PLATES AND 11-.005-INCH ANODE PLATES.  
 CELL B: 5 CATHODE PLATES AND 6-.10-INCH ANODE PLATES.

<u>Cathode</u>	<u>Cell A*</u>	<u>Cell B**</u>
Theoretical capacity	179 amp-min HgO	179 amp-min HgO
Anode, Magnesium C.P.	11 plates, .005,"	6 plates, .005,"
Total active surface area (cm <sup>2</sup> )	362	181
Element volume (in <sup>3</sup> )	0.975	0.822
Element weight, dry (g)	34.5	29.5
Element weight, wet (g)	51.6	46.6
Average voltage to 20% voltage drop (v)	1.68	1.46
Cell capacity to 20% voltage drop (amp-min)	157	90
Watt hours	4.4	2.2
Cathode Efficiency (%)	88	50

\* Cell A: 10 plate, 10:1 HgO  
to Shawinigan plus 5%  
Ag<sub>2</sub>O two g mix per  
.003" grid

\*\* Cell B: 5 plates, 10:1  
HgO to Shawinigan plus  
5% Ag<sub>2</sub>O four g mix  
per .005" grid

The elements were placed in a plastic case with plastic spacers, activated with 2N Mg(ClO<sub>4</sub>)<sub>2</sub> for two minutes, and discharged in a beaker with 140 ml water as a heat sink. Figure 20 shows that a cell made of thin plates of increased surface area gives improved performance. The current density of cell B is 110 ma/cm<sup>2</sup>, which is twice that of cell A.

The discharge characteristics of Mg/Mg(ClO<sub>4</sub>)<sub>2</sub>/HgO cells of various cathode mix ratios were determined at constant current drains of 5 to 15 amperes and are presented in Table VI and Figures 19 and 20.

All cells were placed in a plastic test container to restrict volume and discharged in excess of 2N Mg(ClO<sub>4</sub>)<sub>2</sub> three minutes after activation. Figure 19 represents a 6:1 HgO-to-carbon cell with a 25/0.010-inch silver-plated-copper grid, having a dry element weight of 33.3 grams. The cathode efficiency varied from 74 percent for the cathodes with a 6:1 ratio to 90 percent for the cathodes with a 4:1 ratio. The maximum discharge time was obtained with the highest HgO content. Further studies were made to

CELL CATHODE COMPOSITION	THEORETICAL CATHODE CAPACITY (Ampere- minutes)	DISCHARGE CURRENT (Amperes)	DISCHARGE TIME TO VOLTAGE DROP (minutes)			CATHODE EFFICIENCY (percent)	AVERAGE CELL VOLTAGE AT 20% DROP (volts)
			10% DROP	20% DROP	20% DROP		
4-Plate 4:1 - 5Cu5 grid	122.4	10	10.5	11.0	11.0	90	1.57
4-Plate 4:1 - 5Cu5 grid	122.4	15	6.6	7.1	7.1	87	1.53
8-Plate 4:1 - 5Cu5 grid	244.8	20	10.4	11.1	11.1	91	1.65
4-Plate 6:1 - 5Cu5 grid	150.4	5	23.0	24.3	24.3	80	1.62
4-Plate 6:1 - 25/.010" grid	150.4	10	13.7	14.1	14.1	94	1.61
4-Plate 6:1 - 5Cu5 grid	150.4	10	12.0	12.5	12.5	83	1.58
4-Plate 6:1 - 5Cu5 grid	150.4	15	6.8	7.4	7.4	74	1.51
4-Plate 8:1 - 5Cu5 grid	160	5	23.1	24.2	24.2	76	1.67
4-Plate 8:1 - 5Cu5 grid	160	10	12.3	13.0	13.0	81	1.60
4-Plate 8:1 - 5Cu5 grid	160	15	7.7	8.3	8.3	78	1.56

MT-51

TABLE VI. HIGH-RATE-CAPACITY DATA FOR  $\text{Mg}/\text{Mg}(\text{ClO}_4)_2/\text{H}_2\text{O}$  CELLS OF VARIOUS CATHODE COMPOSITIONS.

determine performance of the silver-plated 5 Cu5 expanded-copper and 25/0.010-inch woven-copper grid against an expanded pure silver 5 Ag 10 grid for optimum design and mix composition.

### 3.2.3.2 Cathode Grid Studies

The grids for the cathode plates in previous studies consisted of silver-plated copper screens used to prevent reaction of the grid with the mercuric-oxide cathode material. A study was made to determine an optimum grid structure before extending cell development. A comparison of cells with various grids discharged at 10 amperes is given in Table VII. The results show that the silver-plated, expanded-copper grid gave the optimum performance and the lightest cell weight. The poorer performance of the pure silver grid is believed due to a weaker plate structure. The 5 Cu 5-4/0 silver-plated grid was used in all further testing.

Mercuric-oxide cathode plates require either a pure silver or a silver-plated copper grid to provide good performance. These grids, however, may be limited in various applications because silver-plated grids break down on activated stand tests. Pure-silver grids also can break down on long discharge rates (24 hours and over) due to amalgamation with the mercury from the cathode reduction. The use of an expanded-titanium grid was studied for use with mercuric-oxide cathodes. Four cells were constructed using 2-inch-square cathode plates made with 10Ti10-1/0 expanded-titanium grids. Theoretical cathode capacity was 277 ampere-minutes. Two cells made with pure-magnesium anode plates were discharged at four-hour and eight-hour rates to a 20-percent voltage-drop end point at an ambient temperature of 70°F.

The results of the tests showed that these cells had a capacity equivalent to cells with a silver-plated copper grid. The initial cell voltage was 0.20 volt lower than comparable silver-grid cells; the voltage then increased to the silver-grid cell value after 25 percent of the discharge.

CATHODE GRID MATERIAL	GRID WEIGHT (grams)	DRY CELL WEIGHT (grams)	DISCHARGE TIME TO VOLTAGE DROP (minutes)		THEORETICAL CAPACITY PER CELL (Ampere-Minutes)	CATHODE EFFICIENCY (10% drop)
			TO 10% DROP	TO 20% DROP		
5Ag10-4/0 Silver	1.8	32.9	11-3/4	13	154	76
5Cu5-4/0 Silver-Plated Copper	0.8	28.4	13	13-1/2	154	84
25/.010" Silver-Plated Bronze	2.5	35.8	12-1/2	13-3/4	154	81

MT-52

TABLE VII. COMPARISON OF  $\text{Mg}/\text{Mg}(\text{ClO}_4)_2/\text{HgO}$  RESERVE CELLS WITH VARIOUS GRIDS.  
DISCHARGED AT 10-AMPERE CONSTANT-CURRENT DRAIN.

This effect is probably associated with a surface film on the titanium grid. Two cells were also made with AZ-31 magnesium anode plates and discharged at the 24-hour rate, both immediately after activation with 5N magnesium-perchlorate electrolyte and after a week of activated stand. The data are plotted in Figure 21 and show a 9-percent drop in capacity after the one-week stand. Anode efficiency measured 64 percent for the cell discharged immediately, and 59 percent for the cell discharged after a one-week stand. It can be concluded from these tests that titanium grids can be used in low-rate mercuric-oxide cells where silver grids are limited.

#### 3.2.3.3 Cathode Mix Studies

The cathode efficiencies of mercuric-oxide cells tested during initial characterization were found to vary from 74 to 90 percent for active material ratios from 4:1 to 8:1. Examination of cathode plates indicated that poor blending was obtained with hand mixing techniques due to agglomeration of mercuric-oxide particles. Ratio and mix blending studies were continued in an attempt to improve cathode efficiency at the higher mix ratios.

Evaluation of various mix blending techniques showed that mixes made by mechanically pre-blending the yellow mercuric oxide and CMC binder solution prior to addition of carbon were the best. No discernible particles of mercuric oxide could be found under 60 X magnification with this type blending. The procedure developed is as follows:

- a. Blend the yellow mercuric oxide with the CMC solution for five minutes in an Osterizer blender.
- b. Add approximately 50 percent of the carbon; follow with further blending in the blender.
- c. Finally, add remaining carbon and blend by hand.

The mix composition and capacity data for lots with various mercuric-oxide-to-carbon ratios made with the preceding mixing procedure are summarized in Table VIII. The cells consisted of four cathode plates and five .014-inch



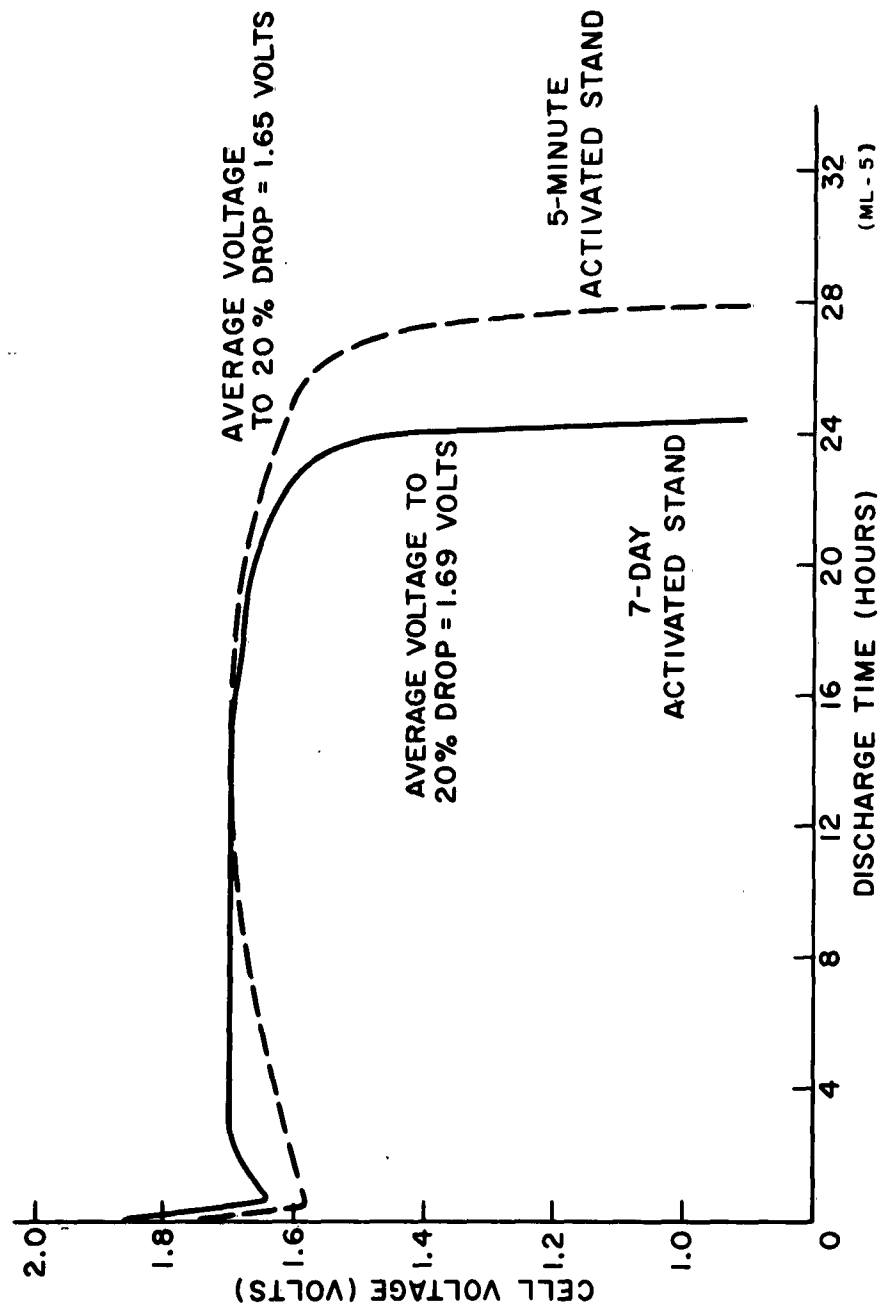


FIGURE 21. CAPACITY DATA FOR  $\text{Mg}/\text{Mg}(\text{ClO}_4)_2/\text{H}_2\text{O}$  RESERVE CELLS WITH A TITANIUM CATHODE GRID AT VARIOUS ACTIVATED-STAND TIMES AT 164 MA CONSTANT-CURRENT DRAIN AT 70°F.

MERCURIC OXIDE-TO- CARBON (Mix Ratio)	COMPOSITION (Percent)			THEORETICAL CAPACITY FOR 4-PLATE CELL (Ampere-Minutes)	DISCHARGE TIME TO VOLTAGE DROP (Minutes)		VOLTAGE AT 20% DROP (Volts, Av)	CATHODE EFFICIENCY AT 20% DROP (Percent)
	HgO	SHAWINIGAN CARBON BLACK	CMC SOLUTION (1.5%)		10% DROP	20% DROP		
6:1	51.8	8.6	39.6	154	13.0	13.9	1.60	90.2
8:1	60.7	7.6	31.6	180	15.4	15.95	1.6525	88.6
10:1	66.8	6.7	26.4	198	16.4	17.0	1.63	85.8
14:1	72.7	5.2	22.1	216	13.0	15.2	1.52	69.5

MT-53

TABLE VIII. COMPOSITION AND CAPACITY DATA FOR MERCURIC-OXIDE BLENDED MIXES WITH VARIOUS ACTIVE-MATERIAL-TO-SHAWINIGAN-CARBON-BLACK RATIOS.

pure-magnesium anode plates with an average wet-element weight of 40.0 grams and volume of 2.25 x 2.5 x 0.25 inches.

Cathode efficiencies over 80 percent were obtained with active material-to-Shawinigan carbon black ratios up to 10:1 at the 10.0-ampere constant current drain. Increasing the ratio to 14:1 resulted in a marked decrease in cathode efficiency and operating voltage level. Discharge curves for the various mix ratios are presented in Figure 22.

#### 3.2.3.4 Mix Additive Studies

During the first one-half minute of discharge, a low discharge voltage is noted for mercuric oxide cells. This might be improved by one of the following methods:

- a. Add a second cathode material to the cathode which operates at near the potential of mercuric oxide and does not polarize. This material does not need a high ampere-minute capacity.
- b. Partially discharge the plate to reach the flat portion of the discharge curve.

Procedure (a) is the more desirable method.

In view of the above, the addition of various cathode mix additives and their effect on this initial voltage drop were considered. Additives used for this purpose consist of the cathode materials with operating voltages equal to, or higher than, mercuric oxide and having a low polarization at high discharge rates in the 2N  $\text{Mg}(\text{ClO}_4)_2$  electrolyte.

The various slightly soluble silver compounds are the most obvious materials for use with the mercuric-oxide system. Figure 23 illustrates the effect of silver (II) oxide on the initial voltage of an 8:1 mercuric-oxide mix under a 10-ampere drain. It is seen that the addition of 5-percent silver (II) oxide is sufficient to raise the voltage to within 10 percent of the maximum operating voltage. Additions in excess of 5 percent result in extended leveling of the voltage within the initial three minutes of discharge. Discharge curves at 10 amperes and 5 amperes are given in Figures 24 and 25.

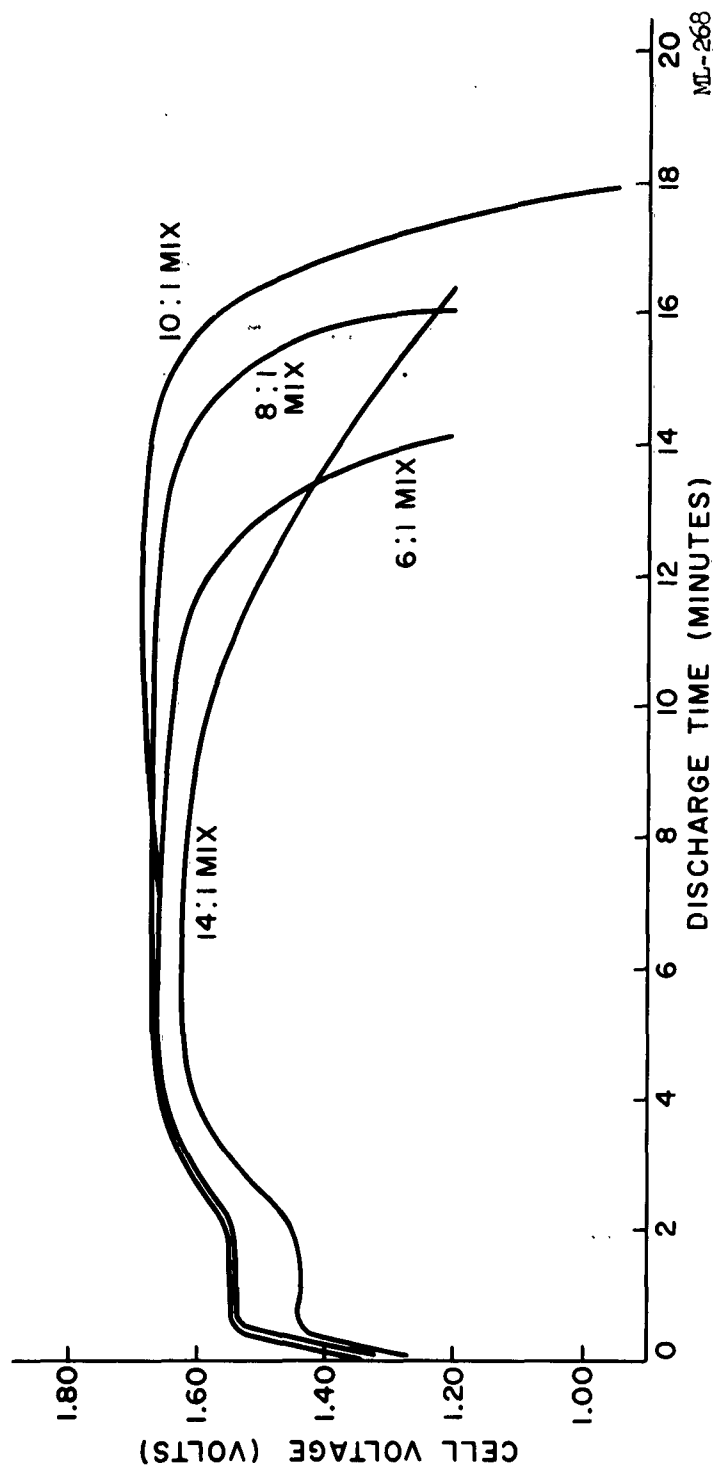


FIGURE 22. CAPACITY DATA FOR  $\text{Mg}/\text{Mg}(\text{ClO}_4)_2/\text{HgO}$  RESERVE CELLS OF VARIOUS ACTIVE MATERIAL-TO-CARBON RATIOS  
DISCHARGED AT 10.0 AMPERES.

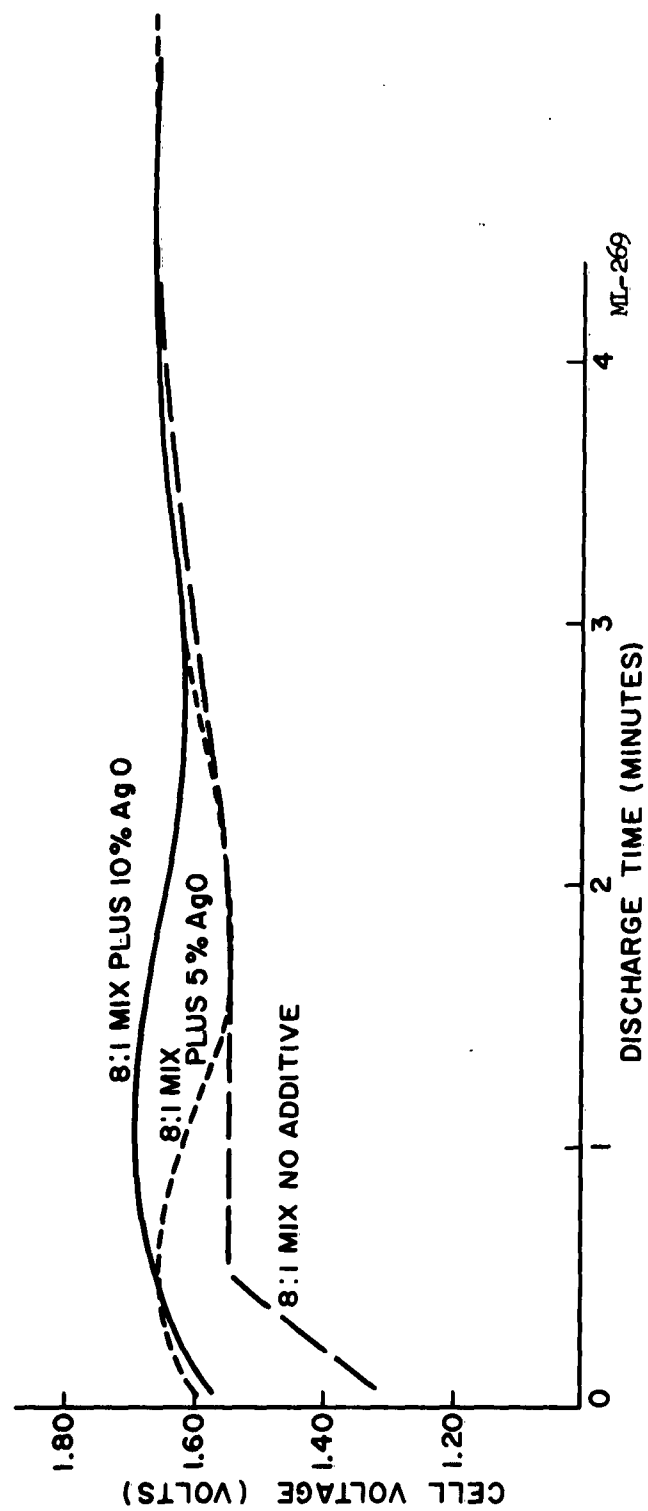


FIGURE 23. EFFECT OF AgO IN THE HgO CATHODE ON INITIAL DISCHARGE VOLTAGE AT 10.0 AMPERES.

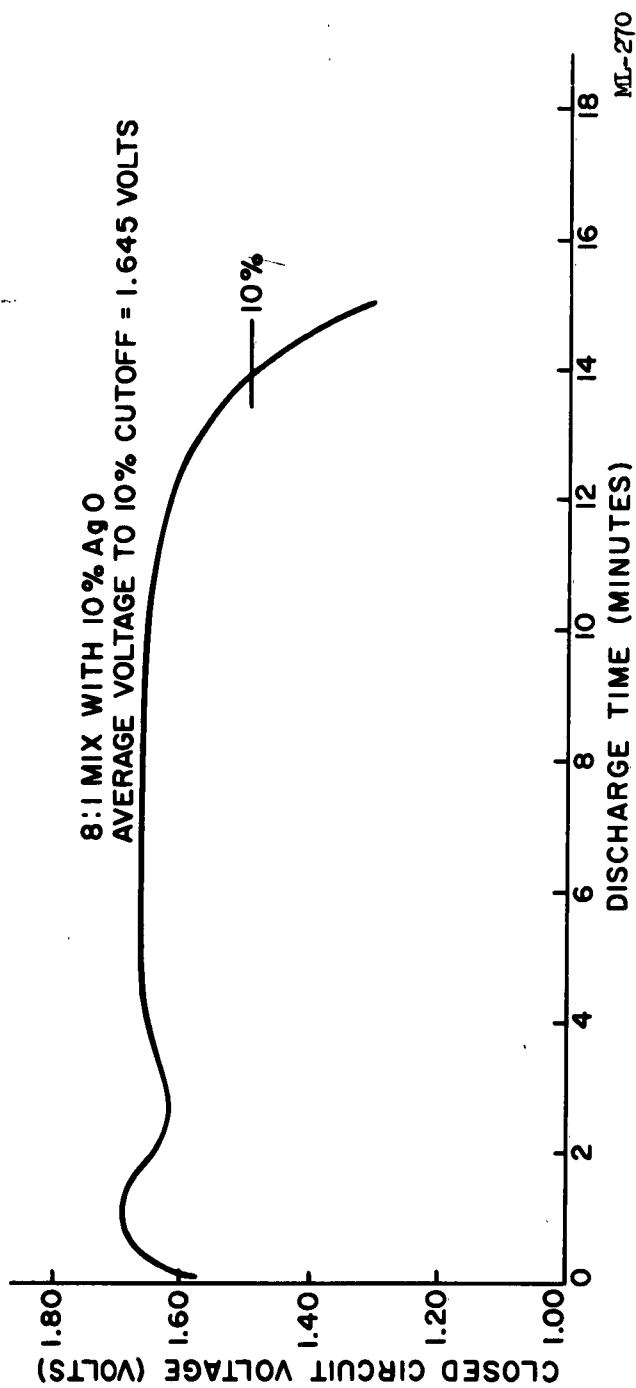


FIGURE 24. EFFECT OF AgO IN THE CATHODE MIX ON THE DISCHARGE VOLTAGE CHARACTERISTICS OF  $\text{Mg}/\text{Mg}(\text{ClO}_4)_2/\text{HgO}$  RESERVE CELLS AT 10.0 AMPERES.

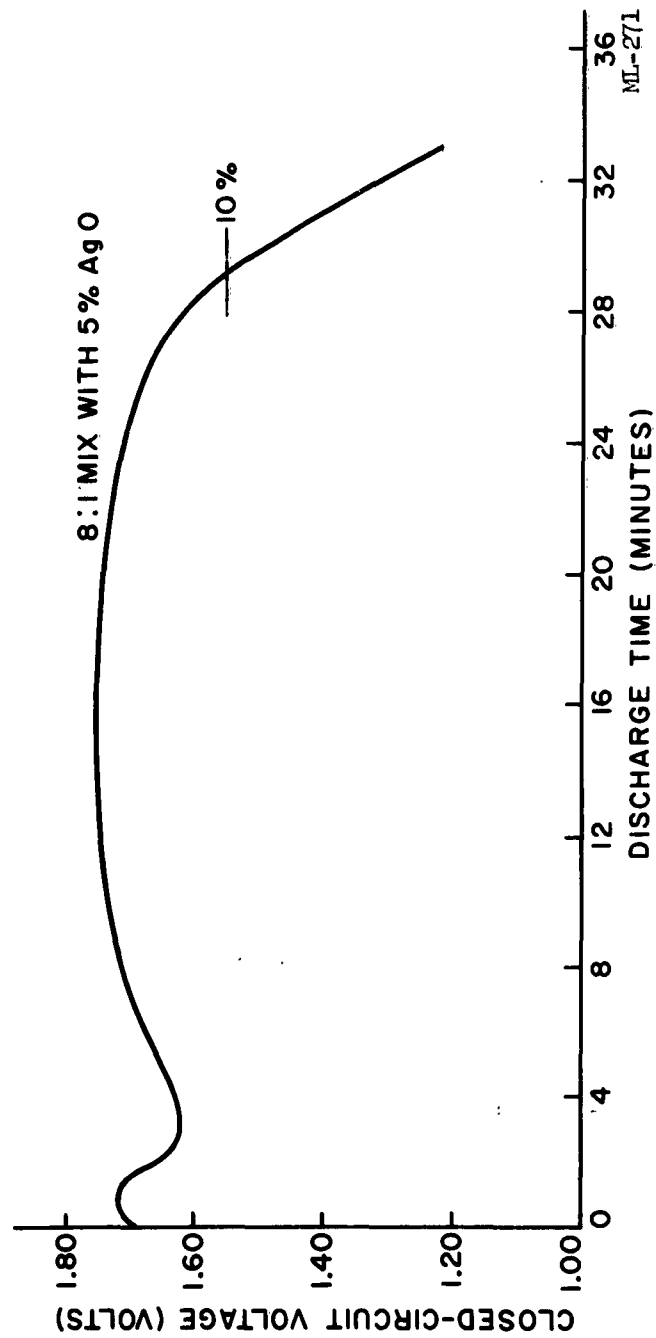


FIGURE 25. EFFECT OF 5% AgO ADDED TO THE CATHODE MIX  $\text{Mg/Mg}(\text{ClO}_4)_2/\text{HgO}$  RESERVE CELL. DISCHARGED AT 5.0 AMPERES.

Addition of a 5-percent silver (I) oxide compound to the cathode mix increased the initial voltage to permit operation of the cell within a 10-percent voltage tolerance. The curve depicting the voltage level of this cell was flatter than that obtained with the silver (II) oxide additive. This improvement probably resulted from the lower activity of the silver (I) oxide compared to silver (II) oxide. Figures 26 and 27 illustrate the effect on the initial part of the 10.0-ampere discharge curve of an 8:1 ratio (mercuric oxide-to-Shawinigan carbon black) cell with a 5-percent silver (I) oxide additive.

A five ampere-hour capacity cell was selected for ease of testing and comparison with other battery systems. A cathode mix of 8:1 ratio of mercuric oxide to Shawinigan carbon black with 5-percent silver (I) oxide was used in all cells tested. Typical wet mix composition was as follows:

- 192 g. mercuric oxide (yellow reagent)
- 24 g. Shawinigan carbon black
- 10.8 g. silver (I) oxide
- 125 ml QMC solution, 1.5%

Cathode plates were processed using silver-plated 5 Cu 5-4/0 expanded-copper screen grids 1.5 x 1.875 inches and 4 grams of wet mix per plate. Theoretical cathode capacity is 32.2 ampere-minutes per plate. A plastic case 1.75 x 2.63 x 0.68 inches was used as the test cell. The cell element consisted of ten cathode plates and eleven 1.5 x 1.875 x .014 inch C.P. magnesium anode plates. A No. 10 copper wire lead weighing 3.5 grams was attached to each electrode for connection. The activated cell weight, including case and leads, averaged 90 grams.

A typical 10-ampere discharge curve for a cell activated with  $2N \text{ Mg}(\text{ClO}_4)_2$  for three minutes at room temperature is presented in Figure 28. Capacity calculated at a 10-percent voltage drop was 42.9 watt-hours per pound and 2.7 watt-hours per cubic inch, neglecting volume for terminal height. Cathode efficiency was 91.5 percent. This data is representative of the state of the art of the present cell. Further studies directed toward reducing element weight should enable a figure of 50 watt-hours per pound to be reached for the 1/2-hour rate.



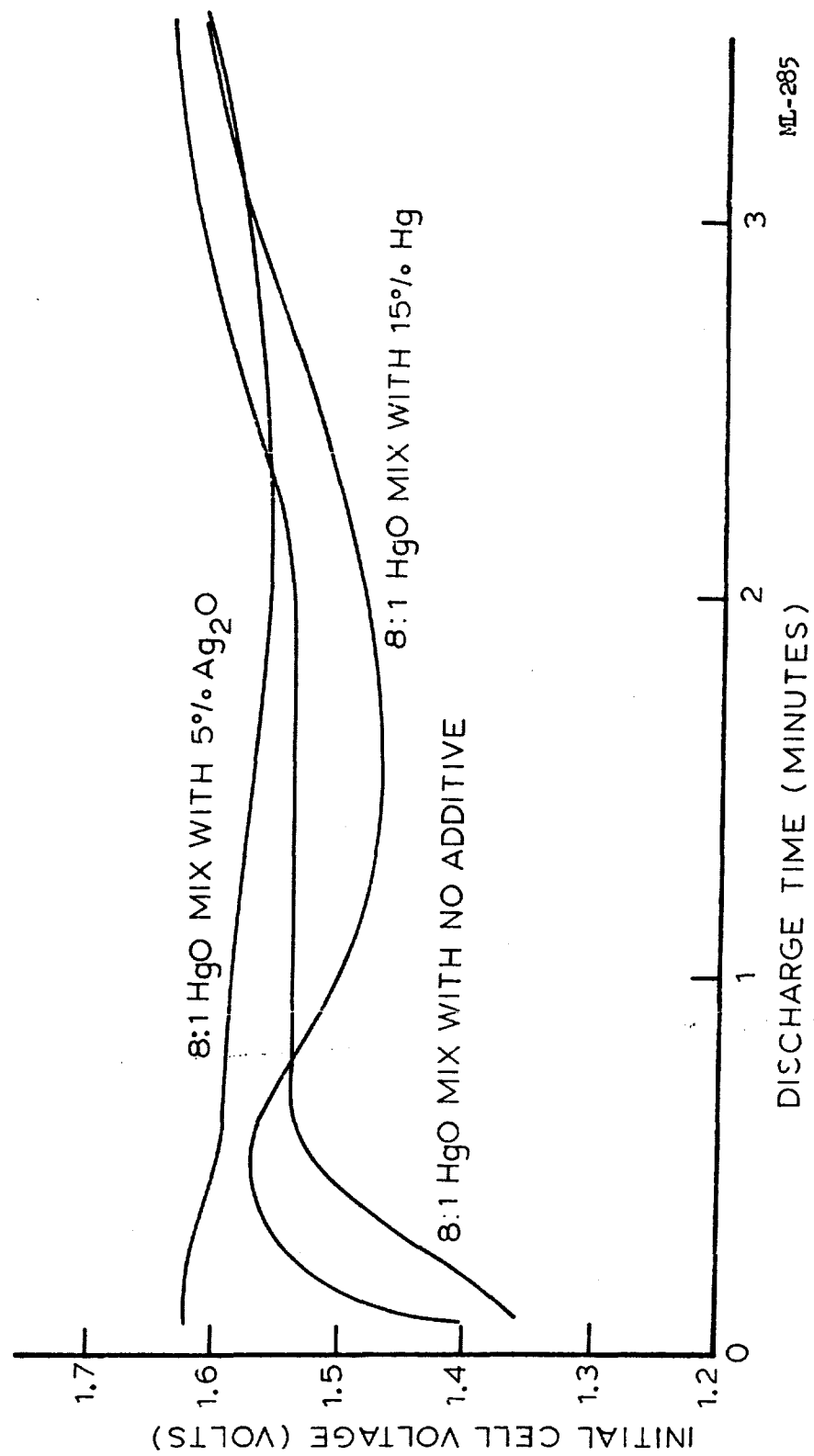
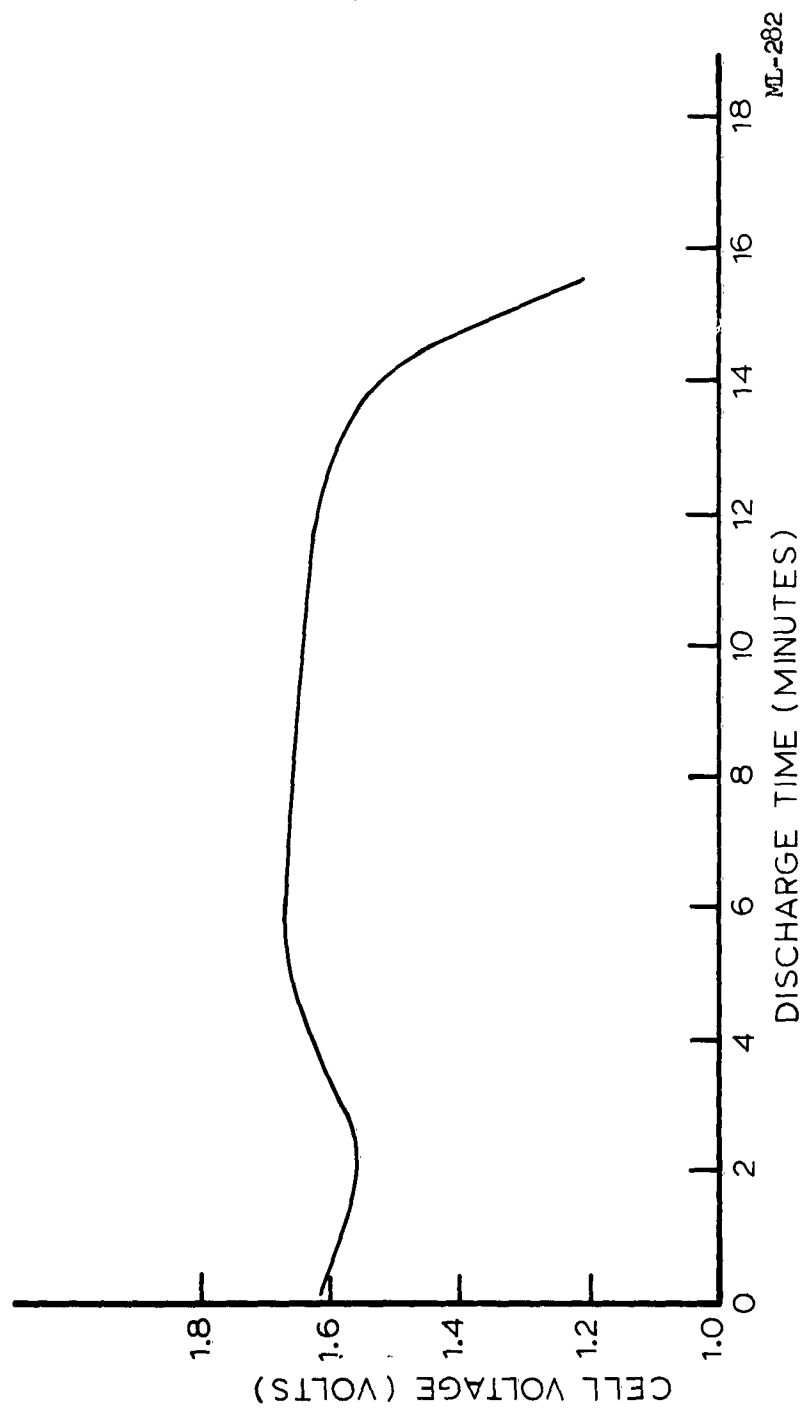
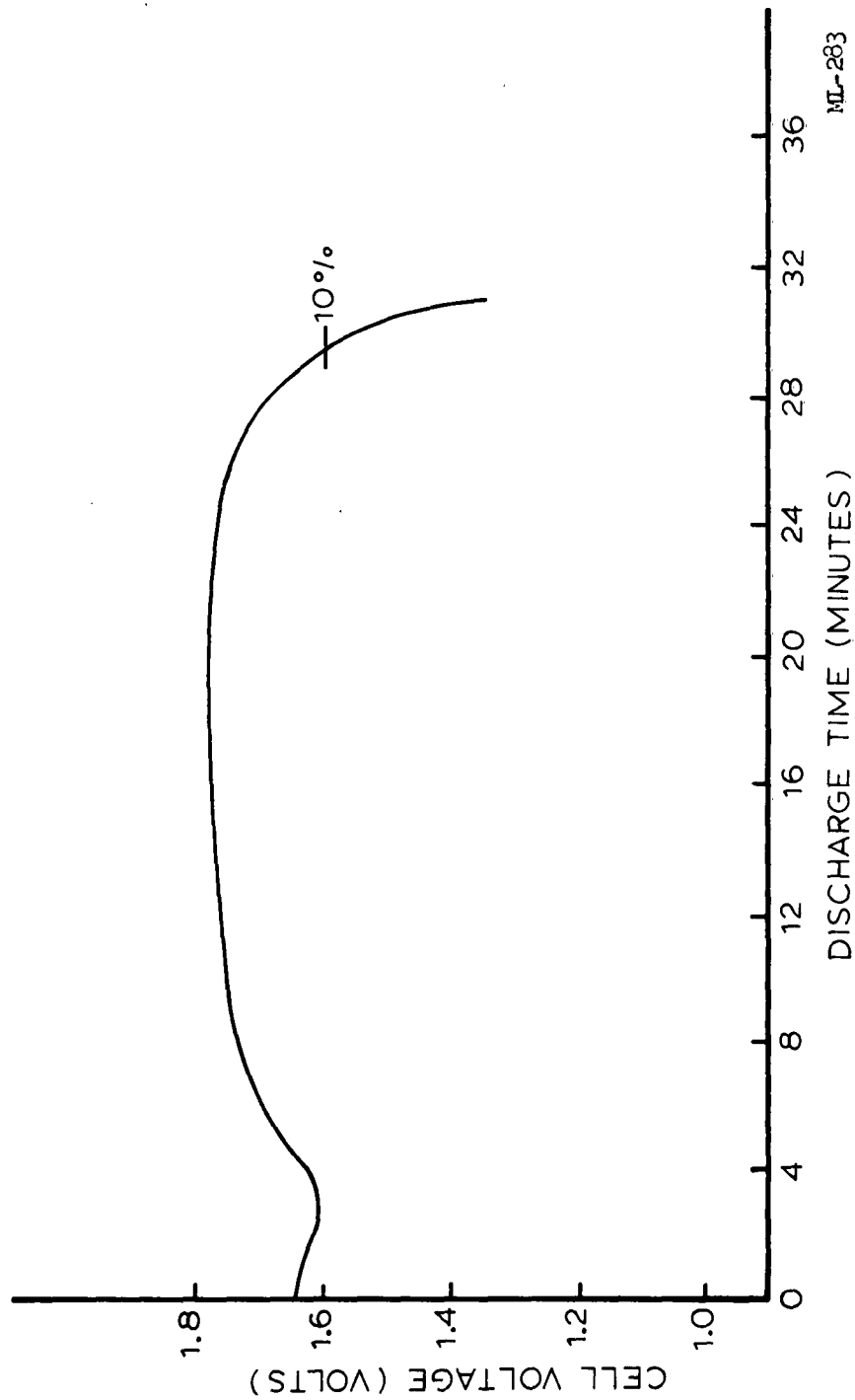


FIGURE 26. EFFECT OF VARIOUS ADDITIVES ON INITIAL VOLTAGE CHARACTERISTICS OF  $\text{Mg}/\text{Mg}(\text{ClO}_4)_2/\text{HgO}$  RESERVE CELLS AT 10.0 AMPERES.



ML-282

FIGURE 27.  $\text{Mg}/\text{Mg}(\text{ClO}_4)_2/\text{HgO}$  RESERVE CELL WITH 5%  $\text{Ag}_2\text{O}$  ADDED TO THE CATHODE MIX DISCHARGED AT 10.0 AMPERES.  
 4-PLATE 8:1 HgO-TO-SHAWINIGAN MIX WITH 5%  $\text{Ag}_2\text{O}$  ADDED. THEORETICAL CAPACITY- 161 AMPERE-MINUTES.



ML-283

FIGURE 28.  $\text{Mg}/\text{Mg}(\text{ClO}_4)_2/\text{HgO}$  RESERVE CELL WITH 5%  $\text{Ag}_2\text{O}$  ADDED TO THE CATHODE MIX DISCHARGED AT 10.0 AMPERES AT ROOM TEMPERATURE. AVERAGE VOLTAGE TO 10% CUTOFF = 1.73 VOLTS. CELL WEIGHT WITH CASE = 90.0 GRAMS. VOLUME = 1.75 X 2.63 X 0.68 INCHES. THEORETICAL CATHODE CAPACITY = 322 AMPERE-MINUTES.

Because of the heat evolved by magnesium cells during discharge, an efficient heat sink must be included in the cell design. For a 10-ampere room-temperature discharge, a 150-ml water heat sink is sufficient to control the temperature for a 10-percent voltage tolerance. The heat dissipation problem increases with increasing discharge rate and the number of cells. One test cell, discharged at 30 amperes without a heat sink, overheated excessively and resulted in an unstable voltage level and early cell failure. Further application studies must include a heat sink as an integral part of the battery design if optimum performance from magnesium cells at high discharge rates is to be obtained.

Cathode mixes were made with five percent of silver iodate and five percent of silver phosphate added to the mix to test the effect of silver solubility on cell performance. Room-temperature discharge at 10 amperes for four 1.5 x 1.875-inch cathode plate cells showed that these compounds had little effect on improving initial cell voltage. Cell capacity for these cells was reduced to 43 percent of the theoretical value for the silver-phosphate mix and 15 percent with the silver-iodate mix. The data show that there is no advantage to using silver compounds of greater or lesser solubility than silver (I) oxide (such as silver iodate and silver phosphate).

Additional mixes made with silver (I) oxide showed the importance of dry-mix blending on cell voltage. A thorough blending of mercuric oxide, silver (I) oxide, and carbon is necessary to obtain a flat voltage level for the first three minutes of discharge. The procedure used for producing the cell described above consists of ball milling the mercuric oxide, silver (I) oxide, and 10 percent of the carbon for one hour. The mixing is then completed in the mechanical blender as described in section on cathode mix studies.

One cathode mix was made with a silver phosphate additive which was prepared in the laboratory. Test results for this cell showed little effect on initial cell voltage.

The addition of silver oxide to the mercuric-oxide cathode mix yielded improved initial voltage levels at room-temperature discharge. At low

temperatures, however, a marked drop in initial cell voltage was noted as shown in Figure 29. This drop is due partly to the failure of the silver oxide to function at low temperature. Other additives or an alternate approach must be used to improve low temperature characteristics.

During the initial thirty seconds of the discharge period of a mercuric oxide cathode, formation of micro particles of metallic mercury forms throughout the plate; this results in a drop in plate resistance and an increase in cell voltage. One mix was made with a fifteen percent metallic mercury addition to simulate the state of the plate after 15 percent discharge. Discharge results presented in Figure 26 show some effect due to this addition. Examination of this mix at 60 x magnification showed a wide range in mercury particle sizes. Special blending techniques would be required to give the micro dispersion of mercury, mercuric oxide, and carbon necessary to raise the voltage level.

An alternative to special blending would be to partially discharge the cathode during processing. Dispersion can be accomplished electrochemically or by partial reduction of the mercuric oxide through chemical means during cathode plate processing.

The partial reduction of mercuric oxide was studied in an attempt to determine the effect of the resultant micro dispersion of mercury on cell voltage characteristics.

Cathode plates of 10:1 ratios were processed and treated with formaldehyde solutions of different strengths. Discharging of single plate cells showed that the reduction with weak solutions had no effect on voltage or capacity. The cells treated with strong solutions showed excess reduction of the mercuric oxide and did not function.

Control cells made with untreated 10:1 cathode plates had an initial five-second voltages of 1.57. This improvement in initial voltage over previously reported results resulted from an improved dry mix procedure. The procedure consisted of ball milling the mercuric oxide with 50 percent of the required carbon for one hour, followed by milling with the remaining carbon for several minutes.

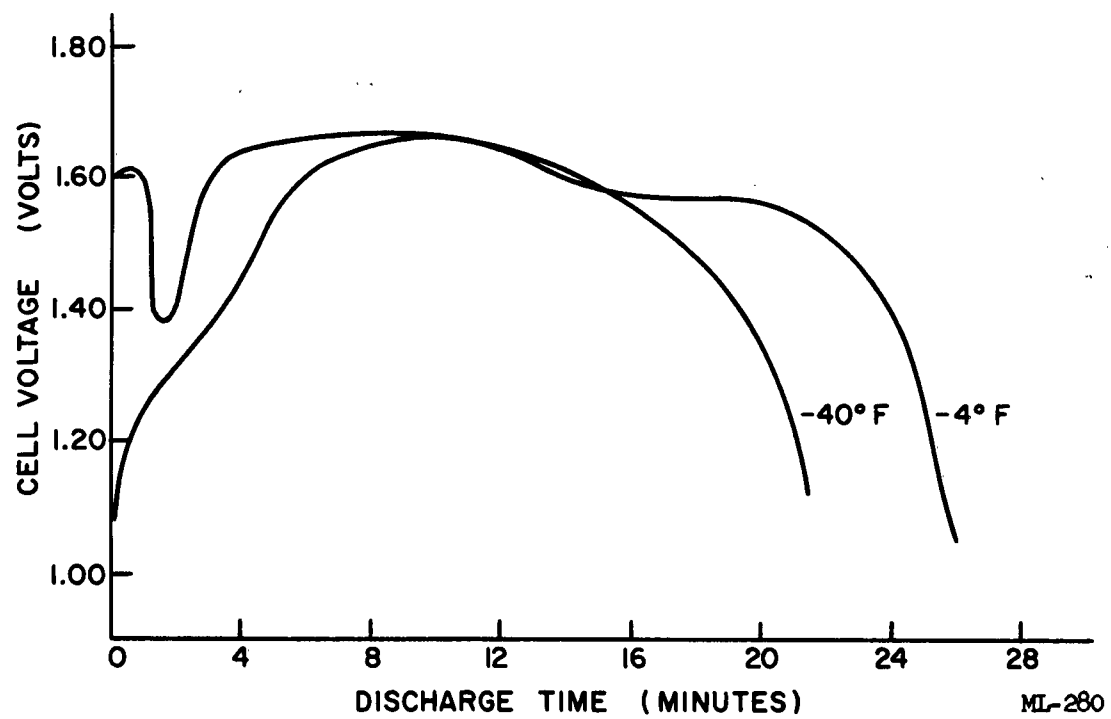


FIGURE 29. LOW-TEMPERATURE CAPACITY DATA FOR  $\text{Mg}/\text{Mg}(\text{ClO}_4)_2/\text{HgO}$  RESERVE CELLS AT 10.0 AMPERES.

#### Partial Reduction in the Cathode Mix

One cathode mix was made with a CMC solution containing two percent formaldehyde to test the effect of partial reduction in the mix. This solution was sufficient to reduce the one 10:1 mercuric-oxide mix by 15 percent. However, no improvement in cell performance was obtained with this mix at the thirty-minute discharge rate compared to an untreated mix. Low-temperature discharge ( $-40^{\circ}\text{F}$ ) showed no improvement in initial cell voltage and showed reduced operating voltage.

#### Partial Reduction by Limited Cell Discharge

Mercuric-oxide reduction, by limited discharge at low rates, resulted in a slight improvement in initial voltage at  $-40^{\circ}\text{F}$ . The test cell was discharged at two amperes for ten minutes at room temperature and then placed at  $-40^{\circ}\text{F}$  until the temperature stabilized. The cell was then discharged at ten amperes. Test results are shown in Figure 30. Magnesium perchlorate (5N) was used as the low-temperature electrolyte for these cells.

Manganese dioxide is another material which has a high operating voltage. Consequently, several mercuric-oxide cathode batches were made, with synthetic  $\text{MnO}_2$  added to the mix. Additions of up to 10 percent type-M or type-L manganese dioxide had no effect on the initial voltage at the 10-ampere drain.

A 6:1 ratio  $\text{HgO}$  cell with 10 percent type-M  $\text{MnO}_2$  gave the equivalent capacity of a 8:1 ratio mercuric-oxide mix. The cathode efficiency for a 20 percent cutoff voltage was 87.3 percent, based on the combined  $\text{HgO}$ - and  $\text{-MnO}_2$  theoretical capacity.

#### Analysis of Heat Evolution in Magnesium Reserve Cells

Data show that heat evolved from magnesium reserve cells during high-rate discharge is a major problem affecting efficient cell performance.

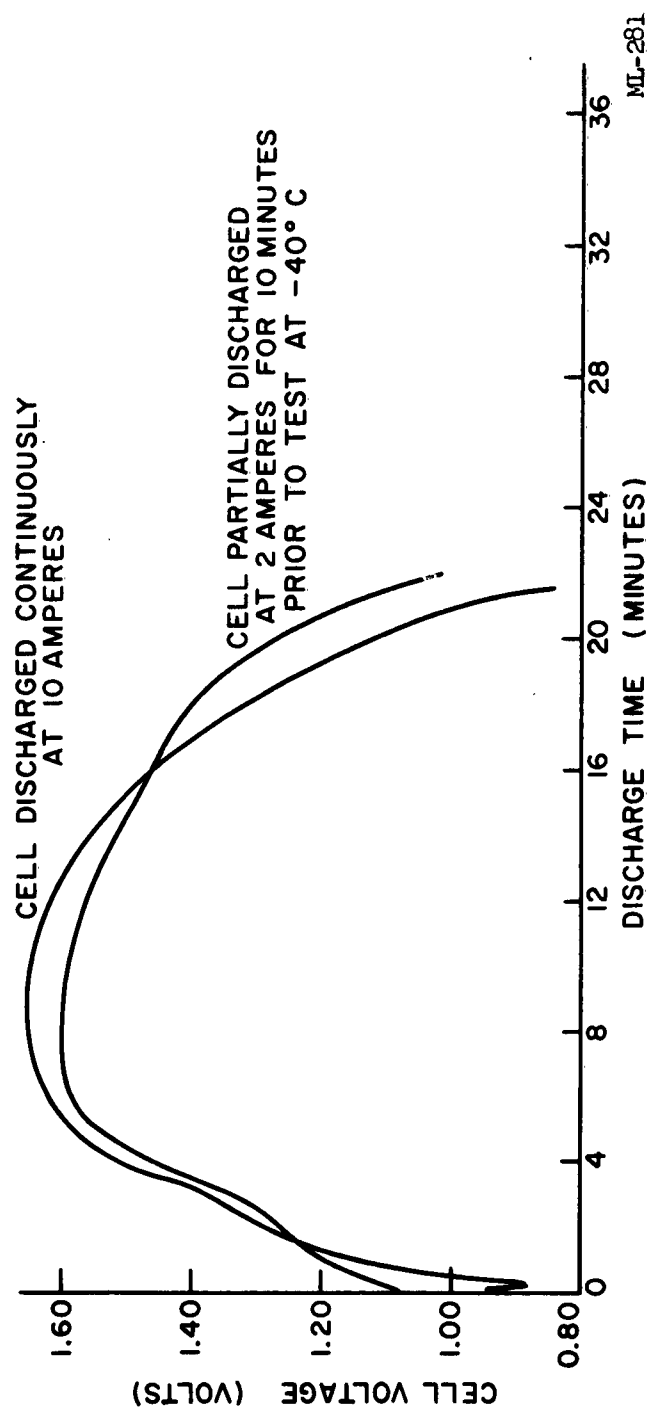


FIGURE 30. EFFECT OF PARTIAL REDUCTION OF MERCURIC OXIDE ON VOLTAGE CHARACTERISTICS OF  
Mg/HgO RESERVE CELLS AT 10.0 AMPERES AT  $-40^{\circ}\text{C}$ .

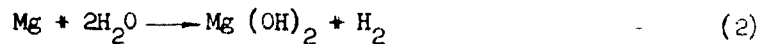


In a magnesium cell, two reactions occur at the anode:

The electrical-energy-producing reaction



The corrosion side reaction



Both of these reactions produce heat. Reaction No. 1 gives off heat because of the irreversibility of the magnesium anode in aqueous electrolytes. Reaction No. 2 is exothermic. The heat given off by these reactions may be calculated with sufficient accuracy for present purposes.

The heat produced by reaction No. 1 may be calculated for any magnesium cell from the following equation:

$$W = A \cdot V \cdot T \quad (3)$$

Where W is watt-hours, A is current drain in amperes, V is the voltage difference between the reversible potential of the magnesium anode and the operating potential of the magnesium anode, and T is the time in hours. V is approximately 1.1 because, under most conditions, the magnesium anode operates at 1.2 to 1.3 volts vs. S.H.E., whereas the reversible potential is 2.34 to 2.40 volts vs. S.H.E. Heat in calories is obtained by multiplying watt hours by 860.

The heat due to the corrosion side-reaction is calculated by first determining the ampere-minutes of magnesium utilized in the corrosion reaction. This is given by the following equation:

$$\text{A.M.} = A \cdot T \cdot E$$

Where A is current drain, T is time and E is an efficiency factor determined by the ratio of percent of anode corrosion to percent of anode efficiency. The heat produced in calories is determined by relating ampere minutes to moles of magnesium multiplied by  $\Delta H$  for the corrosion reaction which is 82.6 Kcal/mole.

The total heat evolved from a magnesium cell per hour is due to the two

heat-producing reactions, and is a function of current drain. Heat evolved under different current-drain conditions is shown in Figures 31 and 32. The 100-percent line represents heat evolved only by the irreversibility of the magnesium. The heat evolved from the corrosion reaction is presented in Figures 33 and 34.

The significance of the thermal data can be realized from the analysis of a mercuric-oxide reserve cell at a constant-current discharge of 10 amperes. Figure 31 shows that 13.5 Kcal are evolved per hour at 10 amperes at 80 percent anode efficiency. For the 5-ampere-hour mercuric-oxide cell, 6.75 Kcal are evolved in the half-hour discharge. This quantity of heat is sufficient to vaporize up to 11.5 grams of water.

Capacity data for a magnesium (AZ-21 alloy) mercuric-oxide reserve cell discharged at a constant current of 10-amperes in  $2N \text{ Mg}(\text{ClO}_4)_2$  is presented in Figure 35. A heat sink of 150 ml of water was used. The cell was discharged for a total time of 36.25 minutes. The magnesium anode efficiency was 80.7 percent, as determined by measurement of weight loss. The total heat evolved during the discharge time was calculated from the data of Figure 31 at 80-percent efficiency and is 8.15 Kcal.

Measurement of the temperature rise in the water heat sink and electrolyte showed a heat output of 4.15 Kcal. The difference in the measured heat and that calculated from the data in Figure 31 may be accounted by these factors:

- a. Reduced anode polarization at high temperatures.
- b. Inhibition of the anode by mercuric ion.
- c. Heat absorbed by the cell.
- d. Heat loss to boiling in center of cell.

The above analysis shows that an efficient heat sink is a necessary requirement in the design of high-rate magnesium cells. Without this heat sink, close voltage tolerances cannot be attained and cell capacity will be limited because of water loss. It should be noted that the resultant heat evolved is independent of cell size; most cathode materials used with magnesium operate close to their reversible potential, and their contribution to the total heat evolved is omitted in this analysis.

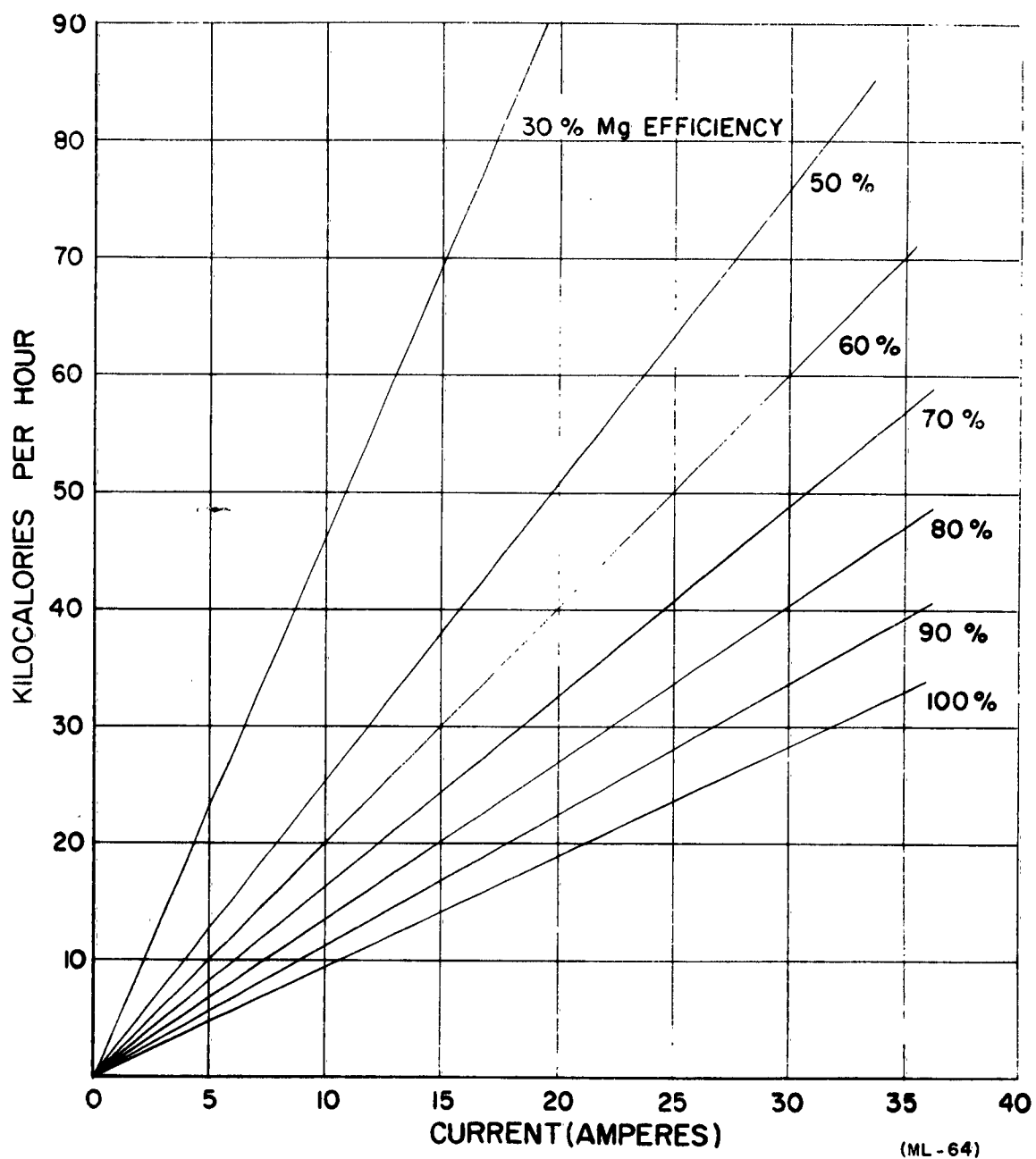


FIGURE 31. CALORIES EVOLVED FROM MAGNESIUM ELECTRODE PER HOUR AT VARIOUS Mg EFFICIENCIES AT HIGH DISCHARGE RATES.

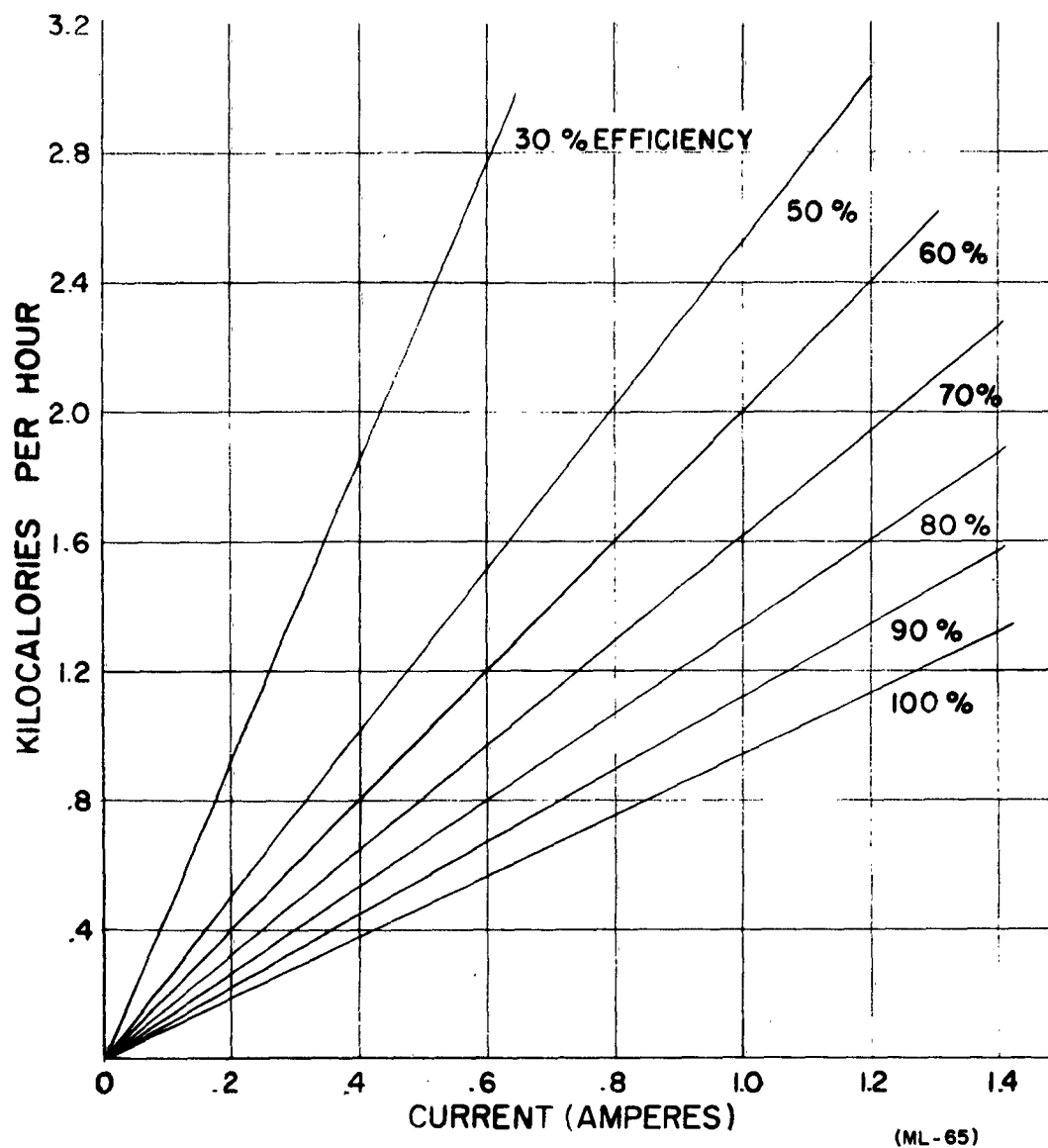


FIGURE 32. CALORIES EVOLVED FROM A MAGNESIUM ELECTRODE PER HOUR AT VARIOUS ANODE EFFICIENCIES AT LOW DISCHARGE RATES. TYPICAL ANODE EFFICIENCY OF A DRY CELL OF THE TYPE PROPOSED HERE IS BETWEEN 60 AND 70 PERCENT.

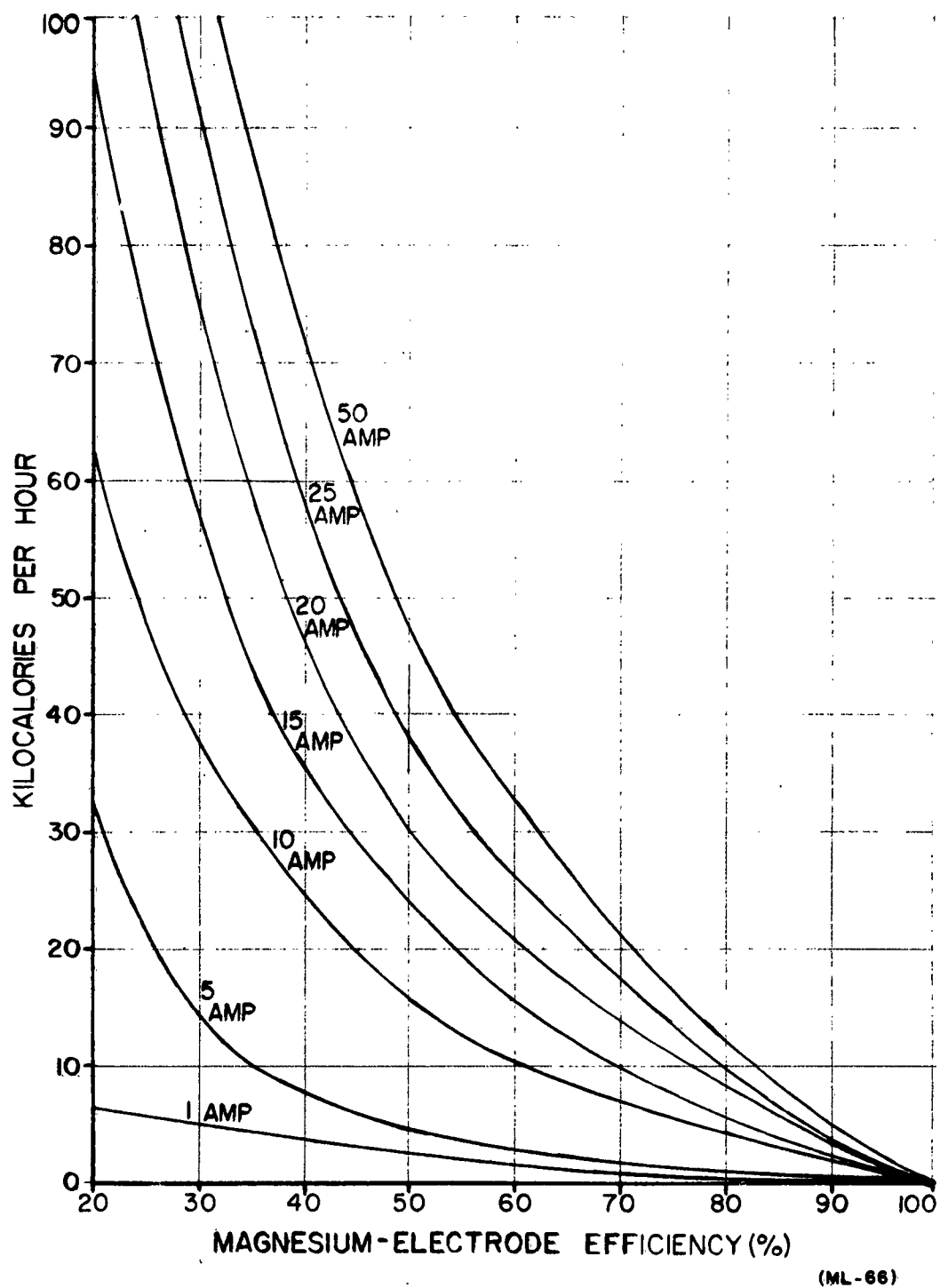


FIGURE 33. CALORIES EVOLVED FROM MAGNESIUM CORROSION REACTION AS A FUNCTION OF ELECTRODE EFFICIENCY AT HIGH DISCHARGE RATES.

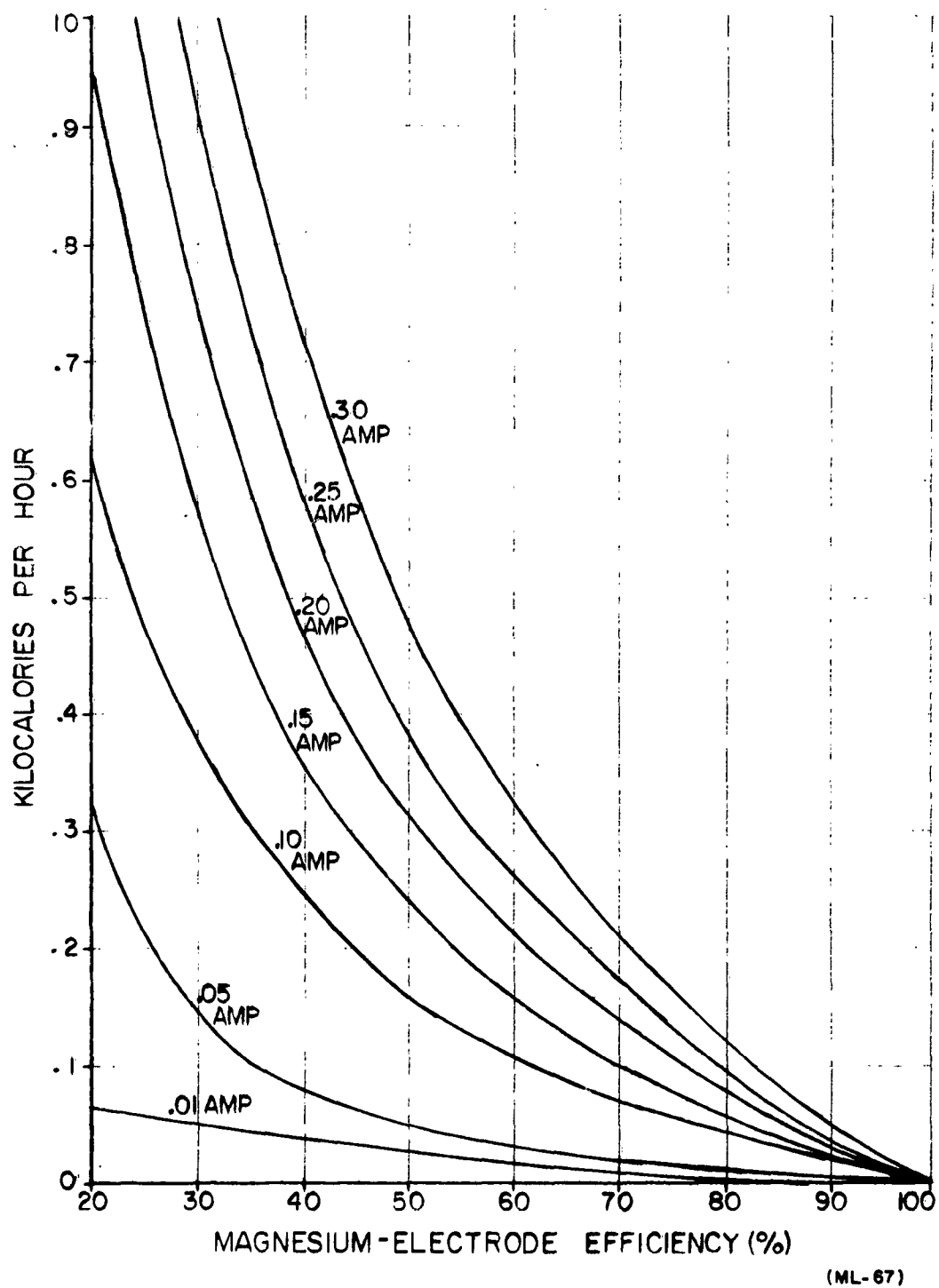


FIGURE 34. CALORIES EVOLVED FROM MAGNESIUM CORROSION REACTION AS A FUNCTION OF ELECTRODE EFFICIENCY AT LOW DISCHARGE RATES.

AV. VOLTAGE: TO 10% = 1.60 VOLTS  
 ANODE: II-PLATE, AZ-21Mg  
 CATHODE: 10 PLATE, 10-TO-1 RATIO HgO-TO-  
 SHAWINIGAN MIX  
 9.0 WATT - HOURS TO 10%  
 2.9 W - HR/IN<sup>3</sup>  
 48 W - HR/lb

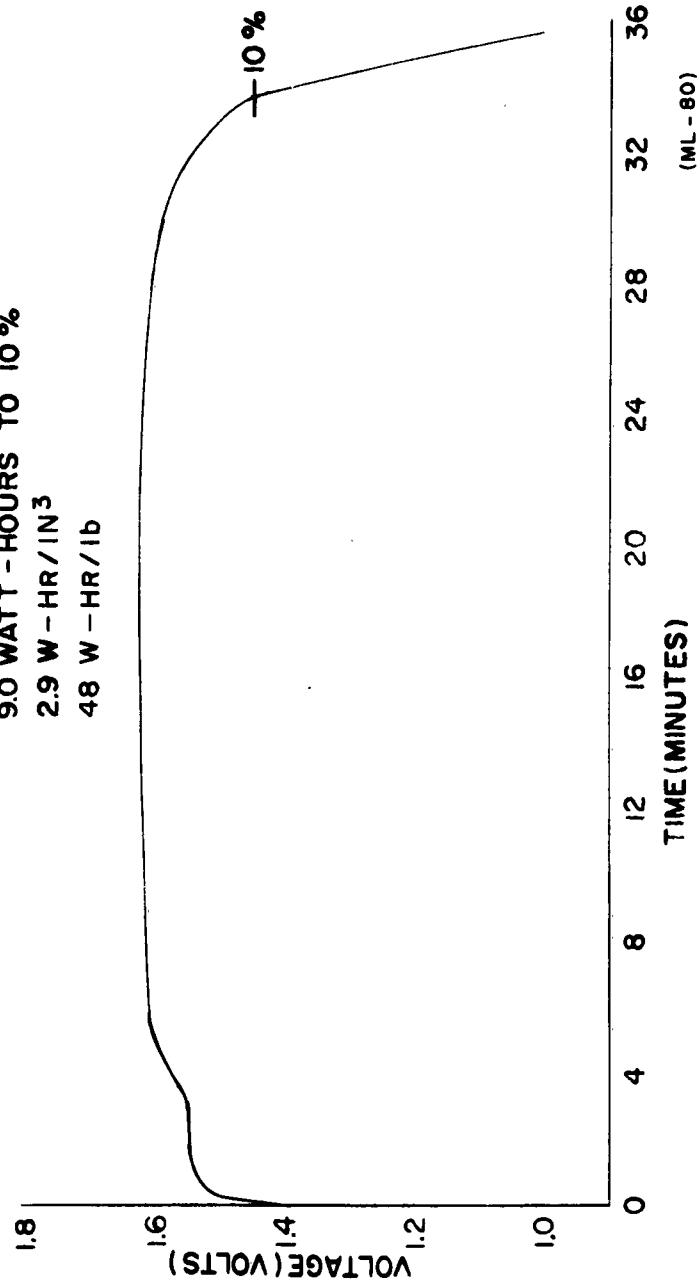


FIGURE 35. CAPACITY DATA FOR  $\text{Mg}/\text{Mg}(\text{ClO}_4)_2/\text{HgO}$  RESERVE CELL DISCHARGED AT 10 AMPERES.

The data given in Figures 31 to 34 can be extended for use in magnesium battery design at any discharge rate. Previous studies of 6-volt magnesium batteries at a 12-hour rate showed excessive heat build-up after three hours discharge at room temperature. These studies indicate that heat evolved from magnesium dry-cell pack batteries can present a problem in confined systems. The data are extremely useful in low-temperature battery design where conservation of heat is important.

#### 3.2.3.5 Voltage Control by Heat Sink Techniques

Previous experiments which used water as a heat sink showed that cells could be operated at the half-hour rate at 10 amperes within a voltage tolerance of  $\pm 5$  percent. Battery design necessitates the use of heat-sink methods other than water. Studies employing metal-jacket techniques were carried out; the results are summarized in the following sections.

##### Effect of Copper-Foil Wrap on Heat Dissipation

A three-cell five-ampere mercuric-oxide reserve battery using single-cell plastic cases wrapped with copper foil was constructed. The three cells were wrapped as a unit and placed in contact with 0.125-inch-thick aluminum plate.

Discharge of the battery at a 10-amperes constant-current drain showed that this method of heat sinking was inadequate for high-rate discharge. Battery voltage could not be maintained at a close tolerance level, and additional water had to be added to the cells throughout the discharge to prevent cells from drying out. The discharge data are presented in Figure 36. Although this method of heat control was unsatisfactory at high discharge rates, it is sufficient for lighter drains.

##### Effect of Aluminum Cell Case with Air-Space on Heat Dissipation

A study was made of the use of an aluminum cell case in place of the rigid plastic case employed in previous tests. Cells were constructed of three cathode plates, measuring  $3 \times 3\frac{1}{8}$ ", and four C.P. magnesium anodes. These cells had a theoretical cathode capacity of 300 ampere-minutes.



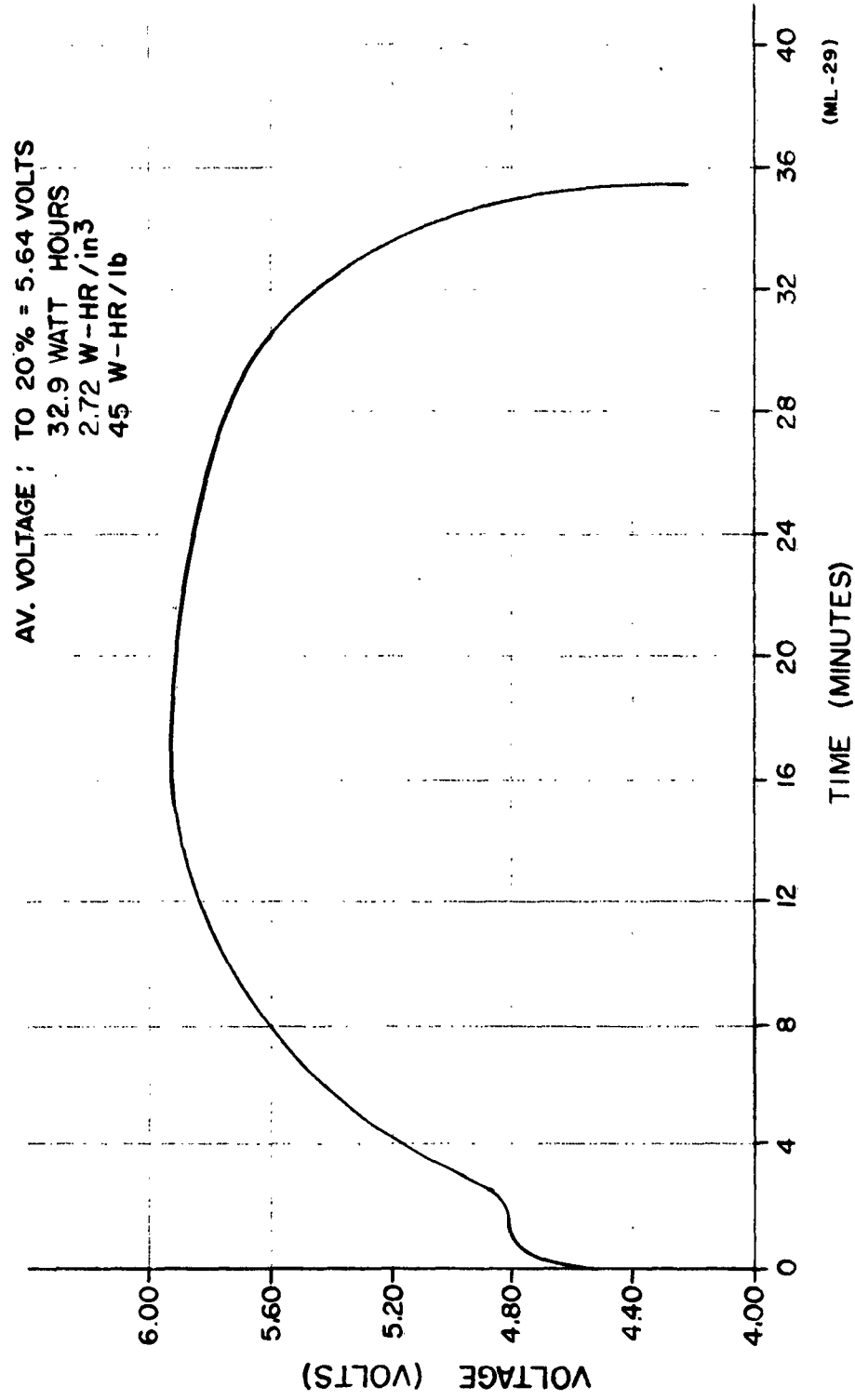


FIGURE 36. THREE-CELL  $\text{Mg}/\text{Mg}(\text{ClO}_4)_2/\text{H}_2\text{O}$  RESERVE BATTERY WITH COPPER-FOIL JACKET DISCHARGED AT 10 AMPERES.

The cell elements were placed in thin polyethylene bags and installed in an 1/16-inch-thick aluminum case with a 3/8-inch air space between cells. The cells were activated with 19 ml of 2N magnesium perchlorate, and discharged at 10 amperes in contact with an aluminum base plate.

Discharge data showed poor voltage regulation because of excessive heat build-up within the cells. Figure 37 shows the discharge characteristics of two 3-cell constructions. The upper curve is for the 3 cell battery described above. The lower curve is based on data from a single cell having a water heat sink. Average voltage for the 3-cell battery was 5.74 volts to the 20-percent voltage drop point. Computed data for the other battery shows an average voltage of 4.56 volts to the 20-percent voltage-drop point.

#### 3.2.3.6 Low-Discharge-Rate Cell Studies

Capacity data were determined for magnesium/mercuric-oxide reserve cells in a 5N magnesium perchlorate solution over a discharge range of two to eight hours. Cells for this study were constructed with five 2 x 2-inch mercuric-oxide cathode plates made with a 10:1 ratio of mercuric oxide to-Shawinigan carbon black, and having a theoretical capacity of 277 ampere-minutes. Six 2 x 2 x .010-inch C.P. magnesium plates were used as the anode. Cells were activated for five minutes with 19 ml of electrolyte, and discharged at constant current drains of 0.5, 1.0, and 2.0 amperes at room temperature and with no heat sink.

The capacity data are presented in Figure 38. These data show that a voltage tolerance within five percent was obtained for most of the discharge. The cathode efficiency was 90.2 percent when measured to a 20-percent voltage-drop point, at a discharge rate of two amperes. The efficiency was 94.6 percent for a discharge rate of one ampere when measured to a 20-percent voltage-drop end point. At the 0.5-ampere discharge the efficiency dropped to 78 percent because of excess magnesium corrosion. Magnesium C.P. cannot be used efficiently at low current drains in a 5N magnesium perchlorate electrolyte; an AZ-21 or AZ-31 magnesium alloy must be used.

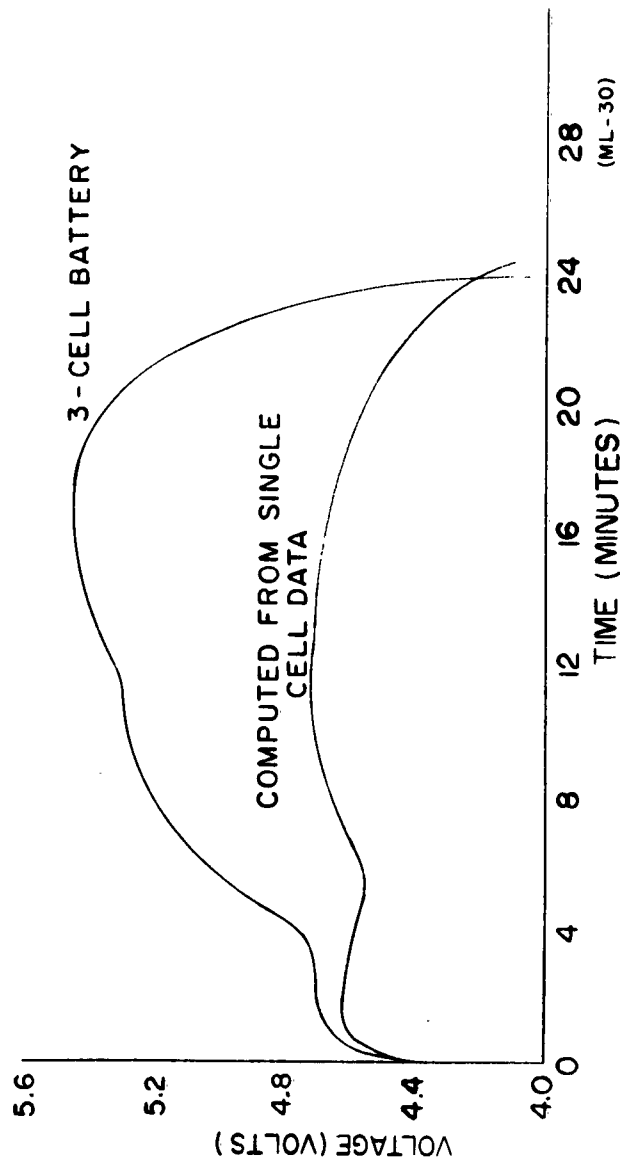


FIGURE 37. CAPACITY DATA FOR A THREE-CELL  $\text{Mg}/\text{Mg}(\text{ClO}_4)_2/\text{HgO}$  RESERVE BATTERY WITH ALUMINUM-CASE CONSTRUCTION. DISCHARGED AT 10 AMPERES.

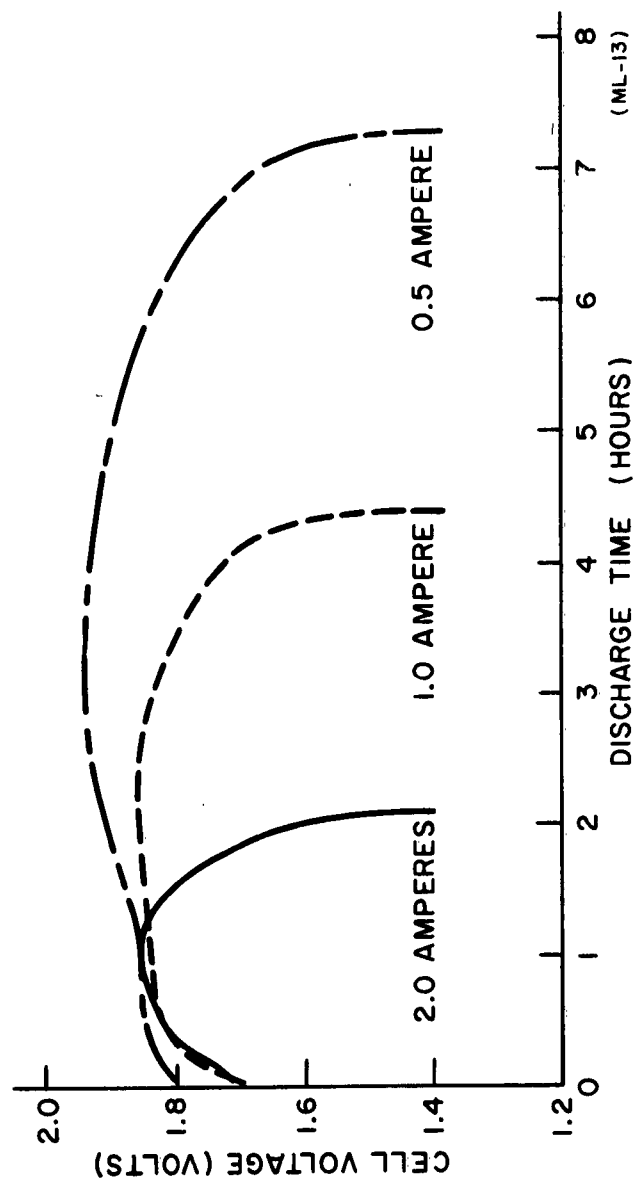


FIGURE 38. CAPACITY DATA FOR  $\text{MC/Mg(ClO}_4)_2/\text{HgO}$  RESERVE CELLS. VARIOUS DISCHARGE DRAINS AT  $70^\circ\text{F}$ .

### 3.2.3.7 Low-Temperature Studies

Mercuric oxide cells of 277-ampere-minutes theoretical cathode capacity were used for all characterization studies. Two types of cell cases were used for the low-temperature studies; a non-insulating rigid plastic case, and a similar case with a one-half-inch-thick polyurethane foam jacket added. The cells were activated with 5N magnesium-perchlorate electrolyte at room temperature and allowed to stand at the test ambient temperature for a period of five minutes prior to starting the discharge. This type of activation procedure is similar to that used in meteorological applications.

The characteristics at  $-4^{\circ}\text{F}$  were obtained for mercuric-oxide cells which were enclosed in a non-insulating plexiglass case. The cells were activated with 5N magnesium perchlorate electrolyte at  $-4^{\circ}\text{F}$  and allowed to stand for 15 minutes prior to the start of discharge. The results of these tests are summarized in Table IX, which also includes data for cells activated and discharged at  $-40^{\circ}\text{F}$ . Figure 39 shows the resulting discharge curves obtained from the data.

The capacity data for single cells discharged at constant-current drains of 0.5 to 4.0 amperes and at temperatures as low as  $-58^{\circ}\text{F}$  are presented in Table X. The data show that room-temperature capacity can be approached at low temperatures by insulating the cell case to conserve the heat evolved from the magnesium reactions. With the 4.0-ampere discharge, a sufficient internal cell temperature is maintained to give room-temperature capacity. The capacity of the non-insulated cell at an ambient temperature of  $-40^{\circ}\text{F}$  drops to 60 percent of the room temperature capacity as shown in Figure 40.

Discharge curves for both cells at an ambient temperature of  $-40^{\circ}\text{F}$  are presented in Figure 41. Data for the cells at an ambient temperature of  $-58^{\circ}\text{F}$  are presented in Figure 42.

Three-cell batteries were constructed of cells similar to those described above to determine the low-temperature characteristics of a multiple-cell unit. The three-cell batteries were activated with room-temperature 5N

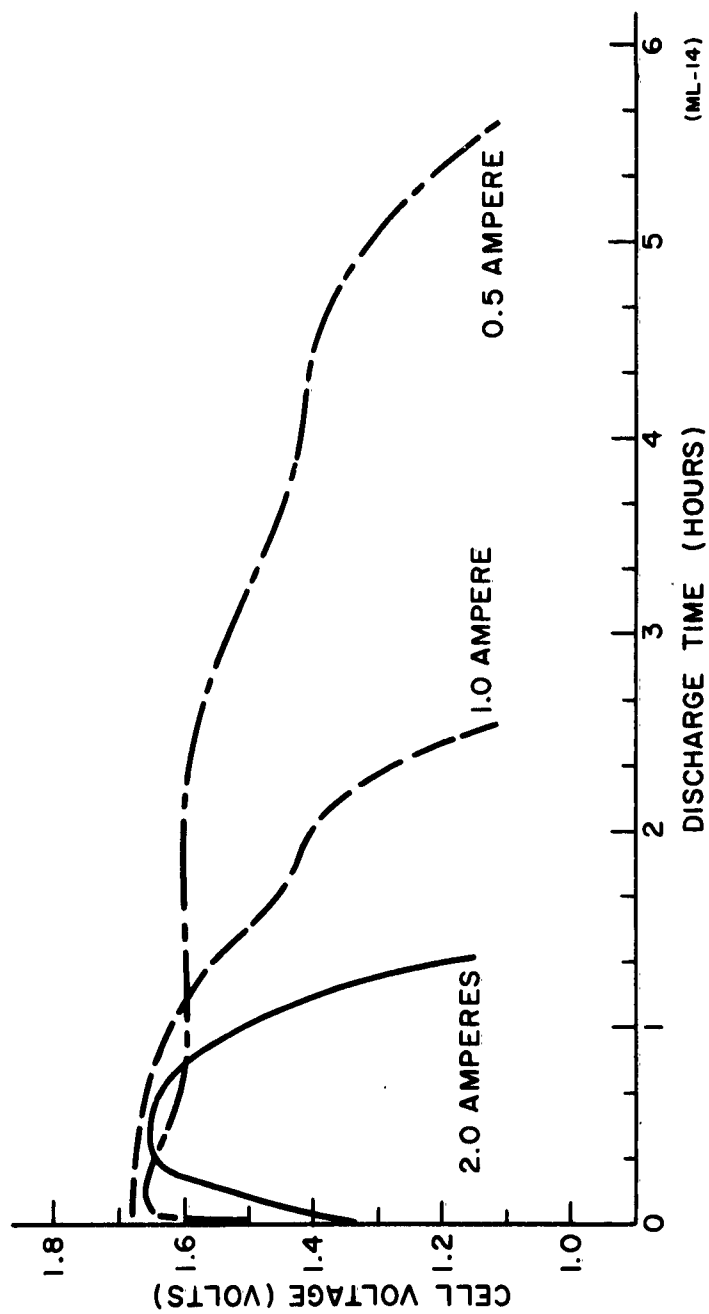


FIGURE 39. CAPACITY DATA FOR  $\text{Mg}/\text{Mg}(\text{ClO}_4)_2/\text{HgO}$  RESERVE CELLS AT VARIOUS DISCHARGE DRAINS AT  $-4^\circ\text{F}$ .

DISCHARGE CURRENT (Amperes)	AMBIENT TEMPERATURE (°F)	CAPACITY TO 20-PER- CENT VOLTAGE DROP			CELL CASE
		DISCHARGE TIME		AVERAGE VOLTAGE	
		(Hours)	(Min.)	(Volts)	
0.5	+70	8	45	1.87	noninsulated plastic
0.5	- 4	5	—	1.53	noninsulated plastic
0.5	-40	6	15	1.18	noninsulated plastic
0.5	- 4	6	30	1.62	1/2-inch polyurethane
0.5	-40	4	10	1.51	1/2-inch polyurethane
0.5	-58	2	—	1.55	1/2-inch polyurethane
1.0	+70	4	22	1.81	noninsulated plastic
1.0	- 4	2	10	1.57	noninsulated plastic
1.0	-40	2	30	1.09	noninsulated plastic
1.0	- 4	3	50	1.67	1/2-inch polyurethane
1.0	-40	3	11	1.69	1/2-inch polyurethane
1.0	-58	3	—	1.64	1/2-inch polyurethane
2.0	+70	2	5	1.79	noninsulated plastic
2.0	- 4	1	15	1.56	noninsulated plastic
2.0	-40	1	14	1.36	noninsulated plastic
2.0	- 4	2	12	1.67	1/2-inch polyurethane
2.0	-40	1	49	1.63	1/2-inch polyurethane
2.0	-58	1	41	1.66	1/2-inch polyurethane
4.0	-58	1	6	1.74	1/2-inch polyurethane

MT-55

TABLE X. CAPACITY DATA FOR  $\text{Mg}/\text{Mg}(\text{ClO}_4)_2/\text{HgO}$  RESERVE CELLS AT  
VARIOUS DISCHARGE RATES AND TEMPERATURES.

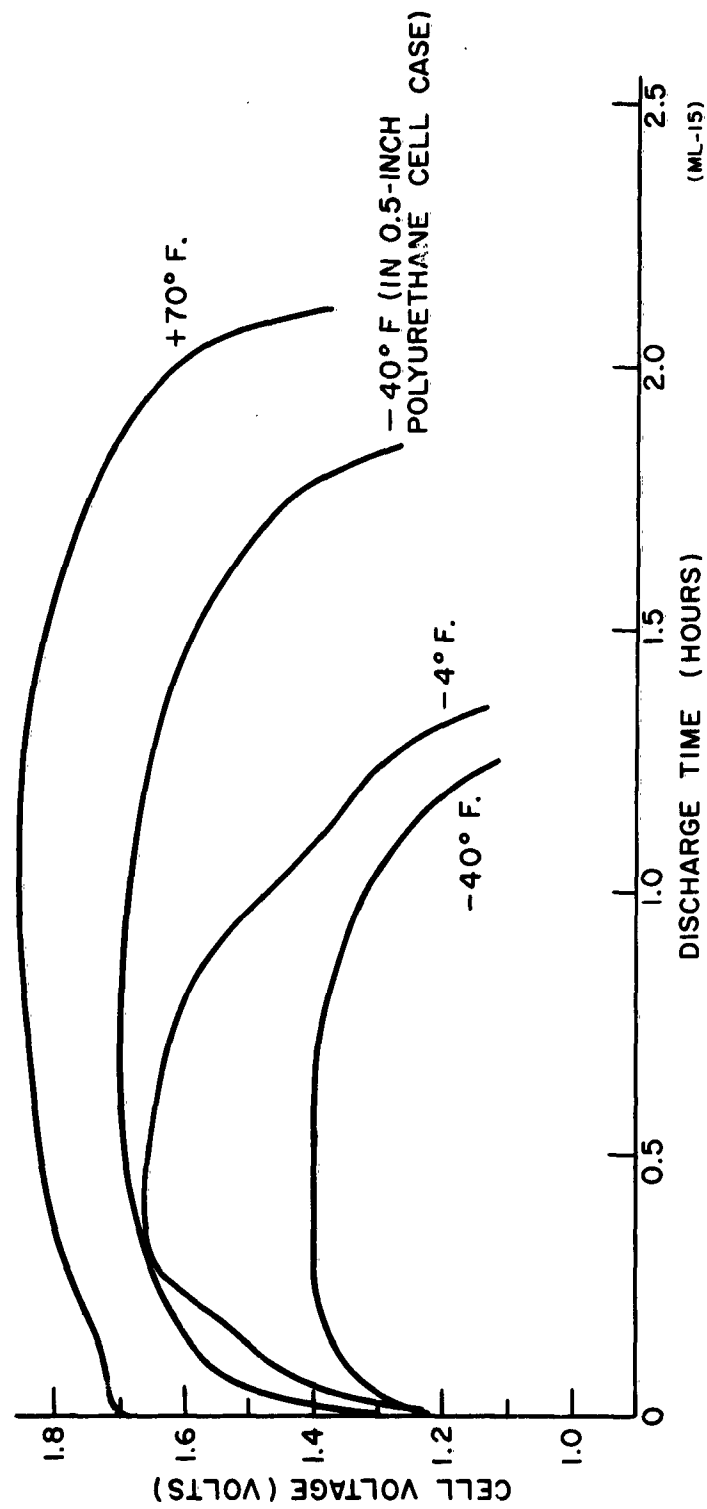


FIGURE 40. EFFECT OF TEMPERATURE ON DISCHARGE CHARACTERISTICS OF  $\text{Mg}/\text{Mg}(\text{ClO}_4)_2/\text{HgO}$  RESERVE CELLS AT 2.0 AMPERES CONSTANT-CURRENT DRAIN.



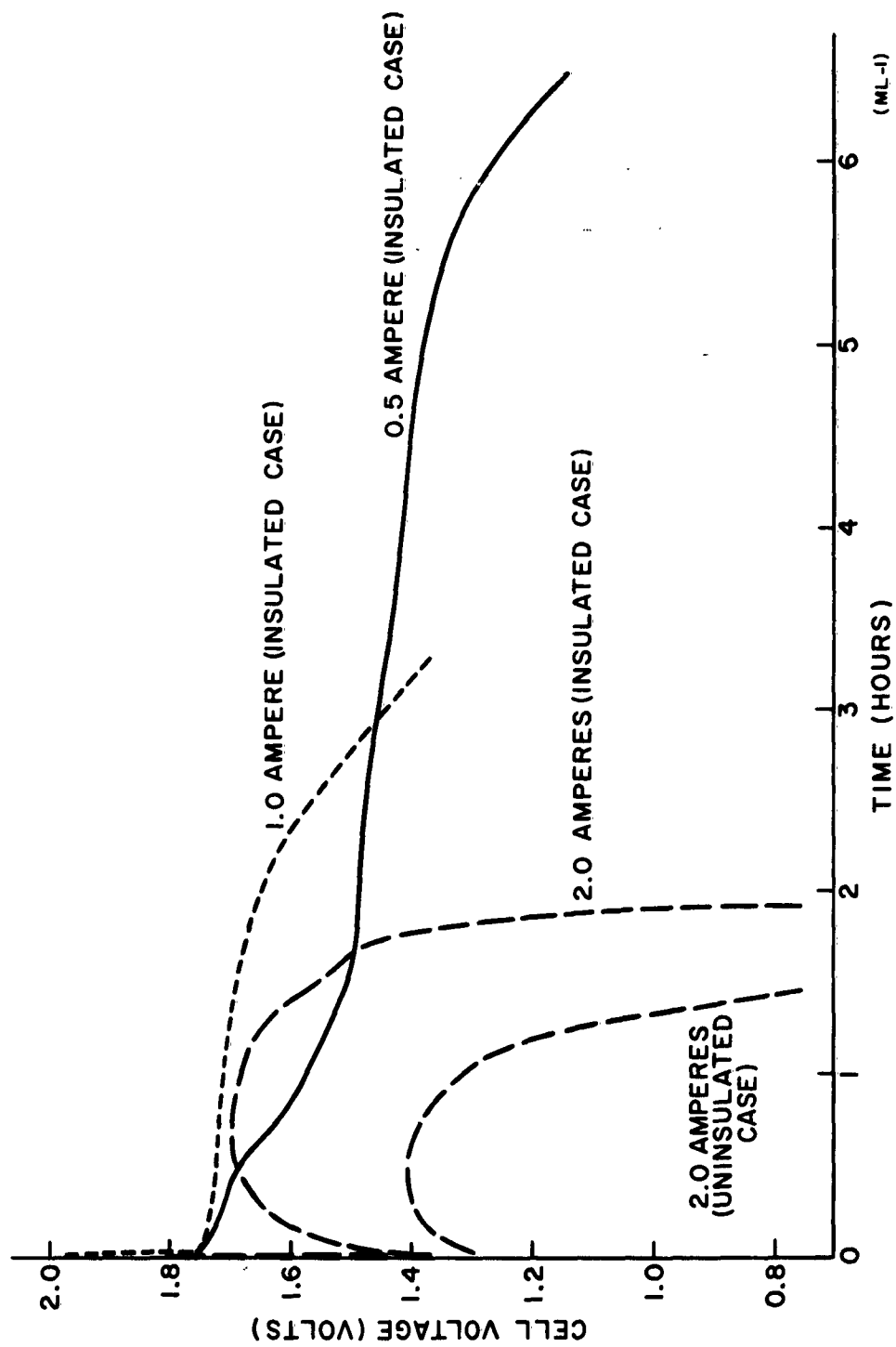


FIGURE 41. CAPACITY DATA FOR  $\text{Mg/Mg}(\text{ClO}_4)_2/\text{HgO}$  RESERVE CELLS AT VARIOUS DISCHARGE RATES AT  $-40^\circ\text{F}$ .

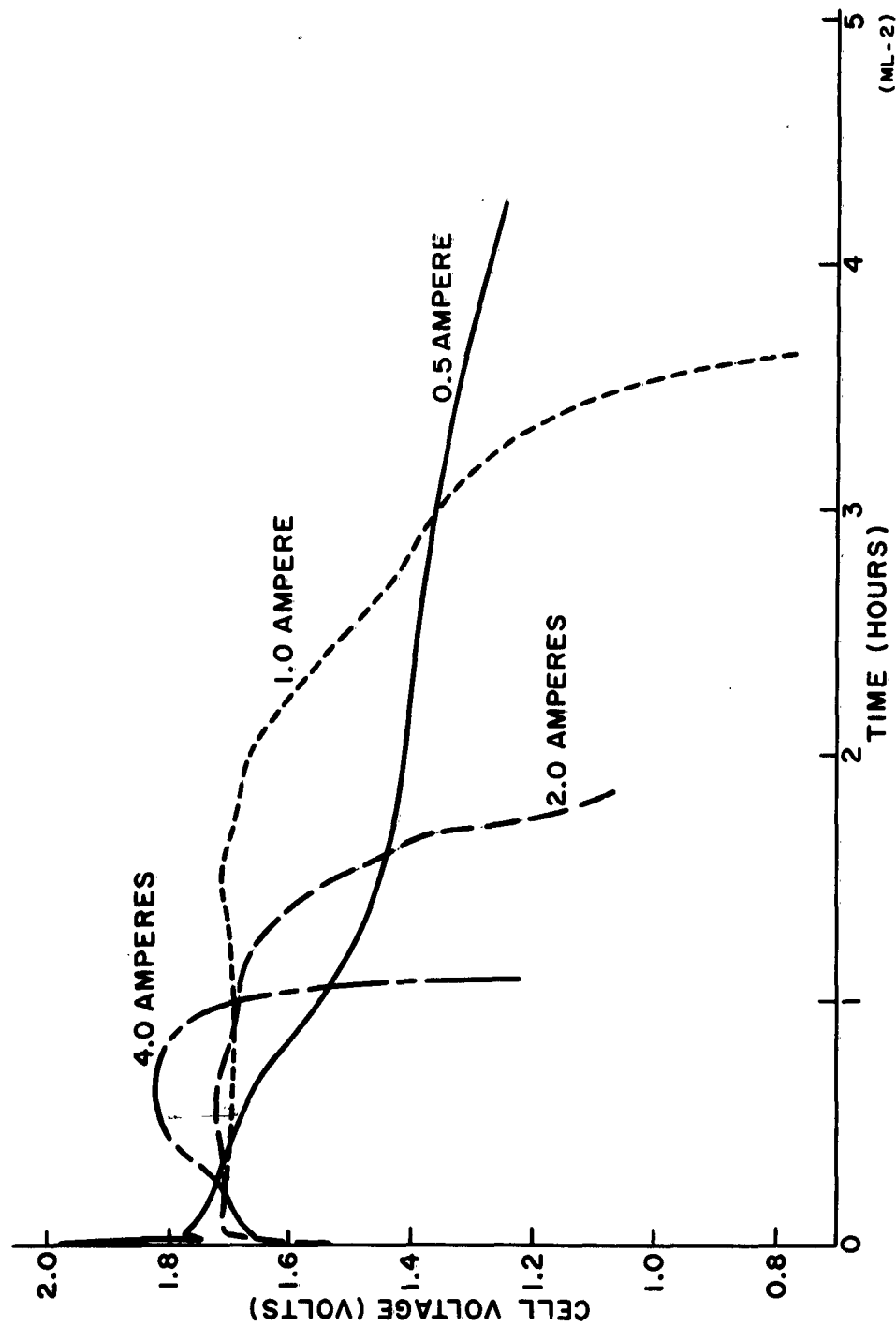


FIGURE 42. CAPACITY DATA FOR  $\text{Mg}/\text{Mg}(\text{ClO}_4)_2/\text{HgO}$  RESERVE CELLS AT VARIOUS DISCHARGE DRAINS AT  $-58^\circ\text{F}$ . ALL CELLS INSULATED.

magnesium-perchlorate electrolyte as in the previous single-cell tests and discharged at a one-ampere rate. Discharge curves for these batteries, both with and without polyurethane insulation, at an ambient temperatures of  $-40^{\circ}\text{F}$  and  $-58^{\circ}\text{F}$  are presented in Figures 43 and 44. The data show that full room-temperature capacity was obtained with the insulated battery at  $-40^{\circ}\text{F}$  and 85 percent of room temperature at  $-58^{\circ}\text{F}$ . For the non-insulated battery a 50-percent capacity was obtained to a 20-percent voltage-drop end point. The gradual decrease in voltage is caused by heat loss from the cells. It should be noted that magnesium/mercuric-oxide cells have an operating voltage of 1.20 volts at  $-40^{\circ}\text{F}$  where no heat is conserved.

Figure 45 shows the discharge characteristics of a six-cell magnesium/mercuric-oxide battery with a theoretical cathode capacity of 44.3 ampere-hours when it is discharged at 1.5 amperes at  $-40^{\circ}\text{F}$ , and is made with a one-half-inch-thick polyurethane foam jacket. Battery specifications and capacity data are summarized as follows:

Battery weight with insulation. . . . .	7.6 pounds
Battery volume with insulation. . . . .	.290 cubic inches
Capacity at $21.1^{\circ}\text{C}$	
Watt-hours per pound . . . . .	55
Watt-hours per cubic inch. . . . .	3.17*
Capacity at $-40^{\circ}\text{C}$	
Watt-hours per pound . . . . .	56
Watt-hours per cubic inch. . . . .	1.47*

\*Function of the design of the foam jacket.

Note: The thermal conductivity of the polyurethane insulation is 0.13 Btu/square foot/hour/inch. Comparison data given at  $68^{\circ}\text{F}$  were computed from a single cell discharged under ideal conditions. The low temperature battery was stored overnight at  $-40^{\circ}\text{F}$  and activated with  $-40^{\circ}\text{F}$  5N magnesium perchlorate electrolyte. The battery was then brought to a higher initial operating temperature by discharging it for five minutes at 10 amperes and using the available heat energy, which is evolved by the irreversibility and corrosion of the magnesium.

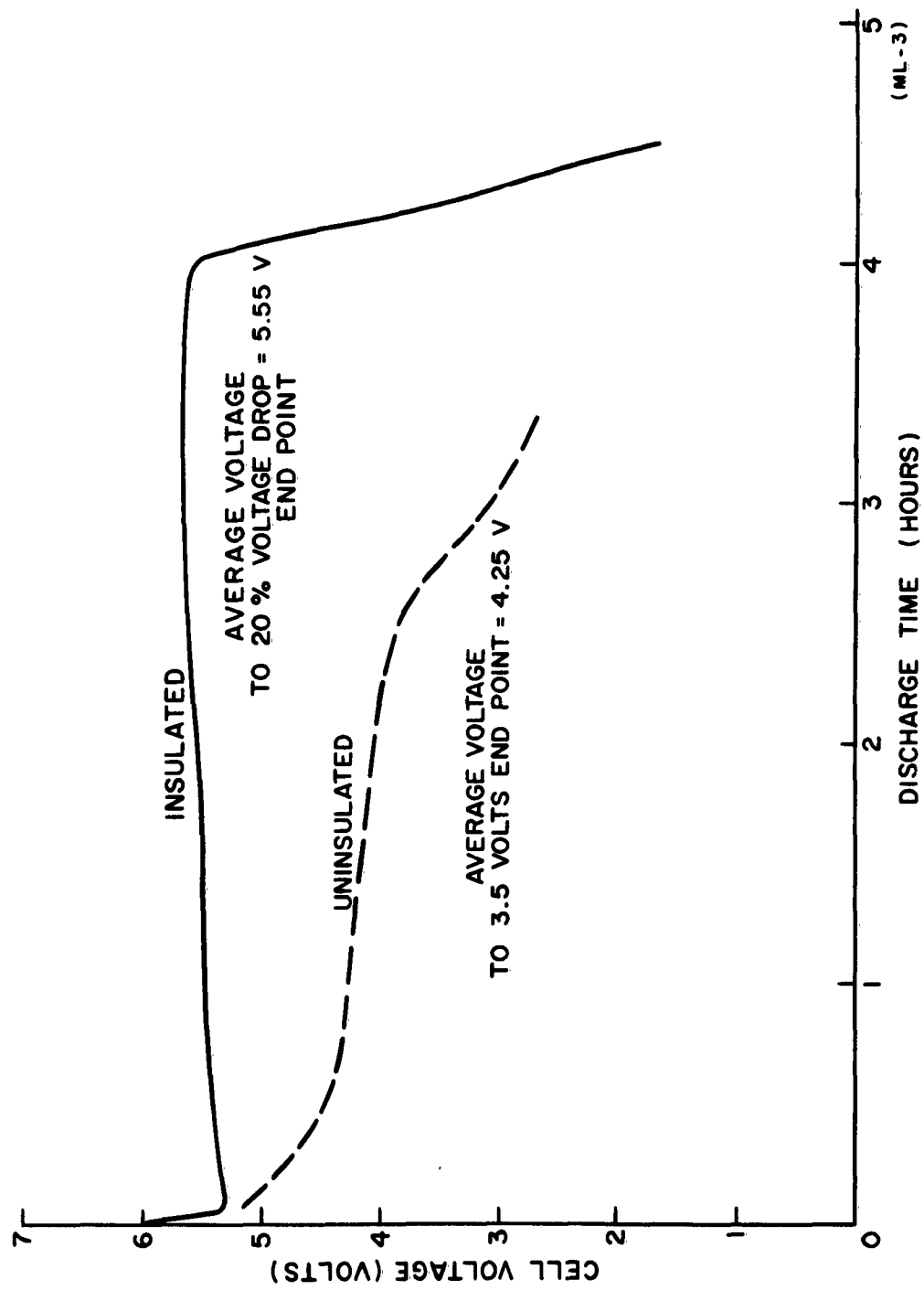


FIGURE 43. CAPACITY DATA FOR A 3-CELL  $\text{Mg}/\text{Mg}(\text{ClO}_4)_2/\text{HgO}$  RESERVE BATTERY AT  $-40^\circ\text{F}$ .

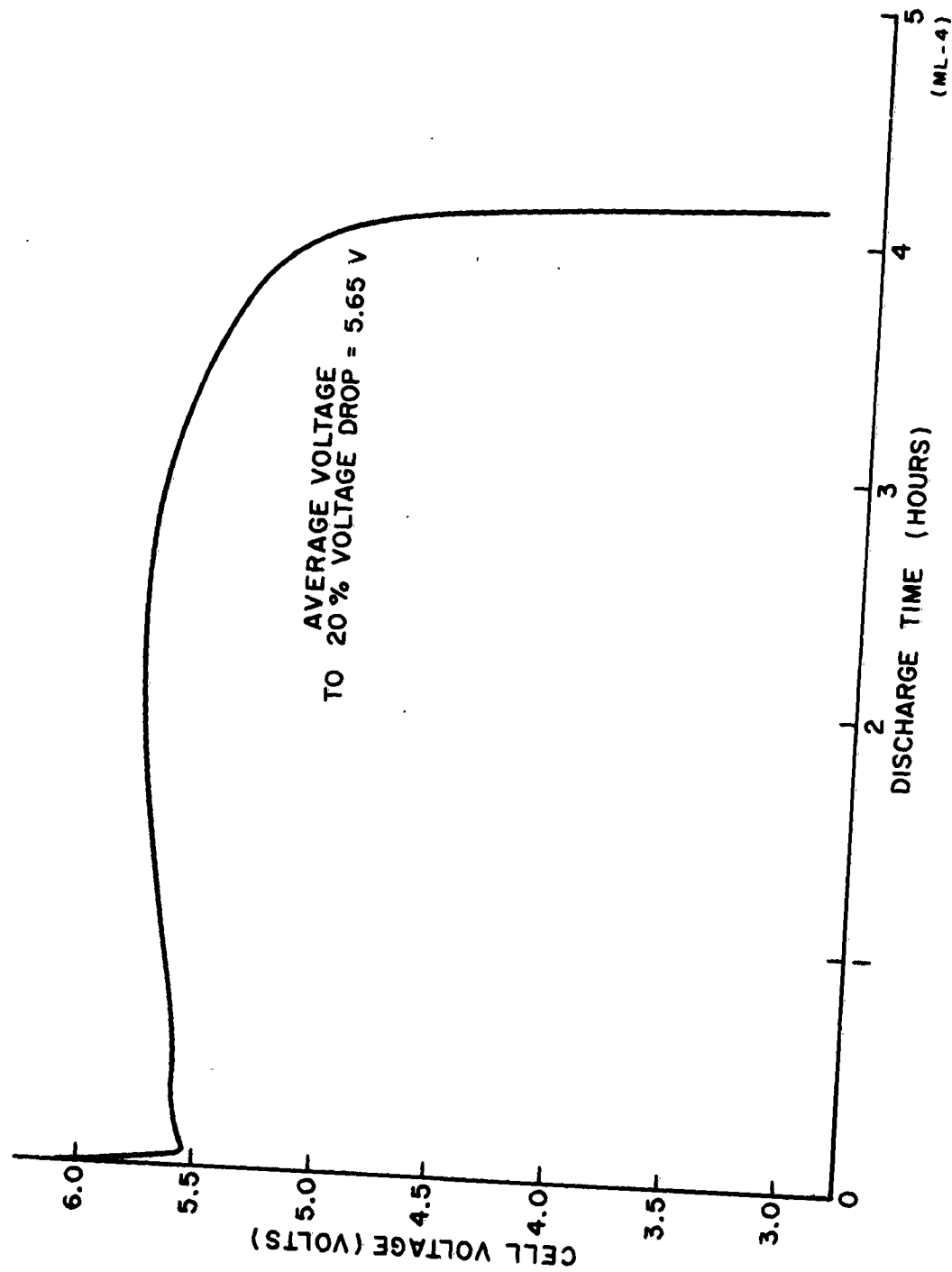


FIGURE 44. CAPACITY DATA FOR A 3-CELL  $\text{Mg}/\text{Mg}(\text{ClO}_4)_2/\text{H}_2\text{O}$  RESERVE BATTERY AT 1.0 AMPERE AT  $-58^\circ\text{F}$ . BATTERY CONTAINED IN AN INSULATED CASE.

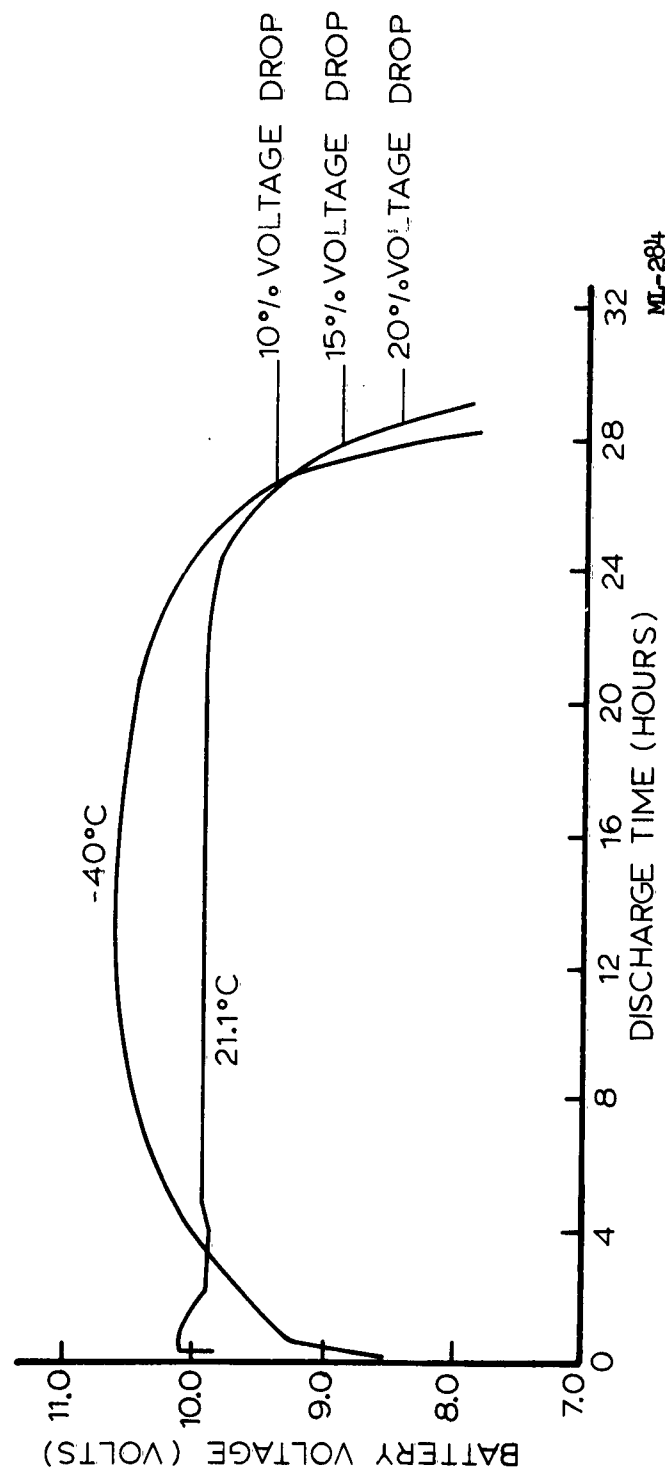


FIGURE 45. DISCHARGE CHARACTERISTICS OF A 6-CELL MAGNESIUM/MERCURIC-OXIDE BATTERY DISCHARGED AT 1.5 AMPERES AT 21.1°C AND -40°C.

### 3.2.3.8 Activated Stand Tests

Mercuric-oxide reserve cells with a theoretical cathode capacity of 185 ampere-minutes were constructed having pure-silver grids and AZ-31 magnesium anodes. The cells were activated in 2N magnesium-perchlorate electrolyte containing 1 gram/liter of lithium chromate, and were discharged at five amperes after various stand times. An activated-stand time of one week revealed a loss of five-percent capacity to a 20-percent voltage-drop point. The average voltage was 0.03 volts lower than a cell discharged after two minutes activation. The data are presented in Figure 46. Cells discharged after an activated-stand time of two weeks revealed complete corrosion of the magnesium. Similar cells tested with silver-plated copper grids failed because of excessive anode and grid corrosion.

The AZ-31 magnesium used in the above tests was not stabilized; surface treatment may offer some improvement in stand time. The data show that an activation-stand time of one week can be expected from the magnesium/magnesium-perchlorate/mercuric-oxide reserve system with its present design. The activation stand time of C.P. magnesium anodes would be much less than magnesium alloys; C.P. magnesium corrodes more readily than magnesium alloys.

### 3.2.3.9 Storage Tests

Capacity data were determined for magnesium/mercuric-oxide reserve cells with a theoretical cathode capacity of 276 ampere-minutes. The cell consisted of six AZ-31 anode plates and five 8:1-ratio cathode plates. These cells were stored at room temperature in plastic bags open to the atmosphere for a period of 19 months. Cell-discharge data at a constant current of 3.0 amperes are presented in Figure 47. A cathode efficiency of 86 percent was obtained as compared to an efficiency of 85 percent for the initial fresh-cell discharge. These results show that there was no loss in capacity over the 19-month storage time, and that this system exhibited good reserve-cell stability.

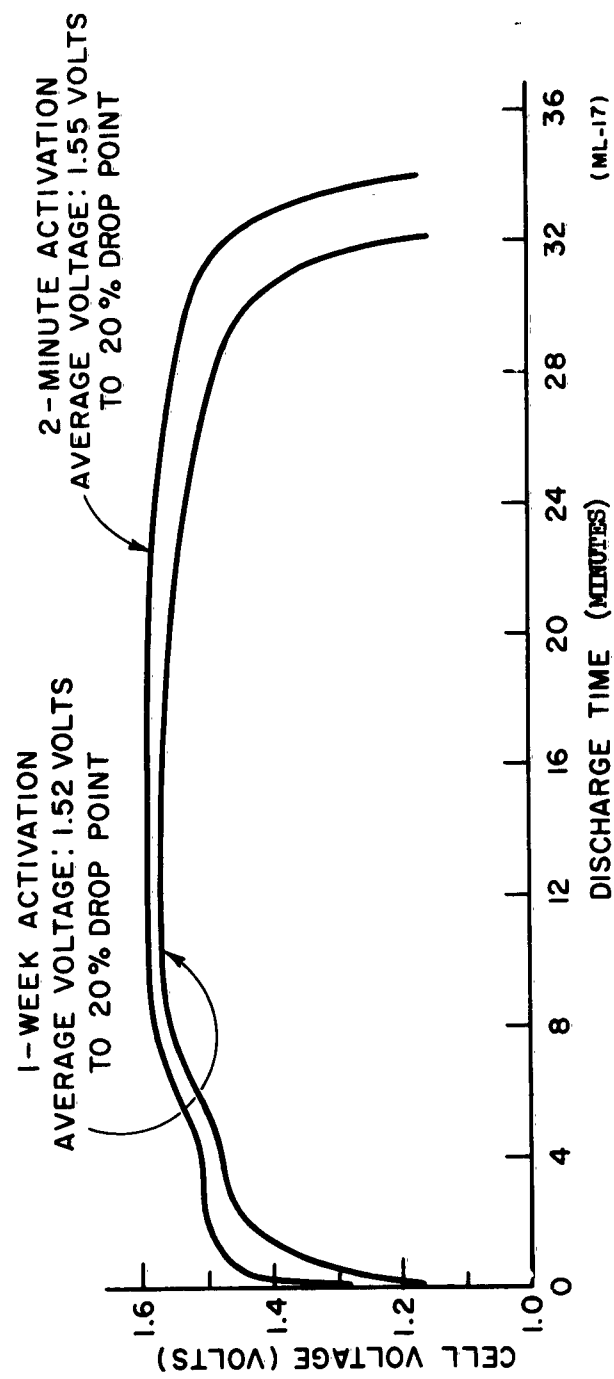


FIGURE 46. CAPACITY DATA FOR  $\text{Mg}/\text{Mg}(\text{ClO}_4)_2/\text{HgO}$  RESERVE CELLS WITH VARIOUS ACTIVATION TIMES DISCHARGED AT 5 AMPERES.



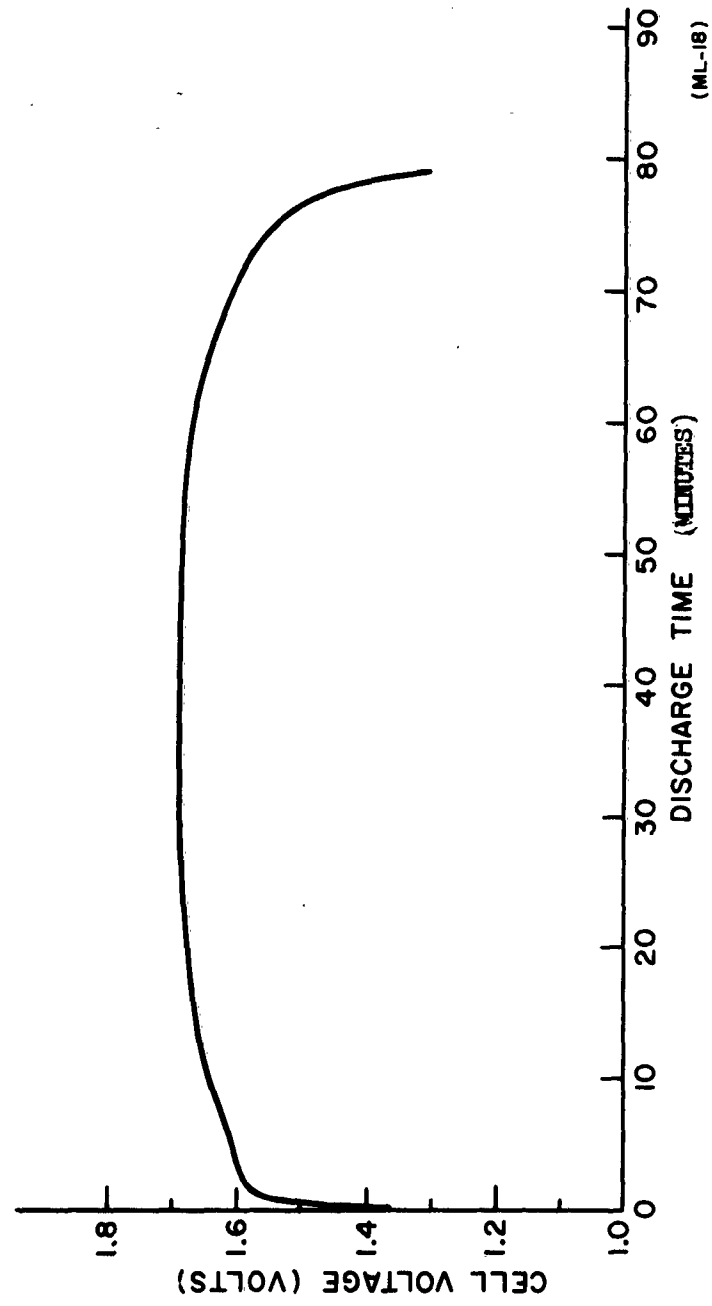


FIGURE 47. CHARACTERISTICS OF  $\text{Mg}/\text{Mg}(\text{ClO}_4)_2/\text{HgO}$  RESERVE CELL DISCHARGED AT 3.0 AMPERES AFTER 19-MONTHS STORAGE.

### 3.2.4 Comparison of Mercuric-Oxide and Cupric-Oxide Reserve Cells

Since the average operating voltage of a mercuric-oxide cell is approximately twice that of an equivalent cupric-oxide cell, a comparison of the discharge capacity between these two systems should be made on an equivalent-power-output basis or discharge rate. It should be noted that the cupric-oxide cell operates at twice the current density of the mercuric-oxide cell with the same number and size of plates.

A comparison of four-cathode-plate and five-anode-plate cells of equivalent size is given in Table XI.

The discharge curve for the cupric oxide cell is given in Figure 48. The discharge curve for the mercuric-oxide cell is given in Figure 24. These data show that the mercuric-oxide cell is more promising at high discharge rates. Further advantages of the mercuric oxide cell are shown in the polarization curves of Figures 49 and 50. These are discussed in detail below.

#### 3.2.4.1 High-Rate Polarization Studies

The beneficial effects of mercury compounds for increasing magnesium-anode efficiency in cupric-oxide cells were shown in the Second Quarterly Report. The mercuric-oxide cathode also acts to increase magnesium efficiency. This is due to the low solubility of mercuric oxide in the electrolyte.

Polarization studies at high current density (70°F) were carried out to determine the maximum current density for operation of the cupric-oxide and mercuric-oxide reserve cells. Test cells consisted of a single two-inch-square, .014-inch-thick C.P. magnesium anode plate and two cupric-oxide cathode plates in excess 2N magnesium-perchlorate electrolyte. A silver/silver-chloride reference electrode was included in the cell. The results are plotted in Figures 49 and 50.

The data shows that both the cupric-oxide and mercuric-oxide cathodes polarize only slightly, while the anode polarizes badly, at the higher

DESCRIPTION	RESERVE CELL	
	MAGNESIUM/ MERCURIC-OXIDE	MAGNESIUM/ CUPRIC-OXIDE
Theoretical Cathode Capacity, (ampere-minutes)	171	340
Discharge Current (amperes)	10	20
Discharge Time, 20% Cutoff (minutes)	13.6	11.0
Average Voltage (volts)	1.645	0.815
Watts	16.45	16.3
Cathode Efficiency (percent)	79.5	64.7
Element Weight, Wet (grams)	41.0	40.4
Watt-Hours Per Pound of Element Weight	41.3	33.6

MT-56

TABLE XI. COMPARISON OF FOUR-CATHODE AND FIVE-ANODE-PLATE RESERVE CELLS OF EQUIVALENT SIZE.

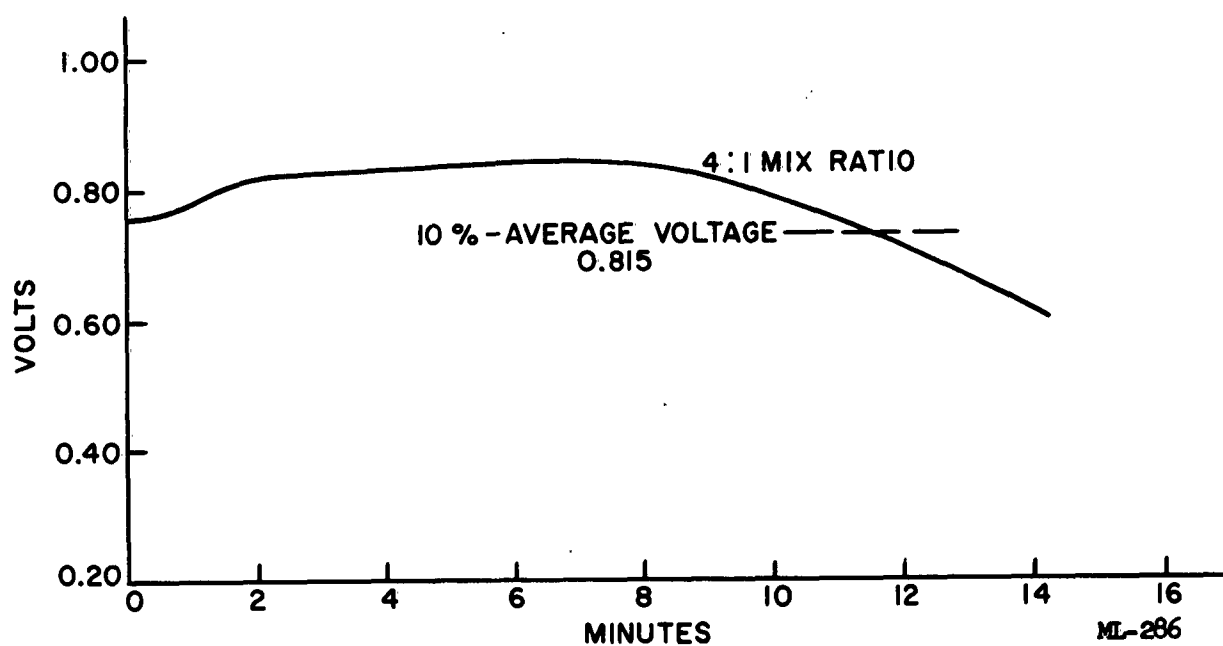


FIGURE 48. CAPACITY FOR A  $\text{Mg}/\text{Mg}(\text{ClO}_4)_2/\text{CuO}$  RESERVE CELL DISCHARGED AT 20.0 AMPERES.

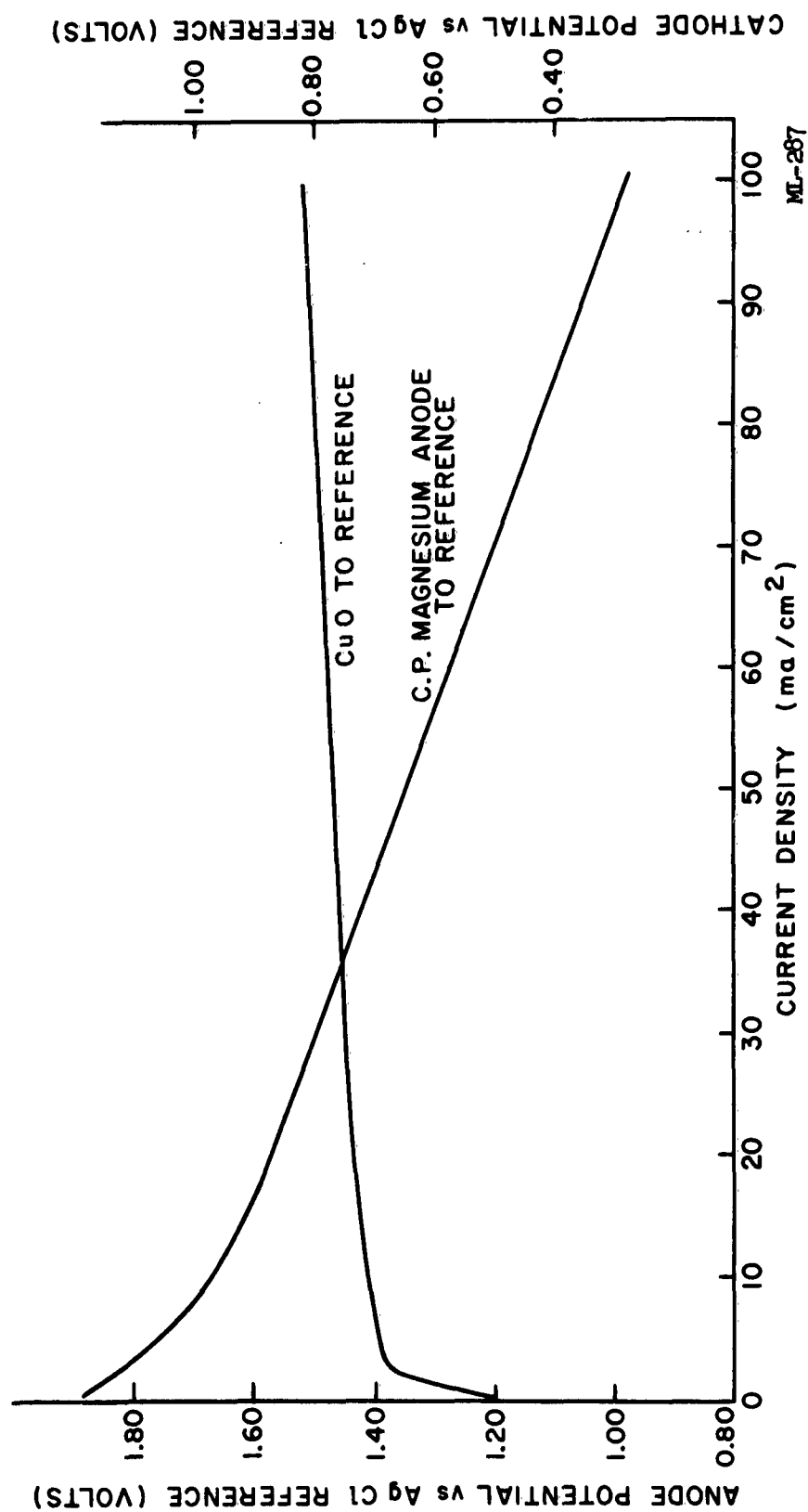


FIGURE 49. EFFECT OF CURRENT DENSITY ON THE ELECTRODE POTENTIALS OF A  $\text{Mg}/\text{Mg}(\text{ClO}_4)_2/\text{CuO}$  RESERVE CELL.

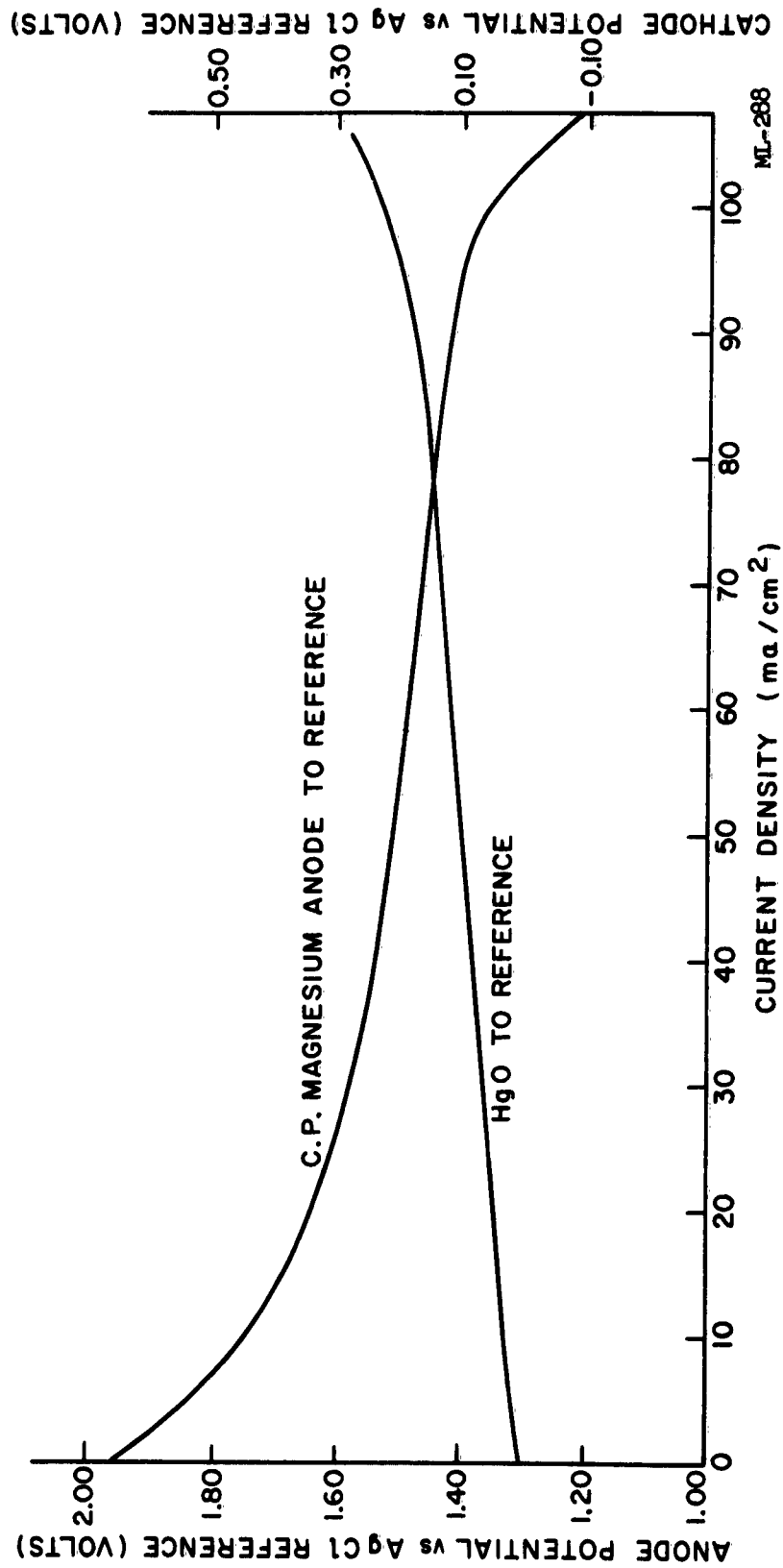


FIGURE 50. EFFECT OF CURRENT DENSITY ON THE ELECTRODE POTENTIALS OF A  $\text{Mg}/\text{Mg}(\text{ClO}_4)_2/\text{HgO}$  RESERVE CELL.

current densities. A marked difference is noted in the magnesium polarization between the two cells. The curve for the mercuric-oxide cell is much flatter with increase in current density and the magnesium operates at a higher potential. These results are probably due to a dual effect of mercury on the magnesium electrode. The mercury disrupts the oxide film, permitting the magnesium anode to operate at a higher potential; the mercury also acts as a cathodic inhibitor, reducing the rate at which hydrogen is evolved at the local cathodes on the magnesium anode.

The data illustrate the advantage of the mercuric-oxide cell over the cupric-oxide in that it operates at a lower current density for the same power output.

Comparison of the data for cupric-oxide and mercuric-oxide cells shows that watt-hour capacities are similar at the one-half-hour discharge rate at the present state of development. The mercuric-oxide system has the advantages, however, of higher, flatter voltage characteristics, lower current density operation, and less heat to dissipate per watt-hour-of-electrical-energy output. Further cupric-oxide mix and component development should result in capacity improvement to the 50-watt-hour-per-pound range.

### 3.2.5 Magnesium-Manganese Dioxide Reserve Cells

#### Room-Temperature Studies

Capacity data were determined for magnesium/manganese-dioxide reserve cells in 5N magnesium-perchlorate electrolyte to the 0.9-volt cutoff point. The cells were discharged at constant-current drains of 2.0, 1.0, 0.5, and 0.25 amperes at room temperature. Cells for this study were constructed with four 2x2-inch manganese-dioxide cathode plates having a 10:1 ratio of manganese dioxide to Shawinigan carbon black, and a theoretical capacity of 205 ampere-minutes.

Five 2 x 2 x .010-inch C.P. magnesium plates were used as the anode. The cell cases were of uninsulated, rigid plastic. Cells were activated for 15 minutes with 30 ml of electrolyte prior to discharge.

The capacity data are presented in Figures 51 and 52. These data show a drop in efficiency for the 0.25-ampere discharge because of excess magnesium corrosion. This condition also existed with the magnesium/mercuric-oxide system, as stated previously. An AZ-21 or AZ-31 alloy must be used to offset the corrosion effects.

#### 3.2.5.1 Low-Temperature Studies

Characteristics at -20 and -40°F were obtained for manganese-dioxide cells enclosed in an uninsulated plexiglass case. The cells and electrolyte were conditioned at the ambient temperature for 16 hours prior to activation and discharge. Discharge was started approximately 15 minutes after activation.

The capacity data for single cells discharged at constant-current drains of 0.25 to 2.0 amperes, and at temperatures as low as -40°F, are presented in Table XII. Figures 53 through 56 show the resulting discharge curves obtained from this data. Cathode efficiencies at various temperatures and current drains are presented in Table XIII, and indicate that efficiency at -20 and -40°F is independent of current drain.

It is apparent from the above studies that magnesium/manganese-dioxide batteries can be designed with excellent low-temperature characteristics. If these cells were insulated for performance at these low temperatures, they would most probably have an increase in capacity similar to that of the magnesium/mercuric-oxide system.

#### 3.2.5.2 Anode Efficiency

During discharge of mercuric-oxide cells, mercury metal is deposited on the magnesium anode causing a decrease in the corrosion reaction and resultant hydrogen evolution. The anode efficiency of cells, with a 6:1 ratio cathode calculated by magnesium weight loss was approximately 81 percent at the 10-ampere drain. This agrees with the data obtained for the mercuric chromate inhibitor in copper-oxide reserve cells.

#### 3.2.5.3 Efficiency vs. Temperature Study

A program was set up to measure the anode efficiency of magnesium/magnesium-



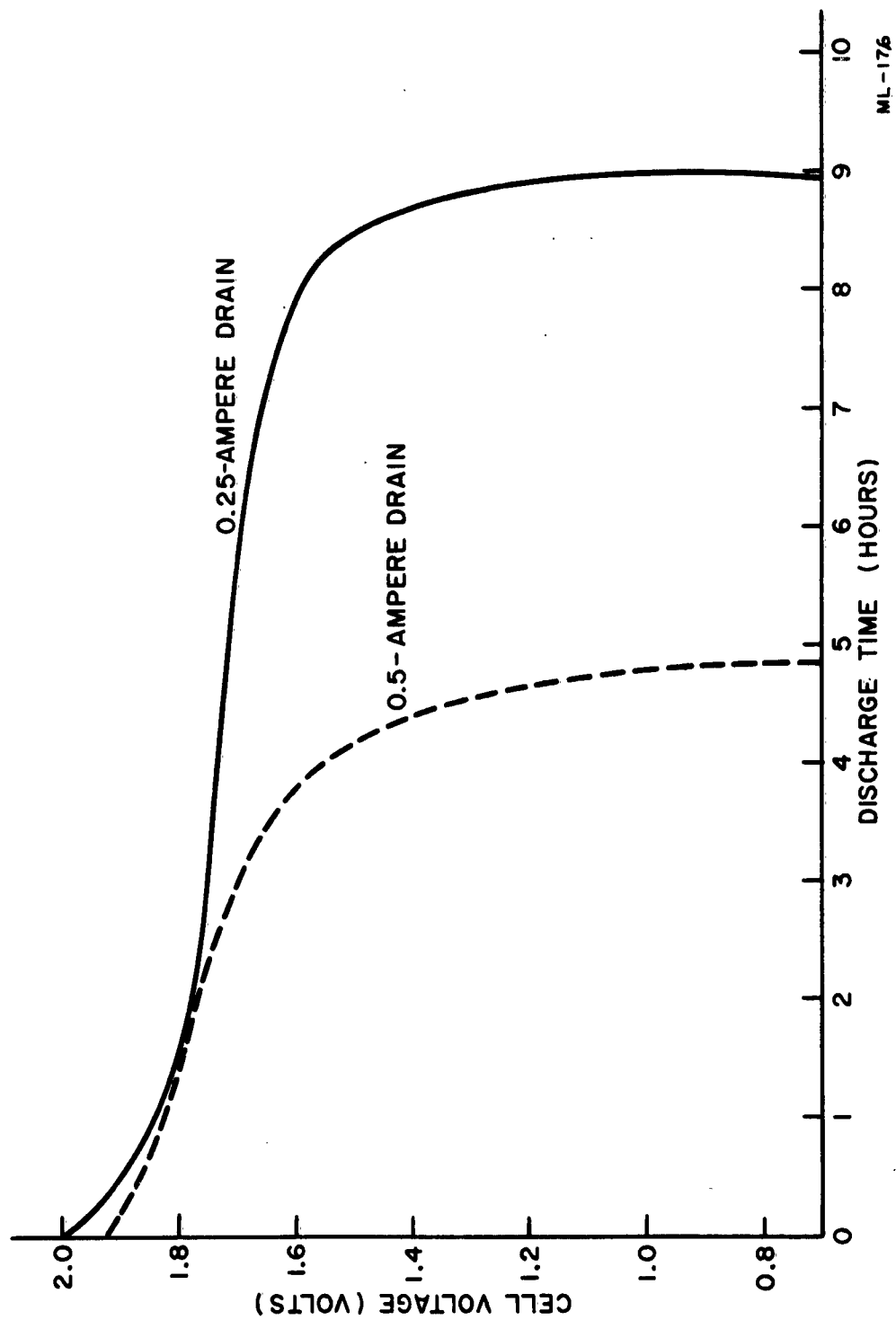


FIGURE 51.  $\text{Mg/Mg}(\text{ClO}_4)_2/\text{MnO}_2$  RESERVE CELLS DISCHARGED AT 70°F.

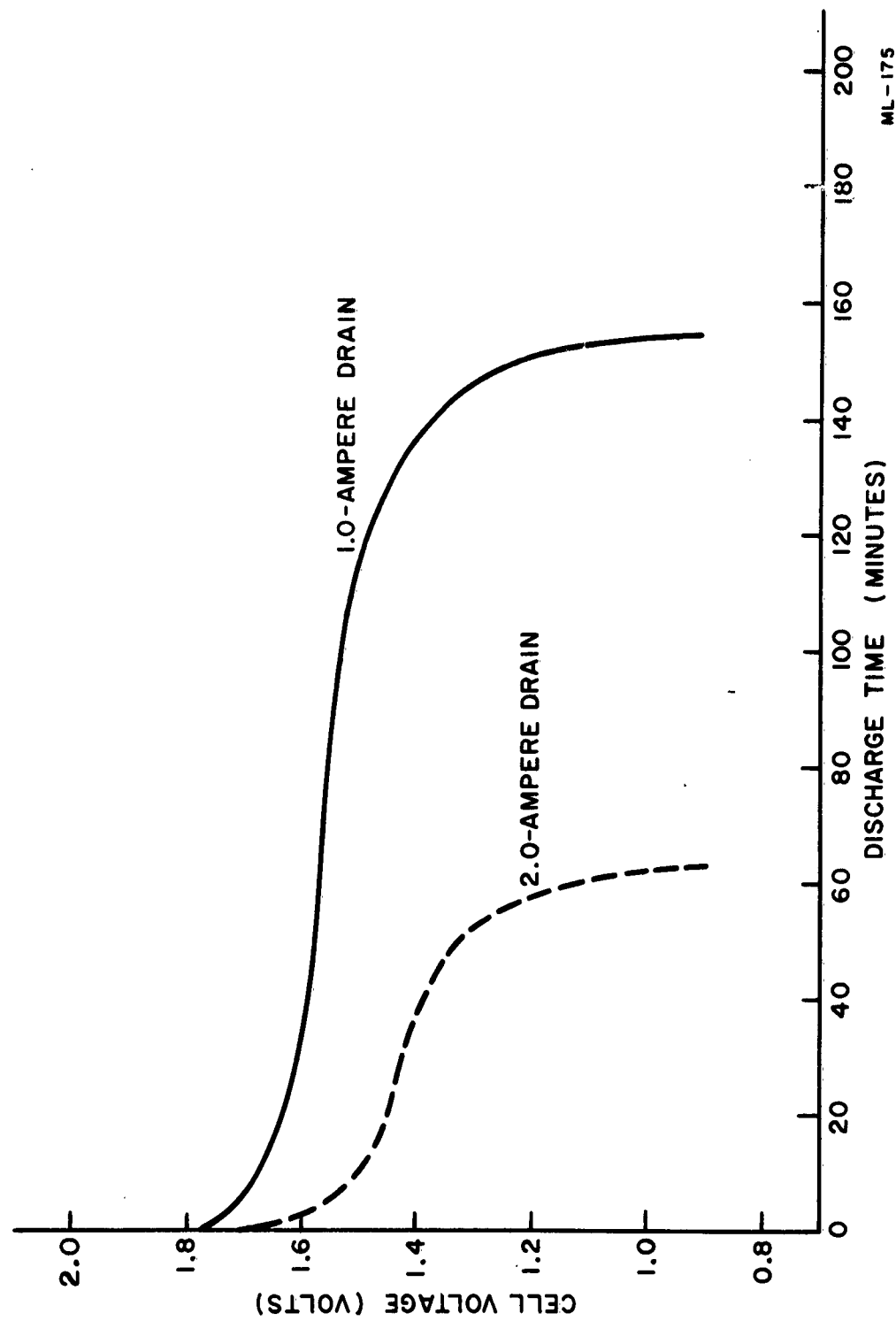


FIGURE 52.  $\text{Mg}/\text{Mg}(\text{ClO}_4)_2/\text{MnO}_2$  RESERVE CELLS DISCHARGED AT 70°F.

DISCHARGE CURRENT (amperes)	AMBIENT TEMPERATURE (°F)	CAPACITY TO 0.9-VOLT CUTOFF	
		DISCHARGE TIME (hours)      (minutes)	AVERAGE VOLTAGE (volts)
0.25	72	9            --	1.60
	-20	5            33	1.38
	-40	5            20	1.26
0.50	72	—            50	1.68
	-20	3            3	1.27
	-40	2            14	1.20
1.0	72	2            35	1.55
	-20	1            27	1.28
	-40	1            8	1.20
2.0	72	1            3	1.43
	-20	-            45	1.22
	-40	-            35	1.11

MT-19

TABLE XII. CAPACITY DATA FOR  $\text{Mg}/\text{Mg}(\text{ClO}_4)_2/\text{MnO}_2$  SYSTEM.

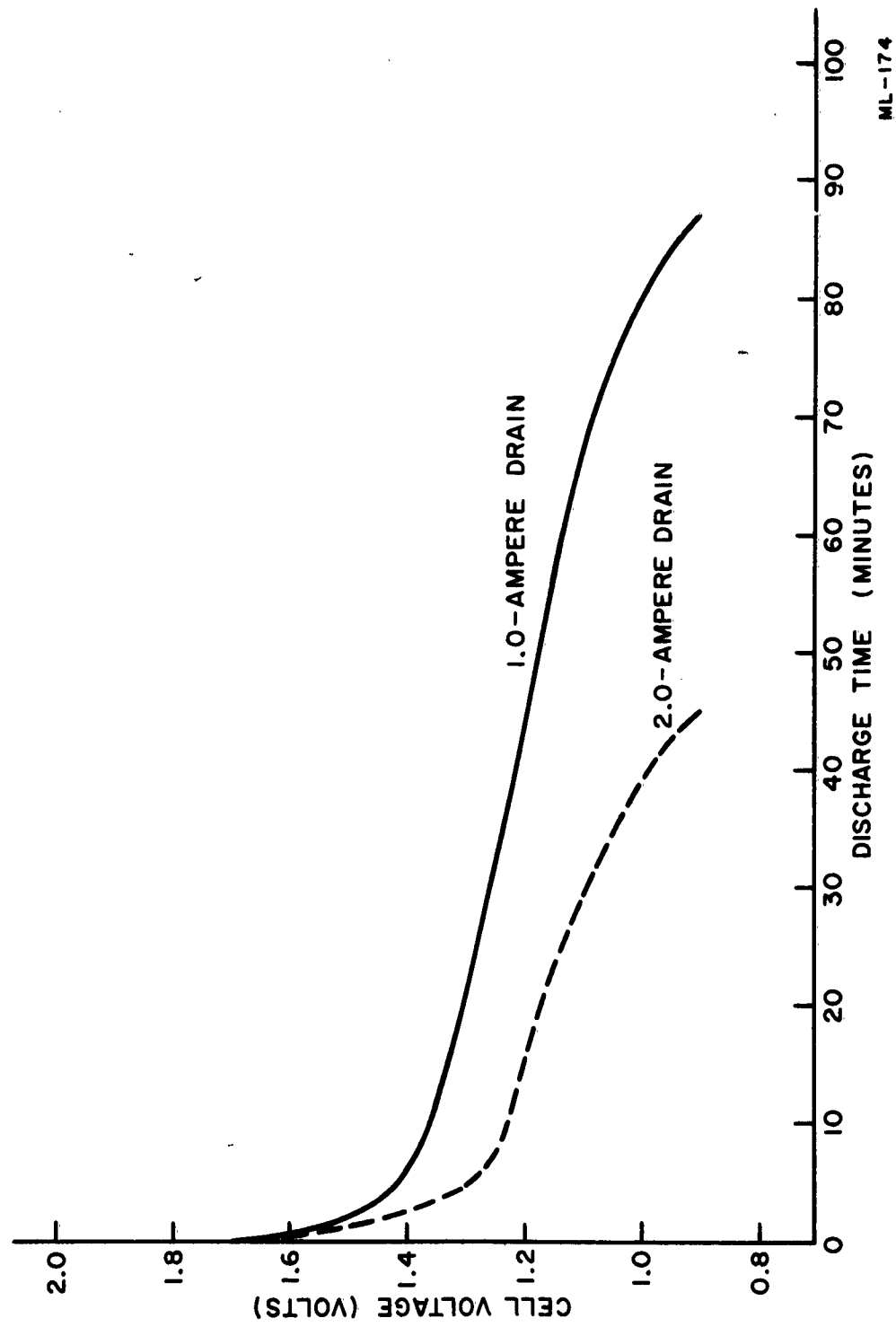


FIGURE 53.  $\text{Mg}/\text{Mg}(\text{ClO}_4)_2/\text{H}_2\text{O}_2$  RESERVE CELLS DISCHARGED AT  $-20^\circ\text{F}$ .

ML-174

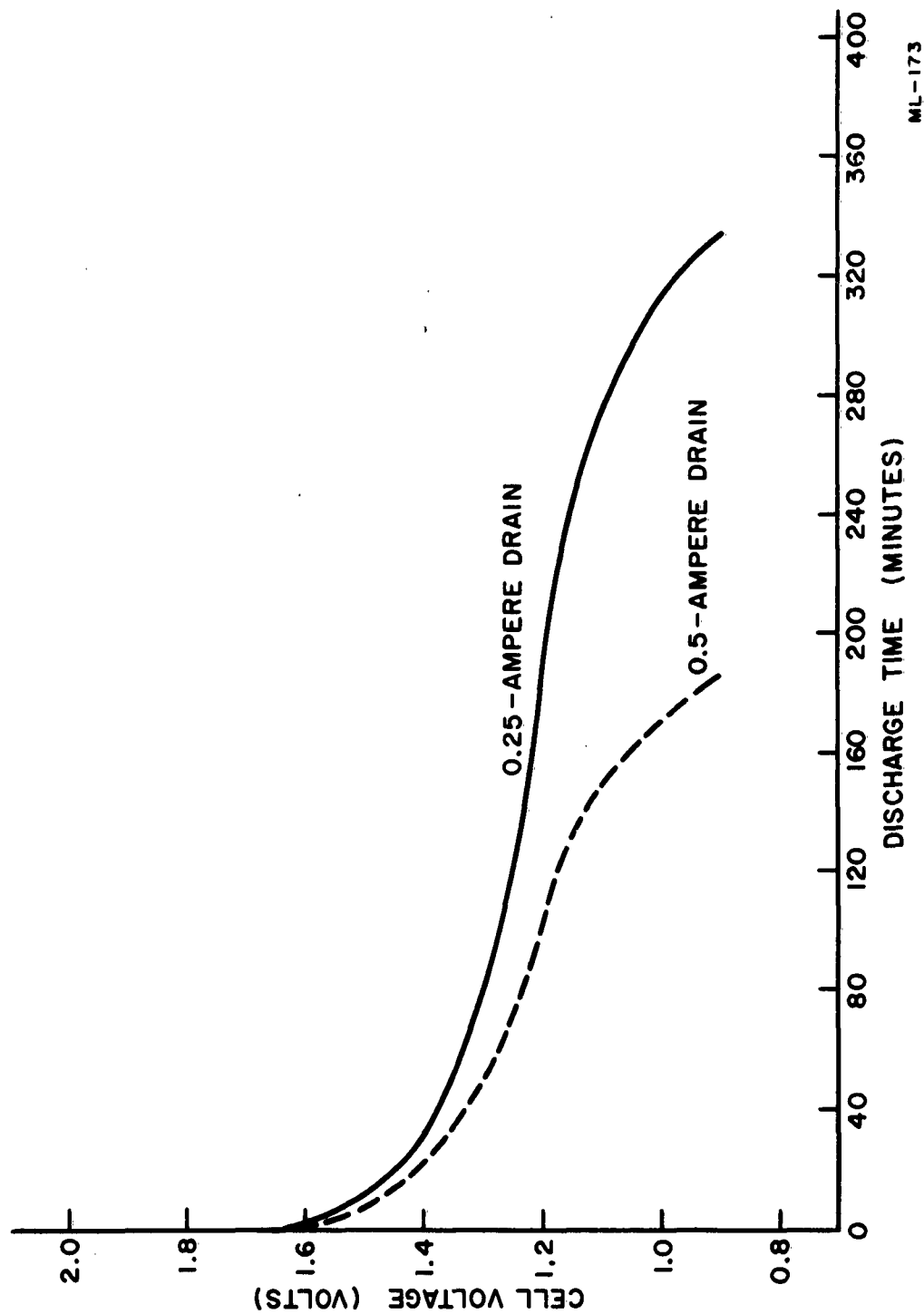


FIGURE 54.  $\text{Mg}/\text{Mg}(\text{ClO}_4)_2/\text{MnO}_2$  RESERVE CELLS DISCHARGED AT  $-20^\circ\text{F}$ .

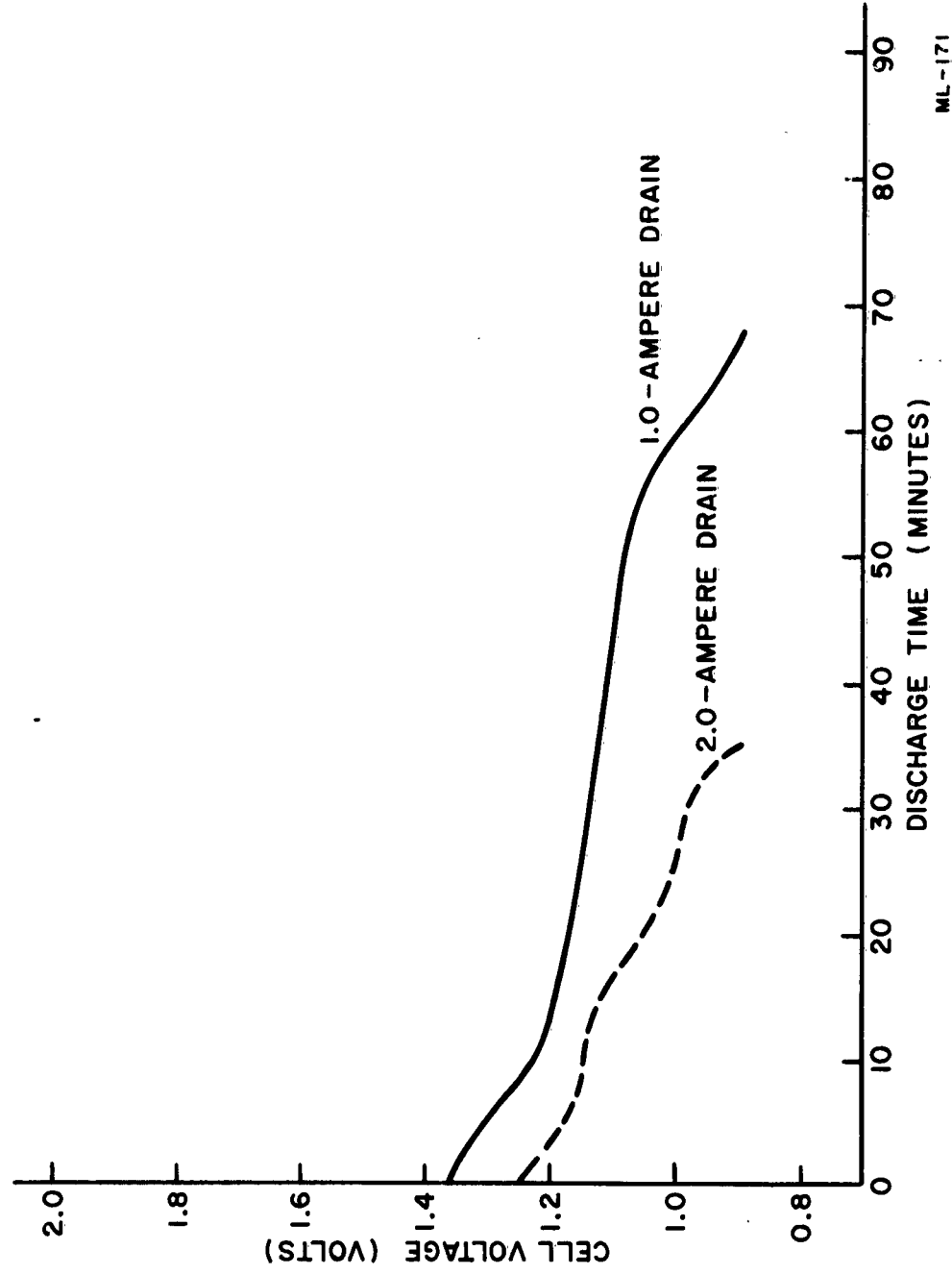
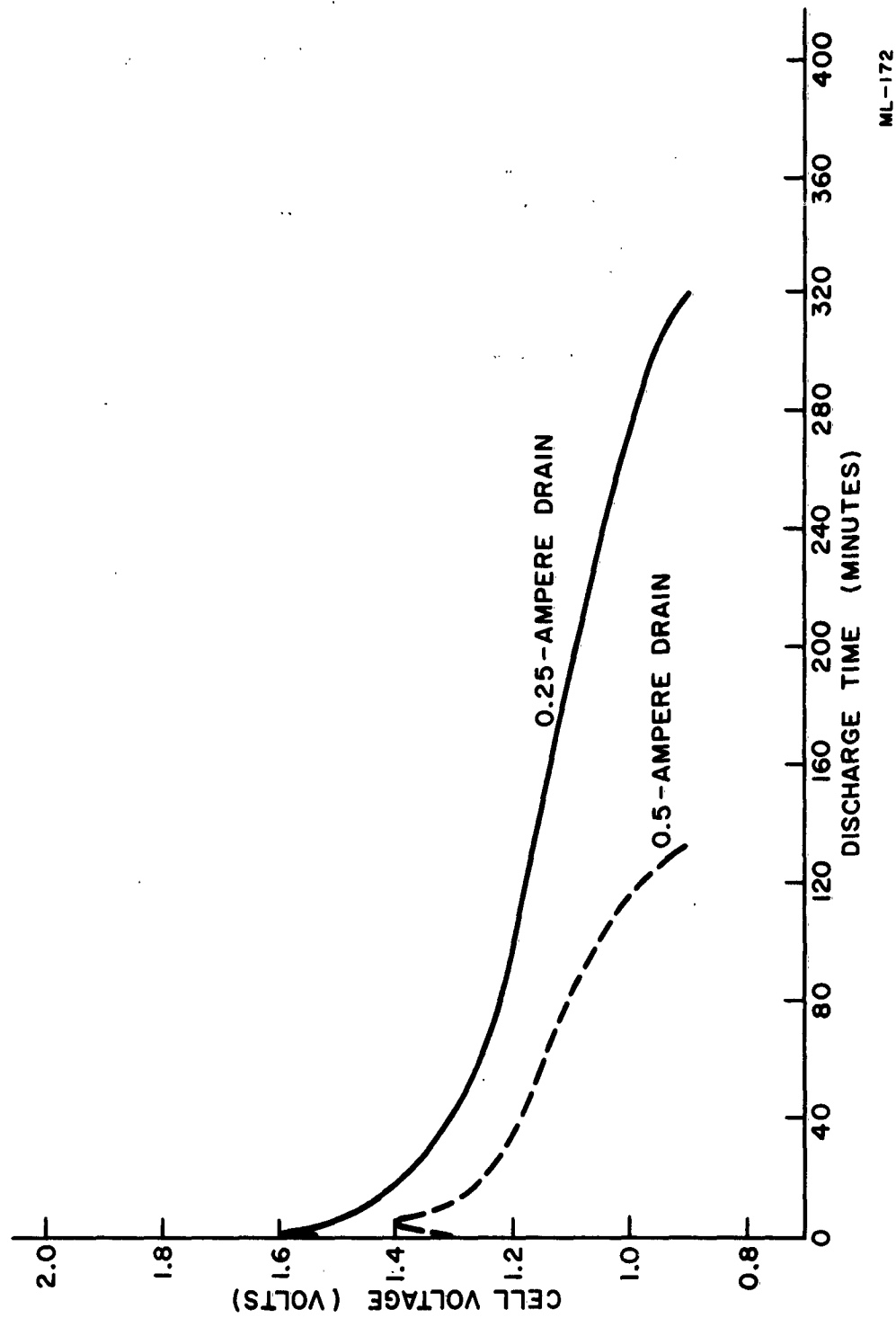


FIGURE 55.  $\text{Mg}/\text{Mg}(\text{ClO}_4)_2/\text{MnO}_2$  RESERVE CELLS DISCHARGED AT  $-40^\circ\text{F}$ .

ML-171



ML-172

FIGURE 56.  $\text{Mg}/\text{Mg}(\text{ClO}_4)_2/\text{MnO}_2$  RESERVE CELLS DISCHARGED AT  $-40^\circ\text{F}$ .

CURRENT DRAIN (amperes)	CATHODE EFFICIENCY TO 0.9 VOLT (PERCENT)		
	72°F	-20°F	-40°F
2.0	61	44	34
1.0	75	43	33
0.5	70	45	32
0.25	66	41	39

MT-20

TABLE XIII. CATHODE EFFICIENCY OF  $\text{Mg}/\text{Mg}(\text{ClO}_4)_2$  AT VARIOUS  
CURRENT DRAINS AND TEMPERATURES.



perchlorate cells as a function of temperature. Tests included efficiency measurements of commercially pure magnesium, AZ-10, AZ-21, and AZ-31 alloys at both high and low current densities. Studies were conducted at a current density of  $1.5 \text{ ma/cm}^2$  and results are included in the following section.

#### Test Procedure

Test cells were assembled using two 1-3/8 x 2-inch copper-oxide reserve-cell cathode plates and one 1-3/8 x 2-inch magnesium anode plate having a total surface area of  $35.5 \text{ cm}^2$ . Anode plates were prepared by degreasing in acetone and pickling in an aqueous solution of 400 cc/l glacial acetic acid and 50 g/l sodium nitrate. The cells were placed in a plastic bag, perforated at top and bottom and held in position with tape. A silver/silver-chloride reference electrode was included in the cells for half cell measurements.

The cells were positioned in a 400 ml beaker with plastic spacers. The beaker was filled with 2N magnesium perchlorate, and immersed in a constant temperature water bath with a  $\pm 1^\circ\text{C}$  variation.

Discharge was started, 15 minutes after filling with electrolyte, at a constant current of  $1.5 \text{ ma/cm}^2$ . The discharge was terminated after several hours and the cells were placed in deionized water. The oxide film was removed from the magnesium anodes by dipping in an aqueous 250 g/l chromate solution with 10 g/l silver nitrate, washing in deionized water, and drying with acetone. The loss in weight was determined by weighing on an analytical balance before and after discharge.

Data for cells containing C.P. magnesium anodes and AZ-10 alloy anodes discharged at  $1.5 \text{ ma/cm}^2$  over a temperature range of  $20^\circ$  to  $70^\circ\text{C}$  are presented in Figure 57. It is seen that anode efficiency decreased sharply initially with increase in temperature and leveled off between  $50^\circ$  and  $70^\circ\text{C}$ . The efficiency of AZ-10 alloy at  $25^\circ\text{C}$  was 62 percent, which is 10 to 15 percent lower than the maximum efficiency obtained at higher current densities.

A  $1.5 \text{ ma/cm}^2$  drain corresponds approximately to a 75-hour rate for an AA-size magnesium/magnesium-perchlorate/magnesium-dioxide (type M) cell and

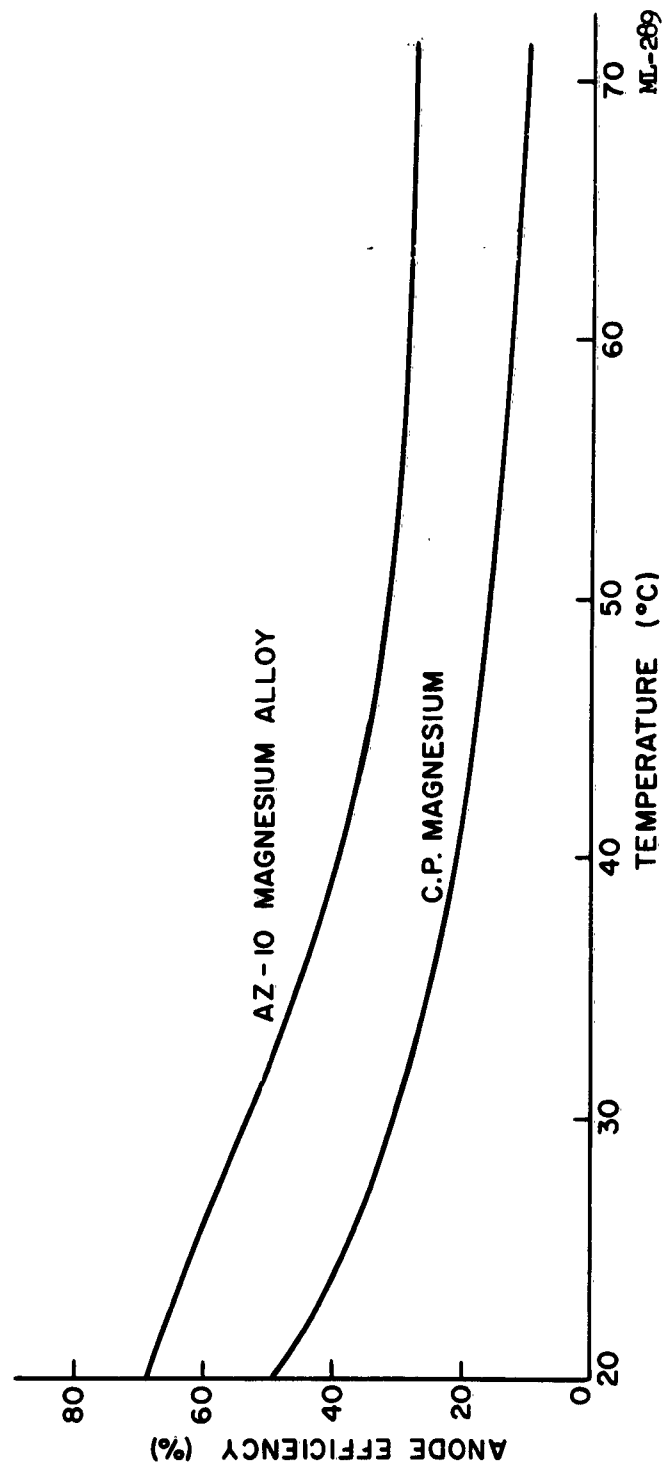


FIGURE 57. EFFECT OF TEMPERATURE ON ANODE EFFICIENCY OF VARIOUS MAGNESIUM ALLOYS IN 2N  $\text{Mg}(\text{ClO}_4)_2$  AT CURRENT DENSITY OF 1.5 MA/ $\text{CM}^2$ .

a 100-hour rate for an AA-size magnesium/magnesium perchlorate/copper oxide cell. It is seen that in batteries without a suitable heat sink, the temperature of the cells could build up during discharge, causing a decrease in the magnesium efficiency and overall cell capacity. This problem is obviously enhanced at higher current densities with the increased rate of heat evolution and presents a very definite design problem. It should be noted that the AZ-10 magnesium anode operates at 30 percent efficiency at 55°C, with the remaining 70 percent going into the heat-producing and water-consuming corrosion reaction.

The data for cells containing C.P. magnesium, AZ-10, AZ-21, and AZ-31 alloys are presented in Figure 58. A slight decrease in efficiency was obtained with the various alloys over the temperature range, 20 to 70°C. This decrease would have little effect on magnesium cell performance. Corrosion of pure magnesium, however, is accelerated above 30°C, with the efficiency dropping to 40 percent at 70°C. This increase in corrosion rate with temperature increase results in an increase in operating voltage level in high-rate reserve cells. However, it will result in a cell-capacity drop if not properly controlled. Proper battery design must be used to distribute heat evolved during the cell reaction and prevent local overheating.

#### Efficiency vs. Duty Cycle Study

Previous studies have shown poor performance of magnesium cells on intermittent service. A program was set up to determine limitations of the magnesium anode in this type of application.

Test cells were constructed with AZ-10 and AZ-21 alloy similar to the efficiency-temperature study cells summarized in the Second Quarterly Report. The test procedure consisted of discharging cells at room temperature in excess 2N magnesium perchlorate electrolyte on a constant-current drain of 10 ma/cm<sup>2</sup> for 15-minute intervals with varying times on open circuit.

The average efficiency data for magnesium are plotted in Figure 59. The efficiency was found to decrease 10 to 15 percent for a 15-minute closed-circuit/two-hour open circuit-duty cycle, with a constant value

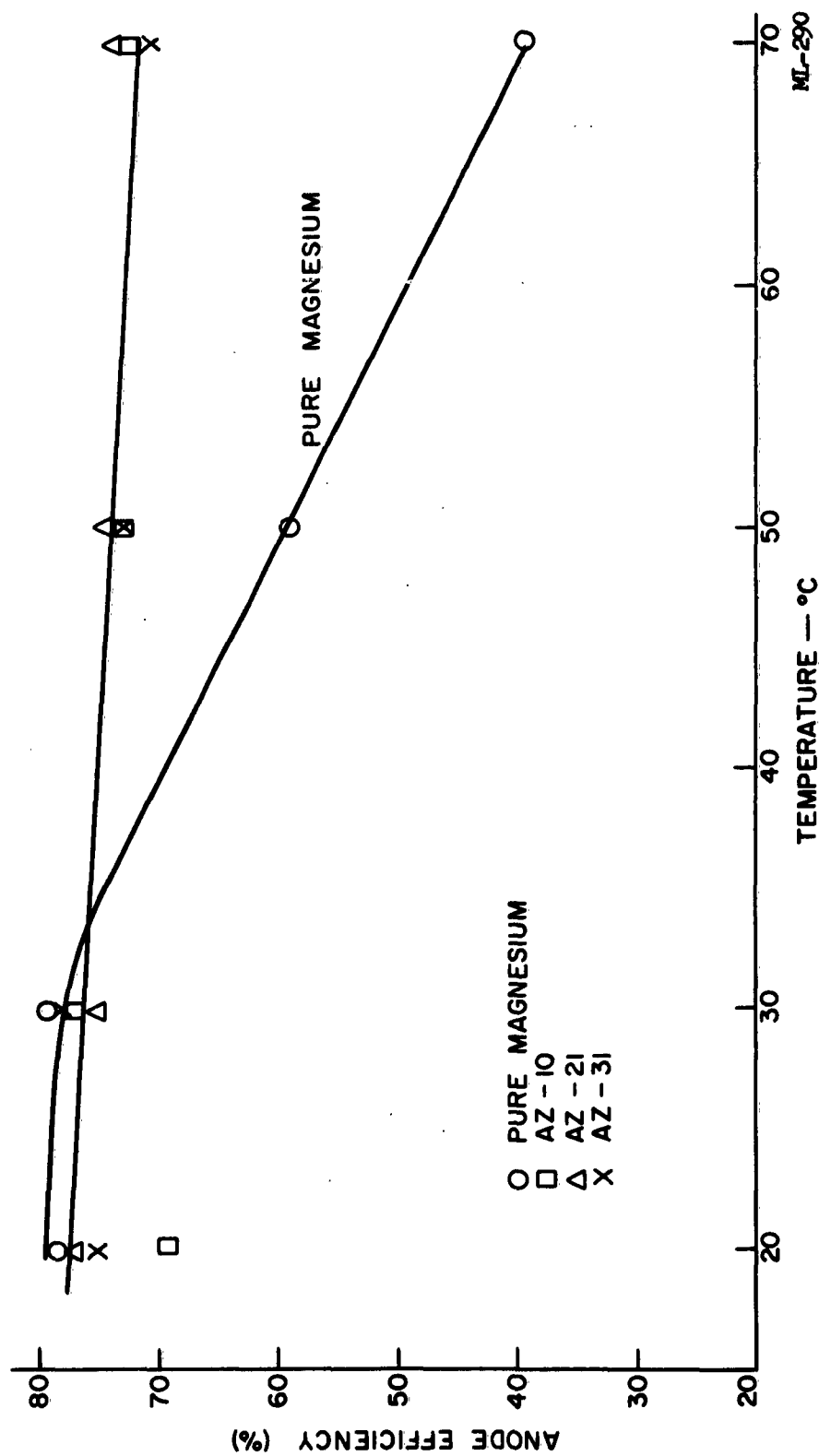


FIGURE 58. EFFECT OF TEMPERATURE ON ANODE EFFICIENCY OF VARIOUS MAGNESIUM ALLOYS IN 2N  $\text{Mg}(\text{ClO}_4)_2$  AT A CURRENT DENSITY OF 10.0 MA/ $\text{CM}^2$ .

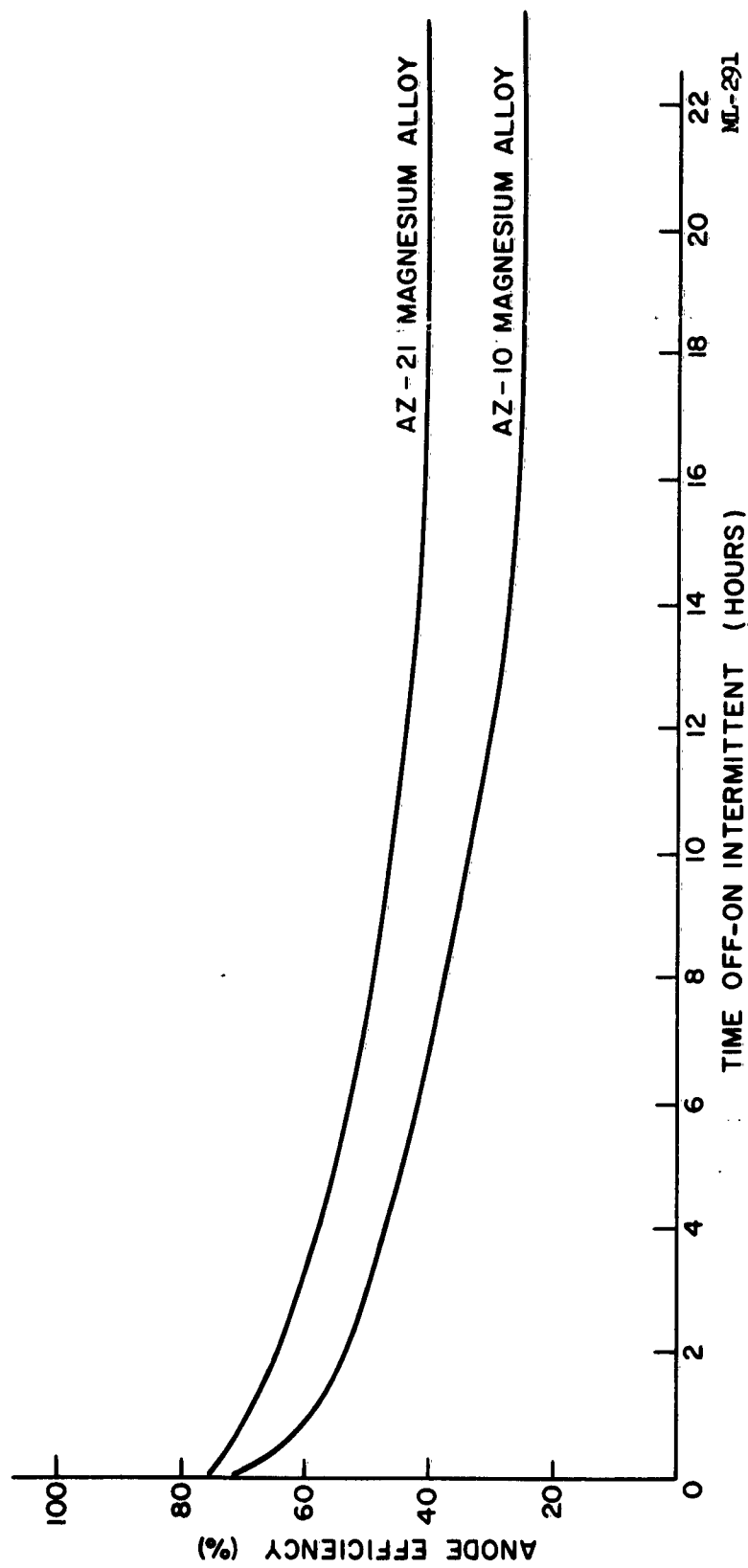


FIGURE 59. EFFECT OF OPEN-CIRCUIT TIME OFF ON THE ANODE EFFICIENCY OF  $\text{Mg}/\text{Mg}(\text{ClO}_4)_2/\text{CuO}$  CELLS DISCHARGED AT  $10.0 \text{ MA}/\text{CM}^2$  FOR 15 MINUTES.

being reached on a 15-minute closed-circuit/16-hour open-circuit duty cycle. The efficiency on a 15-minute closed-circuit/24-hour open-circuit duty cycle averaged 25 percent for the AZ-10 alloy and 40 percent for the AZ-21.

#### Test Cell Composition

A manganese-dioxide cell with a reserve-type cathode, was selected over a cupric-oxide cell to avoid accelerated magnesium corrosion caused by a possible copper solubility at low-current densities. The cathode-mix composition used was as follows:

MnO <sub>2</sub> (Type M). . . . .	148 g
Shawinigan carbon black. . . . .	17.0 g
BaCrO <sub>4</sub> . . . . .	5.0 g
Mg(OH) <sub>2</sub> . . . . .	5.0 g
CMC Solution, 1.5 percent. . . . .	120.0 ml

Cathode plates were made using 1.375 x 2-inch silver-plated 5Cu5-4/0 expanded-copper-screen grids and four grams of the above mixture per plate, with filter paper as the separator. Test cells were assembled using two cathode plates and one 1.375 x 2 x .022-inch AZ-21XA magnesium anode plate. The theoretical cathode capacity was 74.4 ampere-minutes. This is comparable to a AA-size magnesium/magnesium-perchlorate/manganese-dioxide cell which has a theoretical cathode capacity of 69.7 ampere-minutes. The cells were placed in plastic bags, which were perforated at top and bottom. The cells were discharged while immersed in excess 2N Mg(ClO<sub>4</sub>)<sub>2</sub> containing one gram per liter of Li<sub>2</sub>CrO<sub>4</sub> and 0.5 grams per liter of Mg(OH)<sub>2</sub>.

Average test results are summarized in Table XIV for various continuous and intermittent drains. The data show that no significant difference on AZ-21XA magnesium efficiency was obtained over a current-density range of .096 to 5.9 ma per cm<sup>2</sup> and that there was no significant difference in efficiency on several two-minute and 18-minute transceiver-type drains. Two minutes at 100 ma and 18 minutes at 3.4 ma is an equivalent current density to the BA-279-B<sub>2</sub> unit drain for a AA-size magnesium/magnesium-perchlorate/manganese-dioxide cell based on forty-one cells for the unit.

TOTAL CURRENT (milliamps)	CURRENT DENSITY PER CM (milliamps)	TIME TO 0.90 VOLTS (hours)	ANODE EFFICIENCY (percent)
25, continuous	0.70	37	70.4
57, "	1.6	15.5	71.2
210, "	5.9	3.13	71.6
530, "	14.9	1	66.5
305, 2 min } 25, 18 min }	8.6 0.7	15.5	69.5
210, 2 min } 25, 18 min }	5.9 0.7	19.75	71.0
150, 2 min } 10, 18 min }	4.2 0.28	37	68.8
100, 2 min } 3.4, 18 min }	2.8 .096	64.5	74.3
3.4	.096	89.25	74.2

MT-57

TABLE XIV. MAGNESIUM EFFICIENCY AND CAPACITY DATA FOR  
Mg(AZ-21XA)/Mg(ClO<sub>4</sub>)<sub>2</sub>/MnO<sub>2</sub> CELLS AT VARIOUS  
CONSTANT-CURRENT DRAINS.

Cathodes for the cell discharged at 3.4 ma were made using pure expanded-silver grids. Other cells made, using silver-plated-copper screen grids, showed evidence of copper contamination on the drain and therefore, the results are not included. The high anode efficiency at this low drain is explained partially by the beneficial effects of excess chromate in the electrolyte. Previous magnesium studies\* with AZ-10 alloy showed poor efficiency at current densities in this range.

Magnesium corrosion at the 3.4 ma drain was very irregular with the main corrosion occurring around the edges of the plate. This type of corrosion, while maintaining good efficiency, would lead to perforation in a round-type cell and early failure due to loss of water. Low-rate performance of a flat-type cell would not be affected, provided a good seal was maintained.

Data presented previously showed no significant loss in efficiency at discharge rates down to 0.096 ma per cm<sup>2</sup>. Tests were continued at this current density to recheck the results obtained on the AZ-21 alloy, and to determine low-drain efficiency of various alloys and the effect of a chromate inhibitor.

Test cells were the same as in previous tests, i.e., one anode plate and two cathode plates, 1.375 x 2 inches. Manganese-dioxide cathode plates with pure-silver grids were used in all cells except the inhibitor test where cupric-oxide plates were used. Average efficiency data for duplicate cells is presented in Table XV and a typical discharge curve of a manganese-dioxide cell in Figure 60. The data show that magnesium AZ-21 has the highest efficiency of the alloys tested, with an efficiency greater than 70 percent for six manganese-dioxide cells tested. Magnesium AZ-10 had the lowest efficiency.

It should be emphasized that magnesium corrosion at this low current density is very irregular, and results in large holes toward the latter part of discharge. In addition, this high anode efficiency could be realized only in a flat-type cell construction, since round-cell perforation would limit the discharge. The use of a chromate inhibitor increased the efficiency up to ten percent.

\*Unpublished work by R.W. Laity.



MAGNESIUM ALLOY	CATHODE	INHIBITOR	ANODE EFFICIENCY (percent)
AZ-21	MnO <sub>2</sub> (type M)	3% BaCrO <sub>4</sub> , in mix 1g/l LiCrO <sub>4</sub> , in electrode	71.6
AZ-21	MnO <sub>2</sub> (type M)	3% BaCrO <sub>4</sub> , in mix	71.8
AZ-31	MnO <sub>2</sub> (type M)	3% BaCrO <sub>4</sub> , in mix	67.7
AZ-10	MnO <sub>2</sub> (type M)	3% BaCrO <sub>4</sub> , in mix	63.8
AZ-21	CuO	1g/l LiCrO <sub>4</sub> , in electrolyte	61.7
AZ-21	CuO	none	52.8

MT-58

TABLE XV. MAGNESIUM-ANODE EFFICIENCY DATA AT A CURRENT DENSITY OF  
0.096 MA/CM<sup>2</sup> IN 2N Mg(ClO<sub>4</sub>)<sub>2</sub> ELECTROLYTE.

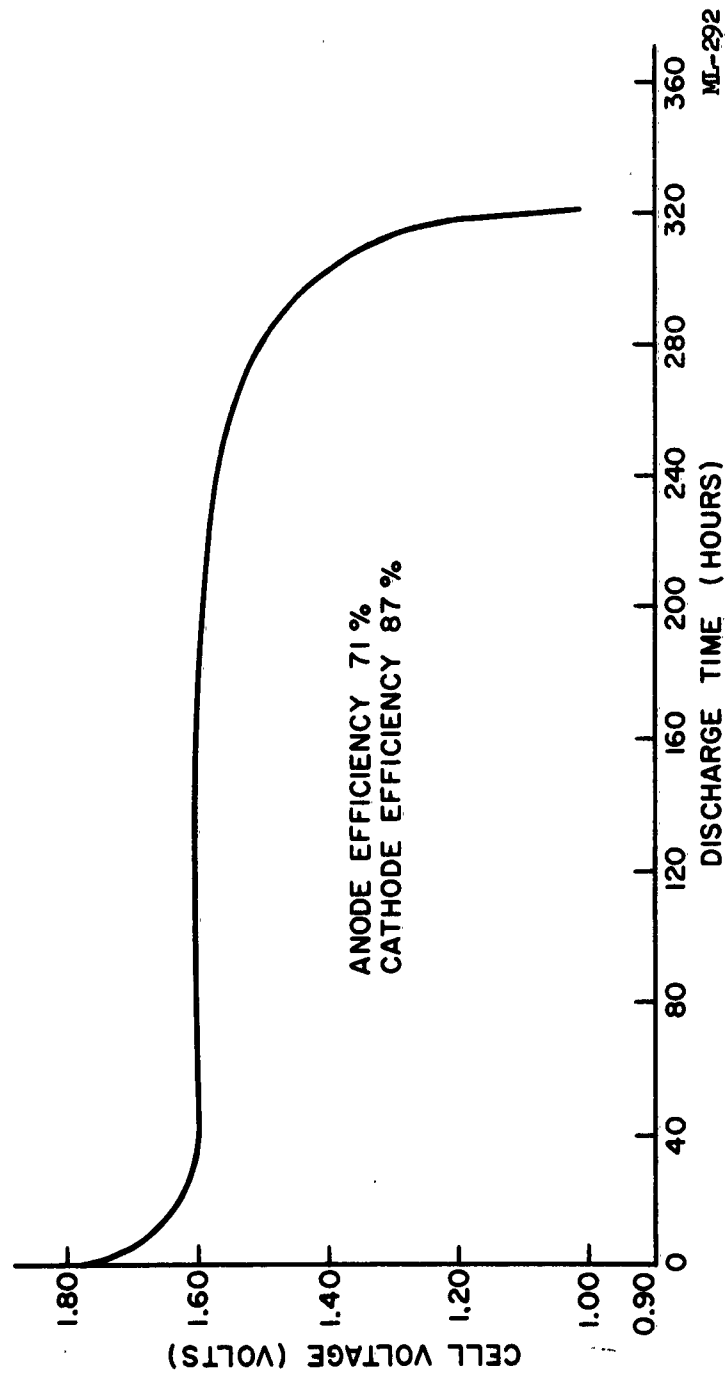


FIGURE 60.  $\text{Mg}(\text{AZ-2LXA})/\text{Mg}(\text{ClO}_4)_2/\text{MnO}_2(\text{TYPE M})$  FLAT CELL. DISCHARGED CONTINUOUSLY AT  $3.4 \text{ MILLIAMPERES } (0.09 \text{ ma/cm}^2)$  DRAIN.

Figure 61 shows the anode efficiency of the two alloys as a function of current density. For the AZ-21X1 alloy, the data show a nearly-constant efficiency. This, together with its excellent low-discharge-rate efficiency, makes this alloy desirable for use in magnesium dry cells and low-rate reserve cells. The efficiency measured for the AZ-21X1 alloy anode was somewhat lower than expected, since in practice, efficiencies as high as 80 percent have been obtained for this material in reserve cells.

The pure-magnesium anode has a much higher efficiency than the AZ-21X1 alloy anode at high-current densities and results in optimum performance in high-rate reserve cells. At current densities below  $3 \text{ ma/cm}^2$  the efficiency falls off sharply, limiting the use of pure magnesium at low discharge rates.

Cell polarization data are presented in Table XVI together with the efficiency data and the anode composition.

#### 3.2.5.4 Correlation of Anode Efficiency with Magnesium Corrosion Film Studies

Measurements of capacitance and resistance of the magnesium corrosion film were related to film area and film thickness, and predictions were made of the anode efficiency of AZ-21X1 and pure magnesium. Figures 62 and 63 show the relationship between exposed anode area and anode efficiency as a function of current density. The data show that the exposed area ( $A_T - A_F$ ) decreases with decreasing current density to a point where the total anode surface is covered with corrosion film. This occurs at  $1.7 \text{ ma/cm}^2$  for pure magnesium, and  $0.3 \text{ ma/cm}^2$  for the AZ-21X1 alloy.

The rate of corrosion film formation is much greater for the pure magnesium, as indicated by the higher current density required to have exposed magnesium present. Below this current density the corrosion film formation rate increases as the load-current density decreases, resulting in a decrease in anode efficiency.

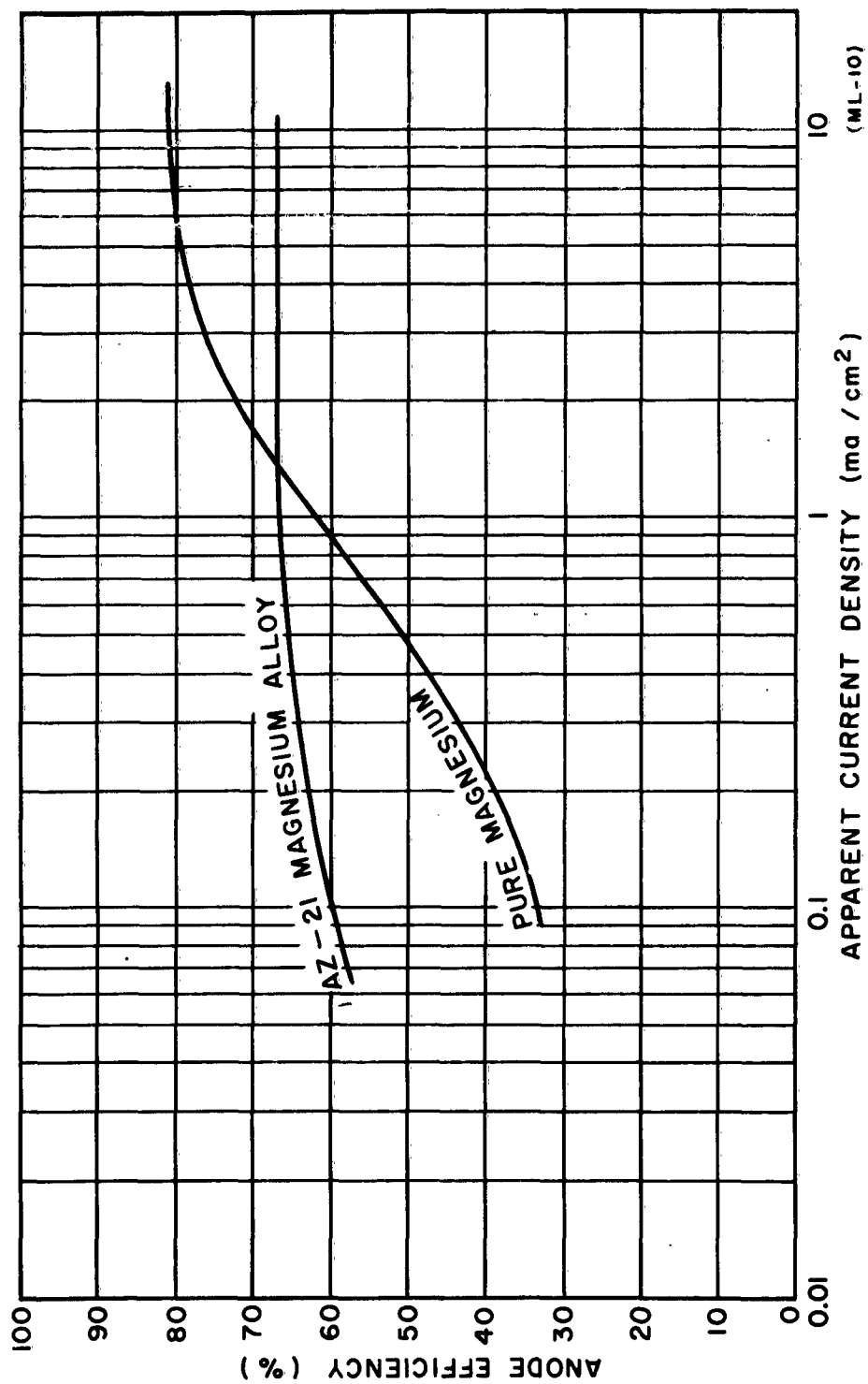


FIGURE 61. MAGNESIUM ANODE EFFICIENCY AS A FUNCTION OF CURRENT DENSITY IN 2N  $\text{Mg}(\text{ClO}_4)_2$  ELECTROLYTE.

APPARENT CURRENT DENSITY (ma/cm <sup>2</sup> )	C. P. MAGNESIUM <sup>(1)</sup>		AZ-21X1 ALLOY (2)	
	CELL <sup>(3)</sup> VOLTAGE (volts)	ANODE EFFICIENCY (percent)	CELL <sup>(3)</sup> VOLTAGE (volts)	ANODE EFFICIENCY (percent)
10.9	0.59	82.3	0.50	66.9
7.8	0.64	81.8	0.54	67.1
3.8	0.73	77.4	0.61	62.2
2.0	0.82	73.6	0.64	67.1
0.46	0.94	49.7	0.64	64.5
0.09	1.20	33.9	0.92	59.0

Notes:

MT-59

(1) Dow Sublimed Mg

<u>%Al</u>	<u>Ca</u>	<u>Cu</u>	<u>Fe</u>	<u>Mn</u>	<u>Ni</u>	<u>Pb</u>	<u>Si</u>	<u>Sn</u>	<u>Zn</u>
<.003	<.01	<.001	<.001	<.001	<.0005	<.002	<.01	<.01	.003

(2) Dow AZ-21X1

1.96	.15	<.001	.0014	.016	<.0005	.004	<.01	<.01	1.08
------	-----	-------	-------	------	--------	------	------	------	------

(3) Magnesium vs platinized-platinum.

TABLE XVI. MAGNESIUM-ANODE EFFICIENCY DATA IN 2N MAGNESIUM-PERCHLORATE ELECTROLYTE.

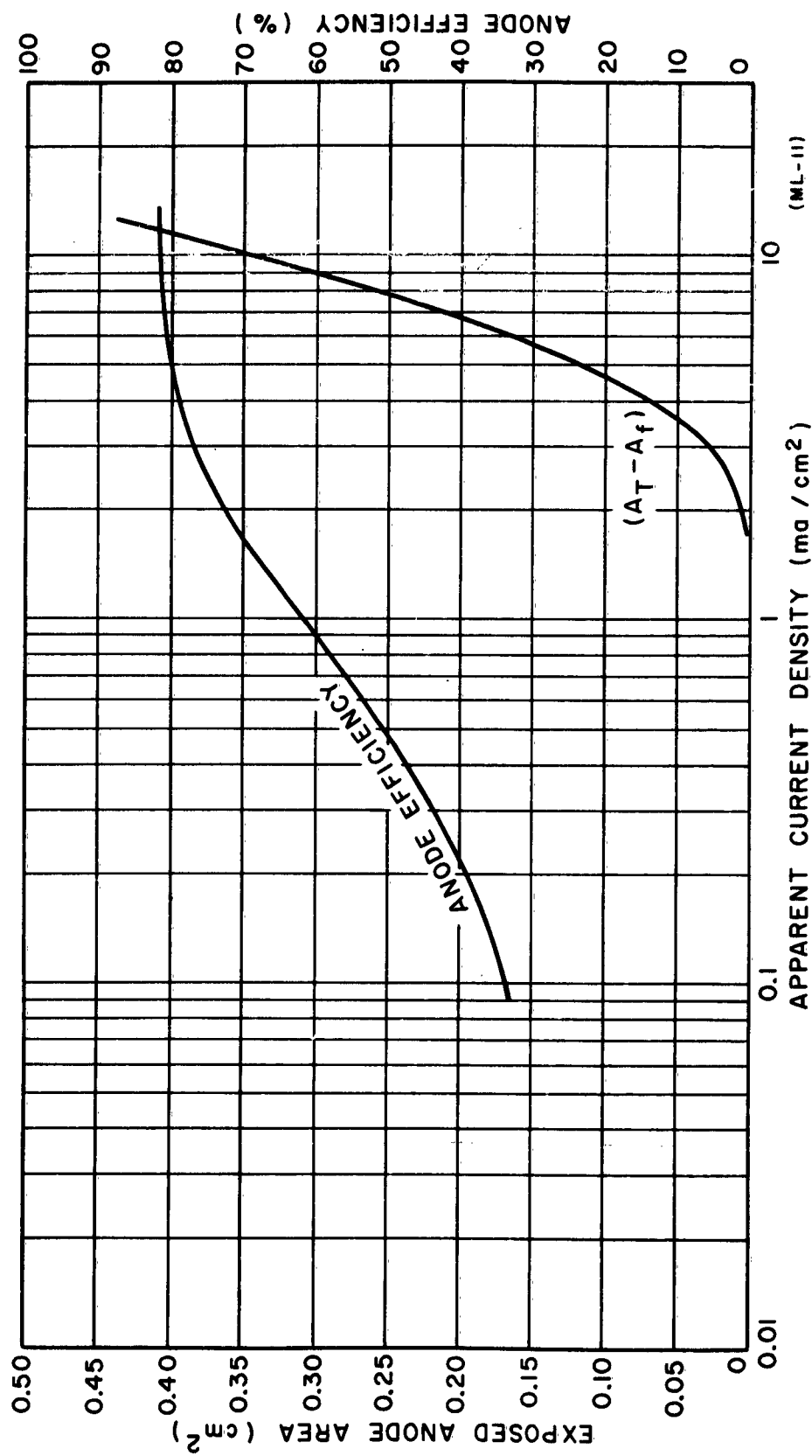


FIGURE 62. EXPOSED-ANODE AREA ( $A_T - A_f$ ) AND ANODE EFFICIENCY VS APPARENT CURRENT DENSITY OF PURE MAGNESIUM IN 2N  $\text{Mg}(\text{ClO}_4)_2$  ELECTROLYTE.

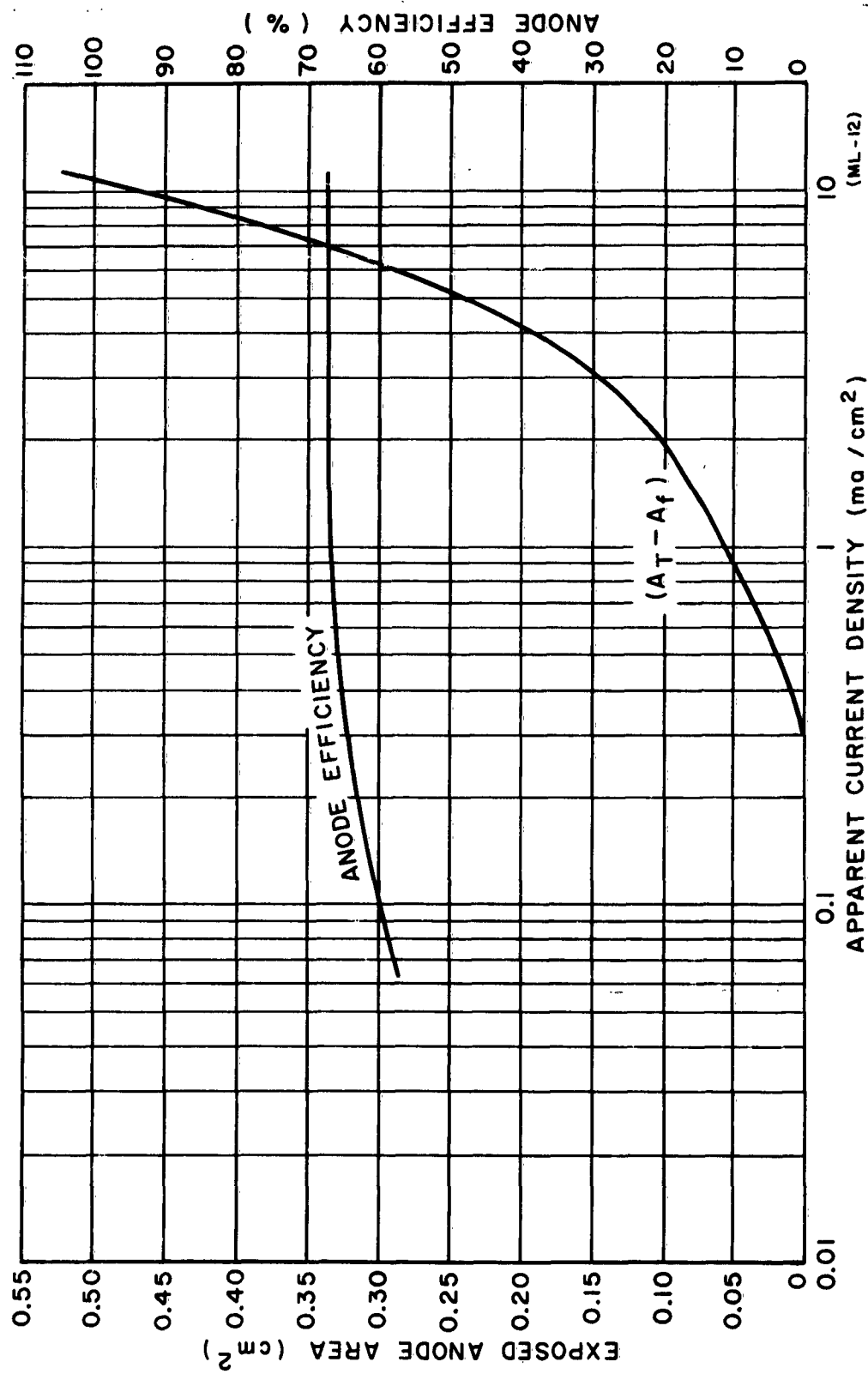


FIGURE 63. EXPOSED ANODE AREA ( $A_T - A_f$ ) AND ANODE EFFICIENCY VS APPARENT CURRENT DENSITY (AZ-21 MAGNESIUM ALLOY) IN 2N  $Mg(ClO_4)_2$  ELECTROLYTE.

### 3.3 ELECTROLYTE RESEARCH STUDIES

#### 3.3.1 Low-Temperature Electrolyte Conductivity

A program was begun to study the conductivity of various perchlorate solutions with respect to temperature and to determine their suitability as a low-temperature battery electrolyte. A literature study showed that little data was available for perchlorate conductivity at low temperatures and high concentrations. It was also found that phase-diagram data on perchlorate-water systems is not available.

The specific conductivity of magnesium perchlorate and lithium perchlorate solutions is presented in Figure 64. Measurements were taken using a conductivity bridge Model RC-16B1 (Industrial Instruments Co), and a conductivity cell with a 1.0-cell constant. These curves show that the magnesium perchlorate electrolyte was superior at low temperatures. At  $-40^{\circ}\text{C}$  the same conductivity was obtained for the 4 and 5N magnesium-perchlorate solutions and both should yield similar cell characteristics at this temperature. The marked decrease in conductivity at the low temperatures is one factor causing initial low voltage on discharge as shown in Figure 29. In Figure 64 the curves are extended down to the approximate freezing point of the materials. The freezing point of 5N magnesium perchlorate was not reached. A study with 5N lithium perchlorate showed results similar to the magnesium perchlorate and is not included in the data of Figure 64.

#### 3.3.2 Specific Conductivity of Various Perchlorates

Electrical conductivity was determined for various perchlorate electrolytes over a temperature range of  $+40^{\circ}$  to  $-70^{\circ}\text{C}$ . Measurements were taken using a Model RC-16B1 conductivity bridge and a conductivity cell with a 1.0-cell constant. Specific conductivity data for these solutions are given in Table XVII. The results show that 6N calcium perchlorate and 6N strontium perchlorate solutions are good electrolyte conductors down to  $-70^{\circ}\text{C}$ . The conductivity at  $-70^{\circ}\text{C}$  is the same as a 5N magnesium perchlorate solution at  $-45^{\circ}\text{C}$ .



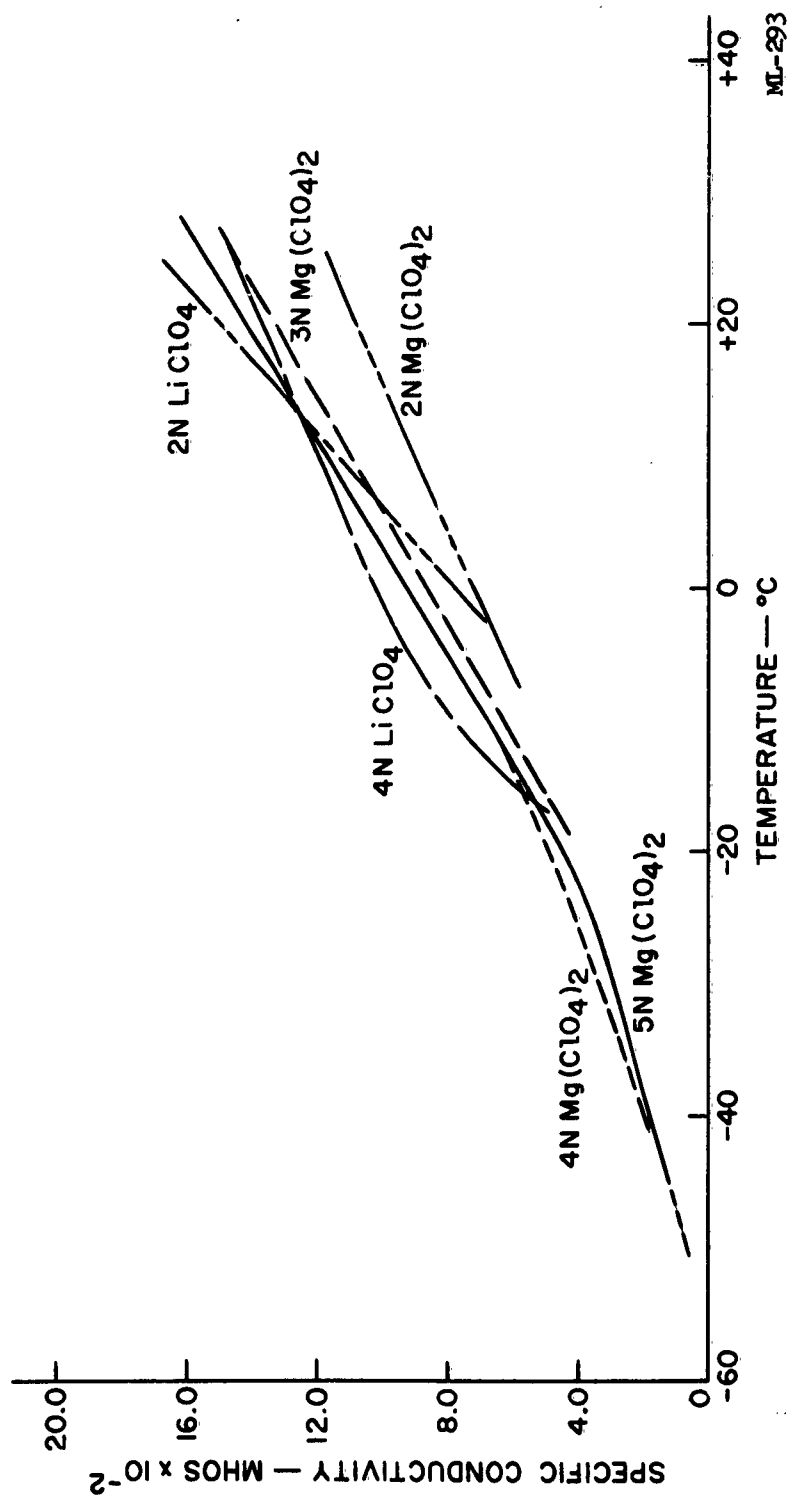


FIGURE 64. SPECIFIC CONDUCTIVITY OF VARIOUS PERCHLORATE ELECTROLYTES AS A FUNCTION OF TEMPERATURE AND CONCENTRATION.

SOLUTION	CONC.	TEMPERATURE (°C)							
		40	23	0	-20	-40	-45	-60	-70
LiClO <sub>4</sub>	2N		0.163	0.072	F*	F			
	3N		.149	.097	F	F			
	4N		.144	.099	.048	F			
	5N		.143	.099	.048	F			
NaClO <sub>4</sub>	2N	0.164	.115	.067					
	4N	.294	.149	.091	.055	.047		F	
	6N	.313	.156	.078	.051	.028		F	
	8N	.192	.124	.060	.036	.020		F	
Mg(ClO <sub>4</sub> ) <sub>2</sub>	2N		.118	.069	F	F	F		
	3N		.141	.083	.049	F	F		
	4N		.149	.092	.053	.020	F		
	5N		.144	.089	.048	.018	.013		
Ca(ClO <sub>4</sub> ) <sub>2</sub>	2N	.167	.132	.073	F	F	F	F	F
	4N	.208	.167	.092	.053	.046	F	F	F
	6N	.167	.116	.078	.055	.036		.019	.014
	8N	.112	.074	.037	.030	F		F	F
Sr(ClO <sub>4</sub> ) <sub>2</sub>	2N	.159	.104	.077	F	F		F	F
	4N	.204	.135	.087	.066	.050		F	F
	6N	.151	.103	.061	.040	.023		.016	.012
	8N	.079	.053	.027	.013	.006		.002	.001
Ba(ClO <sub>4</sub> ) <sub>2</sub>	2N	.030	.086	.059	F	F		F	
	4N	.192	.134	.083	.056	.046		F	
	6N	.170	.127	.067	.044	.027		F	
	8N	.125	.086	.060	.035	F		F	

\*F = frozen

MT-60

TABLE XVII. SPECIFIC CONDUCTIVITY DATA FOR VARIOUS PERCHLORATE-SALT SOLUTIONS AS A FUNCTION OF TEMPERATURE AND CONCENTRATION.

### 3.3.2.1 Effect of Various Perchlorate Electrolytes on the Performance of Magnesium/Mercuric-Oxide Cells

Low temperature capacity at  $-40^{\circ}\text{C}$  was determined for ten-cathode-plate magnesium/mercuric-oxide cells using  $5\text{N Mg}(\text{ClO}_4)_2$ ,  $6\text{N Ca}(\text{ClO}_4)_2$  and  $6\text{N Sr}(\text{ClO}_4)_2$ . The cells were stabilized at  $-40^{\circ}\text{C}$ , activated with  $-40^{\circ}\text{C}$ -electrolyte for 15 minutes, and discharged at the five-hour rate. Internal cell temperature rose during the initial thirty minutes of discharge to a constant temperature of  $-30^{\circ}\text{C}$ . Capacity data for these cells are presented in Figure 65. The results show a decrease in cell capacity for cations of larger size. The cell with  $5\text{N Mg}(\text{ClO}_4)_2$  electrolyte had a cathode efficiency of 56 percent, calculated to a 20-percent voltage drop. Anode efficiency was 70 percent.

Additional studies were carried out at room temperature to determine the factors limiting cell capacity with  $\text{Ca}(\text{ClO}_4)_2$  and  $\text{Sr}(\text{ClO}_4)_2$  electrolytes, and to test the effect of mixtures with  $\text{Mg}(\text{ClO}_4)_2$ . A single-cathode-plate test cell which had a 35.2 ampere-minute theoretical capacity was used for these studies. The cells were discharged at the five-hour rate.

The data show that cell capacity decreases with an increase in salt cation size, similar to those results obtained at  $-40^{\circ}\text{C}$ . Cell voltage also decreased. Mixtures with  $5\text{N Mg}(\text{ClO}_4)_2$  solution showed an increase in cell voltage and capacity.

Half-cell measurements were taken on the  $6\text{N Sr}(\text{ClO}_4)_2$  cell which used a pressed-silver/silver-chloride reference electrode. The mercuric-oxide cathode was found to be the limiting electrode, with the magnesium remaining constant throughout the five hours of discharge. Examination of cells after testing showed evidence of reaction of  $\text{Sr}(\text{ClO}_4)_2$  and  $\text{Ca}(\text{ClO}_4)_2$  solution with the cathode plate. This occurred through increased corrosion of the grid or reaction with the CMC binder.

### 3.3.3 Variation of Electrolyte Viscosity with Temperature

A possible explanation for the decrease in cell capacity at low temperatures lies in the increase in viscosity of the  $\text{Mg}(\text{ClO}_4)_2$  electrolyte with a decrease in temperature.

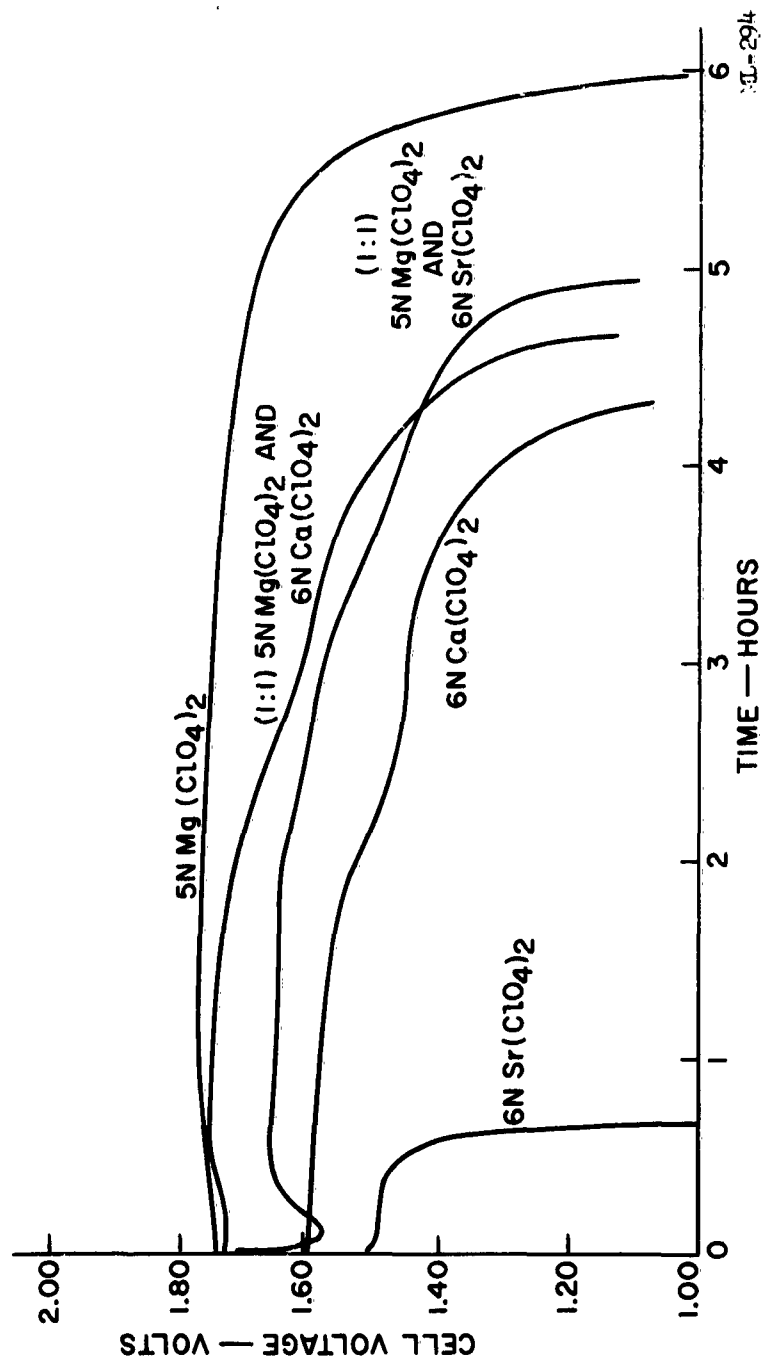


FIGURE 65. Mg-HgO CELLS DISCHARGED AT 0.1 AMPERE AT ROOM TEMPERATURE IN VARIOUS ELECTROLYTES.  
1 CATHODE PLATE. CELLS = 10:1 RATIO MIX. THEORETICAL CAPACITY = 35.2 AMP-MIN.

Viscosity data for a 3.58N  $\text{Mg}(\text{ClO}_4)_2$  electrolyte at various temperatures are as follows:

70°F - 8 centipoises  
32°F - 10 centipoises  
-20°F - 18 centipoises

As may be observed from the above data, an increase in viscosity of 10 centipoises is obtained with a decrease in temperature of 90°F. This increase in viscosity can result in concentration polarization of the cell, thereby decreasing the cell capacity. The increase in viscosity reduces the ionic mobility of the electrolyte which decreases conductance. Data are presented in Figure 64 which shows the decrease in the specific conductivity of magnesium-perchlorate electrolytes with temperature.

Table XVIII lists the viscosity of 5N Ca, Sr, and  $\text{Mg}(\text{ClO}_4)_2$  electrolytes at various temperatures.

It should be noted that  $\text{Ca}(\text{ClO}_4)_2$  is more suitable with respect to viscosity than the other electrolytes tested throughout the entire range. Specific-conductivity data presented in Table XVII show conductivity of  $\text{Ca}(\text{ClO}_4)_2$  and  $\text{Sr}(\text{ClO}_4)_2$  to be better than  $\text{Mg}(\text{ClO}_4)_2$  at low temperature. These electrolytes, however, did not increase the low-temperature capacity of the mercuric-oxide reserve cell.

### 3.4 DRY CELLS

A program was initiated to determine the shelf life of  $\text{Mg}/\text{Mg}(\text{ClO}_4)_2/\text{MnO}_2$  and  $\text{Mg}/\text{Mg}(\text{ClO}_4)_2/\text{CuO}$  dry cells.

#### Cell Formulations:

The  $\text{Mg}/\text{Mg}(\text{ClO}_4)_2/\text{MnO}_2$  (Type M) cell was used for these studies. The composition of this cell is listed below.

<u>Material</u>	<u>Percent by Weight</u>
$\text{MnO}_2$ (Type M)	84.5
Shawinigan carbon black (Acetylene)	9.7
$\text{BaCrO}_4$	2.9
$\text{Mg}(\text{OH})_2$	2.9

TEMPERATURE (°F)	ELECTROLYTE VISCOSITY (CENTIPOISES)		
	$\text{Ca}(\text{ClO}_4)_2$	$\text{Sr}(\text{ClO}_4)_2$	$\text{Mg}(\text{ClO}_4)_2$
70	10	12	10
32	14	16	16
-4	20	20	18
-40	33	40	49
-65	38	74	60

MT-61

TABLE XVIII. VISCOSITY OF 5N  $\text{Ca}(\text{ClO}_4)_2$ ,  $\text{Sr}(\text{ClO}_4)_2$ , AND  $\text{Mg}(\text{ClO}_4)_2$   
ELECTROLYTES AT VARIOUS TEMPERATURES.

Wetness - (per 1000 g dry mix). . . . . 507 ml of 2N  $\text{Mg}(\text{ClO}_4)_2$  with  
 1 g/l  $\text{Li}_2\text{CrO}_4$  and 0.5 g/l  $\text{Mg}(\text{OH})_2$   
 Bobbin - 7 g of wet mix/AA-cell.

A 6:1 ratio of cupric-oxide-to-carbon was selected as a standard lot. The composition is as follows:

<u>Material</u>	<u>Percent by Weight</u>
CuO (reagent powder)	82.4
Shawinigan carbon black (Acetylene)	13.7
$\text{BaCrO}_4$	2.9
$\text{Mg}(\text{OH})_2$	.97
Wetness - (per 1000 g dry mix). . . . .	.473 ml. 2N $\text{Mg}(\text{ClO}_4)_2$ , with 1 g/l $\text{Li}_2\text{CrO}_4$ and 1/2 g/l $\text{Mg}(\text{OH})_2$
Bobbin -	7.5 g wet mix/AA-cell

#### 3.4.1 Synthetic $\text{MnO}_2$ Study

The increased stability in the presence of strong oxidizing agents of the magnesium-perchlorate electrolyte compound to the magnesium-bromide electrolyte permits the use of a more-reactive synthetic  $\text{MnO}_2$  in magnesium cells. A sample of Type-L  $\text{MnO}_2$  was obtained (Manganese Chemical Corp.) to test compatibility and initial characteristics. Magnesium AA-size cells were assembled with this  $\text{MnO}_2$  and used magnesium-bromide and magnesium-perchlorate electrolyte mixes. Cathode mix formulation for these mixes is as follows:

<u>Material</u>	<u>Percent by Weight</u>
Type-L $\text{MnO}_2$	84.7
Shawinigan carbon black (Acetylene)	9.7
$\text{BaCrO}_2$	2.8
$\text{Mg}(\text{OH})_2$	2.8
Wetness - per/1000 g dry mix:	
Magnesium perchlorate mix . . . . .	520 ml 2N $\text{Mg}(\text{ClO}_4)_2$ , with 1 g/l $\text{Li}_2\text{CrO}_4$ and 1/2 g/l $\text{Mg}(\text{OH})_2$
Magnesium bromide mix . . . . .	560 ml 2N $\text{MgBr}_2$ , with 1 g/l $\text{Li}_2\text{CrO}_4$ and 1/2 g/l $\text{Mg}(\text{OH})_2$
Bobbin. . . . .	11 g wet mix/A-size cell

Bromine vapors were evolved in the  $\text{MgBr}_2$  mix, indicating the activity of the Type-L  $\text{MnO}_2$ . Magnesium A-Cells were assembled and discharged characteristics were determined at 4 ohms and 16-2/3 ohms with both electrolytes.

The results are summarized in Table XIX and Figure 66 and 67. The data show that good capacity at a high-voltage level is obtained for the Type-L  $\text{MnO}_2$  cells, while the discharge time is less than for cells with Type-M  $\text{MnO}_2$ . Although the total cell capacity is lower than that for Type-M cells, the Type-L  $\text{MnO}_2$  may be of interest in special applications where the higher voltage would be utilized.

#### Capacity

Shelf-life data, presented in Table XIX and Figure 3, have shown that good capacity retention is obtained with  $\text{Mg}/\text{Mg}(\text{ClO}_4)_2/\text{MnO}_2$  cells and  $\text{Mg}/\text{Mg}(\text{ClO}_4)_2/\text{CuO}$  cells. Although good shelf-life data have been obtained for magnesium perchlorate cells with both  $\text{MnO}_2$  and  $\text{CuO}$  cathodes, some cell lots have shown considerable perforation on both the 70°F and 113°F storage tests. It is believed that these failures are due to variation in can composition and processing.

#### 3.4.2 Dry Cell Parameter Studies

Extensive perforation of magnesium cans of the above shelf studies prompted a re-evaluation of cell materials and assembly techniques. Further dry-cell efforts were directed toward determining the factors causing this perforation.

Analysis of the 2N  $\text{Mg}(\text{ClO}_4)_2$  electrolyte from various sources has shown the electrolyte to be free of impurities. The trace amounts of impurities noted are within tolerance levels as given for a  $\text{MgBr}_2$  electrolyte.

Accelerated corrosion studies with a 2N  $\text{Mg}(\text{ClO}_4)_2$  electrolyte have shown that the magnesium AZ-10A cans badly corroded by the electrolyte after one week at 130°F. The cans tested were from White Metal Co. and late production runs from other sources. These studies indicate that



Cell Type	Resistance (ohms)	End Voltage (Volts)	Capacity (Hours)	Ave. Voltage (Volts)	Ampere Minutes (Act.)	Ampere Minutes (Theor.)	Cathode Efficiency (%)	CAPACITY W-Hr/Lb W-Hr/In <sup>3</sup>	
Mg/Mg(ClO <sub>4</sub> ) <sub>2</sub> /MnO <sub>2</sub> (Type L)	4	0.90	1.88	1.54	43.5	109.0	40.0	26.2	1.82
	16-2/3	0.90	12	1.35	66.2	109.0	60.5	44.6	3.04
Mg/Mg(ClO <sub>4</sub> ) <sub>2</sub> /MnO <sub>2</sub> (Type M)	4	0.90	2.5	1.38	51.7	113.0	45.7	30.8	2.09
	16-2/3	0.90	14	1.46	74.0	113.0	65.5	46.0	3.14
Mg/Mg Br <sub>2</sub> /MnO <sub>2</sub> (Type L)	4	0.90	1.43	1.51	32.1	105.0	30.5	30.6	1.25
	16-2/3	0.90	9	1.56	50.2	105.0	48.0	32.0	2.29
Mg/Mg Br <sub>2</sub> /MnO <sub>2</sub> (Type M)	4	0.90	2.25	1.41	47.6	107.0	44.5	29.7	1.96
	16-2/3	0.90	11.5	1.47	61.0	107.0	57.0	38.6	2.61

MT-62

TABLE XIX. PERFORMANCE DATA OF TYPE-L AND-M MnO<sub>2</sub> A-SIZE CELLS UTILIZING BOTH MgBr<sub>2</sub> AND Mg(ClO<sub>4</sub>)<sub>2</sub> ELECTROLYTES.

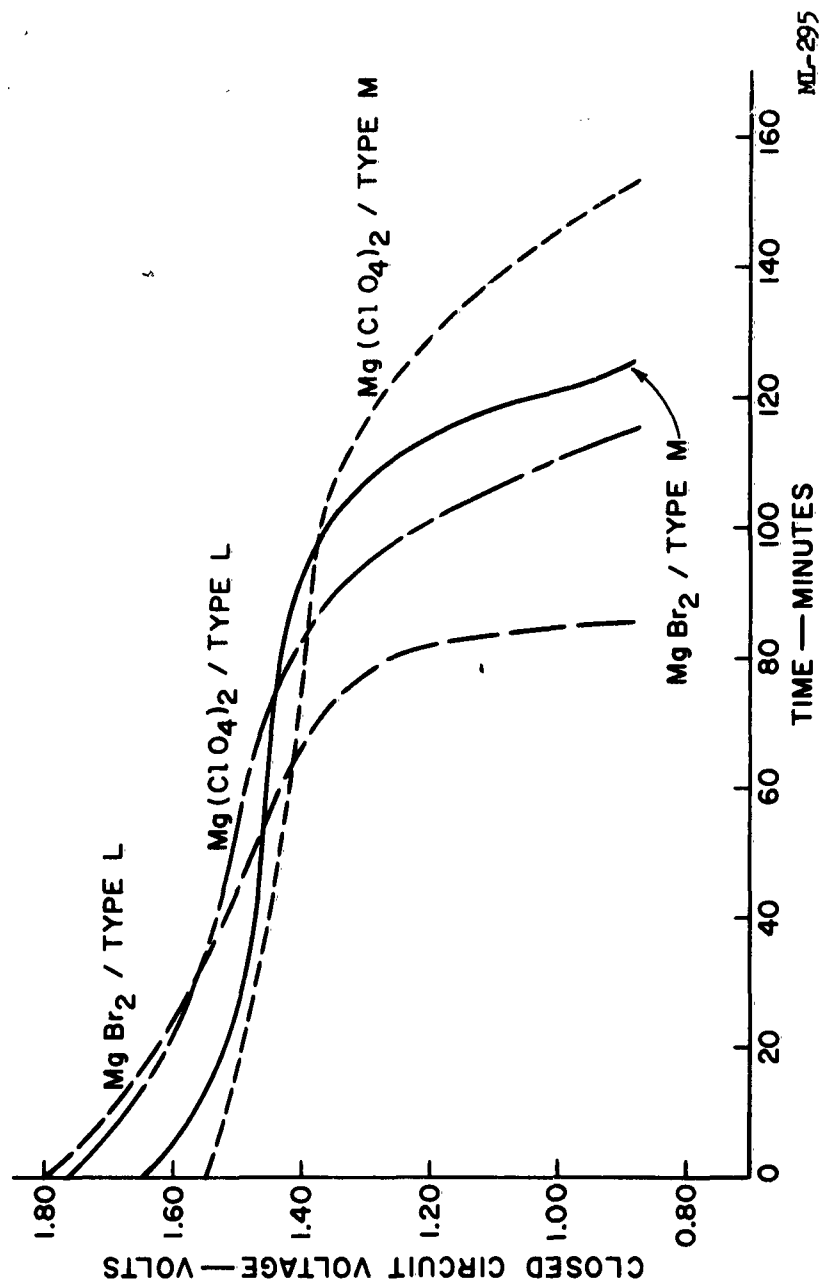
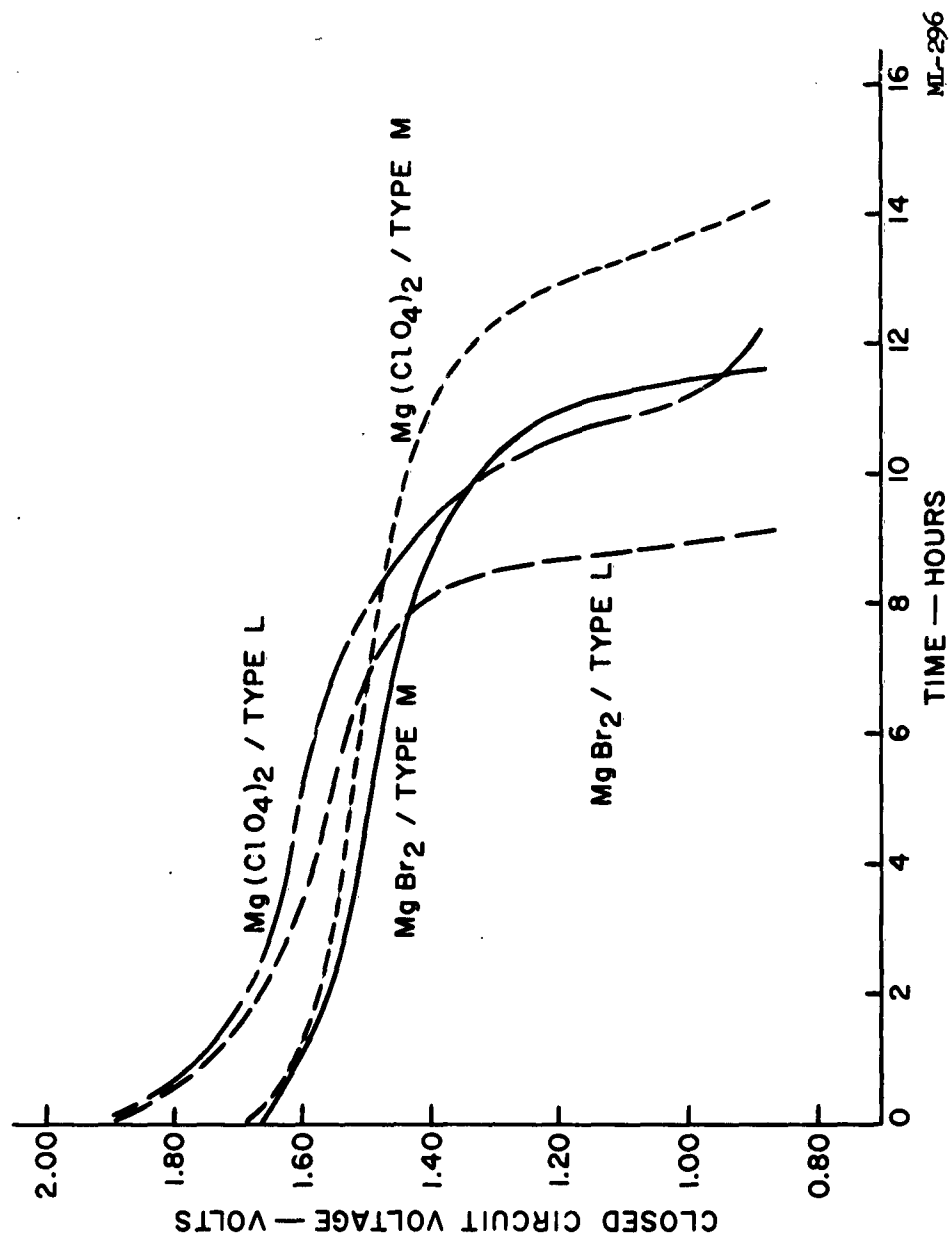


FIGURE 66. COMPARISON OF MAGNESIUM A-CELLS CONTAINING TWO DIFFERENT TYPES OF SYNTHETIC  $\text{MgO}_2$  AND ELECTROLYTE DISCHARGED AT 4 OHMS.



MI-296

FIGURE 67. COMPARISON OF MAGNESIUM A-CELLS CONTAINING TWO DIFFERENT TYPES OF SYNTHETIC  $MnO_2$  AND ELECTROLYTE DISCHARGED AT 16-2/3 CEMS.

shelf-life perforations are probably due to poor magnesium-can quality. Unsupported work prior to this contract had shown that magnesium cans (AZ-10A) were not badly corroded by 2N  $\text{Mg}(\text{ClO}_4)_2$ , and were corroded to a lesser extent than a control sample using a 2N  $\text{MgBr}_2$  electrolyte with and without a chromate inhibitor. Tests have also indicated that air-line perforations in  $\text{Mg}(\text{ClO}_4)_2$  cells are caused by reaction with oxygen.

#### 3.4.2.1 Cell Formulation

The cells were fabricated with the following formulation:

<u>Amount</u>	<u>Material</u>	<u>Percent (By Weight)</u>
391.5 g	$\text{MgO}_2$ (Type M)	66.5
45.0 g	Shawinigan Carbon Black	7.8
13.4 g	$\text{BaCrO}_4$	2.3
13.4 g	$\text{Mg}(\text{OH})_2$	2.3
125.0 cc	3.58N $\text{Mg}(\text{ClO}_4)_2$ electrolyte	22.1

#### 3.4.2.2 Capacity Data

Data on the hours of service, average operating voltage, cathode efficiency, and watt-hours-per-pound of A-cells discharged at the various temperatures are presented in Table XX and XXVI. Capacity data to a 0.9-volt cutoff voltage is presented in Figures 68 and 69. The data show that a decrease in temperature results in a sharp drop in the cell capacity of the system. The cells averaged 2.75 hours for the 16-2/3 ohm drain, and 10 hours for the 50-ohm drain at  $-20^\circ\text{F}$ . This is 18 percent of the room temperature capacity. It should be noted that the low-temperature characteristics of the  $\text{Mg}/\text{Mg}(\text{ClO}_4)_2/\text{MnO}_2$  system are superior to those of the Le Clanché cell.

Figure 70 illustrates the relation of capacity in ampere-minutes to temperature and discharge rate. Figure 71 compares the variation of cathode efficiency and cell capacity with the temperature and discharge rate for  $\text{Mg}/\text{Mg}(\text{ClO}_4)_2/\text{MnO}_2$  A-cells.

TEMPERATURE	AVERAGE VOLTS		DISCHARGE TIME TO 0.90 v (minutes)		AMPERE-MINUTES (TO 0.90 v)		EFFICIENCY (%)		CAPACITY (W-Hr/Lb)	
CURRENT DRAIN (ohms)	16-2/3	50	16-2/3	50	16-2/3	50	16-2/3	50	16-2/3	50
-20°F	1.21	1.30	2-3/4	10	12.0	15.6	9.3	12.1	6.3	8.7
32°F	1.19	1.37	14	50.5	60.1	81.8	46.6	63.5	30.8	48.2
70°F	1.39	1.46	15-1/4	56	76.5	98.0	59.3	76.9	45.8	61.5

MT-63

TABLE XX. PERFORMANCE OF  $\text{Mg/Mg}(\text{ClO}_4)_2/\text{MnO}_2$  A-CELLS DISCHARGED CONTINUOUSLY AT VARIOUS TEMPERATURES THROUGH VARIOUS RESISTANCES.

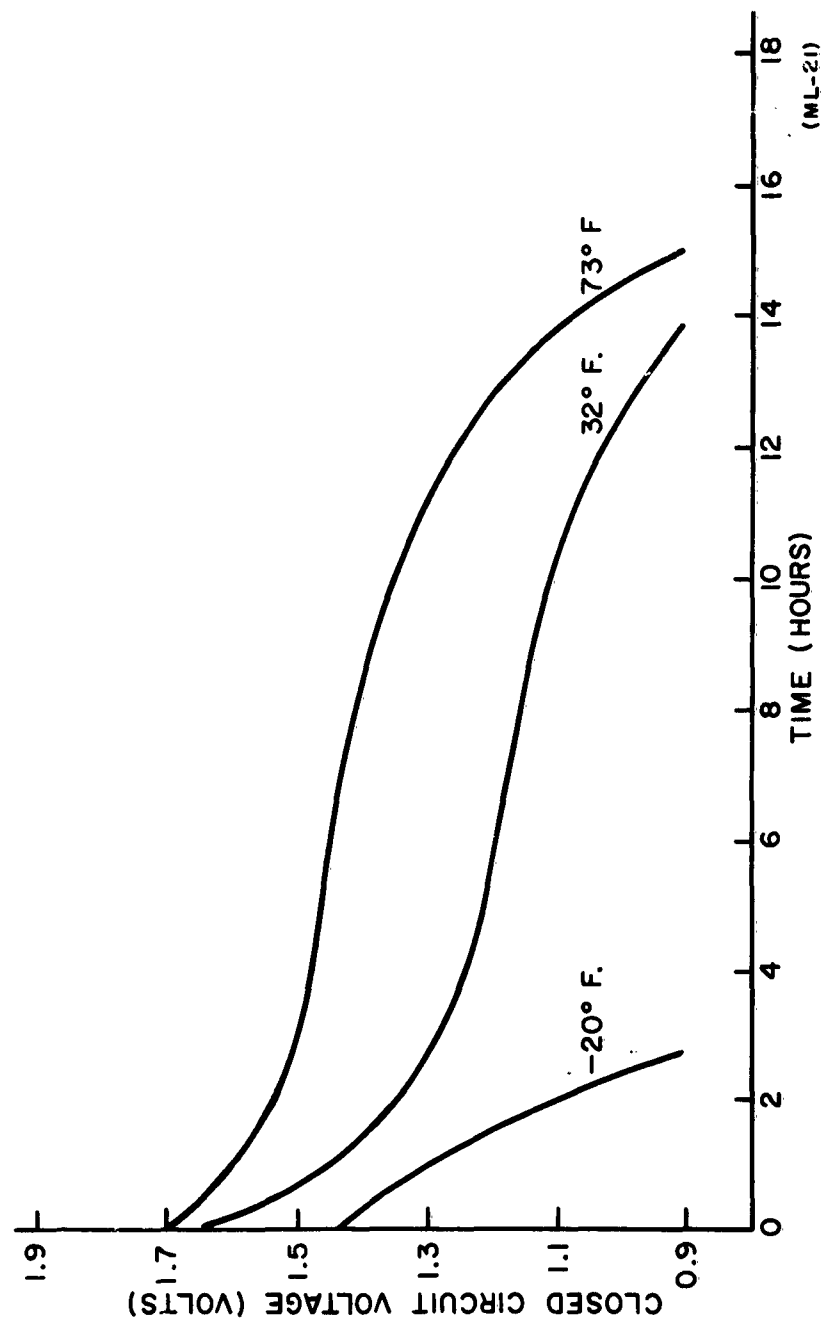


FIGURE 68. DATA FOR  $\text{Mg}/\text{Mg}(\text{ClO}_4)_2/\text{MnO}_2$  A-CELLS DISCHARGED CONTINUOUSLY AT 16-2/3 OHMS AT VARIOUS TEMPERATURES.

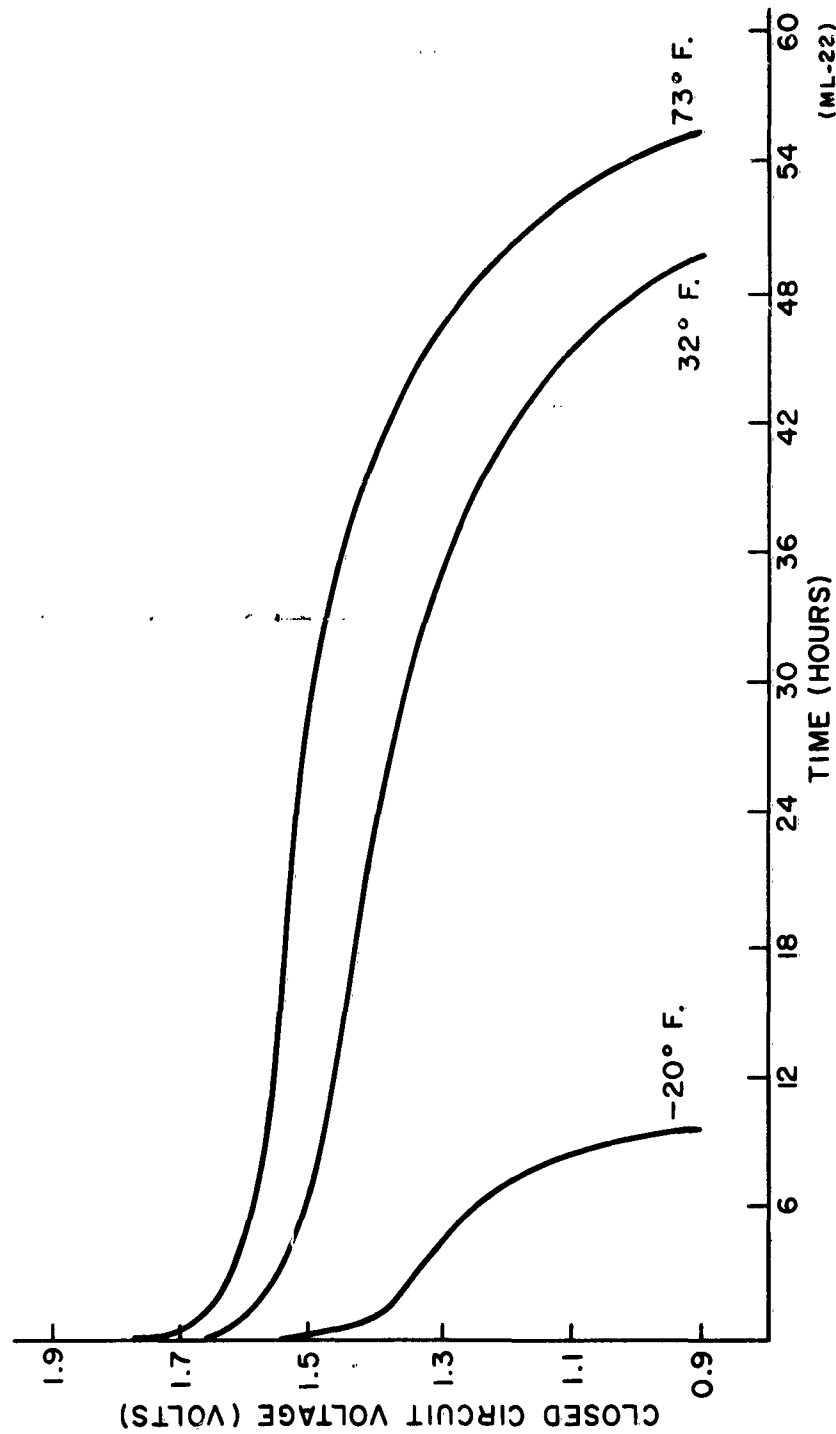


FIGURE 69. DATA FOR  $\text{Mg}/\text{Mg}(\text{ClO}_4)_2/\text{MnO}_2$  A-CELLS DISCHARGED CONTINUOUSLY AT 50 OHMS AT VARIOUS TEMPERATURES.

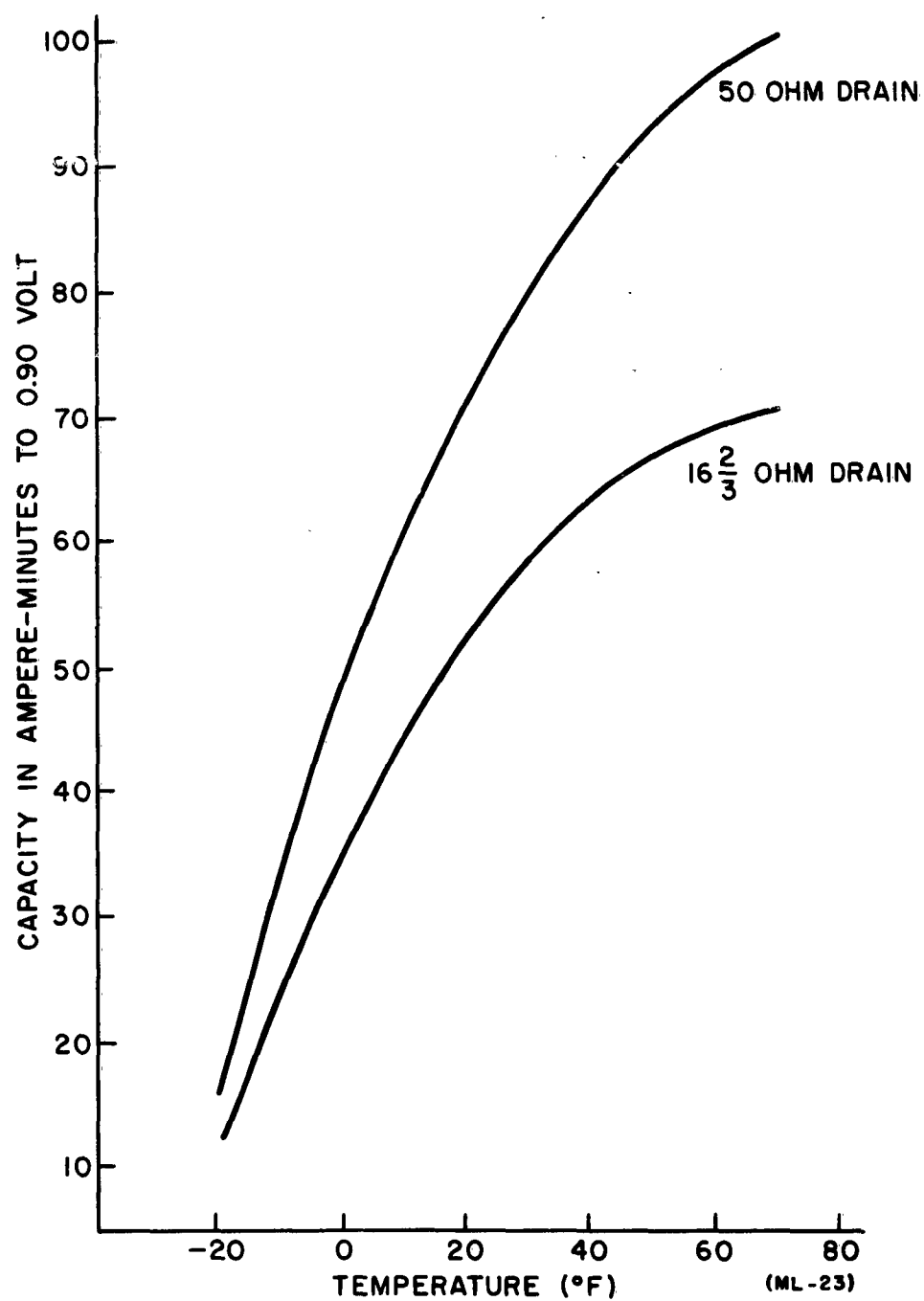


FIGURE 70. RELATION OF CAPACITY TO TEMPERATURE AND RATE OF DISCHARGE FOR  
 $\text{Mg}/\text{Mg}(\text{ClO}_4)_2/\text{MnO}_2$  A-CELLS.



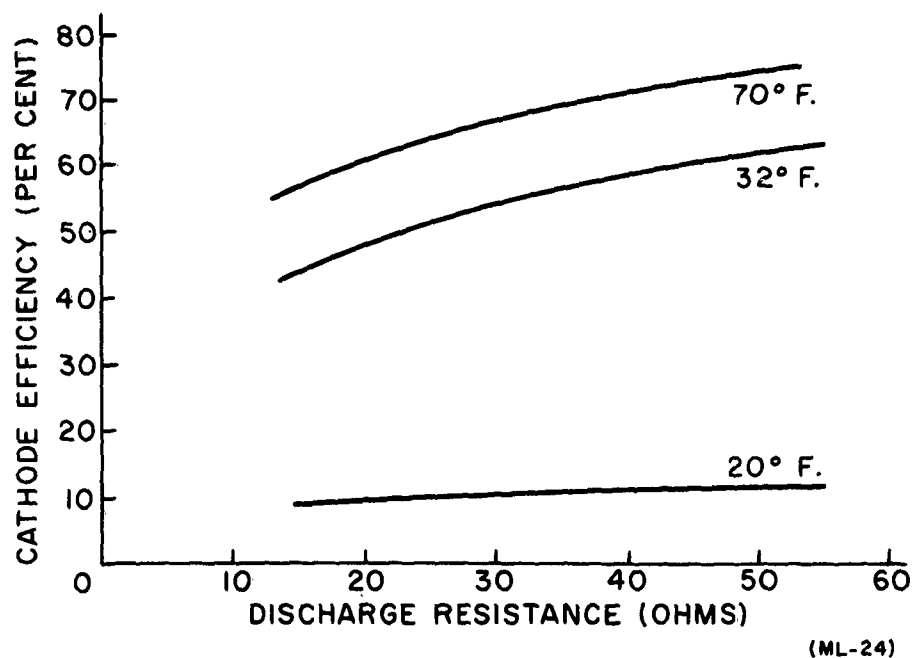
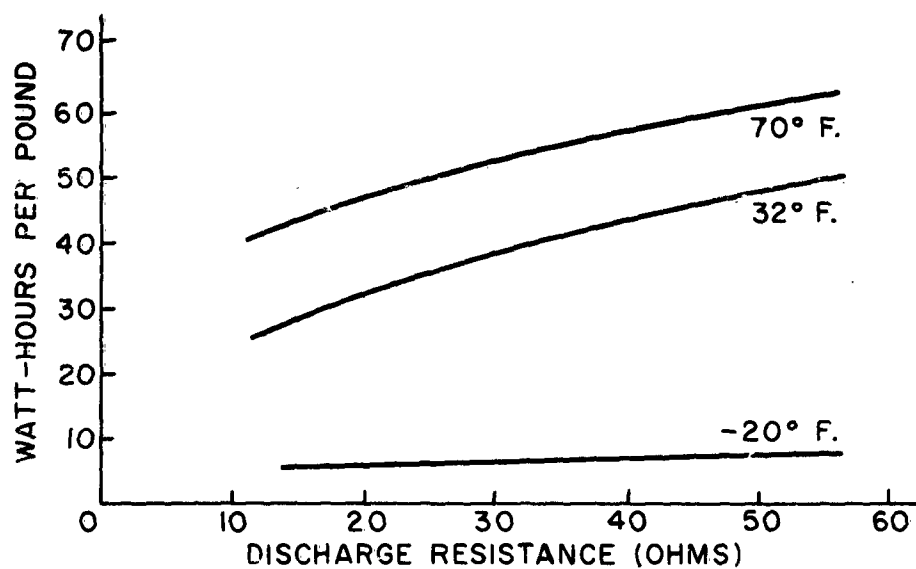


FIGURE 71. RELATION OF  $\text{Mg}/\text{Mg}(\text{ClO}_4)_2/\text{MnO}_2$  CELL CAPACITY AND EFFICIENCY TO TEMPERATURE AND DISCHARGE RATE.

(ML-24)

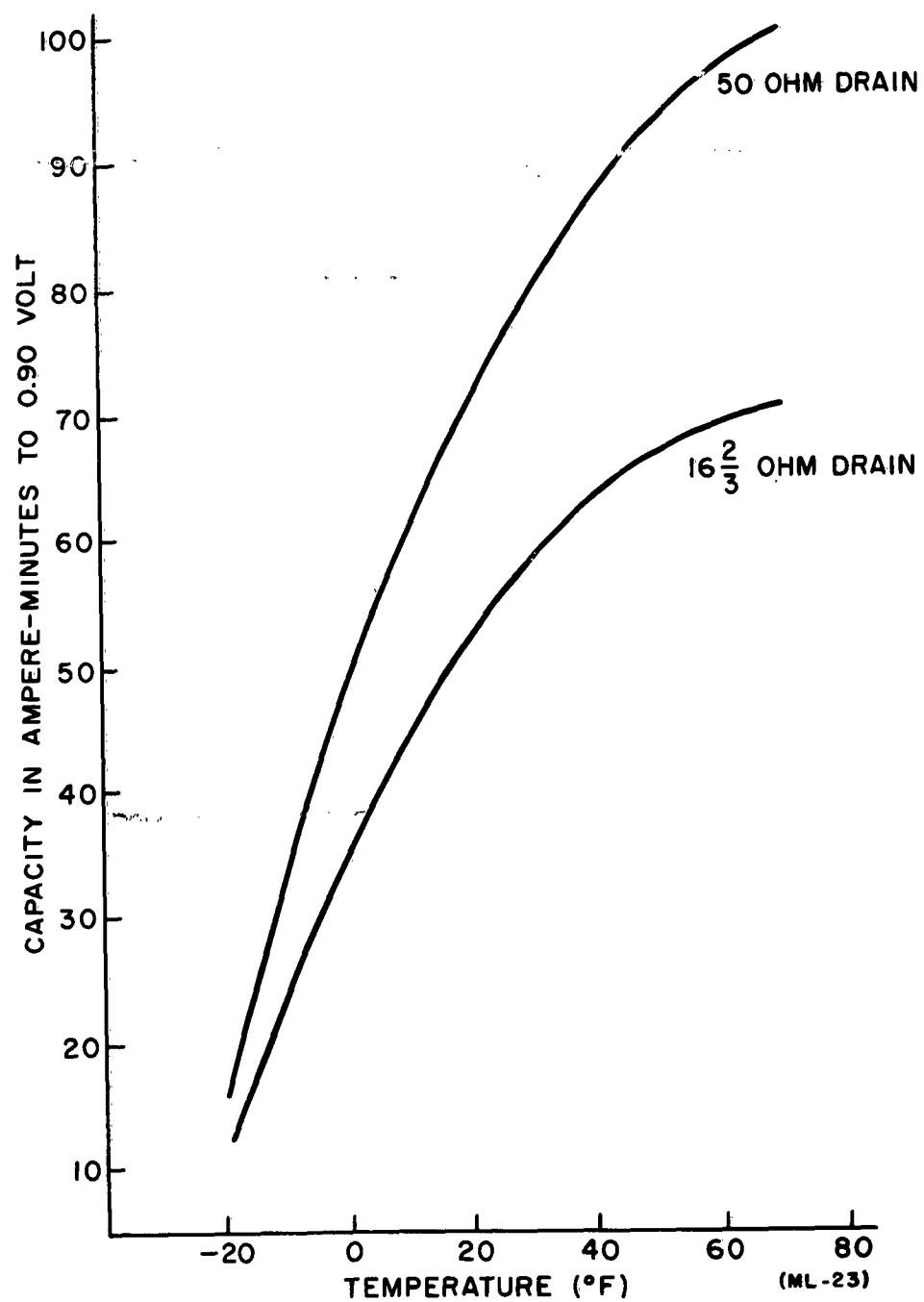
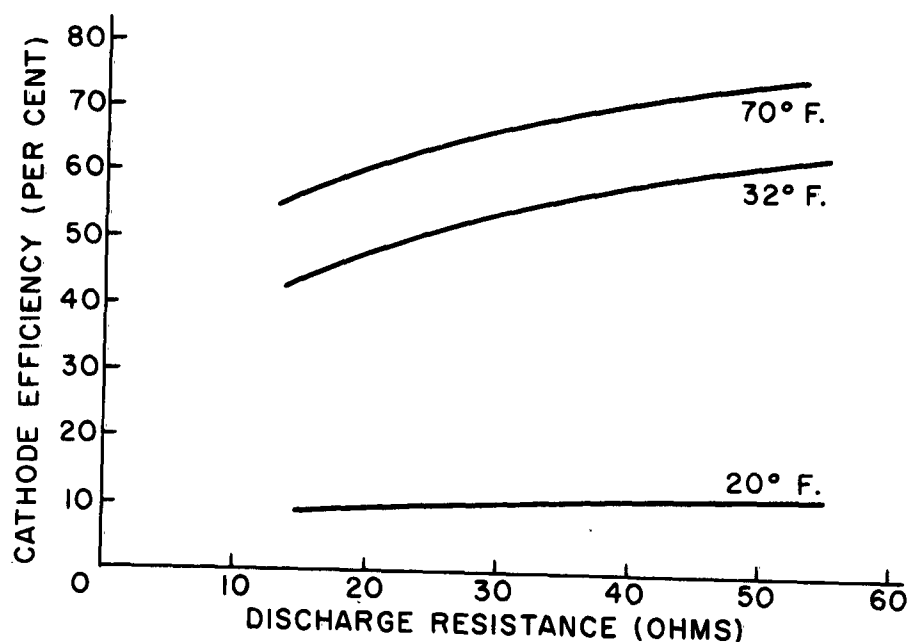
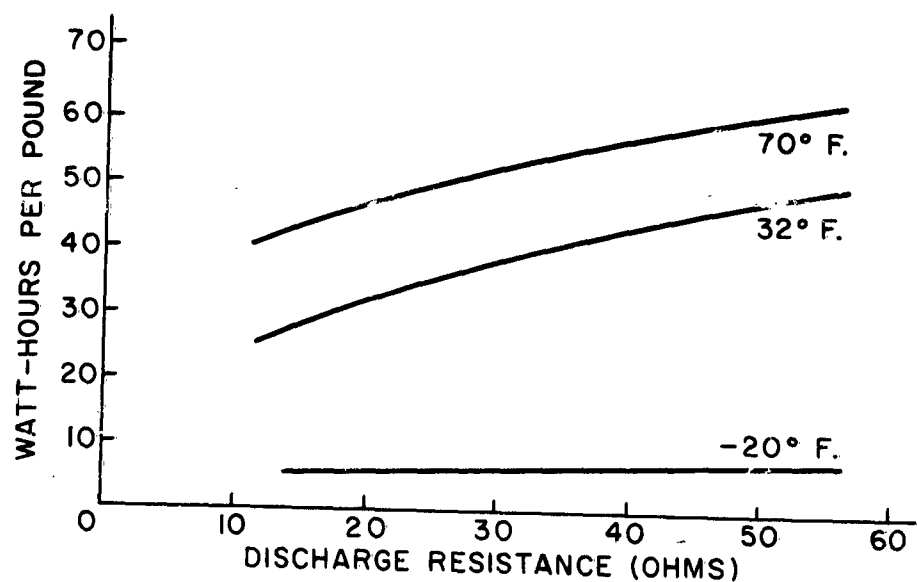


FIGURE 70. RELATION OF CAPACITY TO TEMPERATURE AND RATE OF DISCHARGE FOR  
 $\text{Mg}/\text{Mg}(\text{ClO}_4)_2/\text{MnO}_2$  A-CELLS.



(ML-24)

FIGURE 71. RELATION OF Mg/Mg(ClO<sub>4</sub>)<sub>2</sub>/MnO<sub>2</sub> CELL CAPACITY AND EFFICIENCY TO TEMPERATURE AND DISCHARGE RATE.

### 3.4.3 Low Temperature Studies

Capacity data for A-cells discharged through a 16-2/3-ohm load at 70°F and at -10°F are presented in Figure 72. The data show that the cell capacity is sharply reduced at the lower temperature and the cell retains only 26.5 percent of its room-temperature capacity. The low-temperature tests described above were conducted without covering or insulation.

In an effort to study the effects of insulation on cell capacity, two battery packs (six A-cells per pack) were constructed, one with a cardboard case and one with a polyurethane-foam case. The cardboard-case battery measured 2.05 x 1.425 x 2.175 inches and weighed 123.6 grams; the foam-case battery measured 2.675 x 1.85 x 3.075 inches and weighed 136 grams. The six-cell batteries were tested by storing at -20°F for 16 hours and subsequently discharging them through a 100-ohm resistor. The capacity data are presented in Figure 72. The data show that a discharge time of three hours and 45 minutes was obtained with the foam-insulated battery to a 5.4-volt end point with an average voltage of 7.55 volts; a discharge time of two hours and 10 minutes was obtained for the cardboard-case battery with a 6.2-volt average voltage. Although an improvement was realized with the foam insulation, only one-third of room-temperature capacity was obtained. Examination of cells after low-temperature discharge show some evidence of shrinkage in the Nibroc separator. This would cause poor contact between the anode and cathode and result in reduced cell capacity. Studies were conducted to determine the effect of the separator on low temperature capacity.

A study was made of differences in cell components at temperatures of 70°F and -20°F to determine possible causes of capacity loss at low temperatures. Cell anodes, cathode bobbin, separators, and carbon rods were measured and examined at the two temperatures. No change was noted in dimensions of the anodes or carbon rods. The separator and the cathode mix appeared wet and similar to room-temperature appearance at the -20°F temperature. The only significant variation noted was a slight loosening of the carbon rod in the cathode mix.

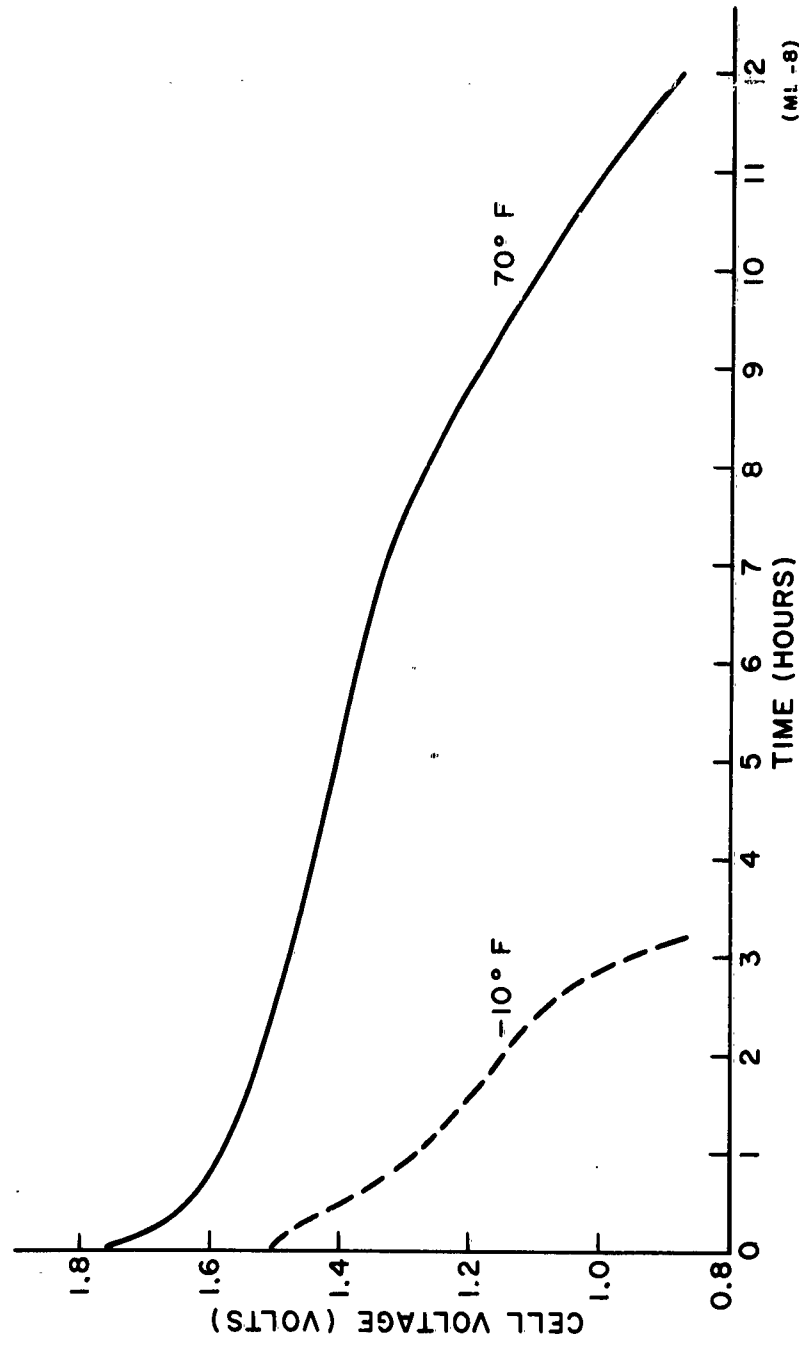


FIGURE 72. CAPACITY DATA FOR  $\text{Mg/Mg}(\text{ClO}_4)_2/\text{MnO}_2$  A-CELLS DISCHARGED CONTINUOUSLY AT 16-2/3 OHMS AT VARIOUS TEMPERATURES.

### 3.4.3.1 Cell Formulation

Cells were fabricated with the following cathode formulation:

<u>Amount.</u>	<u>Material</u>	<u>Percent (By Weight)</u>
783.0 g	MnO <sub>2</sub> (Type M)	53.6
90.0 g	Shawinigan Carbon Black	6.1
26.8 g	BaCrO <sub>4</sub>	1.1
26.8 g	Mg(OH) <sub>2</sub>	1.1
526.0 cc	5N Mg(ClO <sub>4</sub> ) <sub>2</sub> electrolyte	35.9

### 3.4.3.2 Variations in Cell Construction

As suggested previously, poor performance at -20°F is caused by contraction of the cathode mix away from the magnesium electrode and carbon rod. Accordingly, studies were conducted with various separator materials which might expand when wetted by electrolyte.

#### New Separator Material

Separator materials investigated were Webril (R-2601) and microporous polyethylene. Since the Webril material has a large, irregular pore structure, it was necessary to back the Webril with Nibroc paper to prevent shorting. The Webril has a density of 160 g/sq yard, and is .045-inch thick. The microporous polyethylene was .010-inch thick. The assembly of cells with the new separator was identical to that of conventional cells. Little or no improvement in cell performance was realized with the use of either separator material, as evidenced by the data presented in Figure 73. Inspection of discharged cells showed that some cathode material was able to penetrate the Webril separator. The cathode was also hard and dry.

### 3.4.3.3 Excess-Electrolyte Studies

As a result of the observations made on the dry condition of the cathode after discharge, cells were assembled with 25 percent more electrolyte.

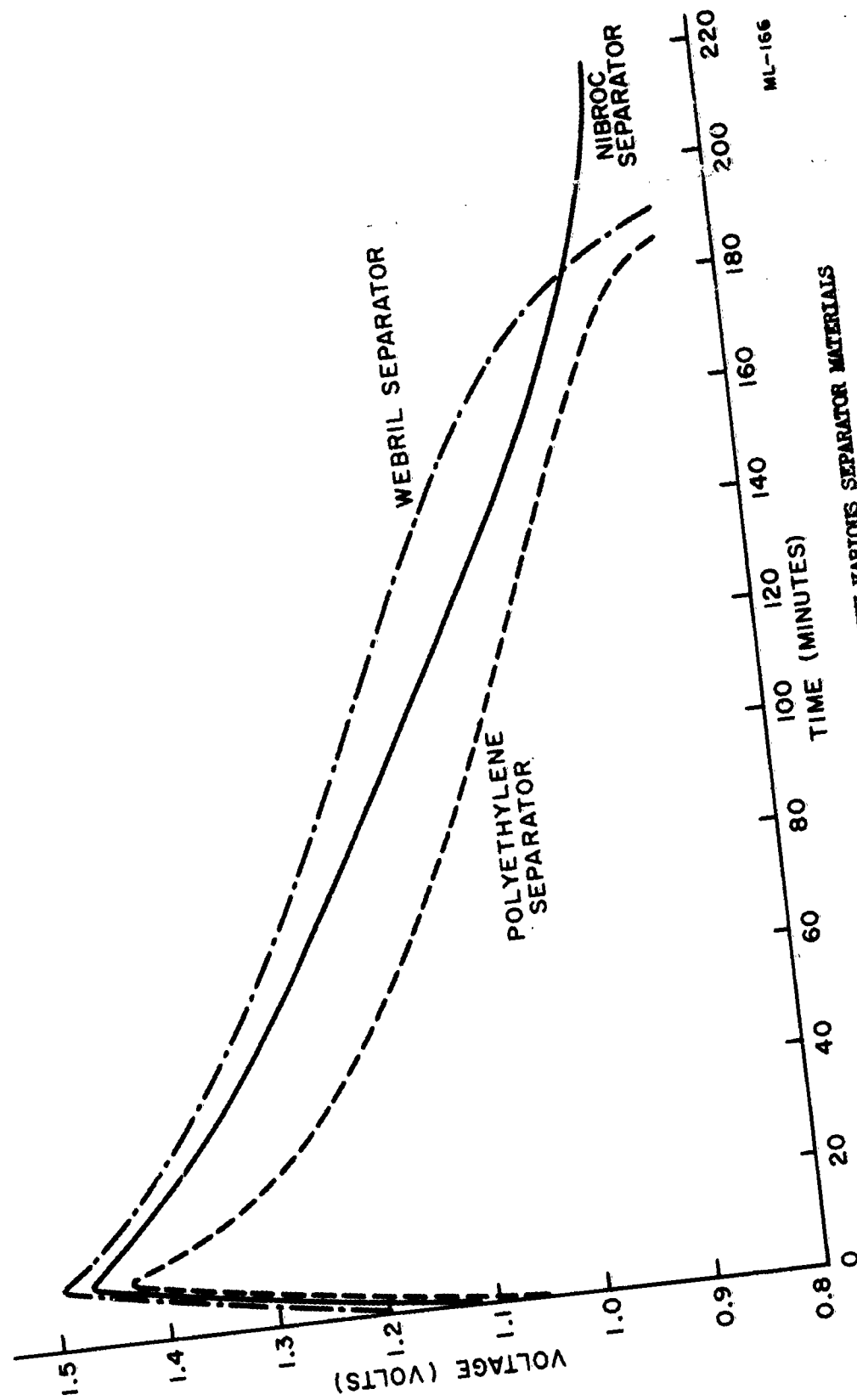


FIGURE 73.  $Mg/MgO_2$  DRY CELLS MADE WITH VARIOUS SEPARATOR MATERIALS AND DISCHARGED ON 16-2/3 OHMS AT  $-20^\circ F$ .

ML-166

Numerous problems were encountered in the assembly of the cells. First, the cathode bobbin could not be extruded, and made filling of the magnesium can an awkward and unpredictable process. Most of the test cells were shorted. Formulation of a  $\text{MnO}_2$ -cathode mix with 10 percent or more excess electrolyte is not ideally suited for the assembly and operation of the present A-cell design.

#### 3.4.3.4 Prepelled Cathode Electrodes

To further study the possibility of capacity loss due to contraction of the cathode bobbin, cells were constructed with pressed cathode electrodes. The following cathode formulation was used:

<u>Amount</u>	<u>Material</u>	<u>Percent</u> <u>(By Weight)</u>
109.5 g	$\text{MnO}_2$ (Type M)	52.6
14.5 g	Shawinigan Carbon Black	7.1
80.0 g	1.5% carboxy methyl cellulose (CMC) solution	38.4

This mix was pressed into a slug having the same dimensions as the extruded bobbin, and a silver wire was inserted into the center of slug to serve as the cathode collector. The pressed cathode slug was dried and inserted into the magnesium can. With the addition of 2.5 grams of 5N magnesium perchlorate electrolyte, the cathode swelled to fit tightly in the can.

Capacity data for 70°F and -20°F operation of these cells are presented in Figures 74 and 75. The cells were discharged on 16-2/3-ohm continuous load without insulation. The room-temperature data given in Figure 74 show an increase in ampere-minute capacity; however, the watt-hour efficiency is approximately the same as that shown by the area under the curves. At -20°F (Figure 75), the cells with prepelleted anodes had a severe loss in capacity. The low ionic conductivity of the electrolyte at this temperature and the increased internal resistance due to the CMC appeared to be responsible for the poor per-



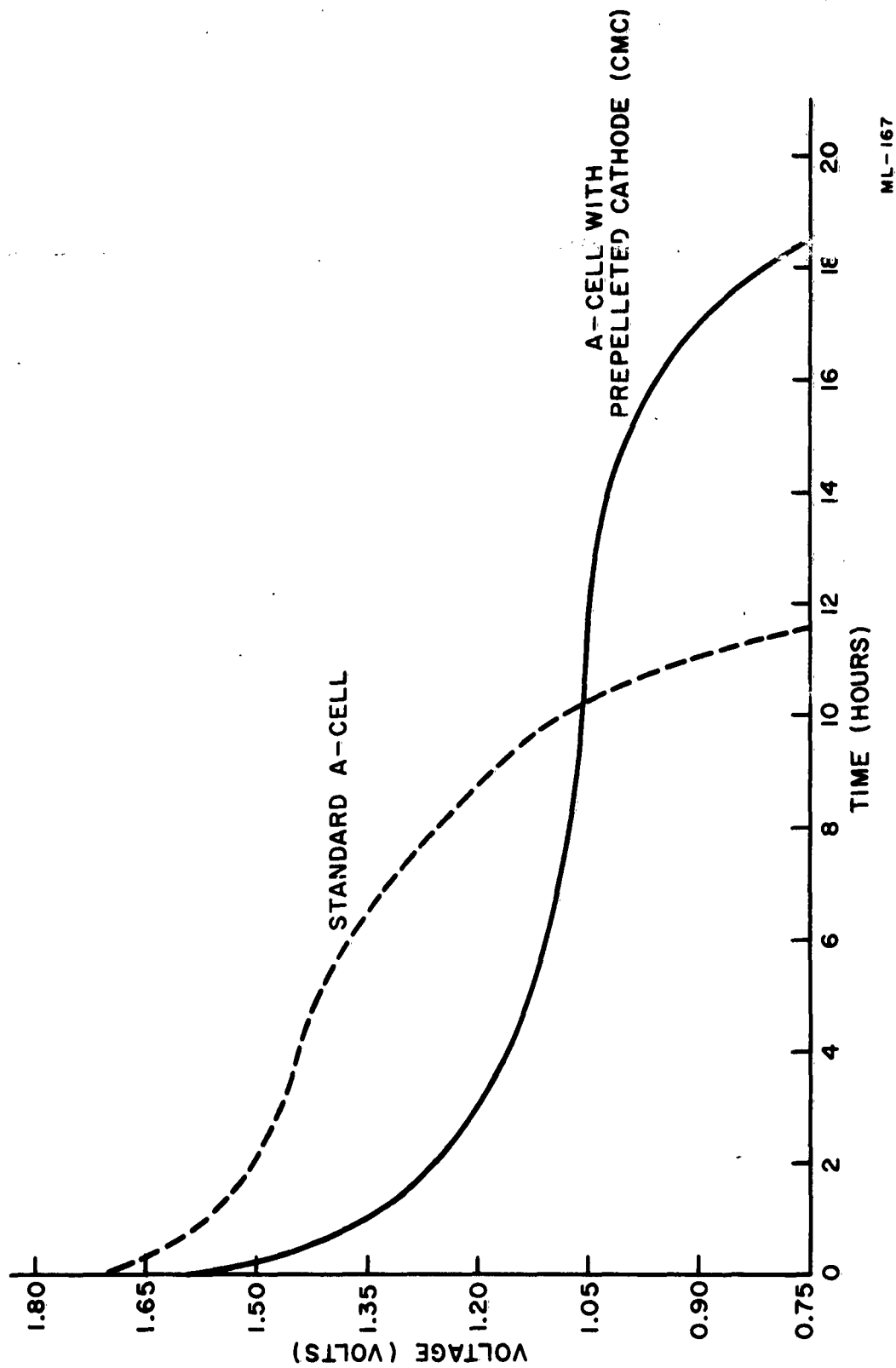
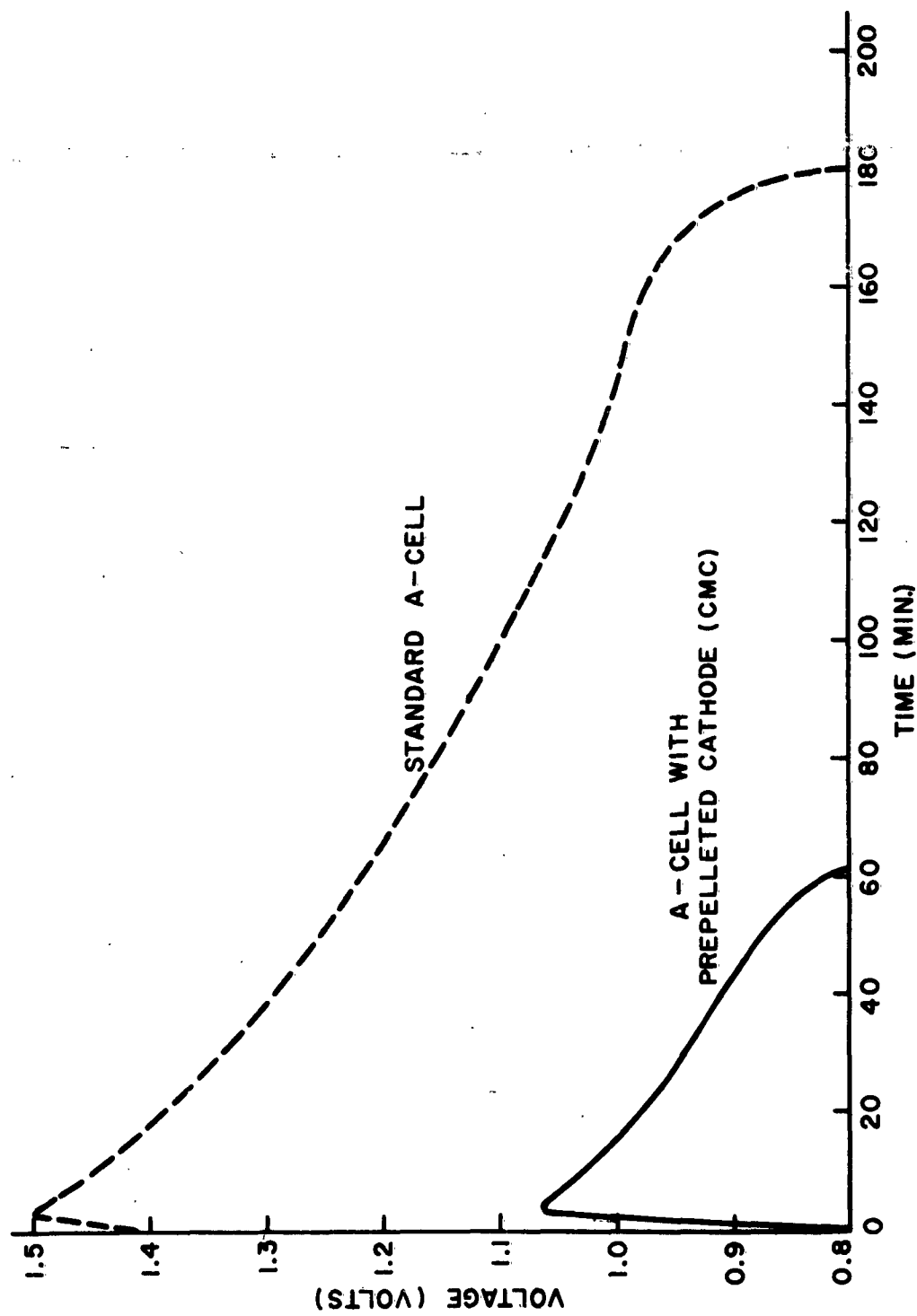


FIGURE 74.  $Mg/MnO_2$  DRY CELLS MADE WITH VARIOUS CATHODE CONSTRUCTIONS AND DISCHARGED ON 16-2/3 OHMS AT 70°F.

ML-167



ML-165

FIGURE 75.  $\text{Mg/MnO}_2$  DRY CELLS MADE WITH VARIOUS CATHODE CONSTRUCTIONS AND DISCHARGED ON  $16\text{-}2/3$  OHMS AT  $-20^\circ\text{F}$ .

formance. The low operating voltage at 70°F most probably was caused by addition of the CMC binder.

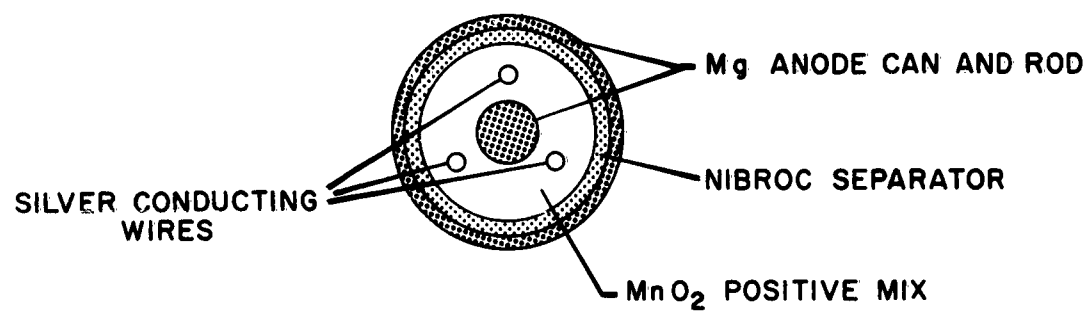
#### 3.4.3.5 Studies of Electrode Surface Area

A good low-temperature battery must possess the same characteristics as a cell performing at room temperature. The efficiency of the electrode reactions involved in the operation of a battery depends largely upon the area of the electrode surface available to the reactions. At low temperatures, the ionic conductivity of an electrolyte is greatly impaired. Therefore, the anode surface area must be made large to compensate for loss in ionic conductivity at lower temperatures. The increased surface area also serves to lower the current density and spread out the poor conducting-reaction products of manganese dioxide. In general, constructions which provide large surface areas are excellent choices for use at low temperatures.

The most convenient method of increasing the anode surface area in the A-cell is to insert a magnesium rod in place of the carbon cathode collector and to externally connect the rod to the can. This procedure increased the anode area by 50 percent. The positive conducting rods were silver wires inserted into the positive mix. Figure 76 is a sketch of the cell construction.

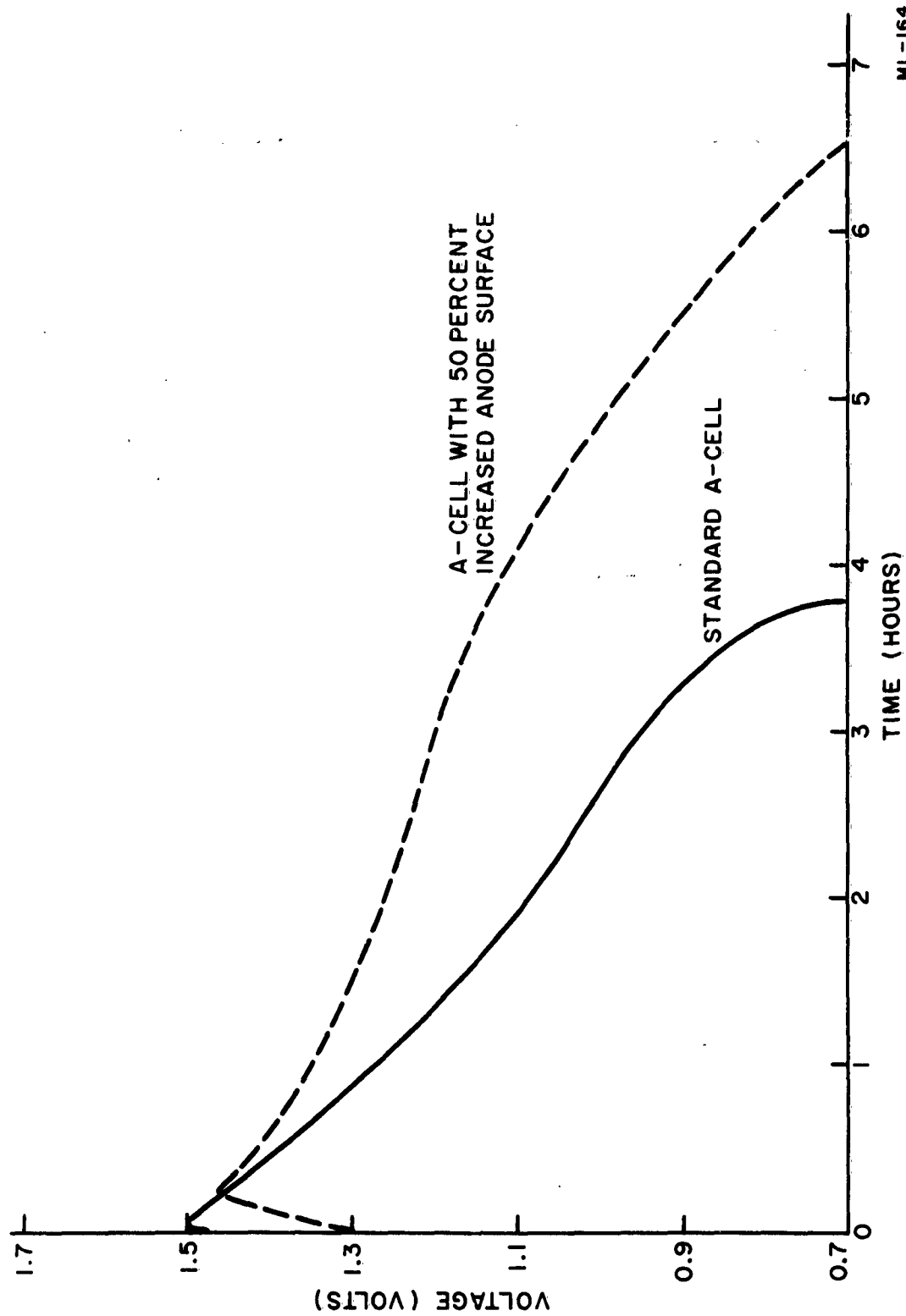
Capacity data for the A-cells described above are presented in Figure 77. These cells had a theoretical cathode capacity of 96 ampere-minutes, and were discharged on a 16-2/3-ohm load. The data show that A-cells with increased anode areas had increased capacity and watt-hour efficiency compared to those of standard construction. A similar improvement in performance was realized at 70°F, as evidenced by the data in Figure 78.

To further determine the effect of surface area on the capacity of the  $\text{Mg/Mg}(\text{ClO}_4)_2/\text{MnO}_2$  system at low temperature,  $\text{MnO}_2$  reserve-type plates were made with 2x2-inch silver grids and 8.7:1 dry-cell-mix ratio.



ML-170

FIGURE 76. BASIC CONSTRUCTION OF LOW-TEMPERATURE A-CELL HAVING INCREASED ANODE-SURFACE AREA.



ML-164

FIGURE 77.  $\text{Mg}/\text{Mg}(\text{ClO}_4)_2/\text{MnO}_2$  (TYPE M) A-CELLS OF INCREASED ANODE AREA. DISCHARGED ON 16-2/3 OHMS AT -20°F.

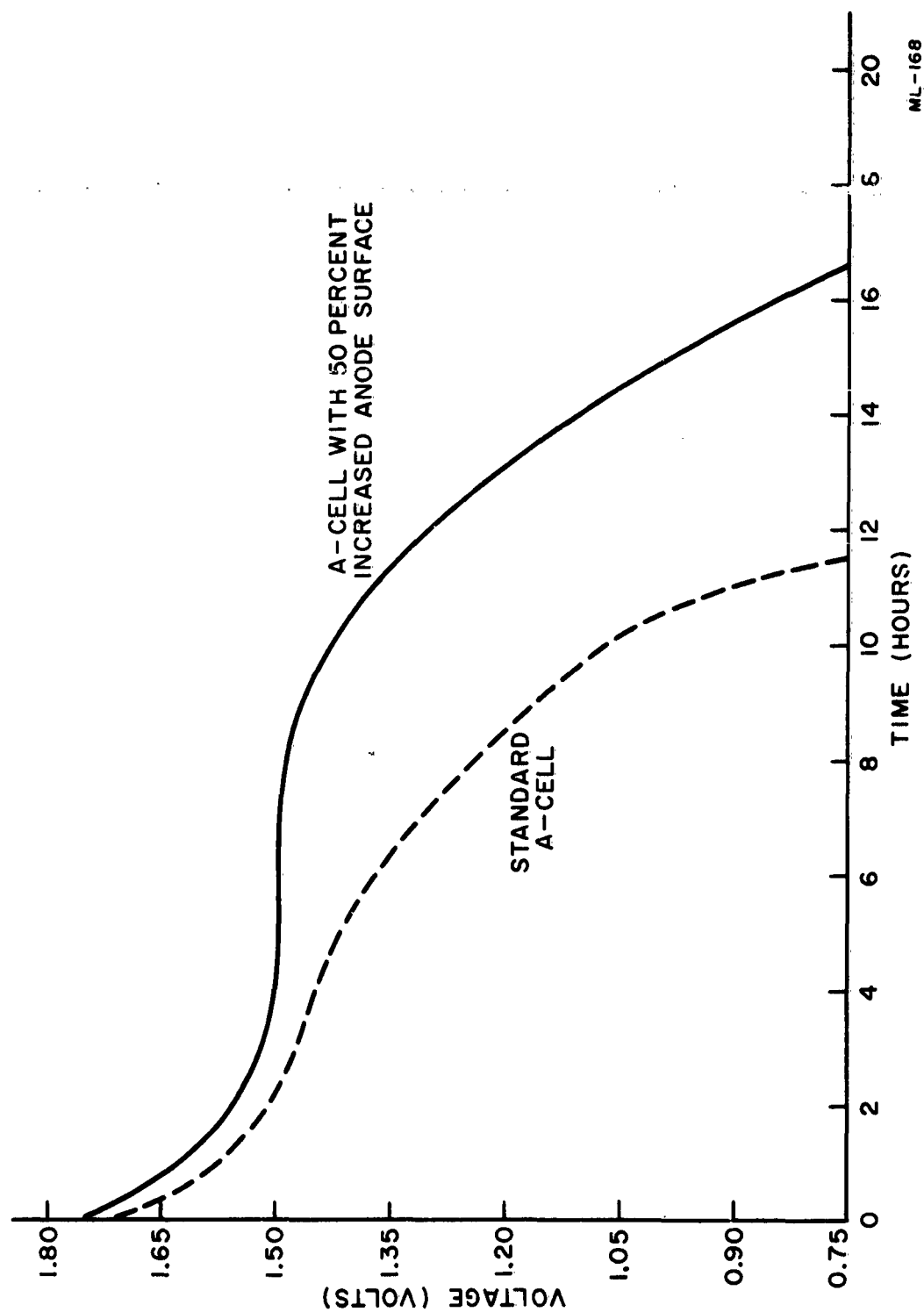


FIGURE 78.  $Mg/MnO_2$  A-CELLS OF INCREASED ANODE AREA, DISCHARGED ON 16-2/3 OHMS AT 70°F.

Two types of cells were made; the first had one cathode and one anode, the second had one cathode and two anodes. The cells were discharged on 16-2/3-ohm load at -20°F without insulation. The results, as evidenced by the data in Figure 79, show capacity increased from two hours and 12 minutes to six hours and 20 minutes by doubling the anode surface area. This increase in performance is similar to that found in the A-cells having increased surface area. An alternate A-cell design which would take advantage of maximum electrode surface area is one which used two thin, flat plates -- one of magnesium and the other of manganese-dioxide spread or pasted onto a flexible grid. The plates are placed on top of each other, with a separator between them, and then rolled. The spiraled element is inserted into a container. Data for cells discharged at -20°F on 16-2/3-ohm load is presented in Figure 80.

#### 3.4.4 Magnesium Can Studies

Fifty AZ-10 magnesium A-cell cans were treated by coating the interior air-space region with a vinylite-solvent mixture. Twenty-five cell lots of  $\text{Mg}(\text{ClO}_4)_2/\text{MnO}_2$  (Type M) and  $\text{Mg}(\text{ClO}_4)_2/\text{CuO}$  cells were assembled and placed on storage tests at 113°F. Two-months storage resulted in four perforations in the  $\text{MnO}_2$  cells and one perforation in the CuO cells. This represents an improvement over the untreated cans. In addition, this treatment yielded a better seal. Corrosion tests on restabilized AZ-10 magnesium A-cell cans in 2N  $\text{Mg}(\text{ClO}_4)_2$  with 1.0 g/l  $\text{LiCrO}_4$  and 0.5 g/l  $\text{Mg}(\text{OH})_2$  showed some improvement over untreated cans. Cell lots were tested for effect of storage.

The reported characteristics of AZ-21XA magnesium which included the low delay of AZ-10XA with the high anode efficiency of AZ-31A made this alloy desirable for extended dry-cell development. <sup>(1)</sup> A lot of A-cell cans was received and evaluation studies made. Tests on these cans in 2N  $\text{Mg}(\text{ClO}_4)_2$  with 1.0 g  $\text{LiCrO}_4$  and 0.5 g/l  $\text{Mg}(\text{OH})_2$  showed evidence of line-type corrosion. This corrosion, however, was very slight and is not expected to affect shelf life. One lot each of  $\text{Mg}/\text{Mg}(\text{ClO}_4)_2/\text{MnO}_2$  (Type M) and  $\text{Mg}/\text{Mg}(\text{ClO}_4)_2/\text{CuO}$  cells was made for 113°F storage. Discharge of these cells showed that the

- (1) R.F. Kirk and R.W. Reid, "Magnesium as a Battery Anode". Proceedings of the 14th Annual Power Sources Conference, U.S. Army Signal Research and Development Laboratory, Fort Monmouth, New Jersey, May, 1960.

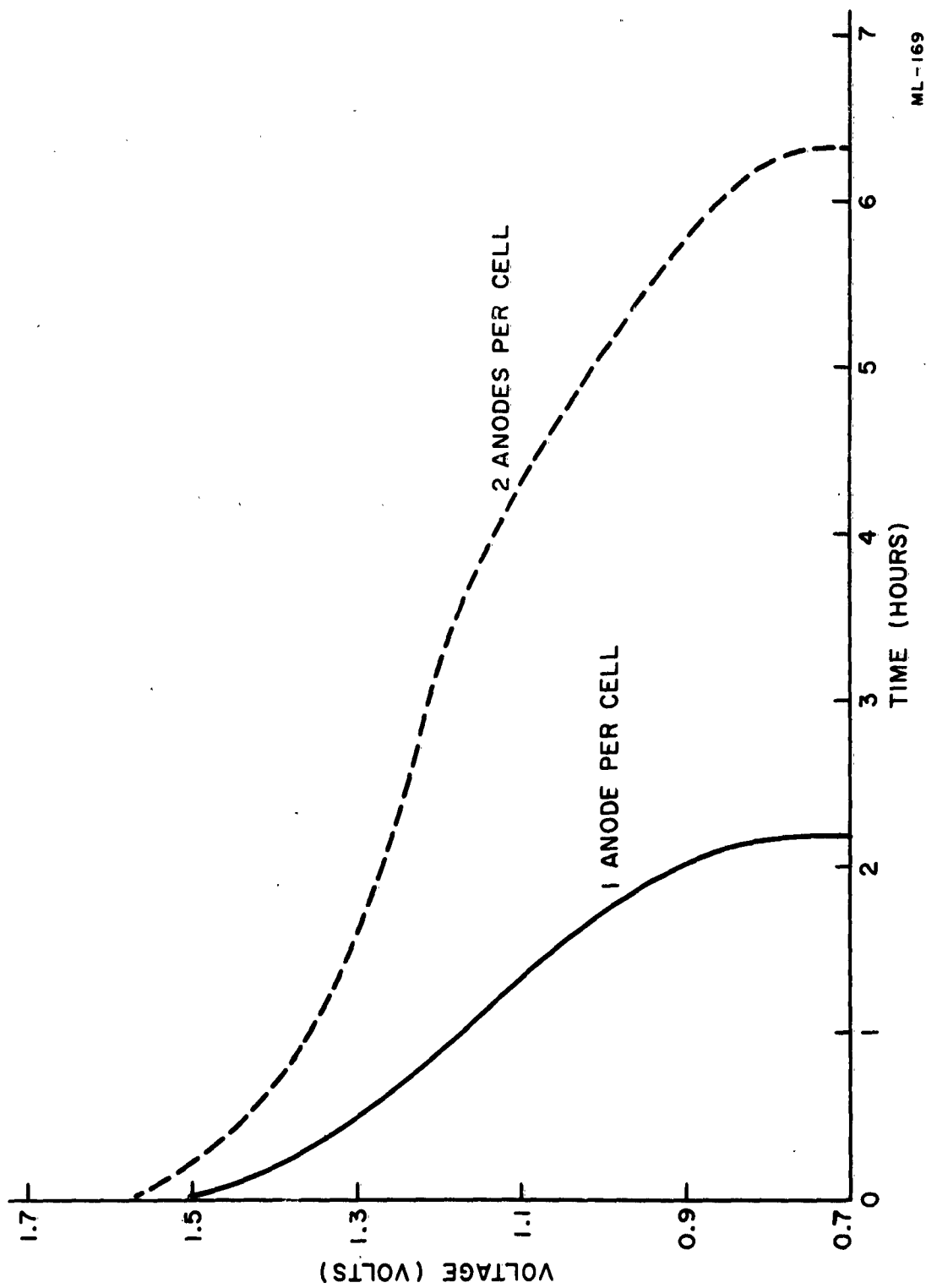


FIGURE 79.  $\text{Mg}/\text{Mg}(\text{ClO}_4)_2/\text{MnO}_2$  FLAT-PLATE CELLS OF VARIOUS ANODE SURFACES.  
CELLS WERE DISCHARGED ON 16-2/3 OHMS AT  $-20^\circ\text{F}$ .



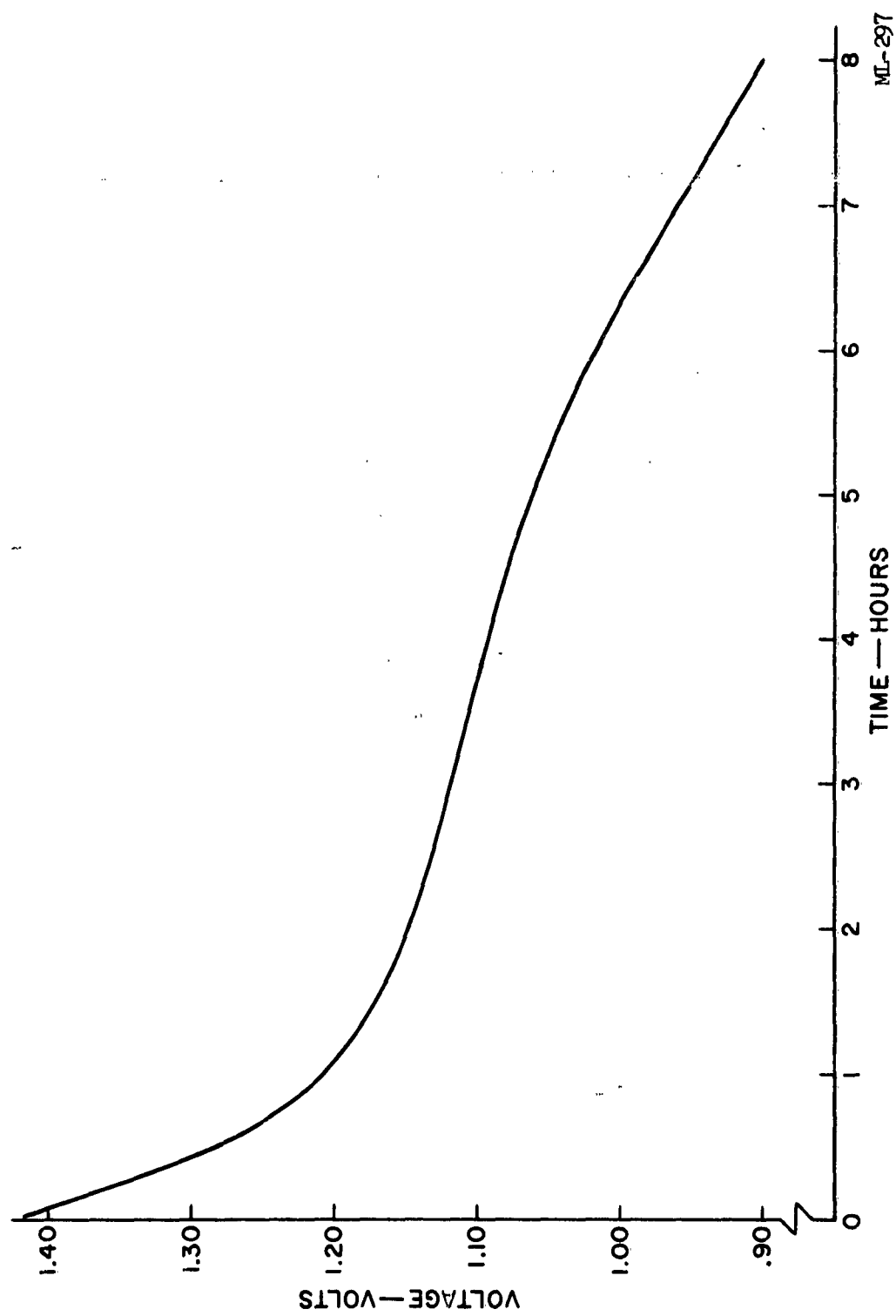


FIGURE 2. VOLTAGE—TIME CURVE FOR CELL WITH SPIRALED ELEMENTS. CELL WAS DISCHARGED ON 16-2/3-OHM LOAD AT  $-20^{\circ}\text{F}$ .

AZ-21XA magnesium operates at 0.03 volts lower than the AZ-10 alloy. Discharge curves are given in Figures 81 and 82. Storage tests for these cells have been evaluated and have been reported in another section of this report. Comparison tests were also run with a magnesium-bromide electrolyte.

Three-month storage of A-cell magnesium AZ-21 alloy/magnesium perchlorate/manganese dioxide (type M), and cupric-oxide dry cells at 113°F and 95 percent relative humidity showed no loss of capacity on 16-2/3-ohm drain. Four can perforations were found in the manganese dioxide cells and one perforation in the cupric-oxide cells, out of original lots of 50 cells each. The manganese-dioxide cells showed evidence of electrolyte leakage past the seal.

#### AZ-21 Magnesium

Six-months storage magnesium (AZ-21)/magnesium perchlorate/manganese dioxide (type M) A-cells at 113°F and 95 percent relative humidity showed a capacity retention of 95 percent. Eight cell perforations were found in the air-space region. The perforations were probably caused by electrolyte leakage resulting from poor seals. Other cells in the lot show evidence of electrolyte leakage around the seal. Additional cells were placed on storage for seal evaluation.

Six-months storage of A -size magnesium (AZ-21)/magnesium perchlorate/cupric oxide dry cells at 113°F and 95 percent relative humidity showed a capacity retention of 65 percent. Water content is a critical factor in cupric-oxide cells. Hence, loss of water through the seal could be a factor in limiting cell capacity. Three cell perforations were found in the lot.

A nine-months storage of A-cell magnesium/magnesium perchlorate/manganese dioxide (type M) dry cells at 113°F and 95 percent relative humidity resulted in 95 percent capacity retention on a 16-2/3-ohm continuous drain. Examination of the cells revealed evidence of leakage of the electrolyte past the seal. This may be caused by an excess of electrolyte in the mix. Additional cells were tested with a reduced amount of electrolyte to determine effect on leakage.

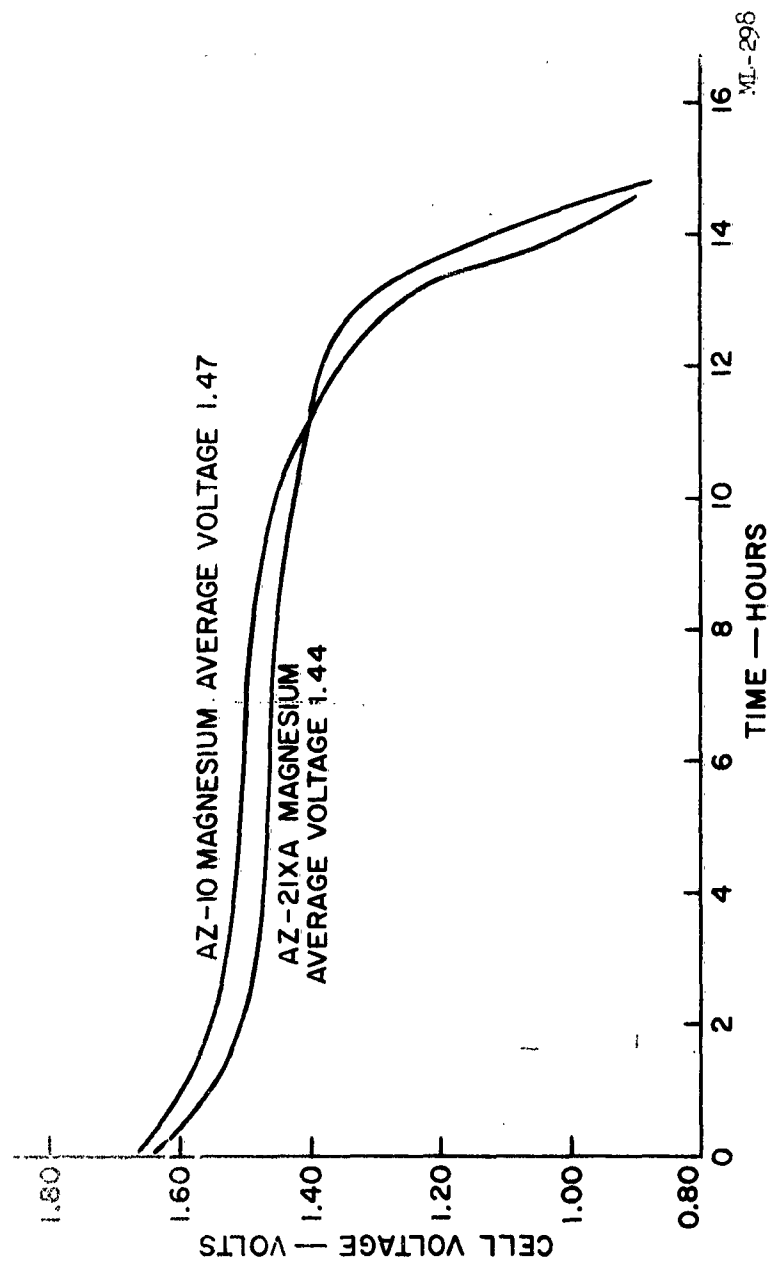


FIGURE 81. CAPACITY DATA FOR  $\text{Mg}/\text{Mg}(\text{ClO}_4)_2/\text{MnO}_2$  (TYPE M) A-CELLS AT 16-2/3 OHMS.

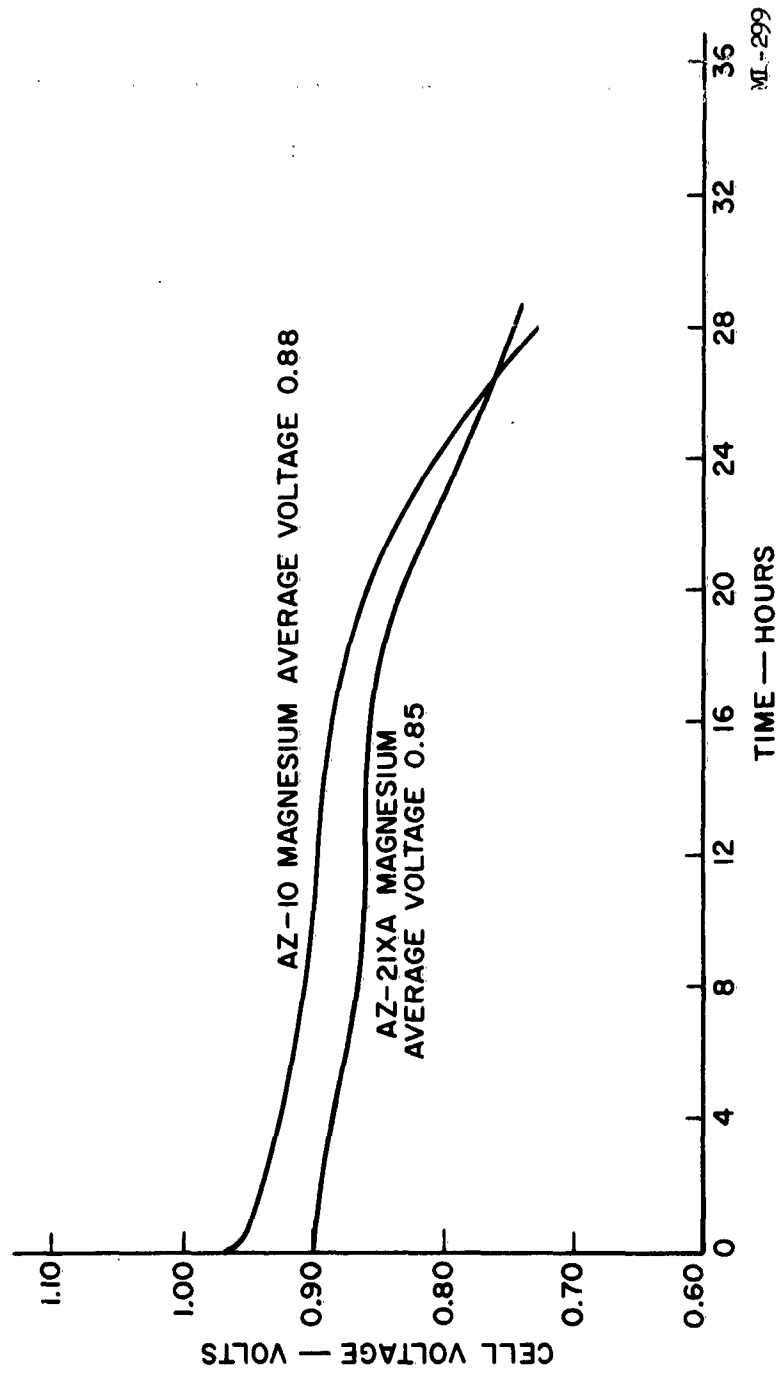


FIGURE 82. CAPACITY DATA FOR  $\text{Mg}/\text{Mg}(\text{ClO}_4)_2/\text{CuO}$  A-CELLS AT 10-2/3 OHMS.

The nine month results of the 16-2/3 ohm tests on magnesium-magnesium perchlorate-cupric oxide A-cells at 113°F and 95 percent relative humidity resulted in a capacity retention of 70 percent. No electrolyte leakage or perforations in the can were detected in these cells.

#### 3.4.4.1 Can Seal Studies

Previous cell storage studies indicated that loss of cell capacity was due to loss of water caused by faulty seals. Therefore, a study was carried out to find a better sealing compound for future storage lots. Tests were run on the sealing compounds presently used plus several additional samples obtained from the Mitchell Rand Manufacturing Corporation.

Evaluation of hot-wax seals to magnesium sheet showed that hard waxes, such as Mitchell Rand No. 1850 black and Mitchell Rand No. 3081 red, had little adhesive strength. Although better adhesion was obtained with the softer materials, these are undesirable for elevated temperature storage. Tests of magnesium A-cell cans filled with 2N  $\text{Mg}(\text{ClO}_4)_2$  electrolyte, sealed, and stored in an inverted position at 113°F and 95% relative humidity showed that the waxes tested were not entirely satisfactory as sealing agents.

The use of an asphalt-base paint pretreatment of the magnesium was studied prior to applying sealing compound as suggested by the Mitchell Rand Corporation. Results of hot-wax seals to magnesium sheet showed that this procedure improves bonding to the surface with most waxes. Best results were obtained by using this paint and a wax consisting of 90% Mitchell Rand No. 1850 black wax and 10% Atlantic shingle saturant. The shingle saturant provided a greater adhesion to the surface.

#### 3.4.4.2 Delayed Action Shelf Study

The delayed action study program was set up to determine cell voltage delay and capacity on a radio transceiver drain. The AN/PRC-35 (XC-2) A<sub>2</sub> unit drain was selected for testing as this represents a more

severe change from low to high current than most transceiver applications. The requirements for the A<sub>2</sub> unit drain are 8 ma for 18 minutes and 138 ma for 2 minutes.

Figure 83 gives a typical discharge curve for the initial capacity of a Mg/Mg(ClO<sub>4</sub>)<sub>2</sub>/MnO<sub>2</sub> (Type M) AA-cell for the above drain. The data are plotted as continuous for the 2-minute and 18-minute cycles.

The delayed-action data for this cell are presented in Figure 84 for the initial 2-minute cycles and at various points during the cell discharge. The delayed action for the initial 2-minute cycle is much greater than for the succeeding cycles and can be attributed to the chromate film obtained in the can pickling process and the concentration of lithium chromate added to the electrolyte. This delay diminishes quickly with subsequent cycling to a relatively constant value of less than one fifth of a second.

#### MnO<sub>2</sub> Cells

A comparison of delayed action characteristics was made between magnesium perchlorate/MnO<sub>2</sub> AA-size cells and magnesium bromide/MnO<sub>2</sub> AA-size cells using both AZ-10 and AZ-31 magnesium alloys.

The improvement in delay with Mg(ClO<sub>4</sub>)<sub>2</sub> cells over MgBr<sub>2</sub> cells was more pronounced with an AZ-31 magnesium anode. These cells exhibited only a slight delay below a 1.1-volt cutoff, whereas the MgBr<sub>2</sub> cells had a delay of several seconds throughout the entire discharge. These results indicated that the perchlorate cells would show favorable delayed-action characteristics with the alloys other than AZ-10.

#### Mg/Mg(ClO<sub>4</sub>)<sub>2</sub>/CuO Cells

The delayed action characteristics of Mg/Mg(ClO<sub>4</sub>)<sub>2</sub>/CuO AA-cells were measured on the Radio Set AN/PRC-35(XC-2) A2 unit drain. Magnesium-

cupric oxide cells were discharged for 18 minutes into 91 ohms and for 2 minutes at 5.39 ohms to a 0.74-volt cutoff.

The delayed action of two-week-old cells on the initial two cycles and at various times throughout the discharge is presented in Figure 85. After the initial cycle, the delay approaches a constant value of less than 1/5 of a second. This agrees with the results found with the magnesium perchlorate/ $\text{MnO}_2$  cells.

Storage of cells at 70°F and 113°F for as long as 13 months showed no effect on the delayed action characteristics. The data curves (Figures 83 and 84) can be considered representative of results up to 13 month storage period. Intermittent capacity data for the above cells are summarized in Table XXI.

### 3.5 BASIC RESEARCH

#### 3.5.1 Impedance of Dry Cells

##### 3.5.1.1 Introduction

Data are presented in Figures 86 and 87 and Tables XXII and XXVIII for the delayed action of the two magnesium alloys measured at various times throughout discharge. The results show that magnesium AZ-21 behaves similarly to AZ-31. The voltage level of the AZ-21 is slightly lower than the AZ-10, as indicated by continuous-drain tests. Cell capacity was equivalent for both alloys, giving 50 hours to a 1.20-volt cutoff. Peak-voltage data are presented in Table XXII. Data are taken from measurements made throughout the first minute of the 18-minute cycle. The results show that both alloys operate with voltage in excess of 1.80-volts in the initial 15 seconds of the cycle during the first eight hours of discharge. The AZ-21 voltage levels off faster than the AZ-10, and operates about 0.1-volt lower on the light drain. Thus, AZ-21 appeared to be the more desirable alloy in applications where peak voltages are a problem.

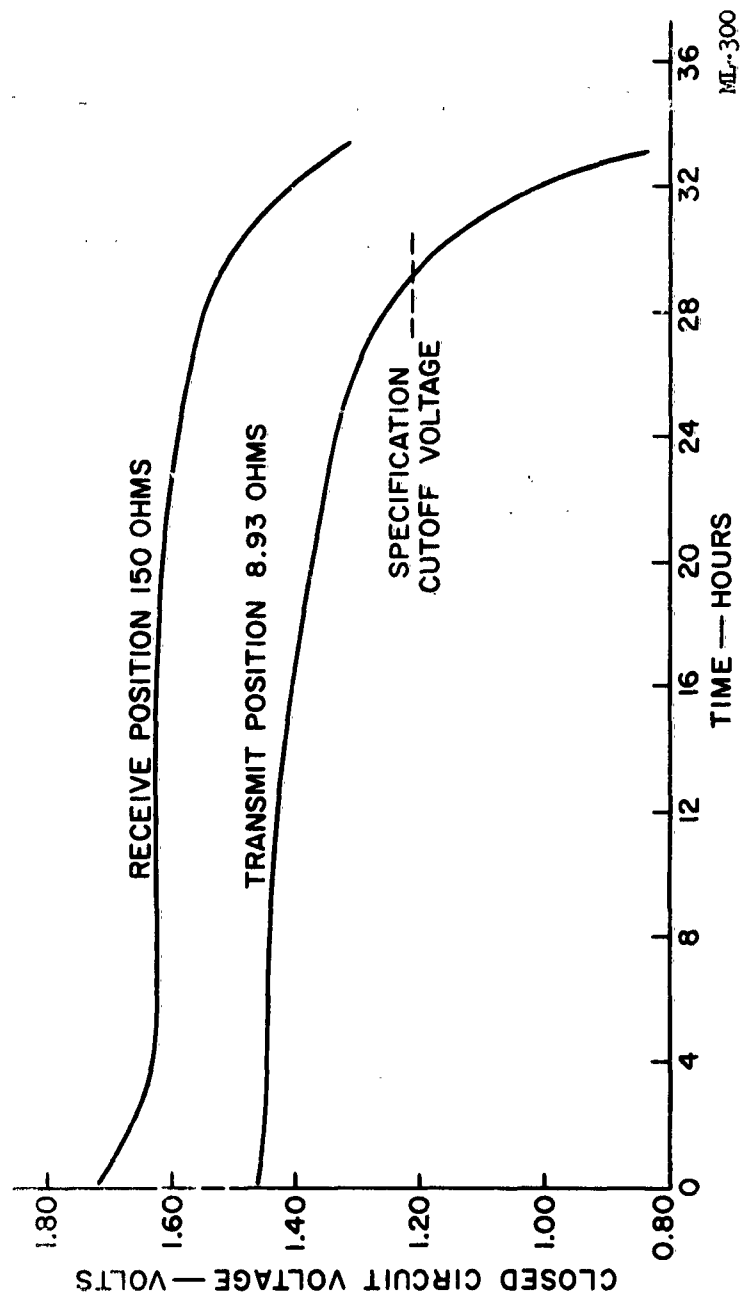


FIGURE 83. CAPACITY DATA FOR  $\text{Mg}/\text{Mg}(\text{ClO}_4)_2/\text{MnO}_2$  (TYPE M) AA-CELLS. DISCHARGED INTERMITTENTLY THROUGH 150 OHMS FOR 18 MINUTES AND 8.93 OHMS FOR 2 MINUTES.



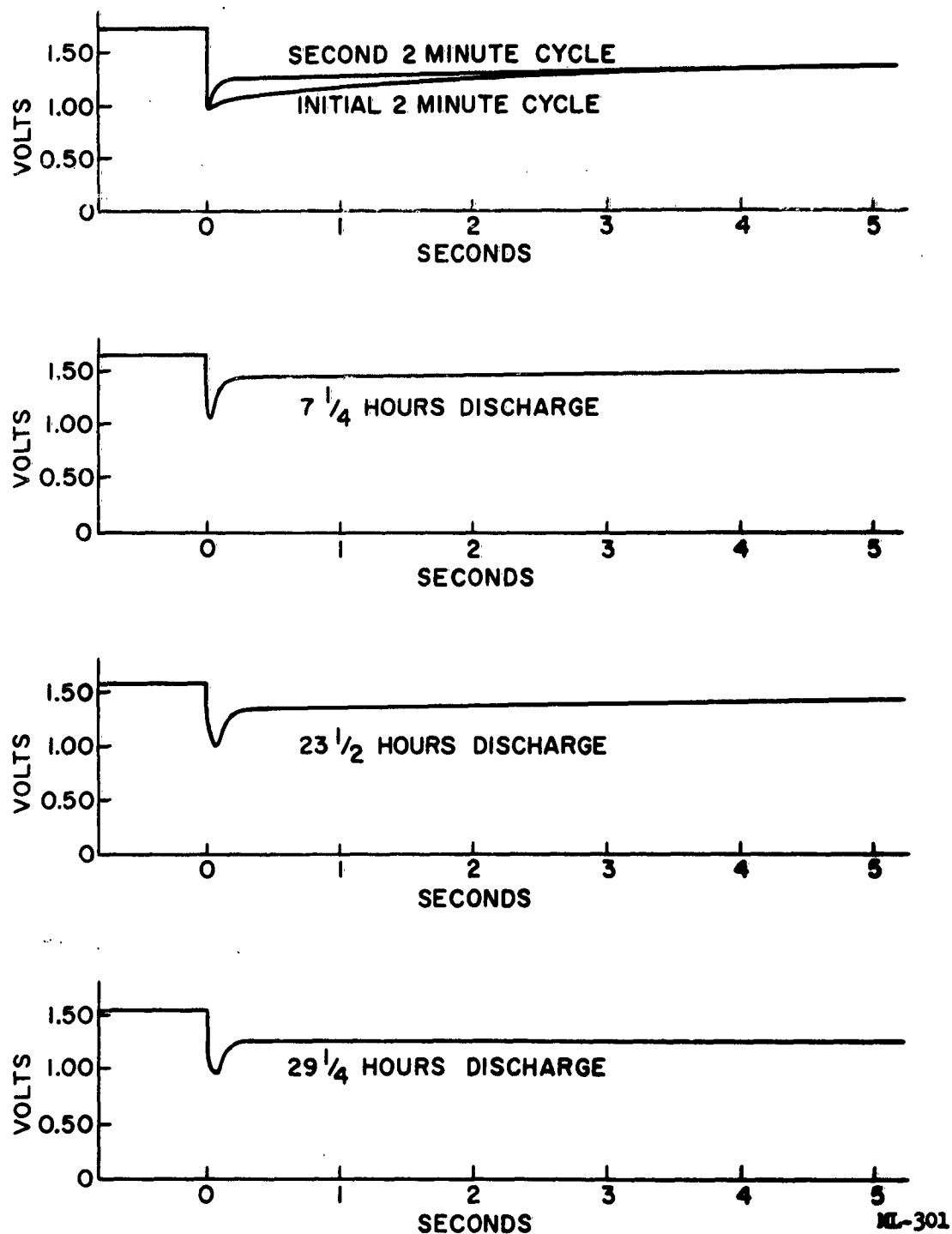


FIGURE 84. DELAYED ACTION CHARACTERISTICS OF  $\text{Mg}/\text{Mg}(\text{ClO}_4)_2/\text{MnO}_2$  (TYPE N)  
AA-CELLS AT 150- TO 8.93-OHM DRAIN.

	CUTOFF VOLTAGE (Volts)	STORAGE CONDITION*	INITIAL CAPACITY (%)	MONTHS		
				ONE	THREE	SIX
Mg(AZ-10)/Mg (ClO <sub>4</sub> ) <sub>2</sub> /MnO <sub>2</sub> (Type M)	1.20 1.10 1.00	A	30 31 33	- - -	28.25 30.25 31.5	27 29 31
Mg(AZ-31)/Mg (ClO <sub>4</sub> ) <sub>2</sub> /MnO <sub>2</sub> (Type M)	1.20 1.10 1.00	A	29 31.75 33.5	- - -	27.25 31.25 32.75	28.5 32 34
Mg(AZ-10)/MgBr <sub>2</sub> /MnO <sub>2</sub> (Type M)	1.20 1.10 1.00	A	28.75 - 31.25	- - -	30.25 32.5 33.5	29.75 32 32.75
Mg(AZ-31)/MgBr <sub>2</sub> /MnO <sub>2</sub> (Type M)	1.20 1.10 1.00	A	25.5 28.25 30	- - -	25.25 - 30.25	- - -
Mg(AZ-10)/Mg (ClO <sub>4</sub> ) <sub>2</sub> /CuO (C.P.)	0.78 0.75 0.73	A	24 37.75 40.75	- - -	24 35 39.25	- - -
Mg(AZ-10)/Mg (ClO <sub>4</sub> ) <sub>2</sub> /MnO <sub>2</sub> (Type M)	1.20 1.10 1.00	B	28.5 30.5 31.5	28 30 31.5	26 28.5 30	32,31.25 35,34.75 37,36.25
Mg(AZ-10)/MgBr <sub>2</sub> /MnO <sub>2</sub> (Type M)	1.20 1.10 1.00	B	32 33.75 34.75	28.25 29.75 30.5	27.5 29.5 30.5	28.5 31 33
Mg(AZ-10)/Mg (ClO <sub>4</sub> ) <sub>2</sub> /CuO (C.P.)	0.78 0.75 0.73	B	26.25 39.25 41.25	23.5 38 45.25	26 34 39	- - -

\*A = 70±2°F, 50% R.H.  
B = 113±2°F, 95% R.H.

TABLE XXI. SHELF-LIFE DATA FOR MAGNESIUM CELLS DISCHARGED UNDER AN INTERMITTENT ANP/RC-35 (XC-2) A2 CURRENT DRAIN.

MT-64

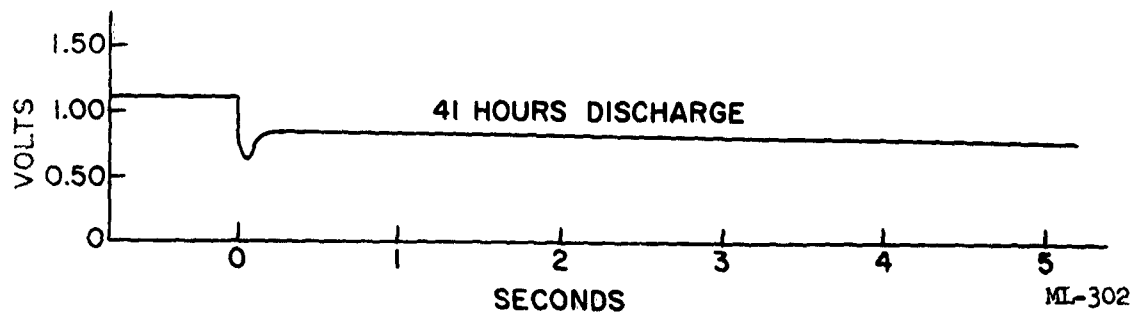
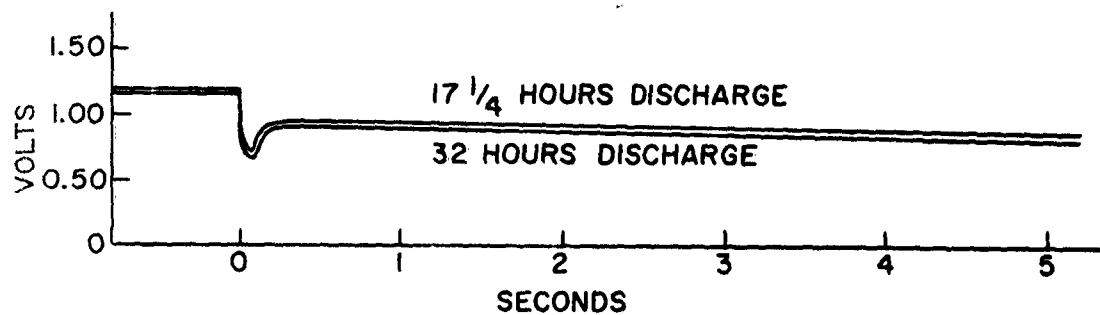
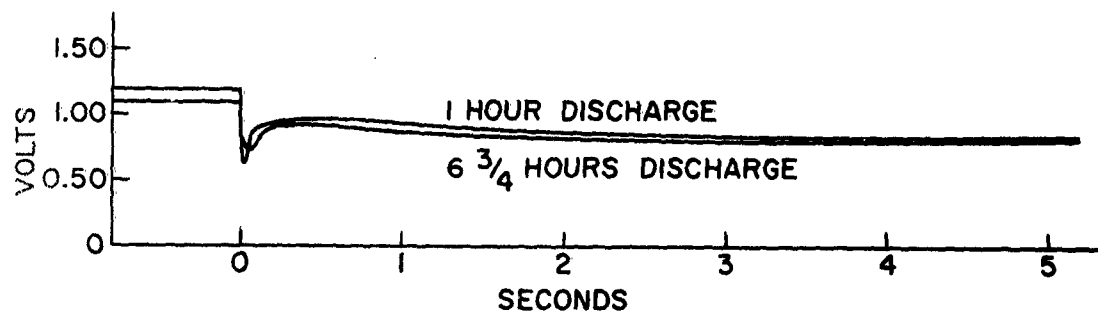
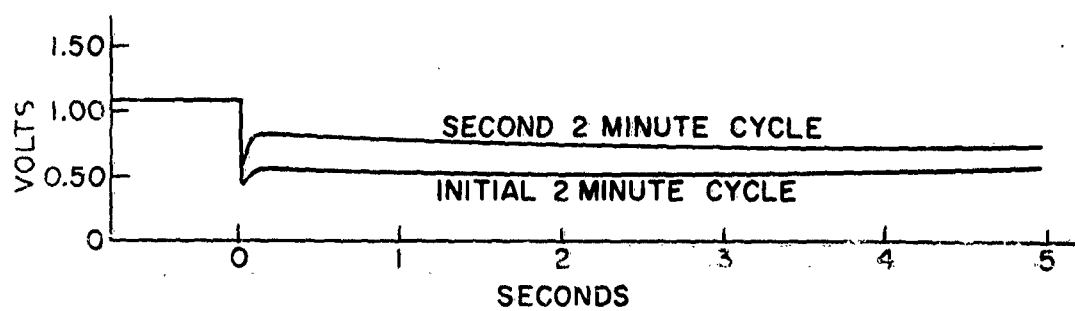


FIGURE 85. DELAYED ACTION CHARACTERISTICS OF  $\text{Mg}/\text{Mg}(\text{ClO}_4)_2/\text{CuO}$  AA-CELLS  
AT 91-OHM TO 5.39-OHM DRAIN.

ML-302

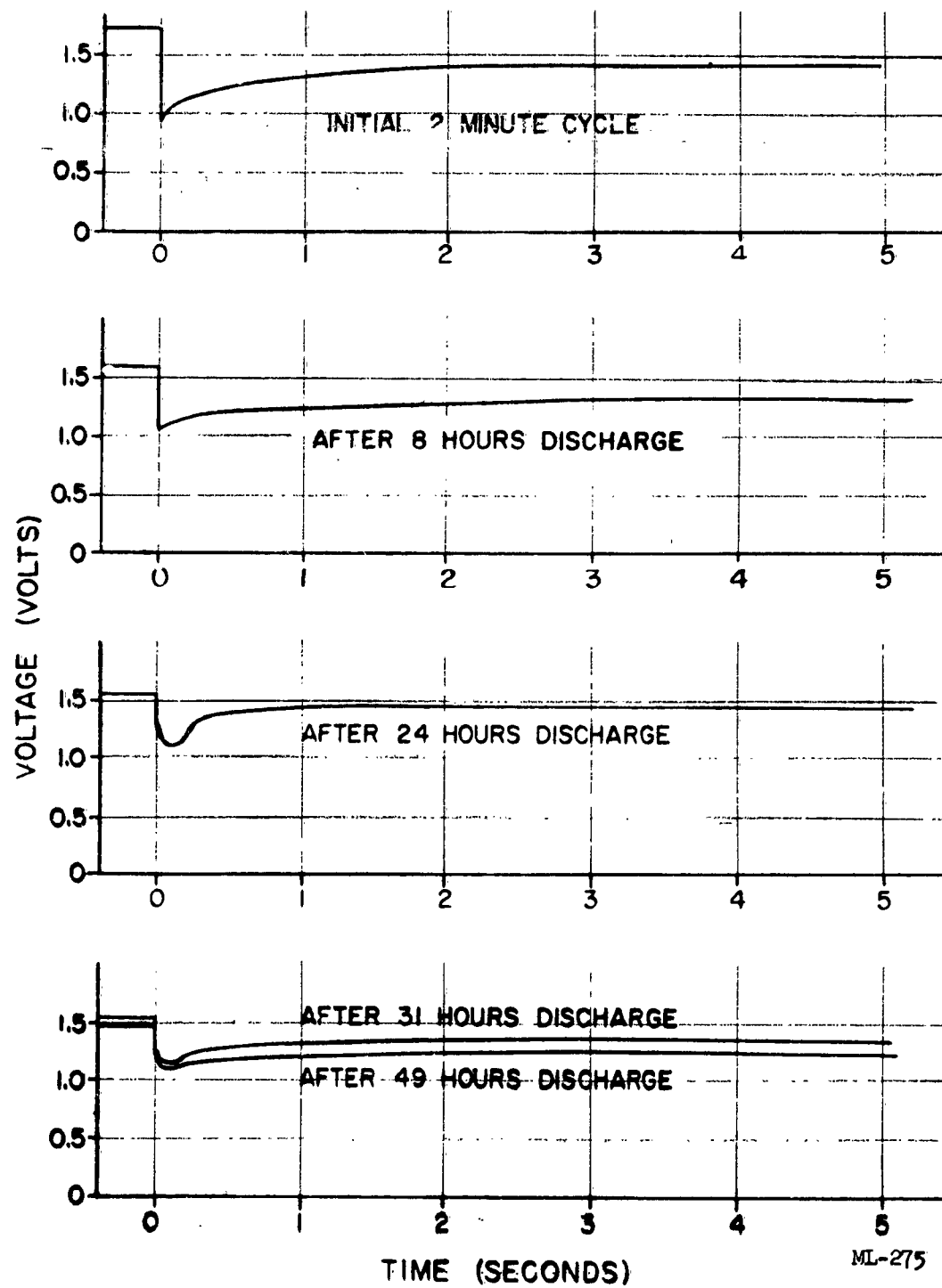


FIGURE 86. DELAYED-ACTION CHARACTERISTICS OF AZ-21  $\text{Mg}(\text{MgClO}_4)_2/\text{MnO}_2$  (TYPE M) A-CELLS AT 150-OHM TO 8.9-OHM DRAIN.

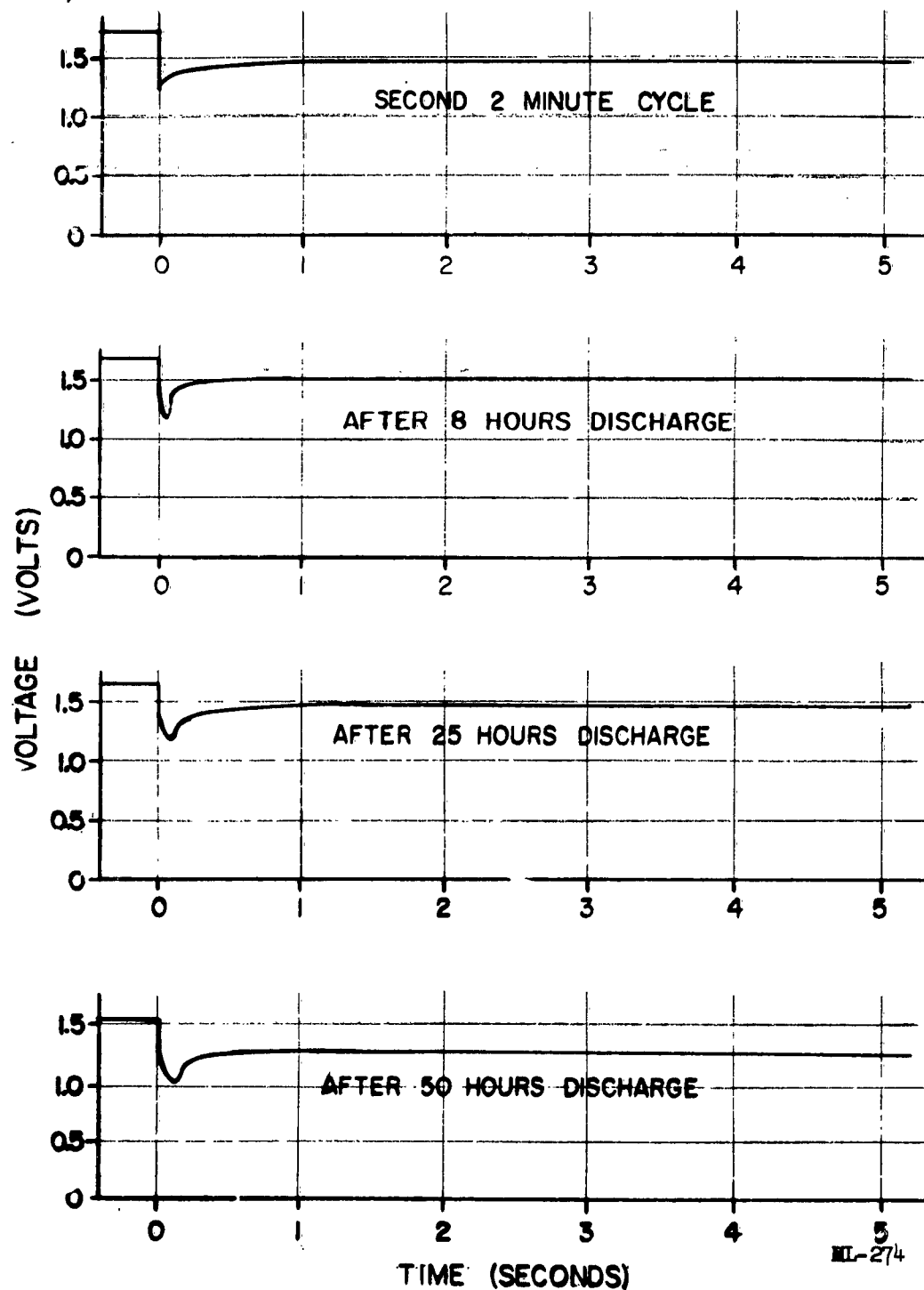


FIGURE 87. DELAYED ACTION CHARACTERISTICS OF  $\text{Mg}(\text{AZ-10})/\text{Mg}(\text{ClO}_4)_2/\text{MnO}_2$  (TYPE M) A-CELLS AT 150-OHM TO 8.9-OHM DRAIN.

CELL VOLTAGE (Volts)																
TIME AFTER DISCHARGE (Hours)	AFTER 18-MINUTE CYCLE of 150 Ohms	SECONDS ELAPSED DURING 2-MINUTE CYCLE (8.9 Ohms)						SECONDS ELAPSED DURING 18-MINUTE CYCLE (150 Ohms)								
		5	15	30	60	90	120	1	5	10	15	30	45	60		
<u>AZ-21 ALLOY</u>																
.5	1.70	1.37	1.43	1.47	1.50	1.50	1.51	1.90	1.88	1.72	1.70	1.72				
8	1.60	1.32	1.35	1.37	1.39	1.40	1.40	1.80	1.77	1.67	1.57	1.58	1.59	1.60		
24	1.55	1.40	1.41	1.41	1.41	1.40	1.40									
31	1.53	1.35	1.37	1.40	1.40	1.40	1.40	1.70	1.67	1.62	1.58	1.50	1.52	1.53		
49	1.48	1.20	1.22	1.23	1.23	1.23	1.24	1.62	1.60	1.55	1.50	1.43	1.45	1.46		
<u>AZ-10 ALLOY</u>																
.5	1.73	1.44	1.45	1.46	1.46	1.47	1.48	1.88	1.83	1.78	1.72	1.73	1.74	1.74		
8	1.66	1.50	1.49	1.49	1.48	1.48	1.48	1.88	1.89	1.88	1.87	1.78	1.72	1.70		
25	1.66	1.45	1.45	1.44	1.44	1.43	1.42	1.76	1.76	1.75	1.73	1.70	1.68	1.68		
50	1.53	1.23	1.21	1.20	1.20	1.19	1.19	1.60	1.63	1.63	1.62	1.61	1.50	1.59		

MT-65

TABLE XXII. VOLTAGE VARIATIONS OF  $\text{Mg}/\text{Mg}(\text{ClO}_4)_2/\text{MnO}_2$  (TYPE M) A-CELLS WITH AZ-10 AND AZ-21 MAGNESIUM ALLOY ON INTERMITTENT SERVICE.

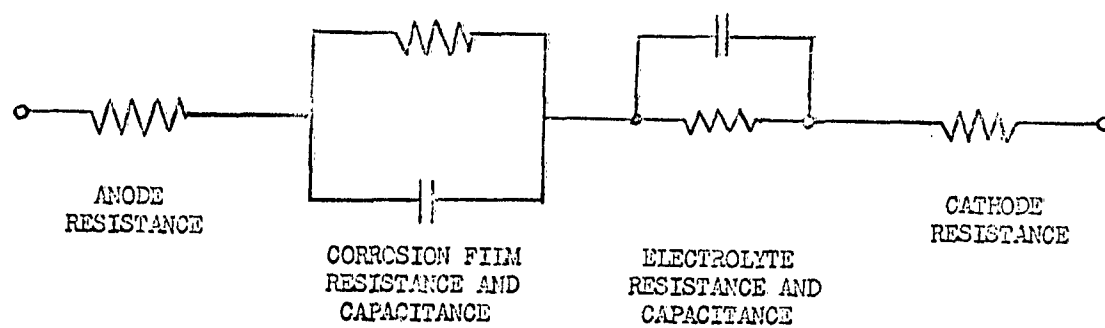
The wide voltage range noted in this type of intermittent service must be considered carefully in the design of magnesium dry-cell packs. Raising the cutoff voltage per cell would minimize the peak-voltage, but would increase the lower delay voltage on the high-drain cycle.

The impedance of cells of the type under consideration is represented schematically in Figure 88. The anode and cathode resistances shown are negligible by comparison with the other ac effects, and may be eliminated from the discussion. Of particular interest is the physical structure of the corrosion film and its effect on the overall cell performance. If a range of frequencies can be found in which the electrolyte capacitance does not affect the cell impedance, the necessary electrical data on the film can be obtained. An ideal two-component system with the equivalent circuit shown in Figure 88 will have a frequency characteristic similar to that shown in Figure 89.

Figure 89 shows a relatively constant-capacitance value followed by an abrupt drop, and a second constant-capacitance value followed by another abrupt drop. The first constant-capacitance value represents the capacitance of both components of the system -- the electrolyte and the anode film. The initial drop in capacitance occurs when the capacitance of the high-capacity element, the electrolyte, is damped by the resistance and ceases to function as a dielectric. At this point, this capacitance ceases to be an operating part of the system. The second constant value represents the capacitance due only to the anode film in the low-capacity parallel branch. The second drop in capacitance occurs when this parallel capacitance is damped by the circuit resistance. Thus, it is possible to separate the effects within a two-component system if a broad range of frequencies can be found to enable the study of a single component.

#### 3.5.1.2 Measurements and Equations

Commercial impedance bridges cannot be used because the capacitance of the cells is very high and the series resistance is often as high as or



ML-277

FIGURE 88. EQUIVALENT CIRCUIT OF THE MAGNESIUM CELL.





ML-278

FIGURE 89. IDEAL FREQUENCY CHARACTERISTICS OF A TWO-COMPONENT SYSTEM.

higher, than the reactance. Therefore, a special resistance-ratio impedance bridge was designed and built; this bridge is shown schematically in Figure 90. The bridge uses very high transformer turn ratios (up to 5000 to 1), two 2500- $\mu$ f capacitors which prevent spurious cell loading by the oscillator and detector circuits, and a load resistor,  $R_L$ , in parallel with the unknown impedance to obtain various current densities. The use of the load resistor,  $R_L$ , necessitates a correction in the measured value of resistance. Direct values for this bridge are obtained with equations (1) and (2), and equation (3) is the corrected value of the equivalent parallel resistance.

$$R_X' = \frac{R_2}{R_1} R_S \quad (1)$$

$$C_X = \frac{R_1}{R_2} \quad (2)$$

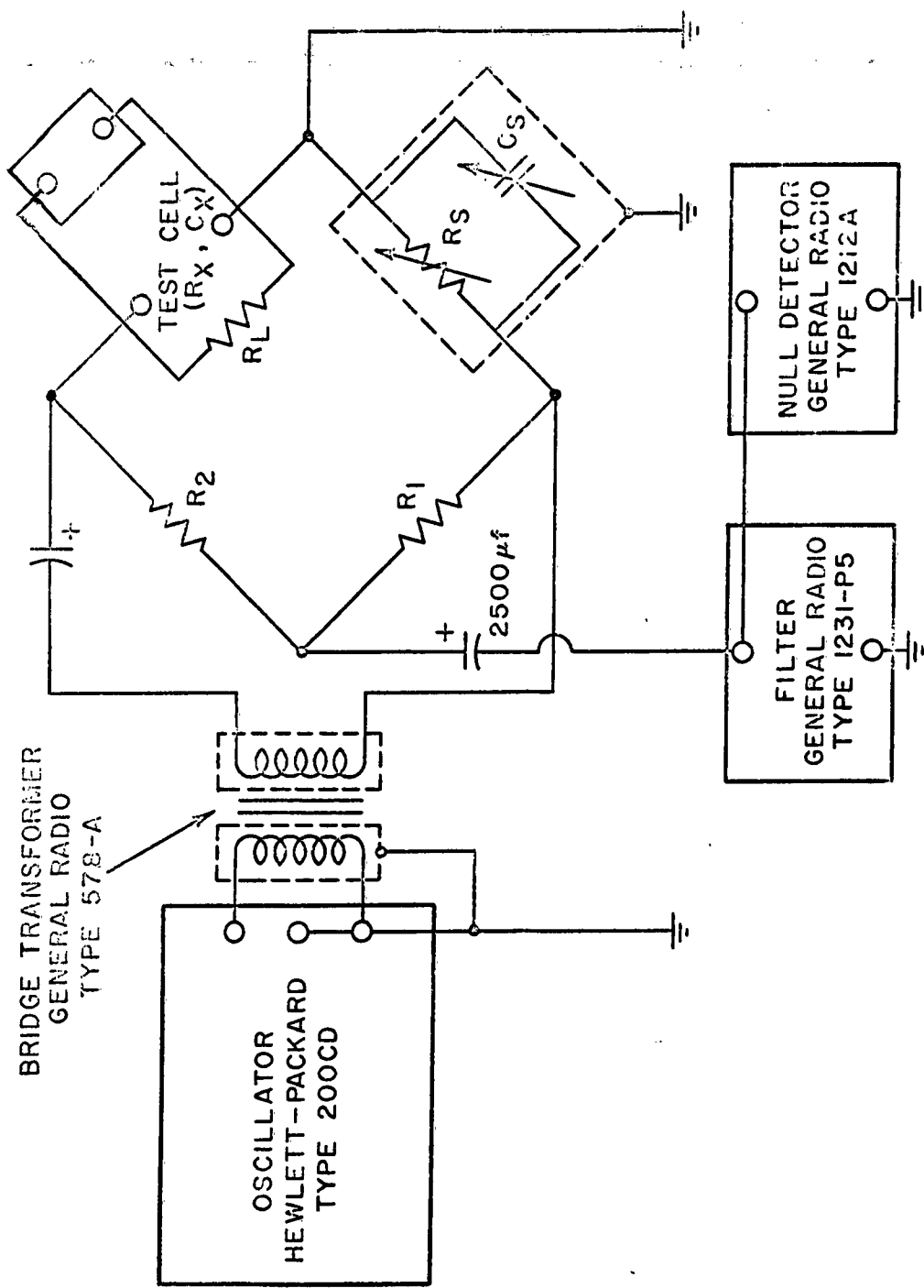
$$R_X = \frac{R_X' R_L}{R_L - R_X'} \quad (3)$$

where:

- $R_X'$  = Equivalent parallel resistance measured value (ohms)
- $C_X$  = Equivalent parallel capacitance ( $\mu$ f)
- $R_X$  = Equivalent parallel resistance, corrected value (ohms)
- $R_S$  = Standard bridge balancing resistor (ohms)
- $C_S$  = Standard bridge balancing capacitor ( $\mu$ f)
- $R_L$  = Load resistor (ohms)

### 3.5.1.3 Cell Analysis

When the polarization of the electrolyte is damped by the cell resistance, the equivalent circuit of the cell shown in Figure 88 is reduced to the simple circuit shown in Figure 91.



ML-279

FIGURE 90. RESISTANCE-RATIO BRIDGE FOR MAGNESIUM CELL IMPEDANCE MEASUREMENTS.

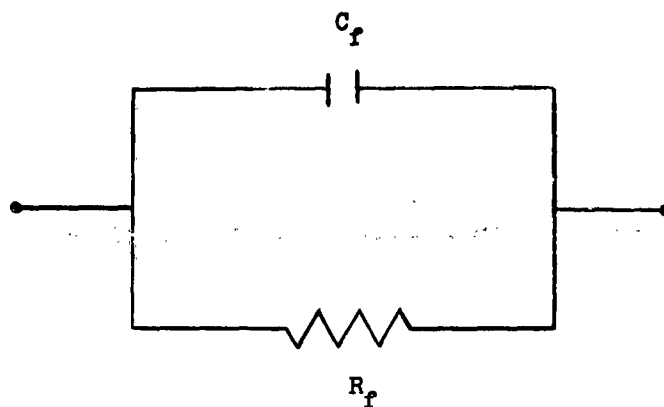


FIGURE 91. EQUIVALENT CIRCUIT OF MAGNESIUM CELL AT FREQUENCIES ABOVE THE ELECTROLYTE CUTOFF FREQUENCY.

At the frequencies where the equivalent circuit shown in Figure 91 is valid, the equivalent parallel capacitance and resistance as measured on the bridge are directly equal to the film capacitance and resistance. The capacitance and resistance of the films may be related to film dimensions and the constants of the materials as follows:

$$C_f = \frac{\epsilon_o K A_f}{t_f} = C_X \quad (4)$$

and:

$$R_f = \frac{\rho_f t_f}{A_f} = R_S \quad (5)$$

where:

$\epsilon_o$  = Permittivity of free space in coul<sup>2</sup>/n cm<sup>2</sup>.

K = Dielectric constant of corrosion film.

$A_f$  = Film area in cm<sup>2</sup>.

$t_f$  = Film thickness in cm.

$\rho_f$  = ac resistivity of film in ohm x cm.

The ratio of the film area ( $A_f$ ) to film thickness ( $t_f$ ) is the only relationship which may be obtained from equations (4) and (5). Solving these two equations simultaneously, the ratio of film area to film thickness is expressed in equation (6).

$$\frac{A_f}{t_f} = \frac{C_X}{E_{OK}} = \frac{\rho_f}{R_X} \quad (6)$$

However, the use of equation (6) is not sufficient to enable the determination of all of the information wanted about the corrosion film. The analysis of the data is not straightforward because of the following characteristics of magnesium anode:

- a. The anode area does not remain constant as a function of the current density.
- b. The anode becomes corroded, etched, and pitted, to varying degrees, at different current drains.

Consequently, the measured plane area of the anode is not the true area. In addition, the corrosion film is not continuous, and the amount of discontinuity or uncovering of the anode surface varies with current density.

Therefore, there are three unknown quantities to be determined as functions of current density are as follows:

- a. the true total anode area ( $A_T$ ).
- b. the part of the total anode area covered by the corrosion film ( $A_f$ ).
- c. the thickness of the corrosion film ( $t_f$ ).

In determining each of these parameters, the dc resistance of the cell must be considered in the calculations. Except for open circuit loads, the dc resistance of the cell is calculated from the cell voltages as follows:

$$R = R_L \left( \frac{V_{oc}}{V} - 1 \right) \quad (7)$$

where:

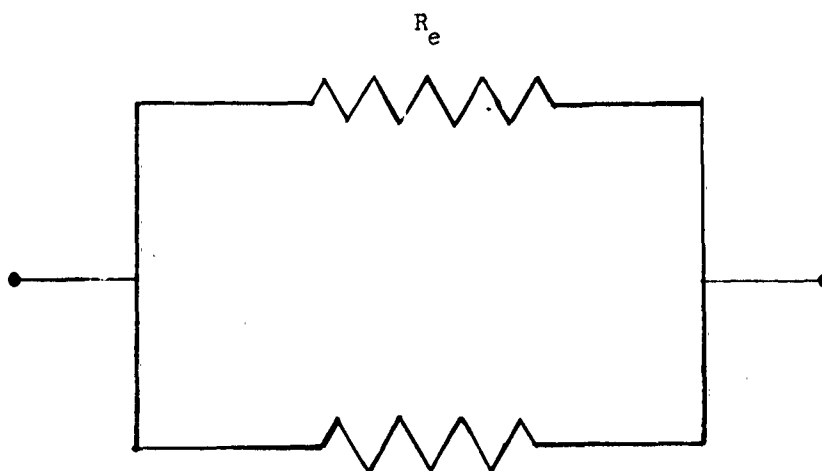
$R_L$  = load resistance

$V_{oc}$  = open-circuit cell voltage

$V$  = output voltage across the load resistor,  $R_L$

At open circuit, the dc resistance of the cell can be found by extrapolating the ac resistance to zero frequency. Note: This precludes the further use of the second part of the equality expressed in equation (6) since it would yield a non-independent equation. The extrapolation implicitly uses the resistance of the film as a basis. Consequently, the ratio of film area to thickness must use the capacitance of the film as a basis.

The dc equivalent circuit of the cell is shown in Figure 92 for all conditions except for an open circuit.



Dc Resistance of the Corrosion Film

FIGURE 92. DC EQUIVALENT CIRCUIT OF A MAGNESIUM CELL.

From Figure 92, the following equation can be derived which relates the total cell dc resistance to the dimensional properties of the film and constants of the materials.

$$\frac{I}{R} = \frac{A_f}{\rho_f t_f} + \frac{A_T - A_f}{\rho_e L} \quad (8)$$

where:

$\rho_f$  = dc resistivity of the corrosion film

$\rho_e$  = resistivity of the electrolyte

$L$  = separation between anode and cathode

By substituting equation (6) into equation (8) and solving for the film area, the expression shown in equation (9) is obtained.

$$A_f = A_T + \frac{C_X \rho_e L}{\rho_f \epsilon_o K} - \frac{\rho_e L}{R} \quad (9)$$

The dc resistivity of the corrosion film is determined at open circuit since  $A_T = A_f$  at this point; therefore, from equation (9) the following relation is obtained:

$$\rho_f = \frac{R C_X}{\epsilon_o K} \quad (10)$$

A third independent equation is still required to complete the analysis. This equation must relate the total anode area ( $A_T$ ) to current density and must come from some source other than the impedance measurements. The possible ways of obtaining the third independent equation are by:

- a. directly measuring the anode area as a function of current density.
- b. assuming that the anode area increases linearly with current density over the limited operating range used in these measurements.

Direct measurement of the surface area can be accomplished by measuring the gas adsorption on the surface, or by electron microscope techniques.

The second method for obtaining the third equation will be used here until a direct measurement technique is made available. The assumption stated in 6. above provides a means of estimating the area at the high current density where almost all of the equivalent parallel resistance of the cell is due to the electrolyte shorting through to the anode. Therefore,

$$A_T = \rho_e \frac{L}{R_X} \quad (11)$$

The assumed variation for  $A_T$  can now be written:

$$A_T = aJ + A_0 \quad (12)$$

where:

$$A_0 = \text{plane area of the anode}$$

The evaluation of the constant,  $a$ , gives the following relation:

$$a = \frac{(\rho_e L/R_X) - A_0}{J_1} \quad (13)$$

where:

$$J_1 = \text{apparent current density at which the anode efficiency curve levels out.}$$

$$R_X = \text{resistance at that point where the anode efficiency curve levels out. This point corresponds to the point where the film is negligible.}$$

It should be noted that the values obtained for total surface area from equation (12) are not absolute since several approximations and assumptions were made in obtaining the equation. Although the data derived from it, along with the data from equations (6) and (9), may be used



as a comparison basis in the study of cells of different composition. Since the same assumptions are made for all cells, a confident comparison between cells can be accomplished.

#### 3.5.1.4 Test Procedure

In using this impedance method as a means of analysis of anode films, the following measurements and calculations are required:

- a. determine resistance and capacitance of cells vs frequency (over a range of 20 cps to 5 kc) at open circuit and at various current densities. Plot the values of capacitance vs frequency over a log-log scale and find that portion of the curve between the electrolyte cutoff and the film cutoff points. Choose a frequency in the middle of this range to evaluate the data.
- b. determine cell voltage vs current density.
- c. determine all of the constants required in the various equations presented in Section 3.5.1.3 of this report.
- d. determine the total anode area vs current density using equation (12), or by direct measurements when possible.
- e. calculate the dc resistance of the cell using equation (7).
- f. calculate from equation (9) the film area and/or the difference between the total area and film area.
- g. determine from equation (4) the thickness of the corrosion film.

#### 3.5.1.5 Comparison of AZ-21 and C.P. Magnesium Anode Cells

##### Cell Geometry

In applying the method of data analysis described in Section 3.5.1.4 small symmetrical cells were constructed. These cells consisted of a cylindrical anode of 0.125-inch diameter suspended in the geometric center of a cylindrical glass container (1.25-inch diameter x 2.5-inches high). A platinized platinum cathode sheet was placed around the inner wall of the glass container. This type of cell construction allows

for easy measurement of the cell dimensions. Since the anode is small, the cell capacitance is also relatively small and can be measured without difficulty. Although the data obtained are specific to this type of cell geometry, the data can be applied to any other cell geometry by simply measuring the plane area of the anode and relating the film area to the new plane area. Note: The thickness of the film remains unchanged regardless of the anode configuration.

#### Constants and Fixed Cell Parameters

The electrolyte and film cutoff frequencies were found to occur close together; this result was anticipated. The frequency characteristics for AZ-21 and pure magnesium indicated that a frequency of approximately 2000 cps should be used in data analysis.

The constants and fixed-cell parameters required in the comparison of AZ-21 and C.P. magnesium anodes are listed in Table XXIII.

#### Corrosion Film Data

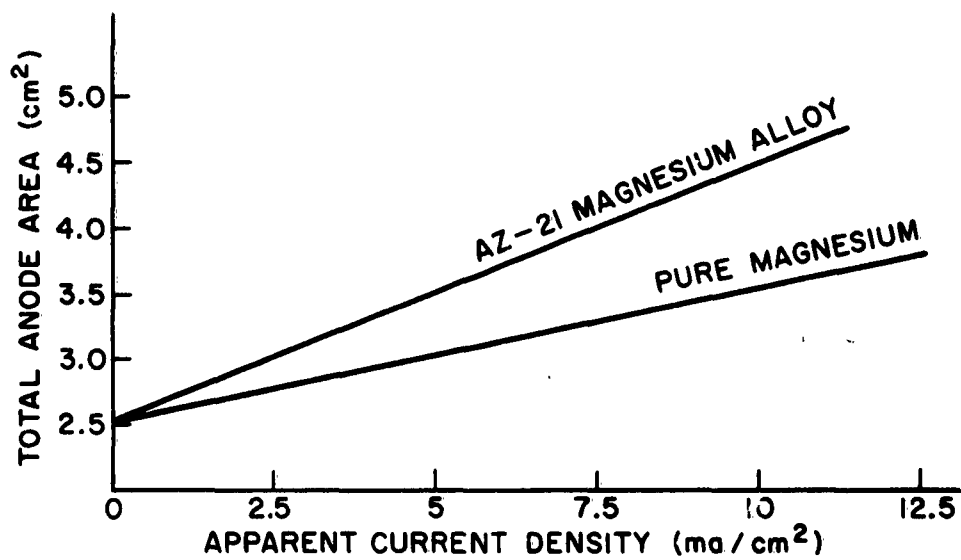
Figure 93 shows the total anode area as a function of the apparent current density. It is noted that the true current density may be calculated with the value of anode area obtained from Figure 93. The values for current density for this type cell are usually based on the anode plane area and not the anode true area. However, these data permit the calculation of current density based on the true anode area.

Figure 94 shows the difference between the total area and the film area, or that portion of the anode which is exposed to the electrolyte. Physically, this area difference is related to the rate of corrosion-film decay. Figure 94 also shows the film volume ( $A_f \times t_f$ ), per unit of total area, as a function of current density. The significance of this figure is that it is a measure of the net rate of growth of the corrosion film. By combining the results shown in Figure 94, the shape

CONSTANT AND FIXED PARAMETERS	AZ-21 ALLOY	MAGNESIUM
$\epsilon_o$ (coul <sup>2</sup> /n cm <sup>2</sup> )	$8.85 \times 10^{-16}$	$8.85 \times 10^{-16}$
K	9.65	9.65
$\rho_e$ (ohm-cm)	9.1	9.1
L (cm)	1.4	1.4
$A_o$ (cm <sup>2</sup> )	2.53	2.53
$\rho_f$ (ohm-cm)	$1.64 \times 10^{12}$	$1.21 \times 10^{11}$
a	0.1975	0.1015

MT-66

TABLE XXIII. CONSTANTS AND FIXED PARAMETERS FOR EVALUATING AZ-21  
C.P. MAGNESIUM ANODES.



(ML - 26)

FIGURE 93. TOTAL ANODE AREA VS APPARENT CURRENT DENSITY FOR AZ-21 MAGNESIUM ALLOY AND PURE MAGNESIUM.

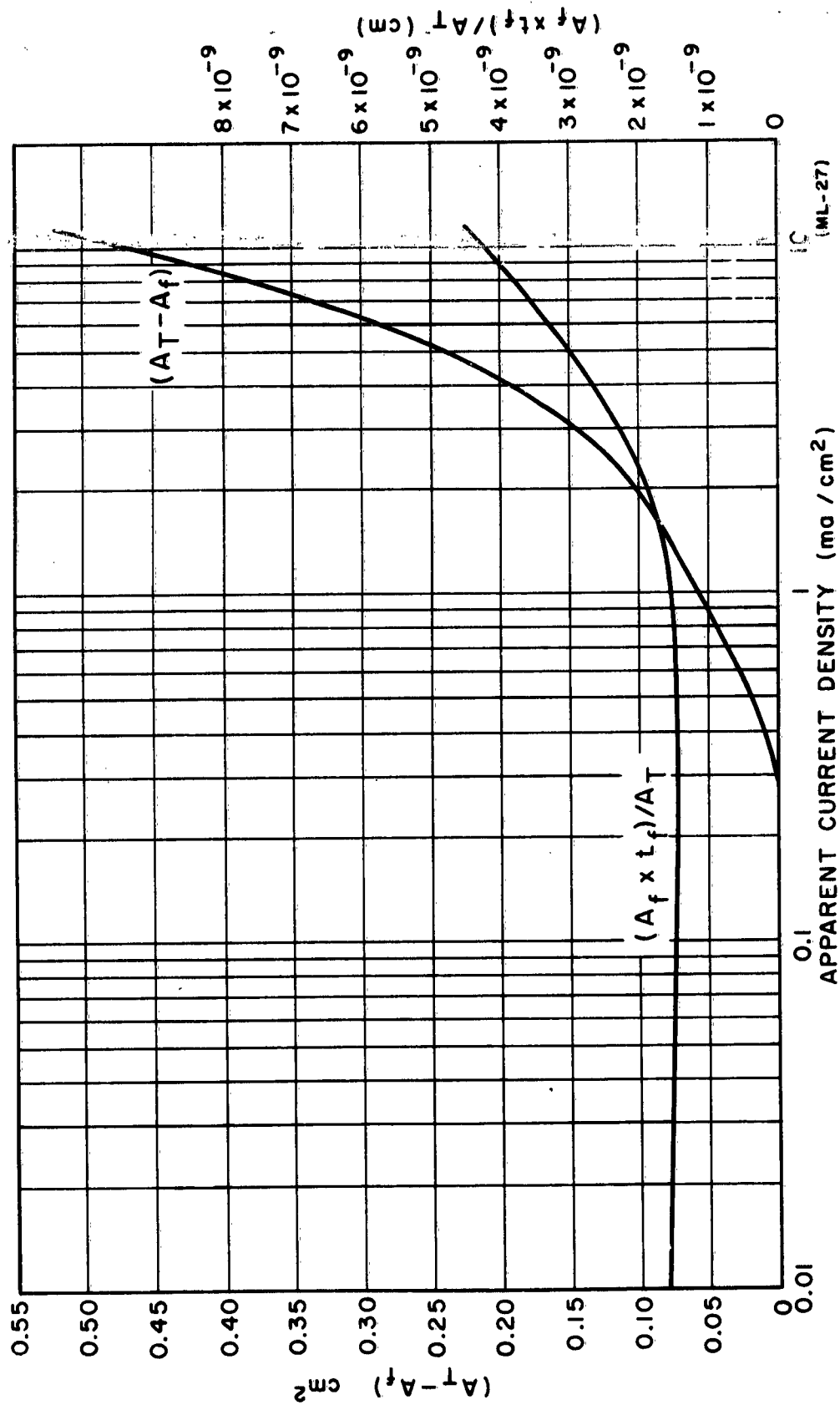


FIGURE 94. EXPOSED ANODE AREA ( $A_T - A_f$ ) AND FILM VOLUME PER UNIT TOTAL AREA VS APPARENT CURRENT DENSITY (AZ-21 MAGNESIUM ALLOY).

of the anode efficiency curve can be predicted. This prediction is possible because the anode efficiency is directly related to the exposed anode surface and to the rate of growth of the corrosion film. Therefore, from Figure 94, the efficiency curve for AZ-21 will rise very rapidly from open circuit to about  $0.3 \text{ ma/cm}^2$ . The curve will then change direction abruptly and level off. The point at which it levels off will occur at about 2 to 4  $\text{ma/cm}^2$ .

The efficiency curve for C.P. magnesium will differ considerably from that for AZ-21. The initial rise in efficiency is inhibited by the excessive growth of film at low current densities. Thus, the initial rise will be more gradual than for AZ-21. The change in direction of the curve will start at about  $2 \text{ ma/cm}^2$  and will be much more abrupt than the change in the AZ-21 curve. The curve will then level out at about 5 to 7  $\text{ma/cm}^2$ . These predictions can be made by comparing the slopes of the film growth curve and the exposed area curve. If the rate of film growth is greater than the rate of surface exposure, the efficiency will be low and vice versa (Figure 95).

### 3.5.2 Impedance Studies

Cell impedance is an important factor affecting the performance of equipment in many electronic applications. Previous data have shown the impedance of magnesium cells to be greater than that of corresponding Le Clanche cells.

The present study includes an intensive investigation of the impedance of  $\text{Mg/Mg(ClO}_4)_2/\text{MnO}_2$  and  $\text{Mg/Mg(ClO}_4)_2/\text{CuO}$  cells as a function of shelf-life for various frequencies and load conditions.

The experimental apparatus is shown in Figure 96. At each frequency, the voltage drop across fixed resistor R is measured at  $V_x$  and  $V_y$ . Then, by Ohm's Law, the ac current flowing through the battery is:

$$I = \frac{V_x}{R+R_b} = \frac{V_y}{R_b}$$

where  $R_b$  is the battery impedance. By making  $R \gg R_b$ , the following approximation can be made:

$$R_b = \frac{V_y}{V_x} R$$

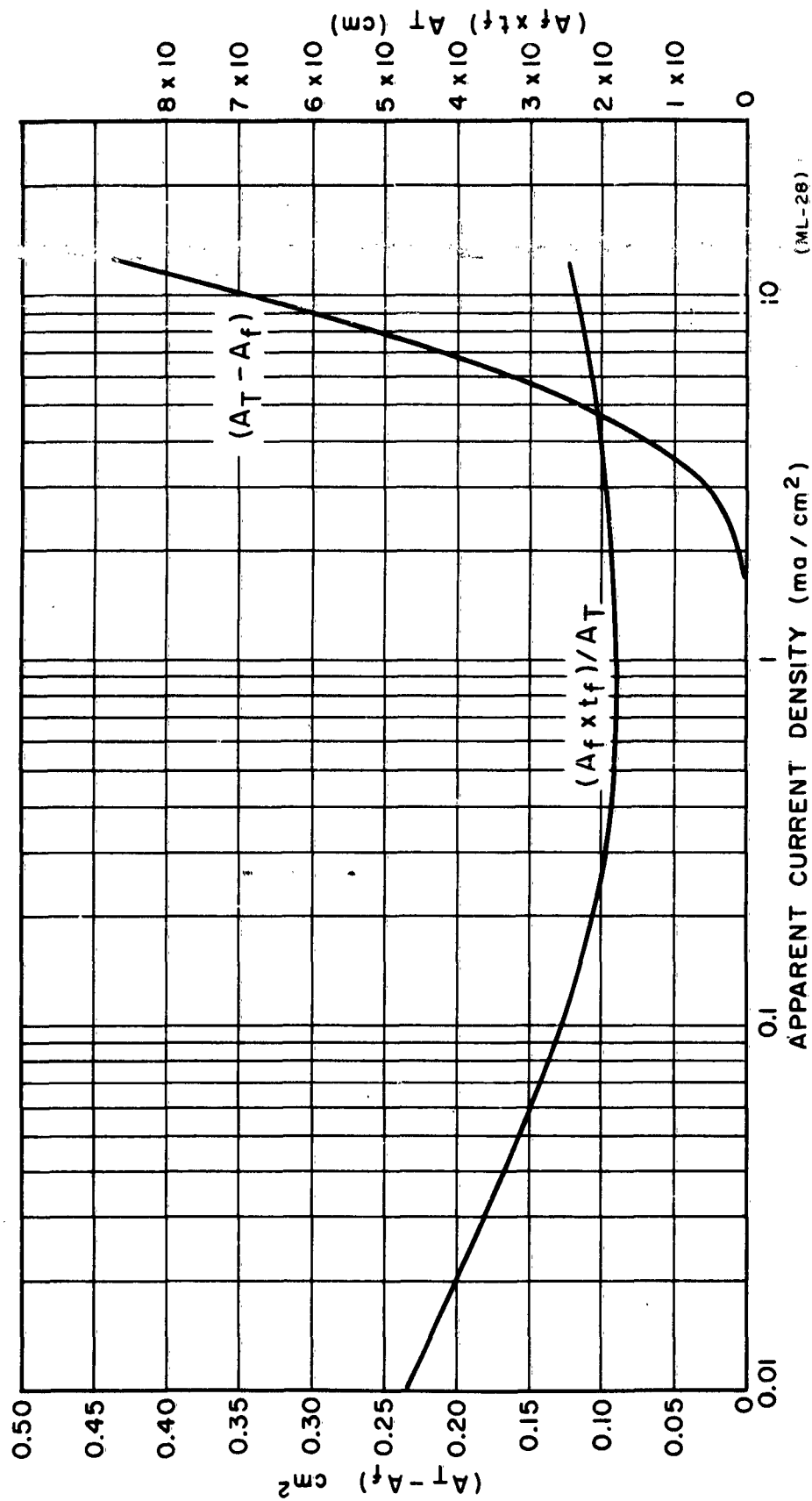
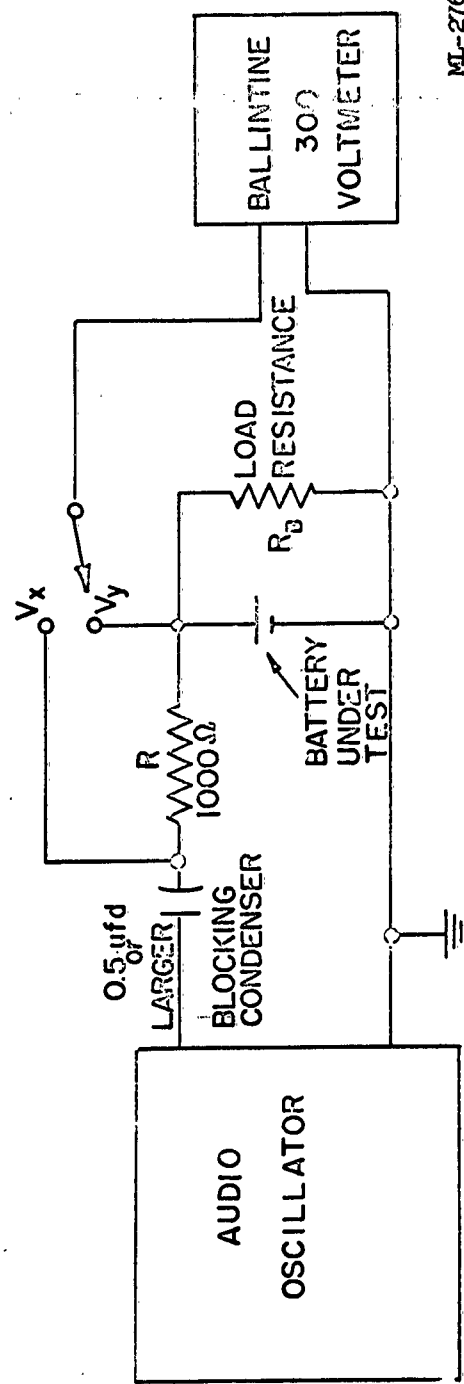


FIGURE 95. EXPOSED ANODE AREA ( $A_T - A_f$ ) AND FILM VOLUME PER UNIT TOTAL AREA VS APPARENT CURRENT DENSITY OF PURE MAGNESIUM.



ML-276

FIGURE 96. EXPERIMENTAL APPARATUS FOR IMPEDANCE MEASUREMENT.



For convenience of calculation, R was set at 1000 ohms and  $V_x$  at 1.00 volt by the amplitude control of the audio oscillator.

The variation in impedance is presented in Figure 97 at 60 and 400 cps as a function of load resistance for  $Mg/Mg(ClO_4)_2/MnO_2$  (Type M) AA-cells. Figure 98 gives the variation in impedance with frequency for the various discharges. The data represent initial impedance measured on cells two weeks old at approximately 50% discharge to a 0.90-volt cutoff.

#### 3.5.2.1 CuO Cells

The impedance of  $Mg/Mg(ClO_4)_2/CuO$  AA-cells was measured at various discharge rates over a frequency range of 6 to 10,000 cps. The variation in impedance is presented in Figure 99 at 60 and 400 cps as a function of load resistance. Figure 100 gives the variation of impedance with frequency for the various discharges. The impedance data were measured on cells two weeks old at approximately 50% discharge to a 0.75-volt cutoff. Results are similar to those obtained with magnesium- $MnO_2$  cells reported above.

Capacity data for the above cells discharged through 4 ohms to 100 ohms are included in Table XXIII. Average voltage and hours of service were computed to a 0.75-volt cutoff.

#### 3.5.2.2 Effect of Storage on Cell Impedance

Results on stored cells from one-month storage at 113°F to six-month storage at 70°F showed little effect of storage on the impedance  $Mg/Mg(ClO_4)_2/MnO_2$  and  $Mg/Mg(ClO_4)_2/CuO$  cells. See Table XXV.

#### 3.5.2.3 AZ-21 Impedance

The impedance of magnesium/magnesium-perchlorate/manganese dioxide (Type M) A-cells with AZ-21 and AZ-10 magnesium alloys was measured at a 50-ohm continuous discharge rate over a frequency range of 60 to 10,000 cps. Test results showed that the impedance of AZ-21 alloy

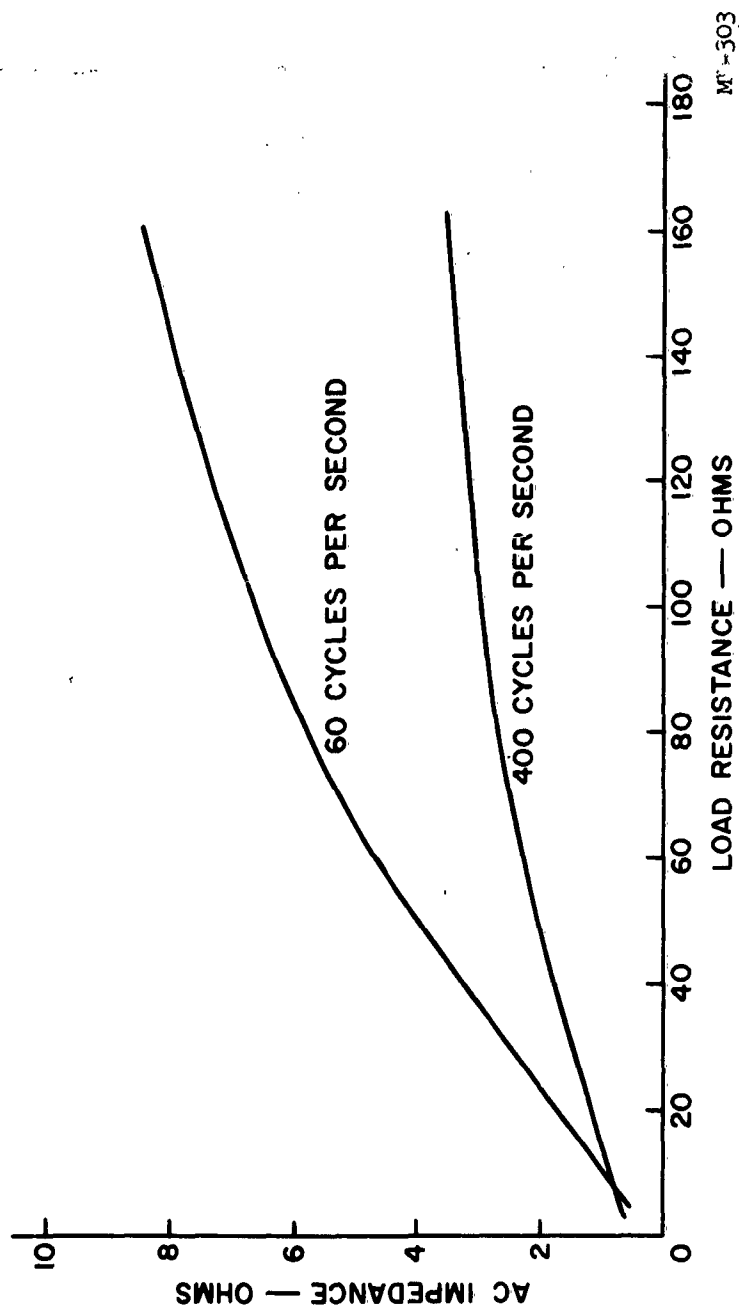


FIGURE 97. AC IMPEDANCE VS LOAD RESISTANCE OF  $\text{Mg}/\text{Mg}(\text{ClO}_4)_2/\text{MnO}_2$  (TYPE M) AA-CELLS DISCHARGED CONTINUOUSLY THROUGH VARIOUS RESISTANCES AT  $70 \pm 2^\circ\text{F}$  AND  $50 \pm 5\%$  R.A.

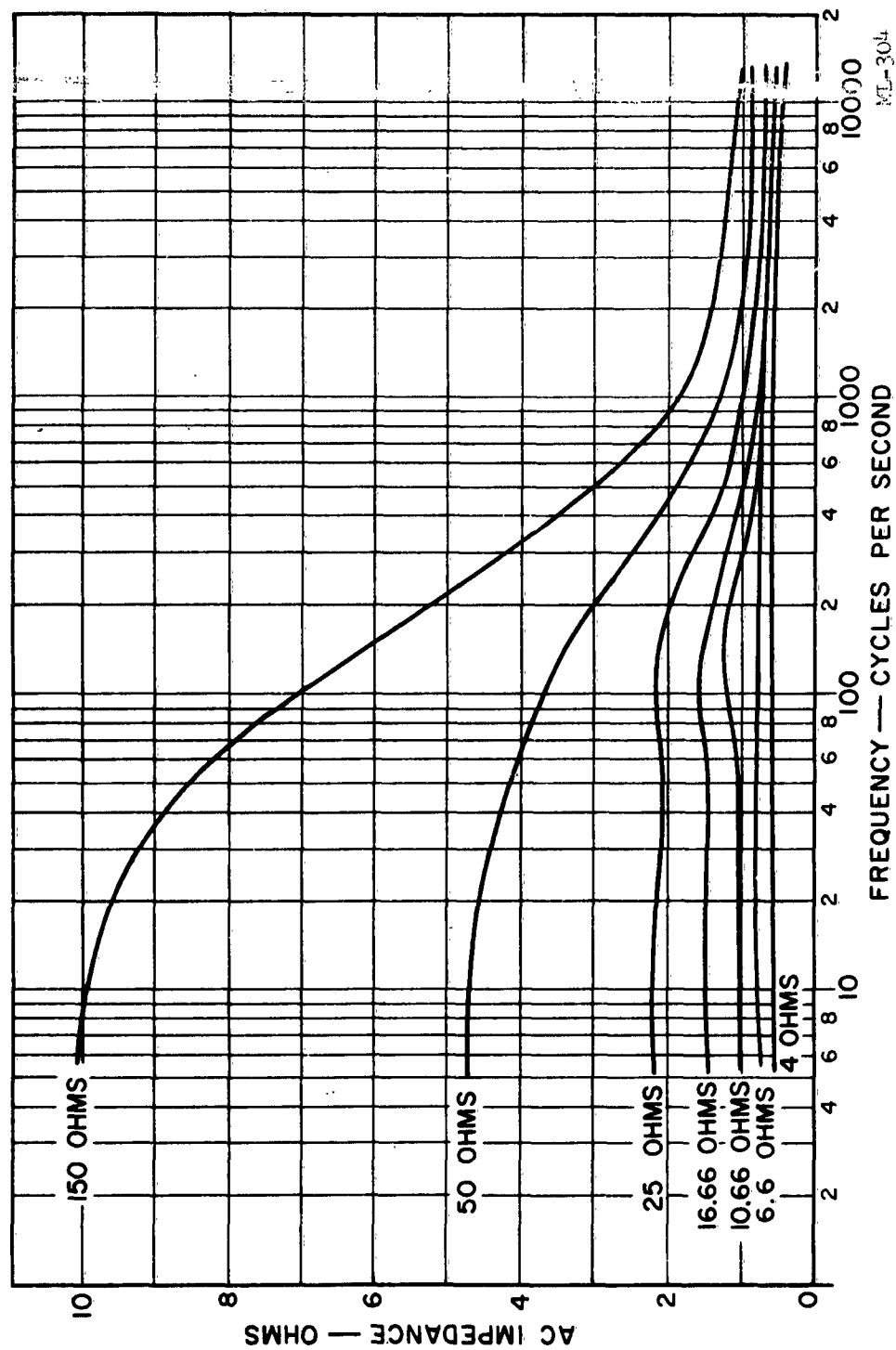


FIGURE 98. AC IMPEDANCE VS FREQUENCY OF  $Mg/Mg(ClO_4)_2/MnO_2$  (TYPE M) AA-CELLS DISCHARGED CONTINUOUSLY THROUGH VARIOUS RESISTANCES AT  $70 \pm 2^\circ F$  AND 50% R.H.

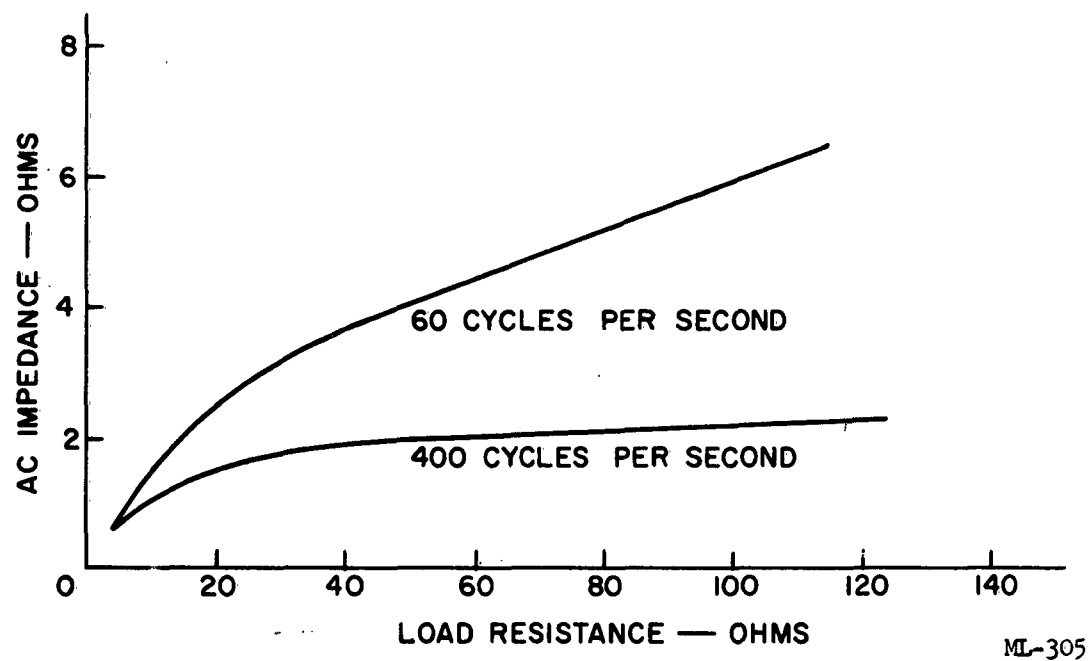


FIGURE 99. AC IMPEDANCE VS LOAD RESISTANCE OF  $\text{Mg}/\text{Mg}(\text{ClO}_4)_2/\text{CuO}$  AA-CELLS  
DISCHARGED CONTINUOUSLY THROUGH VARIOUS RESISTANCES AT  
 $70 \pm 2^\circ\text{F}$  AND  $50 \pm 5\%$  R.H.

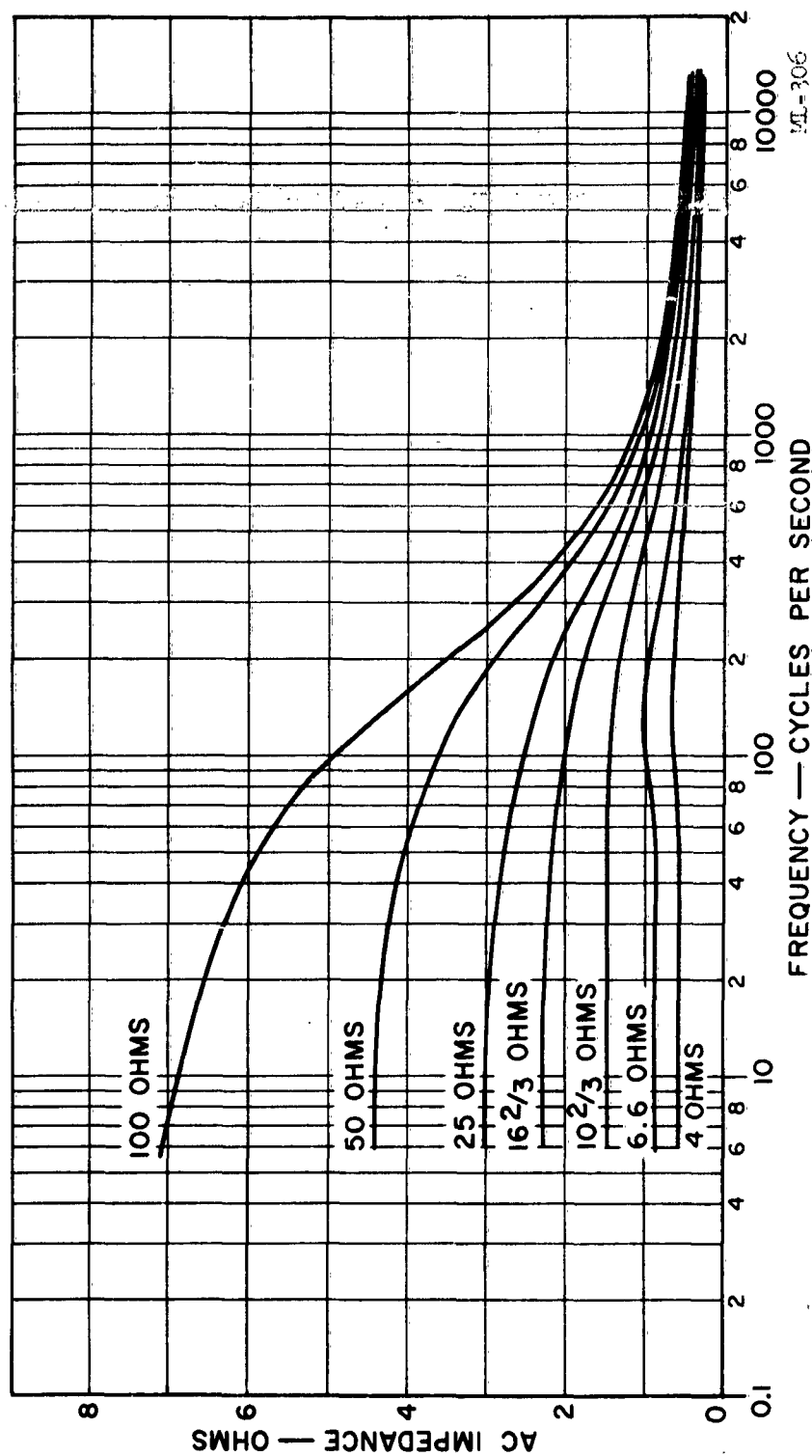


FIGURE 100. AC IMPEDANCE VS FREQUENCY OF  $Mg/Mg(ClO_4)_2/CuO$  AA-CELLS DISCHARGED CONTINUOUSLY THROUGH VARIOUS RESISTANCES AT  $70 \pm 2^\circ F$  AND 50% R.H.

was slightly less than that of the AZ-10 alloy. Impedance tests showed a slight increase in impedance at the 25-ohm drain for cupric-oxide cells and the 50-ohm drain for the manganese-dioxide cells. The cupric-oxide cell impedance was 3.4 ohms at 60 cps and 1.9 ohms at 400 cps as compared to the initial values of 2.8 ohms and 1.6 ohms. The manganese-dioxide cell impedance was 4.2 ohms at 60 cps and 2.1 ohms at 400 cps, as compared to the initial values of 4.0 and 2.1 ohms.

Cell capacities averaged 90% retention. Data for the various lots are summarized in Table XXIV.

#### 3.5.2.4 Magnesium Impedance

It has been shown theoretically that the corrosion film on magnesium anodes can be studied directly by means of cell impedance measurements. The resistance-ratio bridge used for impedance measurements was shown to have more than sufficient accuracy and sensitivity for these studies. From the impedance data, the following may be determined as a function of load current.

- a. an approximation of the true anode area.
- b. the portion of the anode area covered by the corrosion film.
- c. the average thickness of the corrosion film.

This method is useful for the study of various magnesium alloys, inhibitors, and electrolytes and in demonstrating their effects on anode performance.

Because only two independent measurements were made (capacitance and resistance), only two independent values were calculated. The true anode area was estimated on the basis of an equation empirically derived from the test data or measured independently. A BET apparatus was constructed to make accurate measurements of the total surface area.

$R_L$ (ohms)	$C_X$ ( $\mu f$ )	$R_X$ (ohms)	CELL VOLTAGE (volts)	$J$ (ma/cm <sup>2</sup> )	$R(dc)$ (ohms)	$A_T^2$ (cm <sup>2</sup> )	$A_P^2$ (cm <sup>2</sup> )	$t_f$ (cm x 10 <sup>-9</sup> )	( $A_T - A_P$ ) (cm)	FILM VOLUME (cm <sup>3</sup> x 10 <sup>-9</sup> )
20	7.1	2.67	0.57	11.3	24	4.76	4.24	5.1	0.52	21.6
50	10.0	2.65	0.61	4.82	52.5	3.48	3.25	2.78	0.23	9.04
100	10.3	3.00	0.63	2.49	98.5	3.02	2.90	2.4	0.12	6.95
500	14.2	3.71	0.67	0.53	433	2.63	2.61	1.57	0.02	4.10
1000	15.7	4.74	0.68	0.27	840	2.58	2.58	1.4	0.000	3.62
2500	15.2	5.62	0.70	0.11	1970	2.56	2.56	1.44	0.000	3.69
5000	14.4	7.65	1.01	0.08	1200	2.55	2.55	1.51	0.000	3.85
p.c.	13.9	9.83	1.25	0.00	1000	2.53	2.53	1.55	0.000	3.92

MT-71

TABLE XXIV. SUMMARY OF DATA ON AZ-21-ALLOY MAGNESIUM ANODES.

Tests were run using flat AZ-21 magnesium and C.P. magnesium anodes in  $2N \text{ Mg}(\text{ClO}_4)_2$  over a current-density range of 0.1 to 10  $\text{ma}/\text{cm}^2$ , based on the plane area of the anode. See Table XXVII.

### 3.6 METEOROLOGICAL BATTERY

At the request of the Signal Corps, effort was devoted at the end of the contract to the design, testing, and building of the Mg-HgO equivalent of the meteorological battery BA253/u. Four of these batteries have been delivered to Signal Corps for further testing.

#### 3.6.1 Design

The battery consists of four cells, connected in series, each of which have the following design:

Anode material:	C.P. Magnesium
Cathode material:	10:1 HgO + Shawinigan carbon black
Plate Size:	1-1/8 x 2 inches
Separator:	Filter paper
Electrolyte:	5N $\text{Mg}(\text{ClO}_4)_2$

These four cells were assembled with the proper hardware into a battery with a "dry weight" of approximately 60 grams, the battery dimensions are 3-1/2 x 1-3/8 x 15/16 inches and its wet weight, after activation in electrolyte, is approximately 90 grams.

#### 3.6.2 Activation Procedure

The battery is activated by submerging up to "line" in 5N  $\text{Mg}(\text{ClO}_4)_2$  for five minutes. The excess electrolyte is then removed by shaking. Then, after a five-minute stand, the battery is ready to be discharged.

#### 3.6.3 Experimental Data

##### 3.6.3.1 Results Obtained

Samples of the delivered battery were tested by discharging through



12 ohms to a 5.5 volt cutoff under various conditions of temperature. In all cases except room temperature, the battery was insulated by 1/8-inch polyurethane sheet; no insulation was used at room temperature.

The discharge curves appear in Figure 101, and the battery characteristics obtained from these curves appear below:

<u>Ambient Temp.</u> (°F)	<u>Avg. Oper.</u> <u>Voltage</u> (volts)	<u>Capacity</u> (amp/hr)	<u>Utilization</u> (%)	<u>W-hr/lb</u>
*Room	7.24	1.49	95	53.6
-58	6.14	.810	52	25
140 (10 minutes) then -58	6.33	.817	53	25.3

\*Avg. of two cells.

In an attempt to improve the characteristics at the -58°F discharge, batteries were first discharged at room temperature for a five-minute period and for a 10-minute period before being placed into a cold box at -58°F.

The discharge curves for the five-minute and 10-minute pre-cold-box treatment, as well as the curve for no pre-treatment, appear in Figure 102. The characteristics obtained from these curves appear below:

<u>Pre-treatment</u> (minutes)	<u>Avg. Oper.</u> <u>Voltage</u> (volts)	<u>Capacity</u> (amp/hr)	<u>Utilization</u> (%)	<u>W-hr/lb</u>
None	6.14	.810	52	25
5	6.32	.970	62	32
10	6.55	1.09	69	37

#### 3.6.4 Conclusions

The following conclusions can be drawn from an examination of the experimental data obtained:

- A meteorological battery which can deliver in excess of 50 w-hr/lb. has been shown possible using the magnesium/mercuric-oxide system.
- With proper treatment, this battery can deliver better than 30 w-hr/lb. at -58°F.

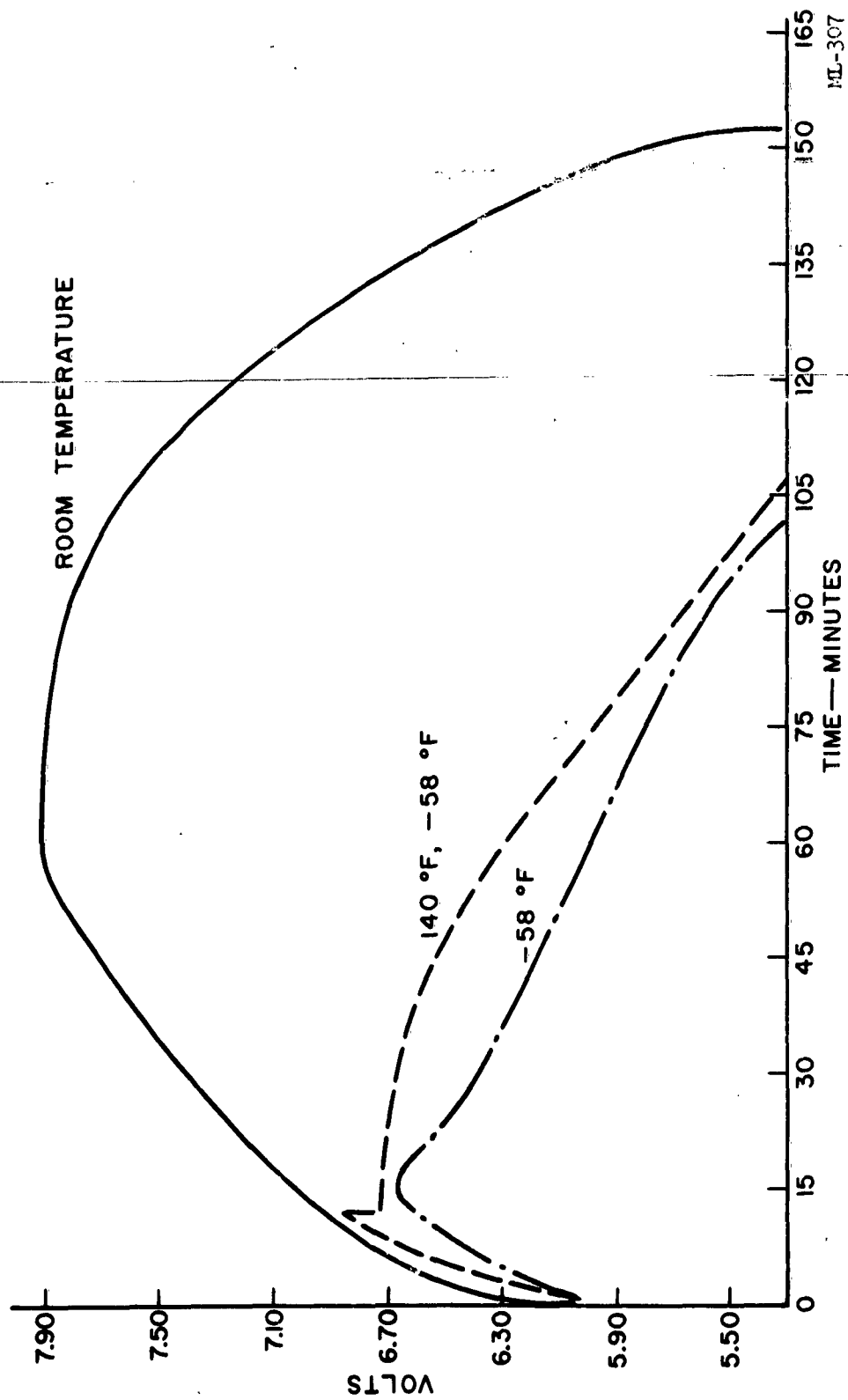


FIGURE 101. FOUR-CELL MAGNESIUM-MERCURIC OXIDE METEOROLOGICAL BATTERY. DISCHARGED THROUGH 12 OHMS.

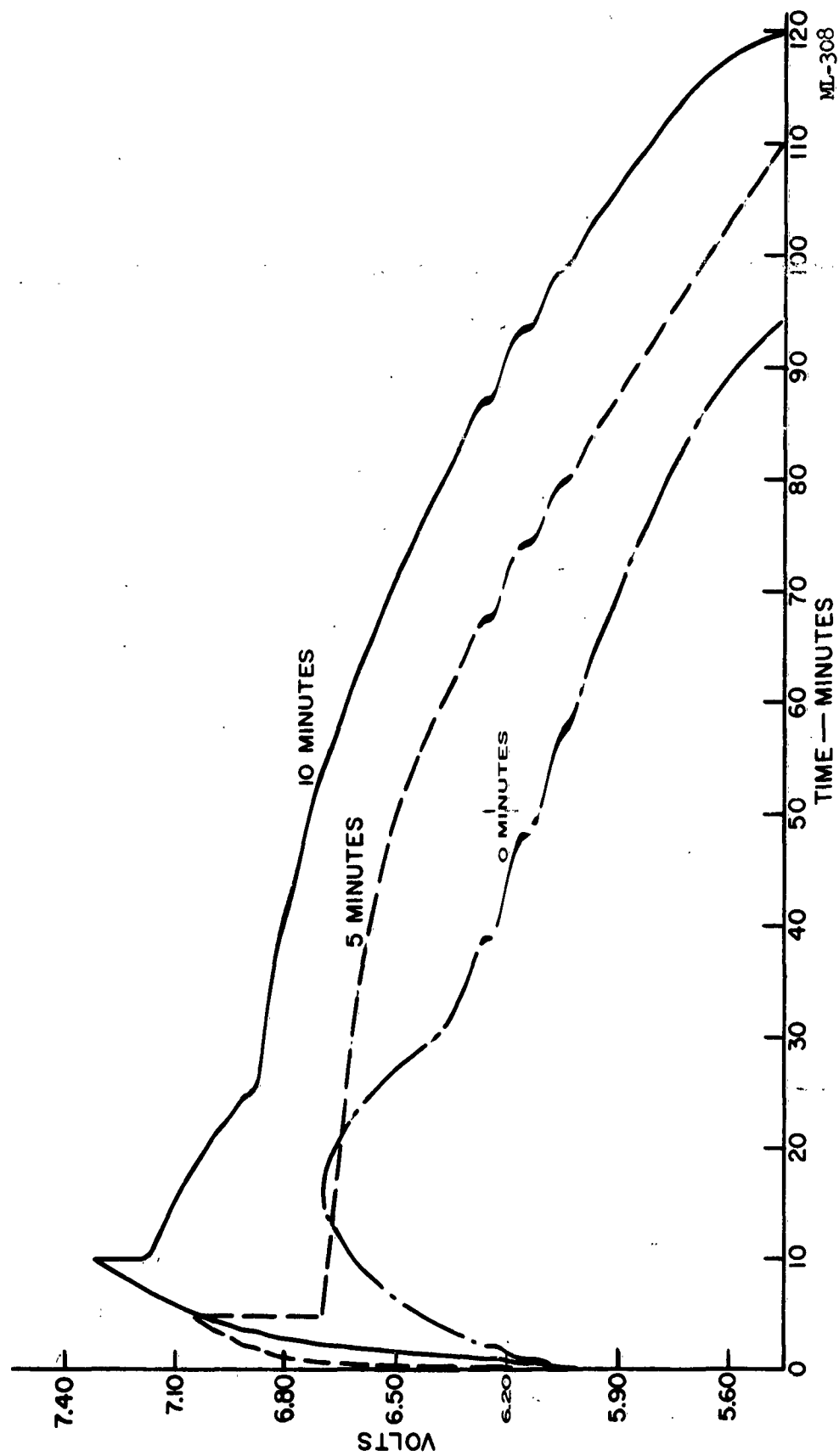


FIGURE 102. FOUR-CELL MAGNESIUM-MERCURIC OXIDE METEOROLOGICAL BATTERY. IMPROVING BATTERY CHARACTERISTICS AT -58°F. BY INITIAL DISCHARGES AT ROOM TEMPERATURE.

STORAGE (Months)	Mg(AZ-10)/Mg(ClO <sub>4</sub> ) <sub>2</sub> /MnO <sub>2</sub> (Type M)				Mg(AZ-10)Mg(ClO <sub>4</sub> ) <sub>2</sub> /CuO (C.P.)							
	10.66-Ω load			50-Ω load		6.6-Ω load		25-Ω load				
	Time To .90v (Hours)	Impedance Ω		Time To .90v (Hours)	Impedance Ω		Time To .75v (Hours)	Impedance Ω				
		60~	400~		60~	400~		60~	400~			
Initial	5.4	1.05	.87	35	4.0	2.1	9.75	.92	.77	58.5	2.8	1.6
1 at 113°F	5.3	1.10	.87	34	3.8	1.9	9.25	1.13	.83	56	2.8	1.6
3 at 113°F	4.75	1.15	.97	36	4.0	2.0	-	-	-	56	2.8	1.6
3 at 70°F	-	-	-	-	-	-	8.0	.96	.83	51	3.1	1.7
5 at 113°F	5.0	1.12	.92	34.5	4.0	2.0	-	-	-	-	-	-
6 at 70°F	4.75	1.25	1.05	30	3.9	2.1	8.0	1.05	.85	51	3.0	1.7

NT-68

TABLE XXV. SHELF-LIFE AND IMPEDANCE DATA FOR Mg/Mg(ClO<sub>4</sub>)<sub>2</sub>/MnO<sub>2</sub> AND Mg/Mg(ClO<sub>4</sub>)<sub>2</sub>/CuO A-CELLS.

DISCHARGE RESISTANCE (Ohms)	SERVICE TO 0.75V (Hours)	AVERAGE VOLTAGE (Volts)	CAPACITY	
			W-HR/LB	W-HR/IN <sup>3</sup>
4	4.5	0.83	28.0	1.85
6.6	9.75	0.84	37.6	2.48
10.66	20.5	0.85	50.2	3.31
16.66	38	0.86	60.7	4.0
25	58.5	0.90	68.7	4.52
50	109	0.97	73.7	4.76
100	184	1.03	70.5	4.65

MT-67

TABLE XXVI. INITIAL CAPACITY DATA FOR  $Mg/Mg(ClO_4)_2/CuO$  A-CELLS. DISCHARGED CONTINUOUSLY INTO VARIOUS RESISTANCES AT  $70 \pm 2^\circ F$  and 50% R.H.

#### 4. RECOMMENDATIONS FOR FUTURE WORK

##### 4.1 RESERVE CELLS

The low-temperature characteristics of the magnesium/mercuric-oxide cell should be more fully exploited. Studies of cell and battery design should be directed toward optimization of the system, especially for applications requiring low-temperature operation.

Methods of controlling or adsorbing the heat generated of magnesium reserve cells at high rates should be continued to obtain maximum performance.

##### 4.2 DRY CELLS

Further data is required describing the characteristics of dry cells with AZ-21 magnesium alloy anodes. The preliminary data on  $\text{Mg-MnO}_2$  is very encouraging. Electrolyte formulations for low-temperature applications should be made a major phase of this program. Package design for low-temperature use should be included in application studies.

##### 4.3 RESEARCH STUDIES

The research studies should be expanded to include the effect of electrolytes, inhibitors, and alloys on impedance, and relation to the efficiency of the magnesium anode.

$R_L$ (ohms)	$C_X$ ( $\mu f$ )	$R_X$ (ohms)	CELL VOLTAGE (volts)	$J$ (ma/cm <sup>2</sup> )	$R(dc)$ (ohms)	$A_T^2$ (cm <sup>2</sup> )	$A_F^2$ (cm <sup>2</sup> )	$t_F$ (cm) x 10 <sup>-9</sup>	$A_T - A_F$ (cm <sup>2</sup> )	FILM VOLUME (cm <sup>3</sup> )
20	10.3	3.33	0.64	12.6	22.4	3.80	3.36	2.79	0.440	9.36
50	11.5	4.81	0.73	5.78	43.0	3.12	2.98	2.22	0.153	6.62
100	12.3	6.31	0.80	3.16	70.0	2.85	2.82	1.96	0.030	5.53
500	12.2	7.80	0.94	0.74	223	2.61	2.61	1.83	0.000	4.77
1000	12.0	8.25	0.97	0.38	400	2.57	2.57	1.83	0.000	4.70
2500	9.36	11.7	1.14	0.18	478	2.55	2.55	2.33	0.000	5.93
5000	9.7	10.6	1.23	0.10	512	2.54	2.54	2.24	0.000	5.70
*	4.8	27.0	1.36	0.00	215	2.53	2.53	4.5	0.000	11.4

\*Open circuit.

MT-69

TABLE XXVII. SUMMARY OF DATA ON C.P. MAGNESIUM ANODES.

TIME (hours)	AZ-21 MAGNESIUM						AZ-10 MAGNESIUM					
	CELL VOLTAGE (volts)	IMPEDANCE IN OHMS					CELL VOLTAGE (volts)	IMPEDANCE IN OHMS				
		FREQUENCY ~						FREQUENCY ~				
		60	100	400	1k	10k		60	100	400	1k	10k
.25	1.69	3.5	4.5	2.0	1.47	0.96	1.71	3.8	4.6	2.4	1.9	1.2
7	1.56	2.6	2.3	0.86	0.69	0.58	1.59	3.4	3.2	1.7	1.09	0.69
24	1.50	2.9	2.8	1.20	0.77	0.57	1.54	3.6	3.2	1.7	1.07	0.69
32	1.46	2.9	2.8	1.14	0.70	0.57	1.50	3.5	3.2	1.6	1.02	0.70
49	1.00	4.0	3.4	1.34	0.91	0.70	0.93	4.0	3.6	1.5	0.99	0.71

MT-70

TABLE XXVIII. IMPEDANCE DATA FOR  $Mg/Mg(ClO_4)_2/MnO_2$  (TYPE 1) A-CELLS  
DISCHARGED AT A CONSTANT RESISTANCE OF 1000 OHMS.



AD	ACCESSION NO.	AD	ACCESSION NO.
<p>UNCLASSIFIED High-Capacity Magnesium Batteries</p>	<p>Radio Corporation of America, Somerville, New Jersey <b>HIGH-CAPACITY MAGNESIUM BATTERIES</b> by G.S. Lozier, R. Ryan, T. R. Krebs</p> <p>Final Report, 1 June 1960 to 30 November 1962. 209 pages, including 102 illustrations and 29 tables.</p> <p>Signal Corps Contract AD-36-039-SC-85340 Department of the Army Project 3A99-09-002, Unclassified</p> <p>The accomplishments and progress made during the U.S. Army Electronics Research and Development Laboratories' High-Capacity Magnesium-Battery Program by the Radio Corporation of America, Semiconductor and Materials Division, Somerville, New</p>	<p>UNCLASSIFIED High-Capacity Magnesium Batteries</p>	<p>Radio Corporation of America, Somerville, New Jersey <b>HIGH-CAPACITY MAGNESIUM BATTERIES</b> by G.S. Lozier, R. Ryan, T. R. Krebs</p> <p>Final Report, 1 June 1960 to 30 November 1962. 209 pages, including 102 illustrations and 29 tables.</p> <p>Signal Corps Contract AD-36-039-SC-85340 Department of the Army Project 3A99-09-002, Unclassified</p> <p>The accomplishments and progress made during the U.S. Army Electronics Research and Development Laboratories' High-Capacity Magnesium-Battery Program by the Radio Corporation of America, Semiconductor and Materials Division, Somerville, New</p>
<p>Jersey, are presented. This program was conducted during the period from 1 June 1960 through 30 November 1962.</p> <p>Characteristic data are presented for magnesium/magnesium-perchlorate reserve cells discharged at temperatures as low as -40°F. Cathode efficiency data as a function of temperature and current drain are also presented.</p> <p>Factors affecting the performance of dry cell batteries were investigated. Cathode efficiencies, storage characteristics, and electrode surface phenomena were evaluated.</p> <p>Data are also presented for a newly developed magnesium/mercuric-oxide meteorological battery, including discharge data for temperatures as low as -58°F.</p>		<p>Jersey, are presented. This program was conducted during the period from 1 June 1960 through 30 November 1962.</p> <p>Characteristic data are presented for magnesium/magnesium-perchlorate reserve cells discharged at temperatures as low as -40°F. Cathode efficiency data as a function of temperature and current drain are also presented.</p> <p>Factors affecting the performance of dry cell batteries were investigated. Cathode efficiencies, storage characteristics, and electrode surface phenomena were evaluated.</p> <p>Data are also presented for a newly developed magnesium/mercuric-oxide meteorological battery, including discharge data for temperatures as low as -58°F.</p>	

DISTRIBUTION LIST  
FINAL REPORT  
CONTRACT NO. DA-36-039-SC-85340

Headquarters U.S. Army Materiel Command Research and Development Directorate ATT: AMCRD-DE-MO Washington 25, D.C.	(1)	Dr. Sidney J. Magram Physical Sciences Division Army Research Office 3045 Columbia Pike Arlington, Virginia	(1)
Commanding General U.S.A. Electronics Command ATTN: AMSEL-RE-A Fort Monmouth, N.J.	(1)	Dr. Ralph Roberts Head, Power Branch Office of Naval Research (Code 429) Department of the Navy Washington 25, D.C.	(1)
Commanding General U.S.A. Combat Developments Command ATTN: CDCMR-E Fort Belvoir, Virginia		Mr. Bernard B. Rosenbaum Bureau of Ships (Code 340) Department of the Navy Washington 25, D.C.	(1)
Commanding Officer U.S.A. Communications and Electronics Combat Development Agency Fort Huachuca, Arizona	(1)	Mr. George W. Sherman Aeronautical Systems Division ATTN: ASRMFP Wright-Patterson Air Force Base Ohio	(1)
Director Fort Monmouth Office U.S.A. Communications and Electronics Combat Development Agency Fort Monmouth, N.J.	(1)	Dr. John H. Huth Advanced Research Projects Agency The Pentagon, Rm. 3E157 Washington 25, D.C.	(1)
Air Force Systems Command Scientific/Technical Liaison Office U.S. Naval Air Development Center Johnsville, Pennsylvania	(1)	Lt. Col. George H. Ogburn, Jr. Auxiliary Power Branch (SNAP) Division of Reactor Development U.S. Atomic Energy Commission Washington 25, D.C.	(1)
Corps of Engineers Liaison Office U.S.A. Electronics Research and Development Laboratory Fort Monmouth, N.J.	(1)	Mr. Walter C. Scott National Aeronautics & Space Adm. 1520 H. Street, N.W. Washington 25, D.C.	(1)
Marine Corps Liaison Office U.S.A. Electronics Research and Development Laboratory Fort Monmouth, N.J.	(2)	Institute for Defense Analysis 1666 Connecticut Avenue, N.W. Washington 25, D.C. ATTN: Dr. Szego & Mr. Hamilton	(1)
AFSC Scientific/Technical Liaison Office U.S.A. Electronics Research and Development Laboratory Fort Monmouth, N.J.	(1)	Bright Star Industries 600 Getty Avenue Clifton, N.J. ATTN: Mr. F. Keller	(1)
Power Information Center Moore School Building 200 South Thirty-Third St. Philadelphia 4, Pennsylvania	(1)		

**DISTRIBUTION LIST**  
**FINAL REPORT**  
**CONTRACT NO. DA 36-039-SC-85340**

Commanding Officer U.S.A. Electronics Research and Development Laboratory Fort Monmouth, N.J.		Rome Air Development Center ATTN: RAALD Griffiss Air Force Base, N.Y.	(1)
ATTN: Logistics Division (MARKED FOR PROJECT ENGINEER)	(11)	Commanding General U.S.A. Electronics Research and Development Activity	
ATTN: SEIRA/P	(1)	ATTN: Technical Library	
ATTN: Dir of Research/Engineering	(1)	Fort Huachuca, Arizona	(1)
ATTN: File Unit #1	(1)		
ATTN: Technical Document Center	(1)	Commanding Officer Harry Diamond Laboratories	
ATTN: Technical Information Div. (UNCLASSIFIED REPORTS ONLY FOR RETRANSMITTAL TO ACCREDITED BRITISH AND CANADIAN GOVERNMENT REPRESENTATIVES)	(3)	ATTN: Library, Rm. 211, Bldg. 92 Connecticut Ave & Van Ness St., N.W. Washington 25, D.C.	(1)
OASD (R&D), Rm 3E1065		Commanding Officer U.S.A. Electronics Material Support Agency	
ATTN: Technical Library The Pentagon Washington 25, D.C.	(1)	ATTN: SELMS-ADJ Fort Monmouth, N.J.	(1)
Chief of Research and Development OCS, Department of the Army Washington 25, D.C.	(1)	Deputy President U.S.A. Security Agency Board Arlington Hall Station Arlington 12, Virginia	(1)
Commanding General U.S.A. Electronics Command ATTN: AMSEL-AD Fort Monmouth, N.J.	(3)	Commander Armed Services Technical Information Agency ATTN: TISIA Arlington Hall Station Arlington 12, Virginia	(10)
Director U.S. Naval Research Laboratory ATTN: Code 2027 Washington 25, D.C.	(1)	Chief U.S.A. Security Agency Arlington Hall Station Arlington 12, Virginia	(2)
Commanding Officer and Director U.S. Naval Electronics Laboratory San Diego 52, California	(1)	Commander Aeronautical Systems Division ATTN: ASAPRL Wright-Patterson Air Force Base Ohio	(1)
Air Force Cambridge Research Laboratories ATTN: CRZC L.G. Hanscom Field Bedford, Massachusetts	(1)	Air Force Cambridge Research Laboratories ATTN: CRXL-R L.G. Hanscom Field Bedford, Massachusetts	(1)

DISTRIBUTION LIST  
FINAL REPORT  
CONTRACT NO. DA-36-039-SC-8 340

Mallory Battery Company  
Tarrytown, New York  
ATTN: Mr. J. Dalfonso (1)

The Dow Metal Products Co.  
Midland, Michigan  
ATTN: Dr. R. Kirk (1)

Burgess Battery Company  
Freeport, Illinois  
ATTN: Mr. M. Wilke (1)

Union Carbide Consumer Products Co.  
Cleveland, Ohio  
ATTN: Dr. F. Granger (1)

Electric Storage Battery Co.  
Ray-O-Vac Division  
212 East Washington Avenue  
Madison 10, Wisconsin  
ATTN: Mr. P. Albert (1)

Marathon Battery Company  
Wausau, Wisconsin  
ATTN: Mr. G. Schroeder (1)

American Cyanamid Co.  
Research Service Dept.  
Bound Brook, N.J.  
ATTN: Dr. C. Maresh (1)

Commanding Officer  
U.S. Naval Ordnance Laboratory  
Corona, California  
ATTN: Library (Spindler) (1)

Electrochimica Corporation  
1140 O'Brien Drive  
Menlo Park, California  
ATTN: Dr. M. Eisenberg (1)

Sandia Corporation  
Sandia Base  
Albuquerque, New Mexico  
ATTN: Librarian (1)